Bifurcations and Symmetries in Viscous Flows

J.J. Kobine

St. Hugh's College, Oxford

Thesis submitted for the degree of Doctor of Philosophy
in the University of Oxford

Trinity Term 1992

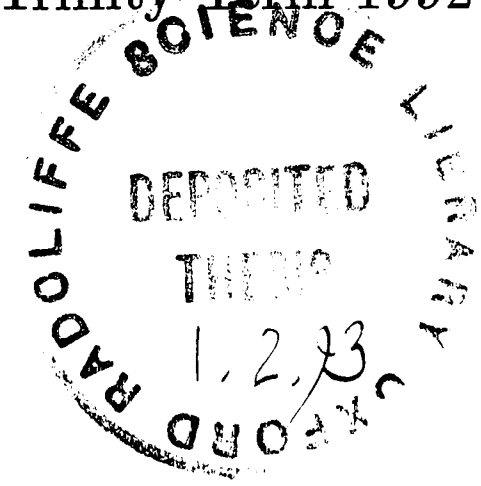

ABSTRACT

Bifurcations and Symmetries in Viscous Flows

J.J. Kobine
St. Hugh's College, Oxford

D. Phil.
Trinity Term 1992

The results of an experimental study of phenomena which occur in the flow of a viscous fluid in closed domains with discrete symmetries are presented. The purpose is to investigate the role which ideas from low-dimensional dynamical systems have to play in describing qualitative changes that take place with variation of the governing parameters. Such a descriptive framework already exists for the case of the Taylor-Couette system, where the domain possesses a continuous azimuthal symmetry group. The present investigation is aimed at establishing the typicality of previously reported behaviour under progressive reductions of azimuthal symmetry.

In the first investigations, the fixed outer circular cylinder of the standard system is replaced with one of square cross-section. Thus there is now discrete $\mathbb{Z}_4$ symmetry in the azimuthal direction. Knowledge of the two-dimensional flow field is used to establish the nature of the steady three-dimensional motion equivalent to Taylor vortex flow. It is shown that similar bifurcation sequences exist in both standard and square systems for the case of very small aspect ratio where a single Taylor cell is formed. This flow develops as the result of a bifurcation which breaks the $\mathbb{Z}_2$ symmetry that is imposed on the annulus by two solid stationary ends.

The study is then extended to consider time-dependent effects in the square system. Two different oscillatory single-cell flows are identified, and it is shown that each is the result of a Hopf bifurcation. Selection of a particular dynamic mode is found to depend on the aspect ratio of the system. A low-dimensional bifurcation structure is uncovered which connects the two modes in parameter space, and involves a novel type of steady single-cell flow. Finally, observations are reported of a nontrivial type of dynamical behaviour which bears strong resemblance to motion found in a circularly symmetric Taylor-Couette system that is related to the Šilnikov mechanism for finite-dimensional chaos.

A second variant on the Taylor-Couette system is considered where the outer cylinder is shaped like a stadium. The effect is to reduce further the overall symmetry of the domain to a $\mathbb{Z}_2 \times \mathbb{Z}_2$ group. The two-dimensional flow field is investigated using both numerical and experimental techniques. Time-dependent phenomena are then investigated in the three-dimensional flow over a relatively wide range of aspect ratio. It is found that a sequence of a Hopf bifurcation followed by period-doubling bifurcations exists up to a certain aspect ratio, beyond which there is an apparently sudden and reversible transition between regular and irregular dynamical behaviour. Although this transition is not of a low-dimensional nature, the experimental results suggest that it exists as the result of a coalescence of the bifurcations which are found at lower values of aspect ratio.

ACKNOWLEDGEMENTS

I would like to take this opportunity to express my gratitude to all those who have helped and supported me in the preparation of this thesis. I am especially indebted to the following individuals.

To Dr. Tom Mullin, for all his guidance, encouragement and positive criticism relating to every aspect of my work.

To Keith Long, whose skill and expertise in the construction and maintenance of experimental apparatus cannot be valued highly enough.

To Dr. Alan Darbyshire, for his generous assistance with all aspects of signal processing and computing.

To Tim Price and Francis Madden, for discussions, ideas, motivation and friendship.

I would also like to thank all past and present members of the Nonlinear Systems Group who have helped and encouraged me. I gratefully acknowledge the financial support of the Science and Engineering Research Council and St. Hugh's College, Oxford.

Finally, much love and thanks to my Mother, to whom I owe everything. And to Laura, without whom this thesis and its author would never have survived, all my love.

CONTENTS

CHAPTER ONE

Introduction

The study seventy years ago by G.I. Taylor of the stability of viscous flow between concentric rotating cylinders provides one of the pillars of hydrodynamic stability theory. Since that time, the system has been used extensively for theoretical, numerical and experimental studies of fluid flow instabilities. In more recent years, this system has become a powerful tool for investigating the role which low-dimensional dynamics have to play in explaining the onset of disorder in the motion of a fluid. This approach represents one of the few areas in which real progress has been made in understanding the origins of complicated flow phenomena.

In this thesis, results are presented from an experimental study of finite-dimensional dynamics in variants of the Taylor-Couette system where the outer circular cylinder is replaced with containers of both square and stadium-shaped cross-section. The aim is to determine whether ideas from systems with a low number of degrees of freedom are valid only in the highly symmetric case of the standard configuration, or persist under reductions of the overall symmetry of the flow domain. In other words, we wish to test the typicality of existing results obtained in the circular system.

A brief discussion is presented in section 1.1 of some of the essential elements in the steady solution structure of the Taylor-Couette problem. The main focus in section 1.2 is then on dynamical phenomena, particularly those aspects relating to behaviour which may be represented in a low-dimensional phase space. In section 1.3, the symmetries of the problem are discussed, and previous work on symmetry variants is reviewed. Finally, a preview of subsequent chapters is given in section 1.4.

1.1 Steady flows in the Taylor-Couette system

The Taylor-Couette system which is taken as standard in the present study is illustrated in figure 1.1. It comprises two concentric circular cylinders with a viscous fluid in the separating gap. Flow of this fluid is driven by rotation of the inner cylinder at a constant angular speed, while the outer cylinder is held fixed. The vertical height of the flow domain is defined by two stationary end-plates horizontal to the axis of rotation.

It was shown analytically by Taylor (1923) that the two-dimensional circular Couette flow for the case of infinite cylinders becomes unstable above a certain critical speed of the inner cylinder. It is replaced by a three-dimensional flow which has the form of a series of axisymmetric cells along the length of the infinite annulus. A similar transition was also found experimentally by Taylor. The new flow is known as *Taylor vortex flow*, and is shown in cross-section in figure 1.2. There is a helical motion in each cell, with a sense that alternates between adjacent cells.

The infinite-cylinder model of the Taylor-Couette system is successful in predicting the onset of cellular motion, and yields a critical Reynolds number which is found to be in excellent agreement with experiment. However, it was first pointed out by Benjamin (1978a) that there are fundamental problems to be considered when attempting to relate such a model to the experimental situation, which is necessarily of finite extent. The distinction between the two cases is represented formally by the fact that solutions in the model are invariant under arbitrary axial

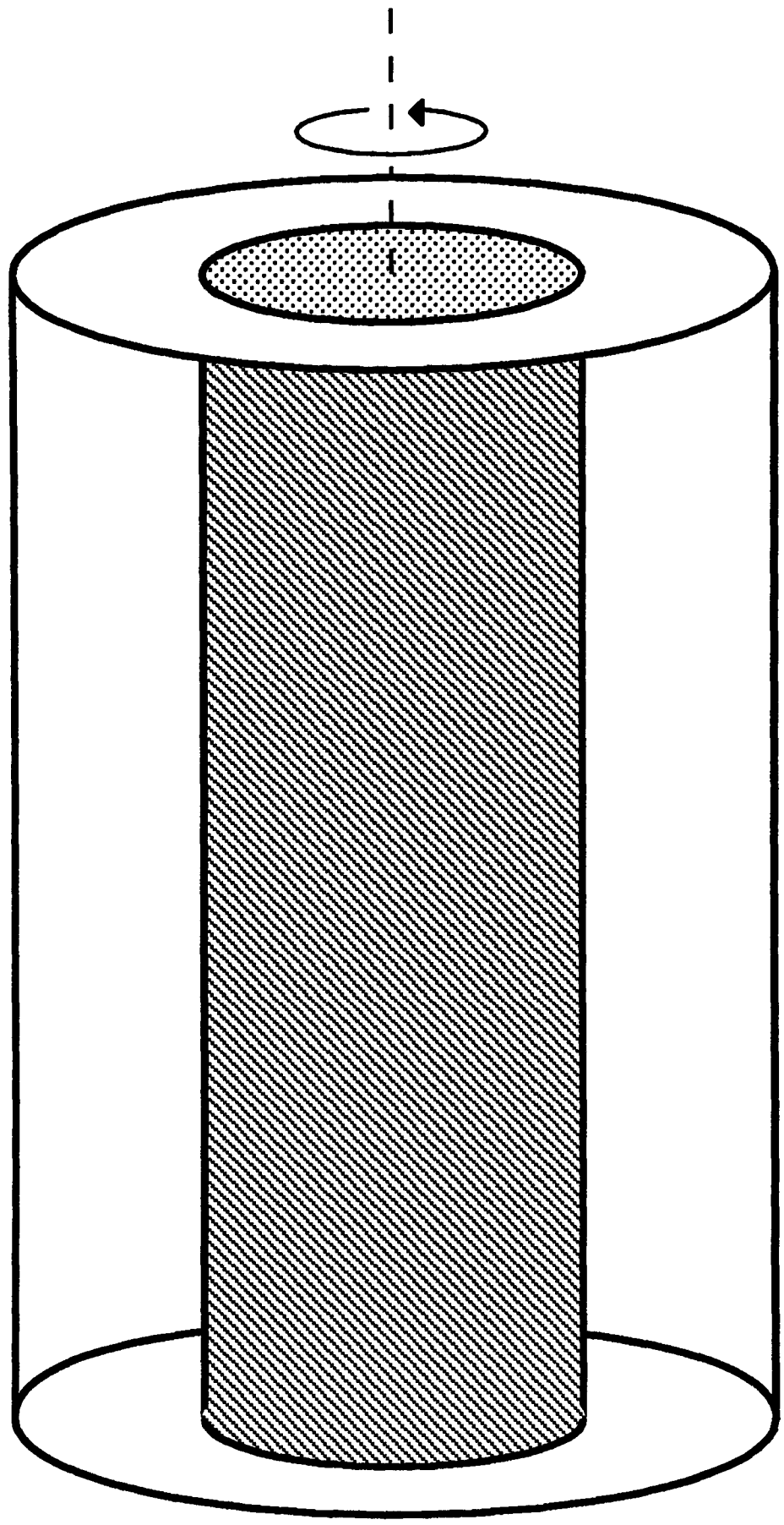

Figure 1.1 : The standard Taylor-Couette system. A viscous fluid is bounded by a stationary outer cylinder, a rotating inner cylinder and two fixed ends.

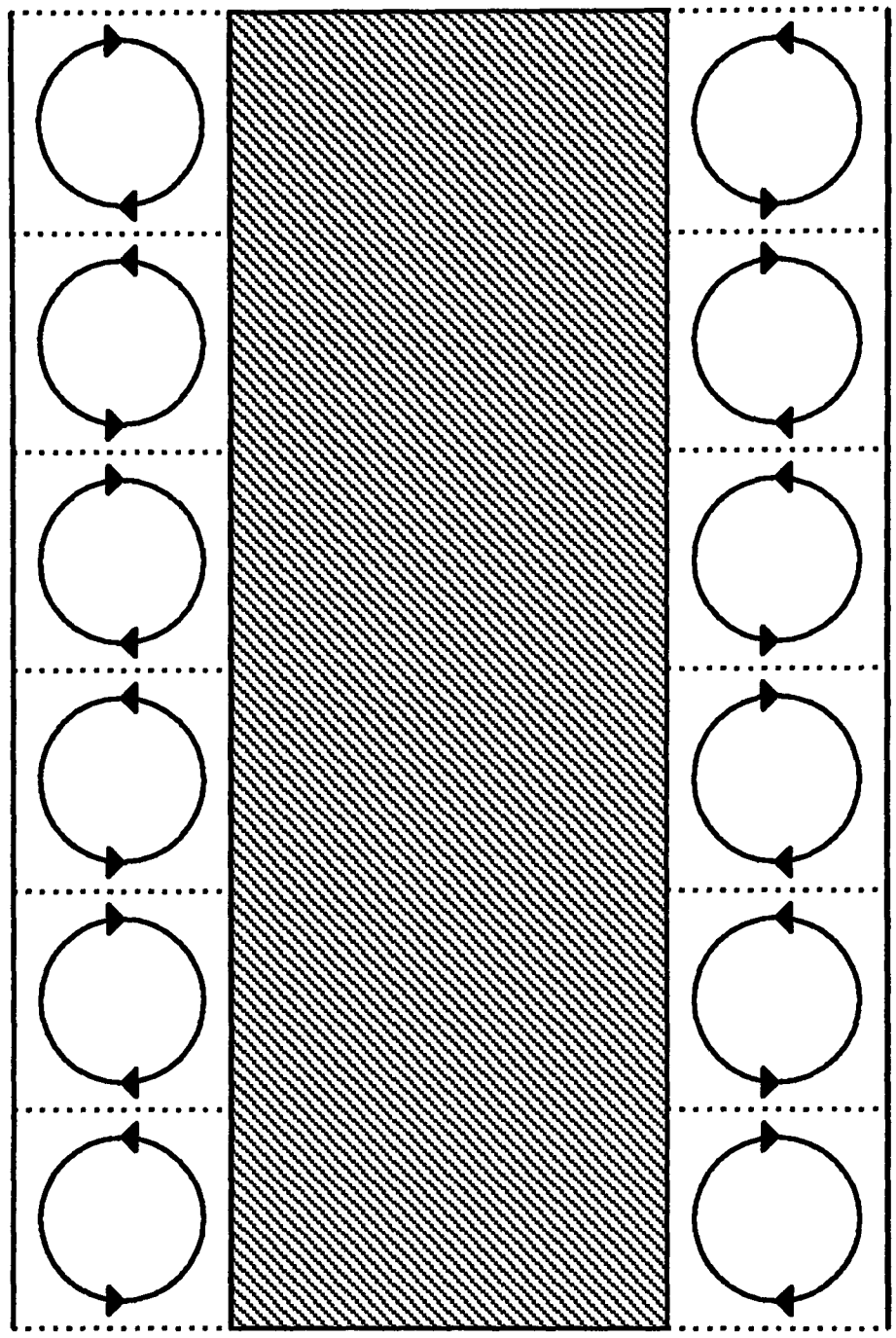

Figure 1.2 : Cross-section of Taylor vortex flow between a rotating inner cylinder and a stationary outer cylinder.

translations, whereas there is no such translational invariance in a finite system. In other words, the ends of the annulus always have a major effect on the flow, no matter how large the system is made.

A mathematical model which addresses the importance of finite length effects was proposed by Schaeffer (1980). The model is parameterized in such a way as to provide a continuous connection between idealized and realistic versions of the problem. This approach was subsequently extended by Benjamin & Mullin (1981) to give a proper understanding of the origin and structure of the many steady cellular flows that are possible in the Taylor-Couette system. A comprehensive review of the Schaeffer model and the steady solution set is given by Cliffe *et al.* (1992), and we consider here only the most basic details.

The mechanism which underlies the observed transition to Taylor vortex flow is found to be that of a supercritical pitchfork bifurcation (see Appendix A). The bifurcation in the model is symmetric, with the two nontrivial solution branches corresponding to stable cellular flows which are related by an axial translation of one cell. When the parameter in Schaeffer's model is changed to incorporate the effects of having solid ends on the annulus, this symmetric pitchfork becomes disconnected. The nature of the disconnection is dependent on whether the bifurcation is to a flow with an axial period which corresponds to an odd or an even number of cells in the model annulus of fixed length. For an odd number of cells, both the nontrivial solutions become disconnected from the trivial branch. However, only one solution is disconnected for the case of even-cell flow. This is the branch which corresponds

to flow where there are outward radial velocity components at both ends of the annulus. The system is biased towards inward flow at the ends because of the action of the no-slip boundary condition in reducing the centrifugal force in these regions.

Benjamin (1978b) observed experimentally that it is always an even-cell mode with inward flow at the ends which evolves with quasistatic increase of the inner cylinder speed. The number of cells is determined uniquely by the length of the annulus, and is referred to as the *primary mode*. However, there are other flows known as *secondary modes* which can be realised by sudden starts of the inner cylinder. These include the flows which correspond to the disconnected elements of the underlying pitchfork bifurcation. Benjamin showed that it is possible to establish experimentally both even and odd numbers of cells where the common characteristic is an outward radial component at one or both ends of the annulus. Such flows are known collectively as *anomalous modes*. All the secondary modes have lower limits on their stability, and these limits for anomalous modes are found to be at least a factor of three larger than the Reynolds number for the onset of the primary mode (see Cliffe *et al.* (1992) and the references therein). This shows that the disconnection of the underlying pitchfork bifurcation is very large compared to the usual 'softening' due to imperfections.

The existence of secondary modes constitutes a multiplicity of solutions in the Taylor-Couette system. This multiplicity is found to be very large even for a modest sized system. Benjamin & Mullin (1982) considered a particular case where the

primary mode contained twelve cells, and showed that there are at least thirty-eight other solutions which exist for the same set of parameter values. This makes it difficult in practice to investigate the detailed interactions between various modes, since there is so much structure which must first be disentangled. An alternative approach is to restrict the size of the annulus to a sufficient extent that only a limited number of solutions exists. In particular, it was shown by Benjamin & Mullin (1981) that a single Taylor cell remains connected to the primary mode when the annulus is as short as the distance separating the two cylinders. Such a regime is therefore suited to the study of low-dimensional dynamics because of the relative simplicity of the underlying solution set.

We will now go on to consider dynamical phenomena in the Taylor-Couette system based on the framework of steady solutions which has been outlined above. In particular, there is a review of work which has shown the applicability of finite dimensional dynamics to the problem. It is stressed that the study of such behaviour is only practically possible under conditions where there is a minimum of multiplicity in the solution set.

1.2 Finite-dimensional dynamics in Taylor vortex flow

The first onset of time-dependent motion in the standard Taylor-Couette system with increase of Reynolds number is typically the appearance of a travelling wave on the basic cellular structure. This was shown both experimentally by Coles (1965) and analytically by Davey *et al.* (1969). The development of temporal disorder in this wavy vortex flow was reported by Gollub & Swinney (1975), who observed the appearance of additional frequency components before the development of a broadband power spectrum. Observations have subsequently been made of a bewildering variety of regular and irregular phenomena in the problem, much of which is discussed by DiPrima & Swinney (1981).

However, despite the large numbers of studies where interesting dynamics have been observed, there have been few attempts to understand the origins of such behaviour. One region where significant progress has been made is in the application of ideas from finite-dimensional dynamical systems to understanding the first transitions to weakly disordered flow (see the review by Mullin (1991), for example). The initial dynamic change from steady to singly-periodic flow was shown by Davey *et al.* (1969) to be the result of a Hopf bifurcation. The behaviour of the system may then be represented by a limit cycle in phase space, as discussed in Appendix A. Ideas from finite-dimensional dynamical systems provide a context in which the stability of this limit cycle and the possible interactions with other solutions may be understood.

One commonly observed low-dimensional route by which a system may proceed from a regular to a chaotic state is a cascade of *period-doubling* bifurcations. This phenomenon is reviewed in detail by Cvitanović (1989), and is essentially an infinite sequence of splittings of a limit cycle with the variation of some parameter over a finite range. The first observation of period-doubling in the Taylor-Couette system was made by Pfister (1985) in a very short annulus where the only possible cellular structures were either a two-cell or a single-cell flow. This is a good example of how reducing the multiplicity in the solution set allows a detailed bifurcation structure to be resolved experimentally.

An important concept is that of *organizing centres* for disordered behaviour. These are points in parameter space where two lines of codimension-1 bifurcations meet to give a multiple codimension-2 bifurcation. This formalism is discussed further in Appendix A. An example of such behaviour was reported by Mullin *et al.* (1987) for the Taylor-Couette system. It was found that a point in parameter space where there was the simultaneous occurrence of a symmetry-breaking and a saddle-node bifurcation was the source of a line of Hopf bifurcations. This behaviour is consistent with predictions of an abstract model forwarded by Guckenheimer (1981) for a similar situation.

The important role of codimension-2 bifurcations in Taylor vortex flow has been confirmed by a series of studies of flow in a variant on the standard system where the end-plates are made to rotate with the inner cylinder. A simultaneous occurrence of a saddle-node and a Hopf bifurcation was identified both numerically

and experimentally by Mullin *et al.* (1989). This point in parameter space was found experimentally to be the origin of lines of bifurcations to quasiperiodic behaviour and then to irregular behaviour.

Mullin & Price (1989) reported the occurrence of *homoclinic* phenomena associated with the interaction of a steady and a time-dependent flow in the system with rotating ends. This is were the period of an oscillation tends towards infinity with the variation of a control parameter. Such a phenomenon can be explained by the approach of a limit cycle and an unstable fixed point in phase space, where trajectories are slowed down as they near the fixed point. It was found that there is a transition between regular and irregular homoclinic behaviour which is similar to that found in a system of ordinary differential equations which has been studied by Langford (1983).

There is no doubting the success of ideas from finite-dimensional dynamical systems in describing the various flow phenomena which are discussed above, and in particular the important role of codimension-2 bifurcations as organizing centres for more complicated behaviour. However, it could be argued that such behaviour in the Taylor-Couette system is highly non-generic. This is because of the high degree of symmetry embodied in the problem which is not generally found in other fluid flow configurations. We will now go on to consider these symmetries, and identify various features of the problem which may be affected by such properties.

1.3 Symmetries in the Taylor-Couette problem

The standard system of concentric circular cylinders with fixed horizontal end-plates, as shown in figure 1.1, possesses two geometrical symmetry groups. One is a discrete $\mathbf{Z}_2$ group corresponding to the reflectional symmetry of the annulus about the horizontal plane mid-way between the stationary ends. The other is a continuous $SO(2)$ group corresponding to the rotational invariance of the annulus in the azimuthal direction. There are various features of the problem which can be assigned to one or other of these groups. We will discuss briefly certain points relating to the $\mathbf{Z}_2$ group before concentrating on the $SO(2)$ group which is of principal interest in this study.

One consequence of the existence of a $\mathbf{Z}_2$ reflectional symmetry about the mid-plane of the annulus has already been encountered in the use of the model due to Schaeffer (1980) to describe the onset of Taylor vortices. It is a fact that the primary mode at onset always comprises an even number of vortices and shares the same $\mathbf{Z}_2$ symmetry as the flow domain. However, it was shown by Mullin & Cliffe (1986) that there is a marked tendency for this symmetry to be broken with further increase of cylinder speed. This occurs as the result of a symmetry-breaking bifurcation as discussed in Appendix A. The initially stable symmetric flow becomes unstable to asymmetric perturbations, and two new stable solution branches appear which correspond to flows where certain cells have grown in size at the expense of other cells to break the mid-plane symmetry. The fact that this bifurcation is in a physical system where imperfections are unavoidable is reflected in the disconnection of one

of the asymmetric solution branches. Flows with the same sense of asymmetry always appear when the angular speed is increased gradually. However, the other asymmetric flow may be established by a sudden change in the rate of rotation.

The breaking of a geometrically imposed $\mathbf{Z}_2$ symmetry by a fluid flow is not restricted to the Taylor-Couette system. Fearn *et al.* (1990) used numerical and experimental techniques to investigate the flow through a nominally two-dimensional channel in which there is a sudden expansion that is symmetric about the mid-plane of the system. The flow at relatively low values of the Reynolds number consists of a symmetric jet into the expanded region, and two corner recirculations of equal size. As the Reynolds number is increased, a pitchfork bifurcation to asymmetric flow is encountered. This results in the bending of the jet towards one of the side walls, and the growth of one of the recirculations. The $\mathbf{Z}_2$ symmetry of the boundary conditions is therefore broken by this change in the flow. A symmetry-breaking phenomenon has also been observed by Winters (1987) for the case of flow in curved ducts, where secondary cellular flow is established by the action of centrifugal instability (see Drazin & Reid (1981), for example). The mid-plane symmetry of the duct is broken by the growth of certain cells at the expense of others.

We now move on to consider the role of the continuous $SO(2)$ symmetry group. One reason for the extensive work carried out to date on the standard Taylor-Couette problem is that many of the results from experiments can be compared directly with numerical solutions of the full Navier-Stokes equations. Such calculations are made possible by utilizing the continuous azimuthal symmetry of the

flow domain. However, the fact that the present studies are all experimental reflects the fact that absence of rotational invariance greatly increases the amount of computational power which would be required in order to solve the governing equations.

The continuous $SO(2)$ symmetry of the standard system has been subject to investigation since the earliest studies of Taylor vortex flow. Terada & Hattori (1926) carried out experiments in a circular container where flow was driven by the rotation of a variety of devices. These included a concentric cylinder with a stationary barrier across the annulus, an eccentric cylinder and double cylinders. In all these cases, the continuous $SO(2)$ symmetry of the original problem is broken by the variations in the geometry of the domain. It was observed by Terada & Hattori that cellular flows could nevertheless be produced in each system given a sufficient speed of rotation of the inner device. The flows were photographed in cross-section, and show the same sequence of alternating cells along the length of the annulus as is the case for the standard Taylor-Couette system.

Observations of cellular flows in variants which break the $SO(2)$ symmetry were also been made by Snyder (1968) in a study into the effects of boundary conditions on geophysical models. Configurations which were studied included a rotating circular cylinder at the centre of a square container, and a rotating square cylinder at the centre of a circular container. Cellular flows were always observed in time-dependent form in the latter system, but the former showed a transition to steady cellular flow as in the standard system. Thus Snyder concluded that altering

the shape of the outer boundary in the Taylor-Couette problem did not alter the underlying stability criterion for the transition to cellular flow.

The above studies were primarily concerned with establishing the existence of steady cellular flows in geometries where the $SO(2)$ symmetry had been broken. Mullin *et al.* (1983) made a preliminary study into the effects on time-dependent flows in a system where the outer circular cylinder was replaced with one of square cross-section. The behaviour of the flow was recorded using a nonintrusive laser system which measured a component of the velocity field at a fixed point within the flow. It was observed that the steady cellular flow becomes unstable to a singly periodic mode with increasing cylinder speed. However, unlike the standard Taylor-Couette system, this mode is not a simple travelling wave but a more complicated motion of the cells. Further increase leads to a second frequency component in the power spectrum of the signal, which results in the formation of side-bands on the main frequency. These merge with the main peak to form a broad band spectrum, which continues to spread until there is no evidence of any temporal structure in the flow. A significant observation of Mullin *et al.* was that the flow in this state is also devoid of any spatial structure. This is in marked contrast to the standard system, where the cellular structure is found to persist well into the turbulent regime (Smith & Townsend 1982). Thus it was concluded that the effect of having discrete azimuthal symmetries was most pronounced in relation to time-dependent phenomena.

The first detailed bifurcation study of flows in a symmetry variant of the Taylor-

Couette system was carried out by Mullin & Lorenzen (1985). They investigated experimentally the exchange mechanism between the four-cell and six-cell primary modes in a system with a stationary square outer cylinder and variable annulus length. It was found that the framework of solutions proposed by Benjamin (1978a) involving secondary modes which are disconnected from the primary mode persists under the change of azimuthal symmetry. Both normal and anomalous types of secondary flow were observed, the latter having both odd and even numbers of cells.

Thus it is established that bifurcation phenomena provide a context for understanding the steady solution set in the square system. The purpose of undertaking the present study is to determine whether the dynamical behaviour of flows in this system can be understood in a similar way.

1.4 Preview of chapters

A description of the experimental rigs which were used to study flows in both the square and the stadium versions of the Taylor-Couette system is given in Chapter 2. The accurate control of such aspects as the rotation speed of the inner cylinder and the viscosity of the working fluid is emphasised. These quantities are then used with others to define the governing dimensionless parameters of the systems, namely the Reynolds number, aspect ratio and clearance ratio. The technique of flow visualization is discussed, and it is shown how the spatial structure of flows may be observed by this means. Laser Doppler velocimetry, on the other hand, provides a nonintrusive point measurement of a component of the flow, and is therefore ideal for studying time-dependent phenomena. Finally, the use of computers in both the control of experiments and in the processing of data is described.

The steady flows which exist in the square Taylor-Couette system at very small aspect ratios are the subjects of Chapter 3. Such a flow domain possesses a discrete $\mathbf{Z}_4$ azimuthal symmetry. Initially, the two-dimensional flow which occurs in such a configuration is considered. Attention is then turned to the bifurcation sequence for single-cell flows. The mechanism proposed by Benjamin & Mullin (1981) for the standard system is described in detail. Experimental results are then presented for a similar sequence in the square system. Comparisons of both a qualitative and a quantitative nature are made with existing results for the standard Taylor-Couette system.

In Chapter 4, results are presented of investigations into basic time-dependent forms of the single-cell flow in the square system. Two distinct modes are identified, and it is shown that these both occur as the result of Hopf bifurcations. These flows are compared with similar states that occur in the standard system. The method by which one mode succeeds the other as the aspect ratio is varied is investigated experimentally. Several bifurcation phenomena are identified over a narrow range of aspect ratio. In particular, there is a bifurcation to a type of steady flow which is not observed in the standard system.

The dynamics of one of the two general types of time-dependent single cells are explored in detail in Chapter 5. It is found initially that there is multiplicity of singly-periodic states. Higher-order effects are then investigated by increasing the Reynolds number beyond the singly-periodic regime. This leads to observations of dynamics which bear strong similarity to finite-dimensional behaviour which is know to exist in a Taylor-Couette system with continuous rotational symmetry around the annulus. The significance of these observations are discussed in relation to the reduction from $SO(2)$ to $\mathbf{Z}_4$ symmetry in the flow domain.

Flows in a Taylor-Couette system where the outer cylinder is shaped like a stadium are considered in Chapter 6. This represents a further reduction of the azimuthal symmetry to a $\mathbf{Z}_2$ group. The two-dimensional flow field is first investigated using both numerical and experimental techniques. Preliminary observations of time-dependent phenomena are then reported from a prototype apparatus. These show potentially significant behaviour, which is then investigated more carefully in

a second apparatus of higher specification. Once again, the results are discussed in relation to the azimuthal symmetry of the domain.

Finally, certain conclusions arising from the findings of this study are made in Chapter 7, along with suggestions for work which may usefully be carried out in the future to extend the present state of knowledge of this subject.

CHAPTER TWO

Experimental apparatus and methods

This chapter is given over to a description of the various experimental apparatus and techniques which were employed in the course of the present study. The technical aspects of two different flow rigs are discussed in detail, along with their respective principles of operation. The main dimensionless parameters which govern the state of both systems are introduced, these being the Reynolds number Re and aspect ratio Γ. Two important techniques for investigating the behaviour of the fluid flow are then discussed. These are flow visualization and laser Doppler velocimetry, and their respective domains of applicability are considered. Finally, the use of computer systems in both the control of the flow rigs and in the acquisition of data is described.

2.1 Taylor-Couette variant with a square outer cylinder

The flow domain which is of primary interest in this study is shown schematically in figure 2.1. The outer boundary is a vertical container with uniform square cross-section, and will be referred to hereafter as a *square cylinder*. It is always held stationary in these experiments. The inner boundary is the surface of a cylinder with uniform circular cross-section. This cylinder is free to rotate at a constant angular velocity. It is positioned so that it is concentric with the square cylinder. The vertical extent of the flow domain is defined by two solid stationary ends. These are perpendicular to the common vertical axis of the inner and outer cylinders, and extend to fill the full horizontal area of the domain.

A photograph of the experimental apparatus which was used to investigate flows in the domain described above is shown in figure 2.2. The flow rig is the same one which was used in the investigations of Mullin *et al.* (1983) and Mullin & Lorenzen (1985), but with some minor modifications and improvements.

The square cylinder was constructed from four uniform glass plates. These were glued together on a milled aluminium former to ensure a precise square cross-section. The length of each side is equal to 63.57 ± 0.05 mm. The inner cylinder was machined from solid stainless steel to a uniform diameter of 31.78 ± 0.01 mm. This value was chosen to give a ratio of the inner diameter to the outer length of side which is equal to 0.500 ± 0.001. A small tapered pin extends from the bottom of the cylinder which allows it to be positioned in the base of the rig. There is a

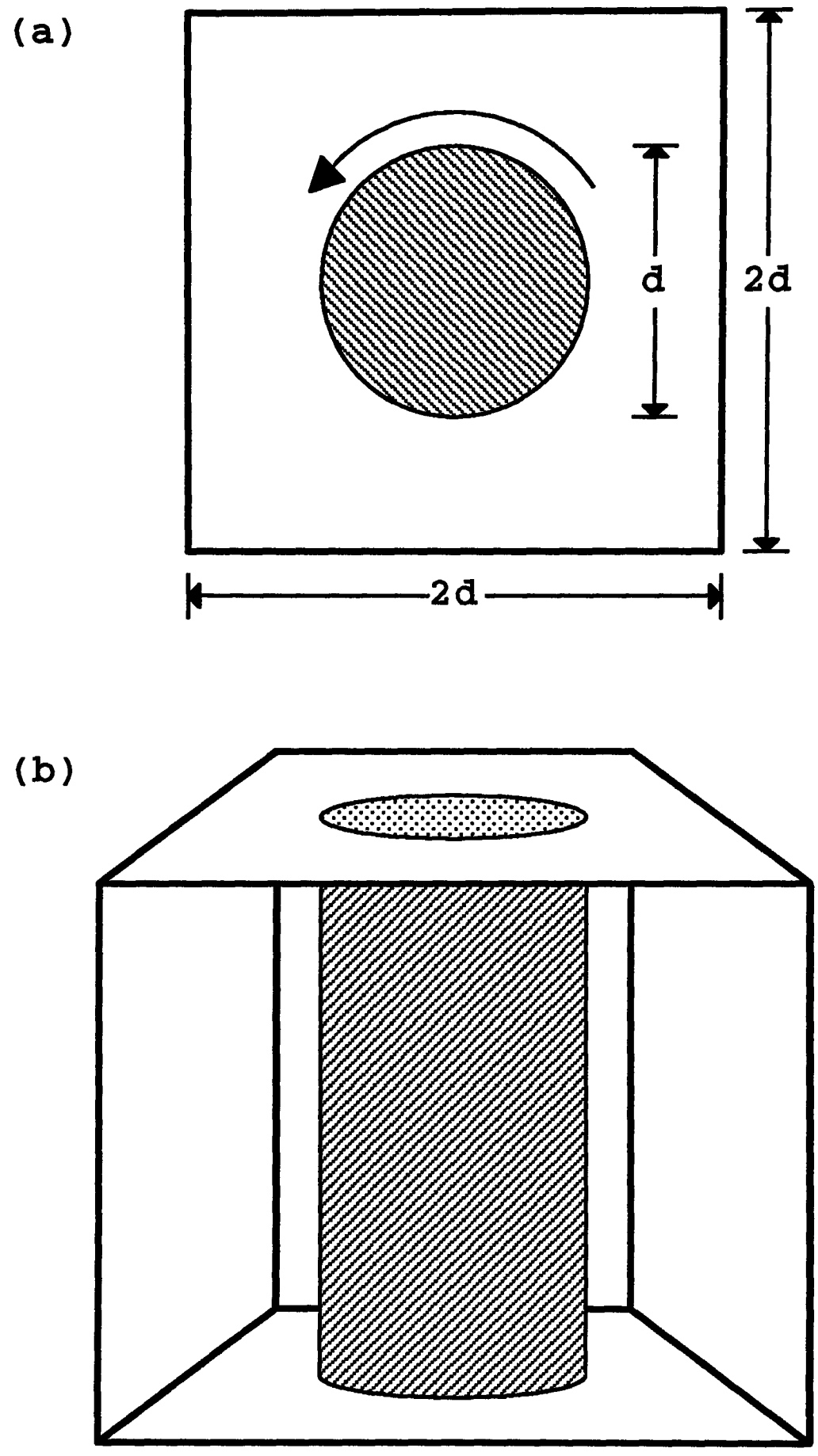

Figure 2.1 : Geometry of the square Taylor-Couette system. (a) plan view. (b) perspective view.

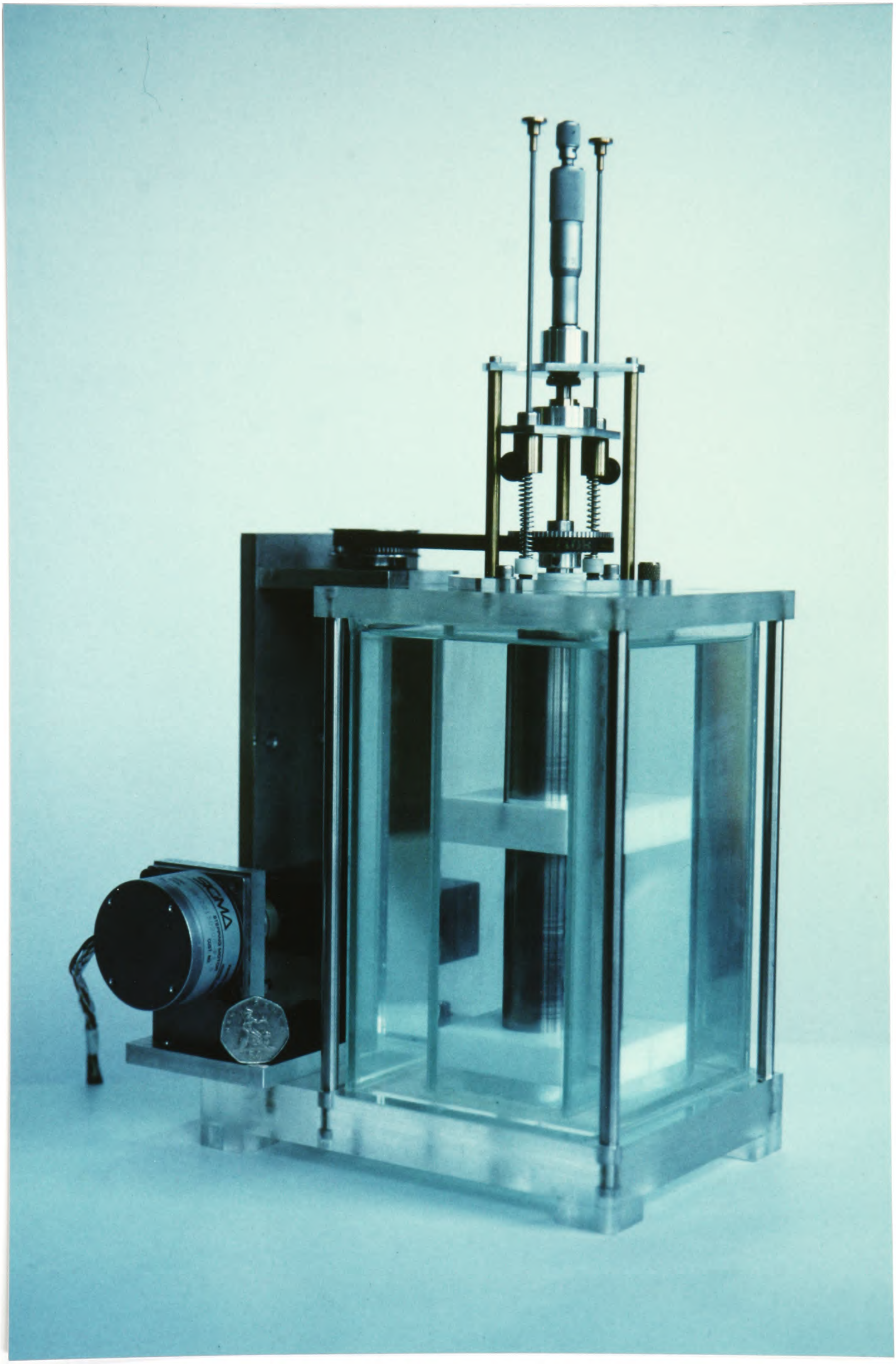

Figure 2.2 : Photograph of the square Taylor-Couette apparatus.

narrow shaft at the top of the cylinder for the purpose of connecting to a driving mechanism which is described later in this section.

The base of the flow rig was made from a thick piece of Perspex. It has a square channel milled into it so that the outer cylinder can be accurately glued into position. In the centre of this square is a sunken bearing made from PTFE into which the tapered pin at the bottom of the circular cylinder is inserted. The depth of the bearing is such that there is a small clearance between the base and the bottom of the cylinder, allowing the cylinder to rotate freely. The top of the rig is covered by a tight-fitting Perspex lid. At the centre of the lid is a PTFE collar bearing which surrounds the shaft of the inner cylinder.

The two horizontal end-plates were cut from 1.6 cm thick pieces of PTFE and were made to fit closely to the outer cylinder, but with a very small amount of clearance at the rotating inner cylinder. The lower block rests on a flat PTFE collar on the base of the rig, while the upper block is supported from above by two metal rods on either side of the inner cylinder. The vertical separation between the horizontal ends can be varied continuously over the range 0–170 mm. The rods extend up through holes in the Perspex lid and are held by grips connected to a micrometer screw assembly. This allows the position of the upper block to be adjusted by small, controllable amounts during an experiment. The holes through which the rods pass are sealed by two tiny rubber rings which are pushed down from above by springs. This helps to prevent contamination of the working fluid by debris which might otherwise enter through the holes in the lid.

The inner cylinder is rotated by a driving mechanism which is attached to the base of the rig. A stepping motor which operates at 400 steps per revolution is supplied by an oscillator whose frequency stability is better than 0.1%. The stepping motor is attached via a 6:1 reduction gearbox to a vertical drive shaft. At the end of both the drive shaft and the shaft extending from the top of the inner cylinder are gear wheels with a relative ratio of 5:6. These are connected together by a toothed drive belt to rotate the inner cylinder at an angular velocity which is constant to within the stability of the oscillator supplying the stepping motor. For this particular apparatus, the angular velocity ω of the inner cylinder is given by $\omega = 2.182f$, where ω has units of seconds^{-1} and f is the frequency of the oscillator signal in kiloHertz. Signals in the range 1–5kHz were used, this being dictated mainly by the need to avoid excessive amounts of heat being produced in the motor when it was operating for long periods of time.

A much larger square box surrounds the outer cylinder of the flow domain. It is made from Perspex and is set into the base of the rig. It is closed at the top by a Perspex cover which extends across to meet the top of the square cylinder. This outer container forms a sealed jacket through which thermally regulated distilled water is pumped at 27.3°C by a Haake temperature controller. As a further precaution, the entire flow rig is housed in a large cabinet in which the air temperature is held at 27°C using an electric fan heater connected to a mercury switch thermometer. These two thermal controls have the effect of holding the temperature of the working fluid constant to better than 0.02°C over the course of the experiments.

2.2 Taylor-Couette variant with a stadium-shaped outer cylinder

In addition to the flow domain discussed in section 2.1, a second configuration was used in the investigation of the effect of symmetry on the nature of rotating flow. The new geometry is shown in figure 2.3. The basic design is similar to the previous case in the sense that the inner and outer cylinders are concentric and the flow domain is bounded by fixed horizontal ends. However, the shape of the outer boundary is now that of a *stadium*. It comprises two parallel plane sides of equal length connected together at each end by semicircular surfaces.

Two pieces of apparatus were constructed, both of which embody this stadium configuration. The first is a basic prototype which was used to investigate the scientific potential of such a flow system. The second piece of apparatus was built to a much higher specification to allow accurate and controllable experiments to be carried out.

A photograph of the prototype flow rig is shown in figure 2.4. The outer container is formed from two Perspex plates and a length of Perspex cylinder which was cut into two halves. These four pieces were glued together to form the required stadium shape. The perpendicular distance between the two parallel sides and the diameter of the semicircular ends are both equal to 107.6 ± 0.1 mm. The length of each of the two straight sides is equal to 109.8 ± 0.1 mm. Thus the prototype rig has a cross-sectional aspect ratio of 2.02. The inner cylinder was made from brass and has a diameter of 88.66 ± 0.01 mm. This gives a clearance ratio of 0.824 based on the

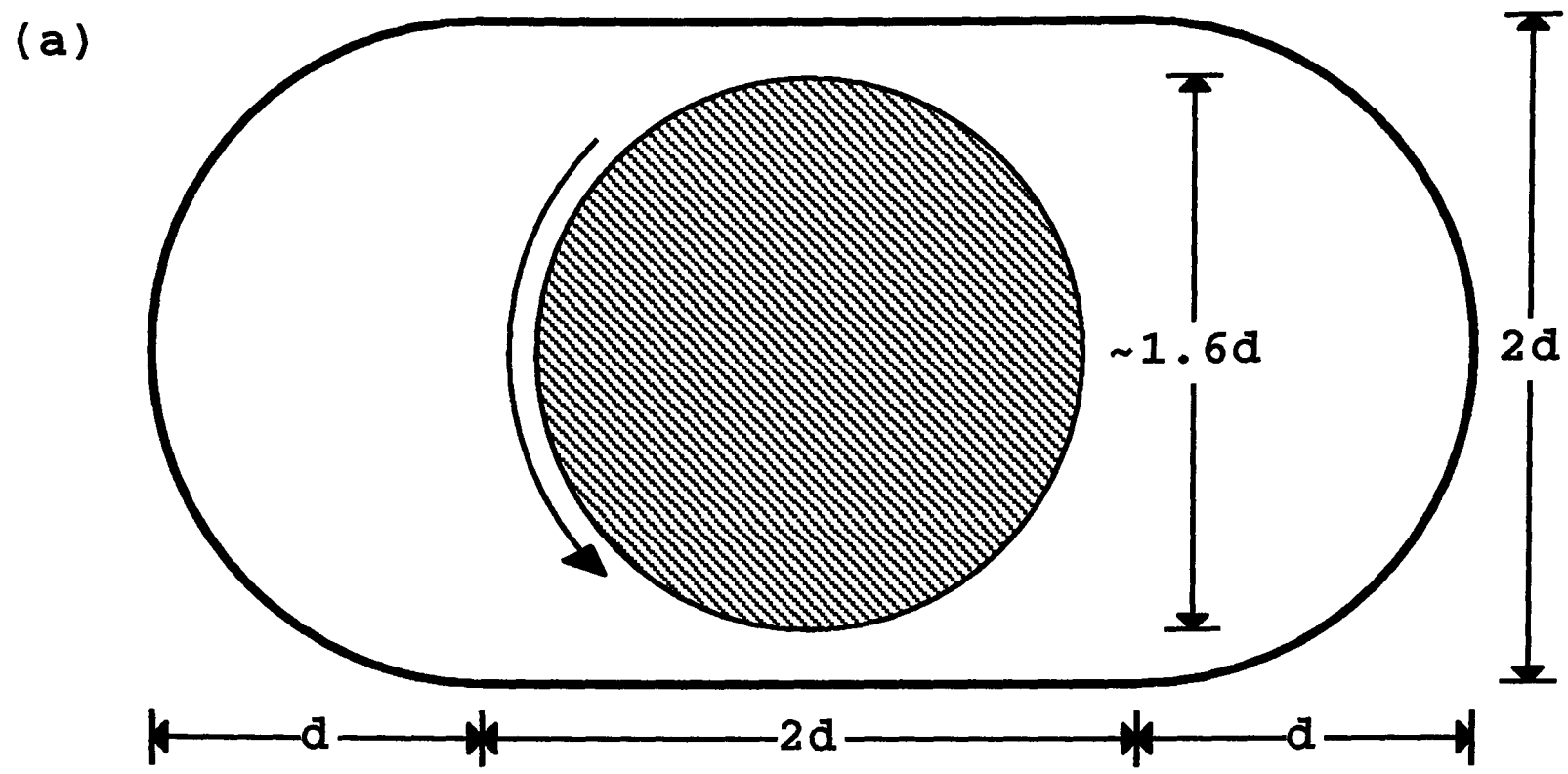

Figure 2.3 : Geometry of the stadium Taylor-Couette system. (a) plan view. (b) perspective view.

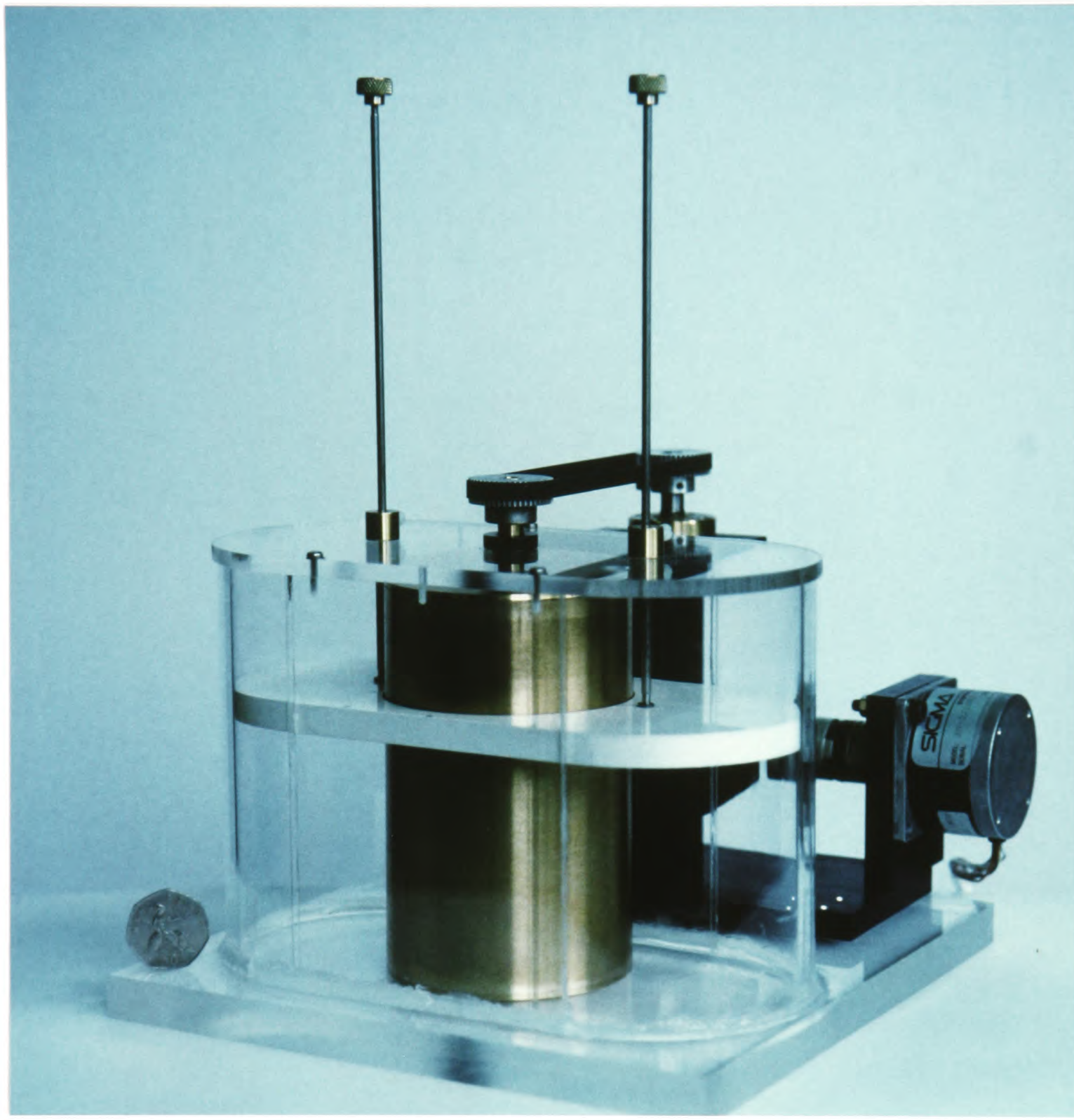

Figure 2.4 : Photograph of the prototype stadium Taylor-Couette apparatus.

minimum gap between inner and outer cylinders. The stadium-shaped cylinder is set into a Perspex base, along with a circular PTFE bearing for the inner cylinder. The height of the flow domain is defined by the position of a horizontal PVC plate which fits inside the stadium and around the circular cylinder. The end-plate is supported from above by two metal rods which pass through the Perspex lid of the flow rig and are held by two screw grips.

The second piece of apparatus is shown in figure 2.5. The stadium is now made from two Perspex plates and the two halves of a glass cylinder. The choice of glass as the material for the curved surfaces results in a more accurate radius than is the case when Perspex is used. The inner diameter of the glass cylinder is equal to 75.00 ± 0.02 mm. The length of each straight side and the perpendicular distance between them are both equal to 75.00 ± 0.05 mm. Thus the cross-sectional aspect ratio is 2.00. Two different brass inner cylinders were used, with radii of 60.00 ± 0.01 mm and 61.80 ± 0.01 mm. These values give clearance ratios of 0.800 and 0.824 respectively. The base and cover of the flow rig are made from aluminium, and extend out to allow the flow region to be surrounded by a water jacket with Perspex walls. The water jacket is used to provide thermal control in the same way as was detailed in section 2.1. The flow domain is bounded vertically by two PVC end-plates. One rests on the base of the flow rig, while the other is connected by two metal rods to a micrometer assembly. The height of the flow domain can be varied between zero and 115 mm.

The driving mechanism for each of the two stadium rigs described above is

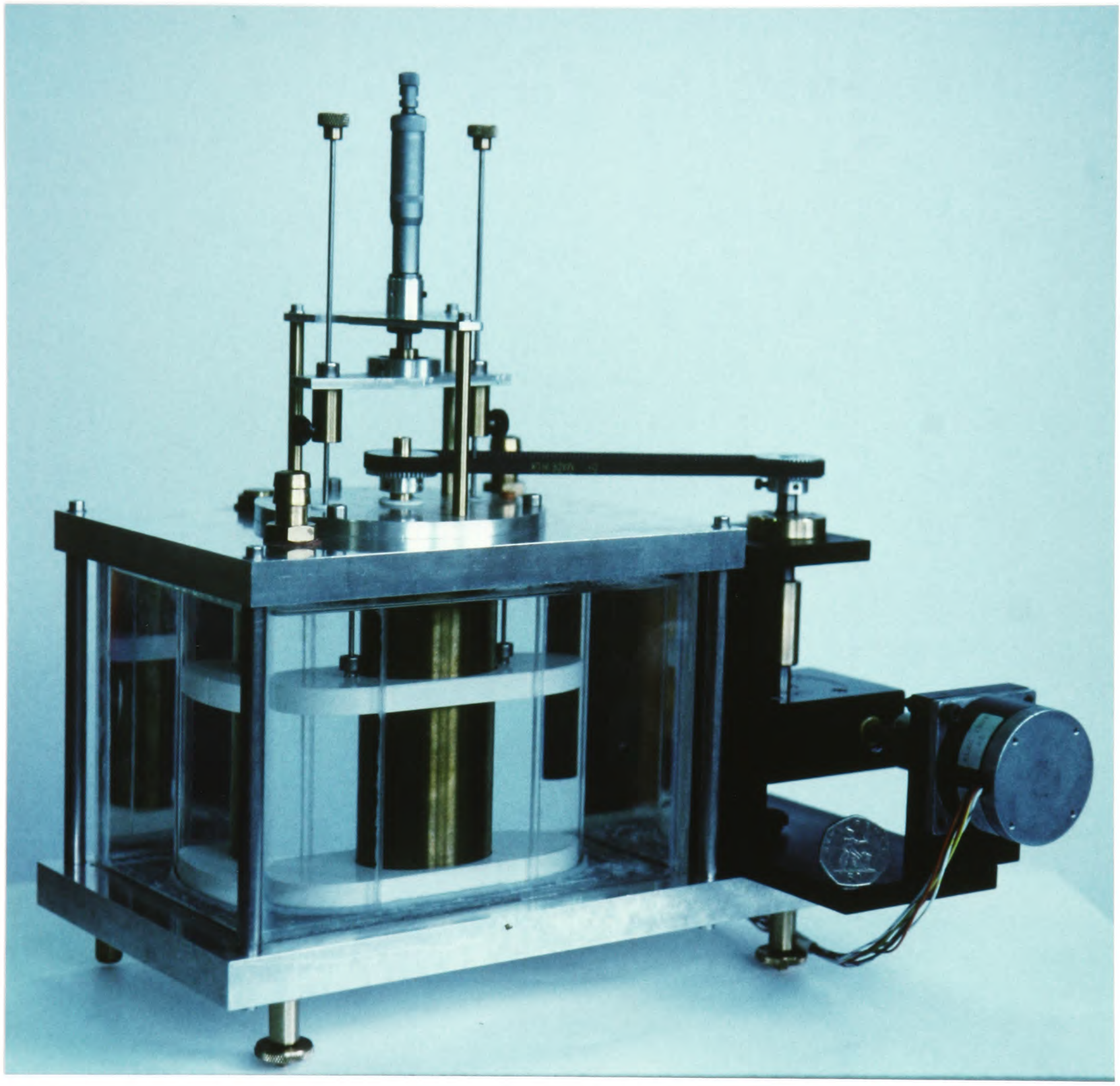

Figure 2.5 : Photograph of the second stadium Taylor-Couette apparatus.

essentially the same as the one which is used in the case of the square configuration. The only difference is that the ratio of the gear wheels which are linked by the drive belt is 1:1 instead of 5:6. Thus the relationship corresponding between driving frequency and angular speed is now $\omega = 2.618f$. Once again, ω is the angular velocity in units of seconds^{-1} and f is the frequency in kiloHertz of the signal being supplied to the stepping motor.

2.3 Governing parameters

The main dimensionless parameter in both the square configuration and the stadium-shaped configuration is the *Reynolds number Re*. This is defined as

$$Re = \frac{UD}{\nu}, \tag{2.1}$$

where U is a representative speed in the flow, D is a representative distance and ν is the kinematic viscosity in appropriate units. In Taylor-Couette problems generally, the speed U is taken as the tangential speed on the surface of the rotating cylinder. For the case of a circular cylinder at the centre of a noncircular container, we will choose the distance D to be the minimum gap between the inner and outer cylinders. Although the choice could be made from any other distance in the flow domains under consideration, we shall see in Chapters 3 and 6 that there are good reasons for this particular choice. Thus the definition of Reynolds number for both systems becomes specifically

$$Re = \frac{\omega r d}{\nu}, \tag{2.2}$$

where ω is the angular frequency of the inner cylinder, r is the radius of the inner cylinder, d is the minimum gap between inner and outer cylinders and ν is the kinematic viscosity of the fluid.

Two different types of fluid were used separately throughout the course of this study. Mixtures of distilled water and Glycerol were the preferred choice for flow-visualization experiments (see section 2.4), whereas silicone oil was used for many of the laser Doppler velocimetry measurements (see section 2.5). However,

silicone oil was found to cause a deterioration of the silicon rubber sealant which is used around the base of the square cylinder. As a result, Glycerol solutions were used latterly for laser Doppler work as well. In every case, the fluid was prepared with the aim of selecting a value of the kinematic viscosity that would allow the Reynolds numbers of interest to be obtained within the optimum frequency range of the stepping motor. Viscosity measurements were performed using a suspended level viscometer which allowed the value of ν to be determined to an accuracy of 0.01 mm^2s^{-1}. Fluids used in the square-shaped system had viscosities ranging from 2 mm^2s^{-1} to 6 mm^2s^{-1}. Those used in the stadium-shaped system were required to be more viscous, with ν taking values from 16 mm^2s^{-1} to 25 mm^2s^{-1}.

In addition to the Reynolds number, there is a dimensionless geometrical parameter which is known as the *aspect ratio* Γ. It is defined as

$$\Gamma = \frac{h}{d}, \tag{2.3}$$

where h is the perpendicular distance between the stationary ends of the flow domain and d is the minimum distance between the inner and outer cylinders. Once again, this latter distance is chosen over others on the basis of certain two-dimensional flow features which are discussed in Chapters 3 and 6. The value of h was determined using a precision travelling telescope which was located externally from the flow rig and its temperature-controlled environment. The telescope has a cross-hair eyepiece and an integral spirit level to ensure correct and repeatable positioning during the taking of measurements. The vertical separation h between the two fixed ends was measured to an absolute accuracy of 0.02 mm.

Thus each system is described by three dimensionless parameters. One is the clearance ratio η based on the minimum clearance between the inner and outer cylinders. This ratio remained fixed throughout the course of individual experiments. The other geometrical parameter is the aspect ratio Γ, the dimensionless height of the flow domain. Finally, there is the Reynolds number Re. The latter two parameters are variable in experiment, and are used as the coordinates of a two-dimensional parameter space. The usual method of experimental investigation was to fix the aspect ratio at a chosen value and then vary the Reynolds number to observe changes in the nature of the flow. However, it was necessary in certain situations to vary the aspect ratio at a fixed value of Reynolds number in order to obtain an accurate measurement of certain critical transitions.

2.4 Flow visualization technique

Flow visualization is a technique which allows the qualitative nature of a flow field to be observed directly by eye. It has been used extensively in this study for investigating steady flow phenomena and the spatial structure of time-dependent flows. The technique involves the distribution in the fluid of a small quantity of particles which move with the fluid as it flows. These particles should ideally have the same density as the surrounding fluid so that they follow the flow exactly and do not experience any net buoyancy effects. In addition, the particles themselves should not alter the nature of the flow. This is achieved by using particles whose size is much less than the smallest structure in the flow, and by working with minimum concentrations.

Two flow visualization materials have been used separately in the work reported in this thesis. One is *Mearlmaid AA* natural pearl essence and the other is *Superpearl 100* mica/titanium dioxide flakes. Both are made up of tiny anisotropic platelets which are essentially neutrally buoyant in the working fluid. Concentrations of approximately 0.01% were used in the experiments. The platelets are individually aligned by the local action of shear in the flow, and reflect light in a way which depends on their orientation relative to the direction of observation. A detailed discussion of reflection in seeded flows is given by Savaş (1985), who considered a viscous fluid containing ellipsoidal particles and derived a probability density function for their orientation in a given flow field.

The flow is illuminated by projecting a narrow slit of light through the fluid. This allows the structure of three-dimensional flows to be viewed in two-dimensional cross-section. Such a representation is ideal for looking at Taylor vortex flows generally, since the secondary motion in each Taylor cell is perpendicular to the main rotating flow. Thus if the light is in a vertical plane, the cellular structure is seen very clearly.

2.5 Laser Doppler velocimetry technique

In addition to flow visualization, the technique of *laser Doppler velocimetry* (LDV) was used to investigate flow phenomena. Whereas flow visualization results in qualitative information about spatial aspect of the flow, LDV yields a local measurement with quantitative results. These are in the form of real-time values of one of the velocity components in the flow. As such, LDV is an ideal tool for investigating time-dependent flow fields. A full discussion of the laser Doppler technique is given by Drain (1980). We will restrict ourselves here to the more important principles of operation.

Two equally intense beams of laser light are focussed to an intersection within the fluid. This intersection occurs at the Gaussian waists of the two beams, and defines a small region known as the *measuring volume.* Interference fringes are formed in the measuring volume, and the motion of a solid particle through these fringes causes light to be scattered with an associated Doppler beat frequency which is directly proportional to the velocity component of the particle normal to the fringes. The frequency of the scattered light is independent of the direction of scattering.

The LDV system which was used in the present study has a 2 mW He-Ne laser as its source. The emitted beam is directed into a beam-splitter to produce two beams of equal intensity. Both beams then pass through Bragg cells which shift the frequency of the beams to give a relative difference in frequency of 100 kHz. This

has the effect of producing a moving interference pattern in the measuring volume, allowing the direction of scattering particles through the fringes to be determined unambiguously. The particular particles which were used are latex spheres with an average diameter of 6.4 μm. These are distributed uniformly in the fluid by the action of an ultrasonic bath prior to the fluid being poured into the flow rig.

The alignment of the beams was such that measurements were made of the radial velocity component of the flow. A photomultiplier was used to detect the light scattered from the measuring volume in the forward direction, and the Doppler frequency was transformed into a voltage by a phase-locked loop circuit. The fact that the frequency of the scattered light is independent of the direction of scattering means that the positioning of the photomultiplier was not critical. In practice, it was orientated so as to produce the maximum response from the processing electronics.

2.6 Computer control and data acquisition

The output voltage from the phase-locked loop circuit was fed through a low-pass filter with a cut-off frequency of 5 Hz. This value was chosen on the basis that there are no significant components in the signal above this frequency. The filtered signal was then amplified and level-shifted before being displayed on the screen of an oscilloscope. In this way, the variation with time of the radial velocity component of the flow through the measuring volume was viewed as a continuous time-series. A *Masscomp 5600* computer with integral 12-bit analogue-to-digital converters was used to sample the velocity time-series, and a range of standard signal processing techniques were used to analyse recorded data. These include calculation of the power spectrum of the signal, and phase-space reconstruction using the method of singular value decomposition as developed by Broomhead & King (1986).

In the initial experiments of this study, variation of the Reynolds number was performed by manual adjustments of the signal generator supplying the stepping motor of the flow rig. However, in the latter stages a computer was used to obtain more exacting control over the setting of the Reynolds number. The system which was used is essentially the same as the one documented by Price (1991), with a number of minor alterations. It is built around an Atari 1040 ST microcomputer. The computer is linked to a Yamaha TX81Z synthesizer which acts as a variable frequency signal generator for the stepping motor. The output extends from 16 Hz to 16 kHz, with a constant resolution of just under 0.1% over the full range. The stability of the synthesizer was found to be better than 0.01% for even the longest

time-scales involved in the experiments.

The use of the synthesizer as a controllable oscillator allowed the computer to remain free for other tasks. An external analogue-to-digital converter with 8-bit resolution was used to sample the output from the LDV system, and the discretized time-series was displayed on the Atari screen as on an oscilloscope. This allowed recordings to be made of the response of the flow to variation of the Reynolds number between an initial and a final value. Such parameter sweeps are extremely useful in locating bifurcation points in parameter space, subject to sufficient time being allowed for the system to settle between parameter changes. The Reynolds number was incremented typically by steps of the order of 0.1%, with a time corresponding to approximately five cylinder rotations being allowed between each step. This allowed measurements to be made which were repeatable.

Another use of the computer was in controlling the position of the vertical lift which supported the flow rig during an experiment. By raising and lowering the lift, the vertical position of the LDV measuring volume in the flow could be varied. This allowed radial velocity profiles of the cellular flow to be recorded and stored for subsequent reference.

CHAPTER THREE

Steady flows in a square Taylor-Couette system

We are concerned in this chapter with the steady flows which exist in the Taylor-Couette variant where the outer cylinder has a square cross-section. The discussion begins with a consideration of the two-dimensional flow in such a system. This is then used as the basis for understanding the nature of the three-dimensional flow equivalent to Taylor vortex flow. The specific regime which is of interest is when the annulus is sufficiently short that a single Taylor cell is formed. There is then a copy of the bifurcation sequence proposed by Benjamin & Mullin (1981) for the single cell in the standard system. Experimental results are then presented which show that a similar sequence exists in the square system. Finally, there is a discussion of the similarities and differences between the behaviour in the two systems.

3.1 Two-dimensional flow

Two-dimensional flow exists in cylinders which are considered to be infinitely long so that all properties of the flow are independent of translation along the vertical axis. In addition, it is assumed that there is no component of flow in this direction. Thus the problem reduces to one of determining the motion in a plane, perpendicular to the vertical axis, with the appropriate boundary conditions applied at the inner and outer walls.

The two-dimensional flow between concentric circular cylinders is known as *circular Couette flow.* The derivation of this solution from the Navier-Stokes equations is now a standard exercise (see Tritton (1988), for example), and is facilitated by the continuous azimuthal symmetry of the domain. However, when the cross-section of the outer cylinder is square rather than circular, there is no continuous azimuthal symmetry group to call upon. The flow field can now be expected to depend on both spatial coordinates. This fact greatly increases the complexity of any analytical approach.

The problem may be tackled instead using numerical techniques. Lewis (1979) considered the problem of solving for steady two-dimensional flow in the geometry under consideration. This was achieved using a finite-difference scheme applied to a nonuniform cartesian grid fitted to the flow domain. Lewis obtained solutions for a range of *clearance ratios* which he defined as the ratio of the inner cylinder diameter to the length of side of the outer cylinder. Results were obtained for a

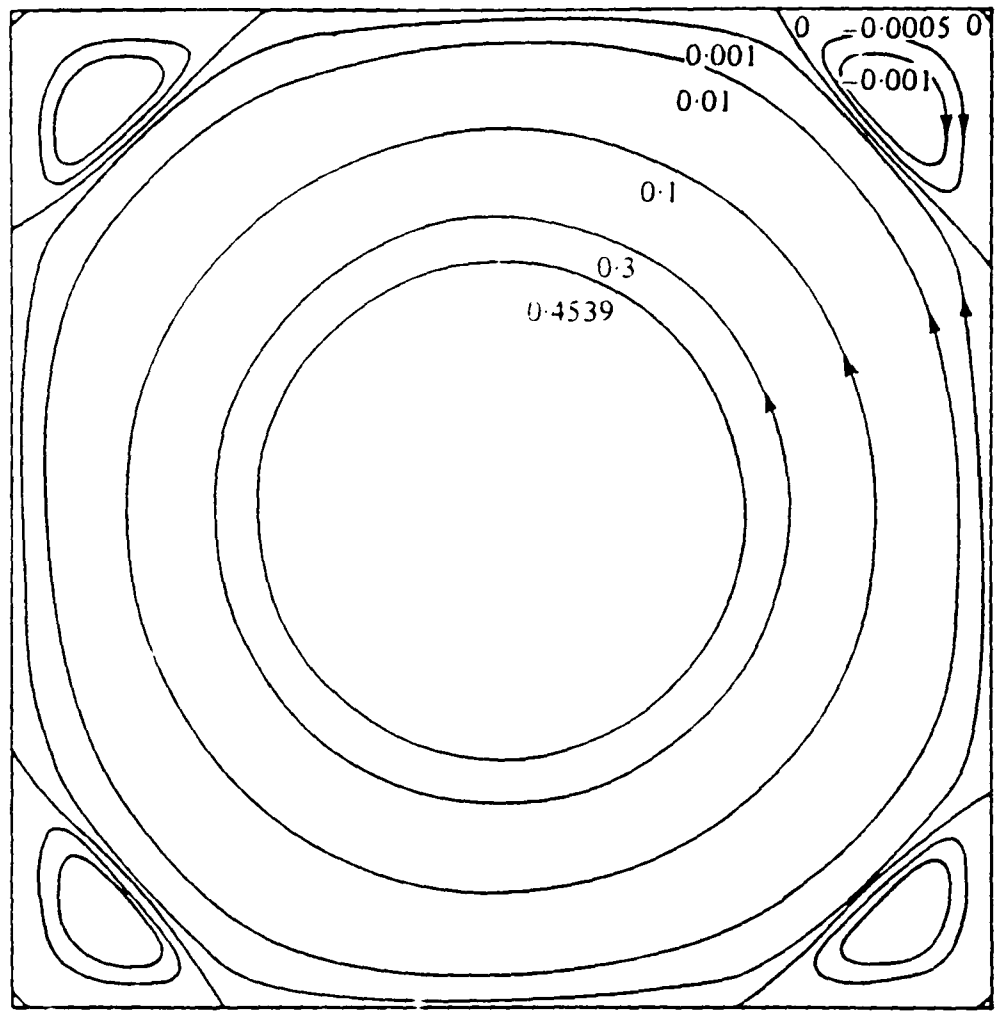

Figure 3.1 : Numerical solution for two-dimensional flow between a rotating cylinder and a square container at $Re = 1$. From *Lewis (1979)*.

clearance ratio of 0.5, which is the value used in the present study. An example of the flow field which was calculated by Lewis for the Reynolds number $Re = 1$ is shown in figure 3.1. Close to the inner cylinder, the streamlines are essentially circular. However, as the distance from the inner cylinder increases the streamlines tend towards the shape of the outer boundary. In each corner of the flow domain there exists a small recirculation region. This corner eddy is the first of the infinite sequence of rapidly decaying eddies identified by Moffat (1964) for flow near a sharp corner. Lewis showed that the effect of increasing the Reynolds number was to increase both the size and the strength of the corner circulations relative to the main flow. Nevertheless, the recirculations remain very weak features of the overall flow, even up to a value of $Re = 1400$.

Hellou & Coutanceau (1992) have tackled the related problem of purely viscous two-dimensional flow induced by a rotating cylinder in the centre of a rectangular domain. The analytical complexity is reduced to an extent by restricting attention to *creeping flow*, where the Reynolds number is zero. This is achieved by eliminating inertial terms from the governing equations of motion. Under these conditions, the two-dimensional flow is described by a streamfunction ψ satisfying the equation $\nabla^4\psi = 0$. Hellou & Coutanceau proceed to a truncated series solution of this equation in polar coordinates, with a numerical optimisation method applied to the boundary condition on the rectangle. The solutions obtained over a wide range of aspect ratio of the outer boundary show excellent agreement with photographs of experimental flow patterns. In particular, Hellou & Coutanceau consider the case of unit aspect ratio, that is with a square outer boundary. The results for this

configuration are virtually identical to those obtained by Lewis (1979) for $Re = 1$.

An example of the two-dimensional flow in the apparatus used for the present study is shown in figure 3.2. Glycerol was seeded with a small quantity of flow visualization material as described in Chapter 2. It was poured into the flow rig to form a layer on top of the transparent bottom approximately 2 cm deep. Flow was driven by slow rotation of the inner cylinder and was illuminated by a thin horizontal sheet of light through the centre of the fluid. The motion was recorded using an Olympus OM-4 Ti camera with Fujichrome 64T colour slide film. Exposure times of approximately 30 seconds were required to capture the paths of individual particles. The flow visualisation photograph shown in figure 3.2 was taken at a Reynolds number approximately equal to one, and is in excellent agreement with the numerical results of Lewis (1979) and the analytical and experimental results of Hellou & Coutanceau (1992). In addition, it is clear that the two-dimensional flow shares the same $\mathbb{Z}_4$ symmetry group as the flow domain. This fact is used by both Lewis and Hellou & Coutanceau to increase the efficiency of their respective techniques.

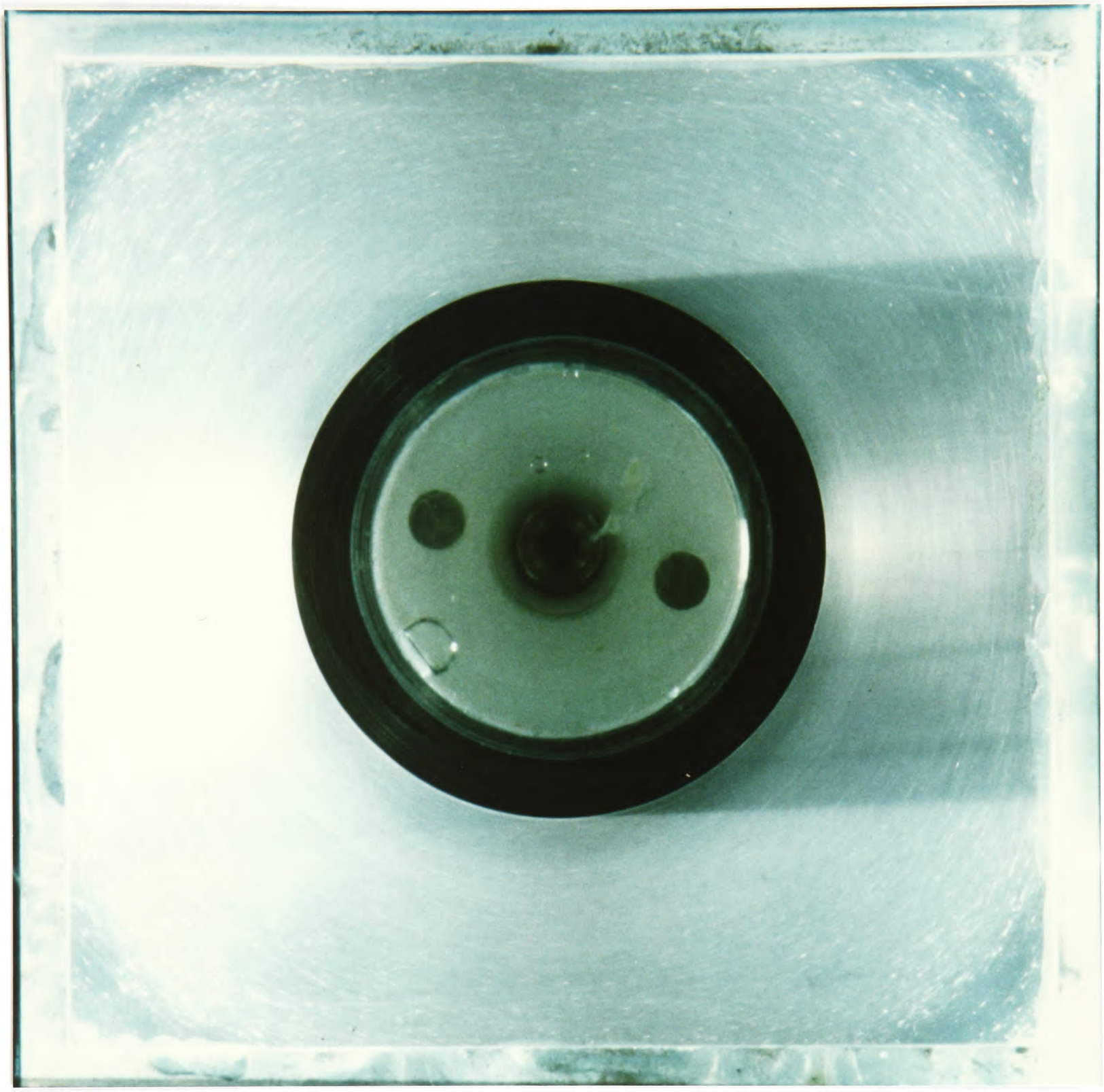

Figure 3.2 : Photograph of two-dimensional flow in the square Taylor-Couette system at $Re \approx 1$.

3.2 Three-dimensional flow

We will now use the results for the two-dimensional flow to help interpret the structure of the three-dimensional flows which exist in the square Taylor-Couette system. It was shown in the Introduction that there is a transition to cellular motion in the square system when the inner cylinder rotates at a sufficiently high speed. This can be understood from the fact that Rayleigh's criterion (see Chandrasekhar (1961), for example) for the stability of rotating inviscid flow is violated in the main region of the two-dimensional flow. However, unlike the Taylor vortex flow in the standard system, the cellular flow in the square system cannot be axisymmetric because of the $\mathbb{Z}_4$ azimuthal symmetry of the domain. Instead, we must expect some variation in the nature of the cells around the annulus related to the recirculations which exist in the corners of the system.

It can be seen from figures 3.1 and 3.2 that the corner recirculations in the two-dimensional case are relatively small features of the overall flow. This makes a direct observation of three-dimensional effects in these regions very difficult in practice. However, it was the case that the measuring volume of a laser Doppler system could be located within one of the corner flows. Velocity profiles which were taken across the vertical extent of the system showed there to be a periodic structure in this region, with a spacing which is equal to that of main cellular flow. Thus it is possible to deduce that the cellular structure in the square system is of the type shown schematically in figure 3.3. The secondary flow in the narrow gaps of the annulus is exactly that which is found in the standard system. However, the cells

in the widest sections do not occupy the full width of the gap. Instead, the main Taylor vortex flow drives oblate secondary motion within the corner recirculations.

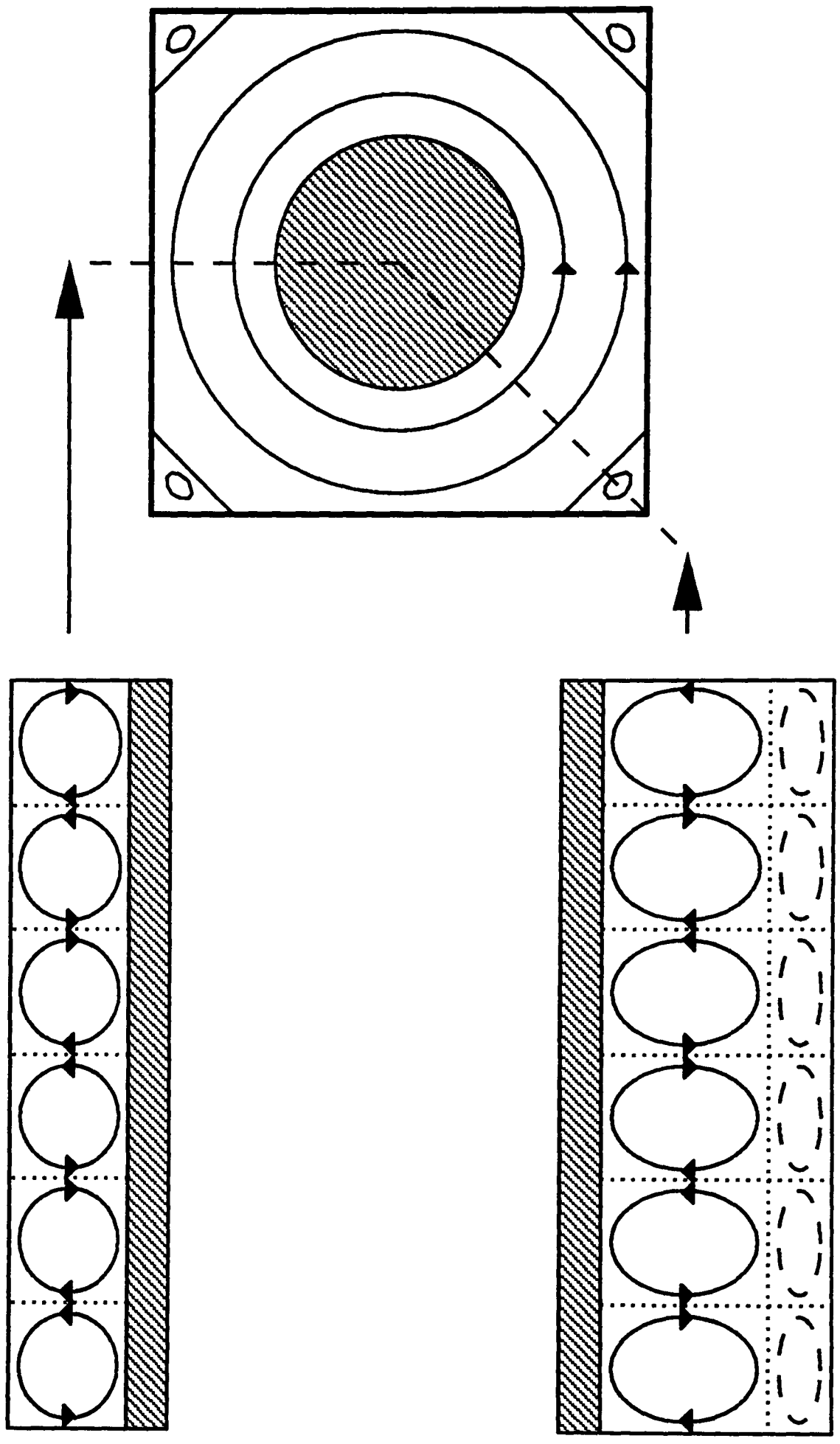

Figure 3.3 : The nature of steady Taylor vortex flow in the square system in both the narrowest and the widest gaps around the annulus.

3.3 Single-cell Taylor flow in the standard system

It was stressed in the Introduction that a proper understanding of observed behaviour in the Taylor-Couette system is only really possible if care is taken to limit the multiplicity of flows. Otherwise, a complicated structure must be untangled in which there is a plethora of interacting solutions. One approach by which the multiplicity can be reduced is to make the annulus very short so that the flow typically consists of a single Taylor vortex. This is the approach which is adopted for the present study of behaviour in the square Taylor-Couette system. Therefore we will consider first the steady bifurcation structure associated with the single-cell flow in the standard system before proceeding to present results for the square system.

Steady flow at very small aspect ratios in the standard Taylor-Couette system was first considered by Benjamin & Mullin (1981) as part of a wider study of anomalous modes. It was found that unlike all other flows with an odd number of cells, there is a range of aspect ratio over which the single-cell solution remains connected to the primary mode. Benjamin & Mullin applied the model due to Schaeffer (1980) to the case where the bifurcation from Couette flow is to flow with a single Taylor cell. This then led to a proposed sequence of bifurcations in the real system which took the single-cell mode from a connected to a disconnected solution with increasing aspect ratio. The sequence was confirmed experimentally by Benjamin & Mullin, and subsequently also by Cliffe (1983) using numerical techniques.

The steady bifurcation sequence for single-cell flow in the standard system when the annulus length is of the order of the gap between the cylinders is shown in figure 3.4. In each case, the primary mode corresponds to a flow with two Taylor cells which is symmetric about the midplane of the annulus. This flow exists from very small values of the Reynolds number due to the strong three-dimensional effects of the fixed ends. The bifurcations which subsequently break the $\mathbb{Z}_2$ symmetry are shown in their connected forms in figure 3.4 for the sake of simplicity. It should be stressed, however, that there will always be disconnection of one or other of the asymmetric branches due to the presence of unavoidable imperfections.

In figure 3.4a, the first feature is that of a supercritical symmetry-breaking bifurcation. The two-cell flow becomes unstable at this point, and the new stable branches correspond to asymmetric flow where one cell grows to fill the domain while the other cell is reduced to a small corner circulation. A second feature is another pitchfork bifurcation at a higher value of Reynolds number. Here the symmetric solution is restabilized by the creation of two unstable asymmetric solutions. As Γ is increased, the two pitchfork bifurcations approach each other. This is accompanied by a change in the first pitchfork from supercritical to subcritical, as shown in figure 3.4b. At a critical value of aspect ratio, the two bifurcation points coalesce, resulting in the disconnection of the asymmetric solutions and the full stabilization of the symmetric branch at larger values of Γ. The corresponding bifurcation diagram is shown in figure 3.4c.

The validity of this bifurcation sequence was first established by Benjamin &

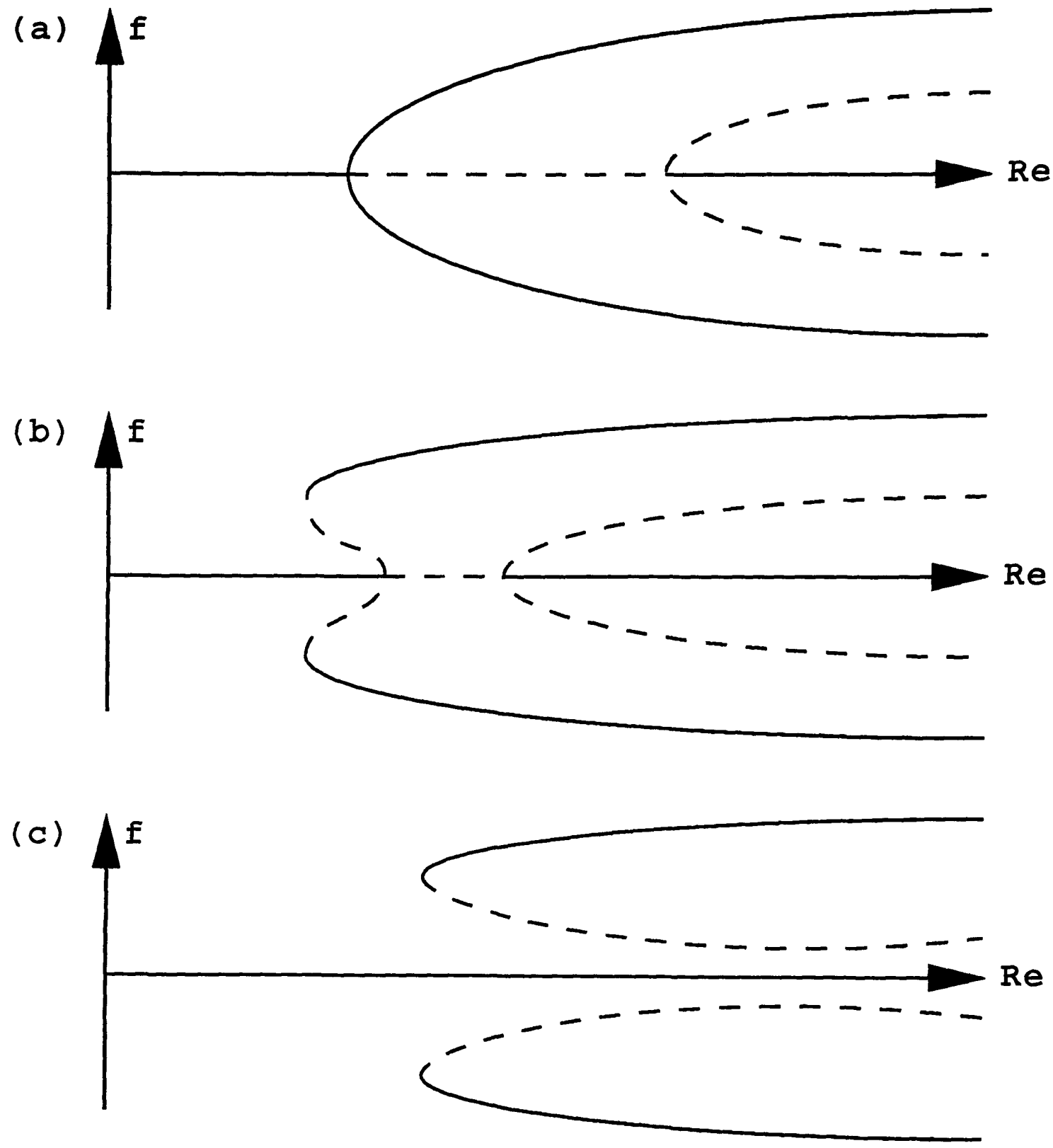

Figure 3.4 : Bifurcation sequence for single-cell flow with increasing aspect ratio. The primary solution branch represents a symmetric two-cell flow. Bifurcations from this solution are to asymmetric single-cell flow.

Mullin (1981) with the experimental identification of the initial symmetry-breaking, the restabilized symmetric two-cell flow, the small hysteresis in the primary pitch-fork bifurcation, and the limit points that terminate the disconnected asymmetric branches corresponding to single-cell flow. A significant contribution of Cliffe (1983) was the direct calculation of the unstable solution branches as well as the stable ones. In this way, it was possible to confirm the picture presented in figure 3.4

3.4 Experimental results from the square system

We now wish to investigate the robustness of the bifurcation sequence which is found in the standard Taylor-Couette system and which was discussed in section 3.3. This consists of an experimental investigation of the effects of the change of the outer boundary on the steady solution set at small aspect ratios.

The investigation of was carried out using flow visualisation as described in Chapter 2. The first result is a sequence of photographs showing the symmetry-breaking phenomenon in the square Taylor-Couette system at an aspect ratio $\Gamma = 1.5$. In figure 3.5a, the Reynolds number is such that the flow consists of two somewhat compressed Taylor cells which are symmetric about the midplane of the annulus. On increasing the Reynolds number, one of the cells begins to grow at the expense of the other. This symmetry-broken state is shown in figure 3.5b. Finally, with further increase of Re, the dominant cell grows to fill the majority of the annulus as shown in figure 3.5c. The other cell is reduced to the role of a small corner circulation. It is also possible to observe the other single-cell flow by sudden increase of the Reynolds number from the symmetric regime.

The next stage of the study was to measure the critical Reynolds numbers for the qualitative changes which occur in the flow. For this purpose, the illuminated region of the flow was observed through a travelling telescope with a cross-hair eye piece. In order to measure the critical values of Reynolds number associated with symmetry-breaking in the two-cell flow, the horizontal cross-hair was positioned so

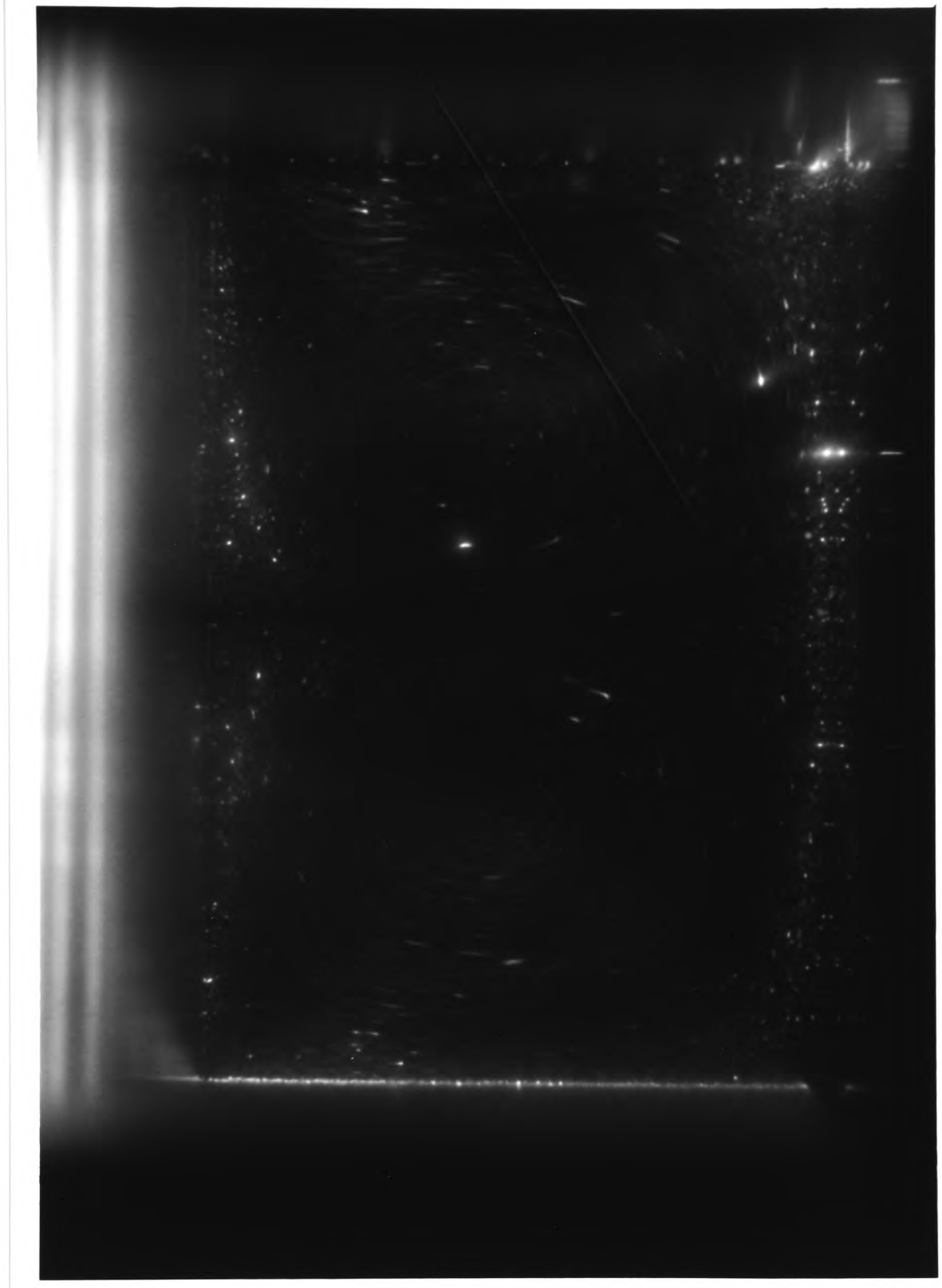

Figure 3.5 : (a) Symmetric two-cell flow in the square system at $\Gamma = 1.5$, $Re = 95.43$.

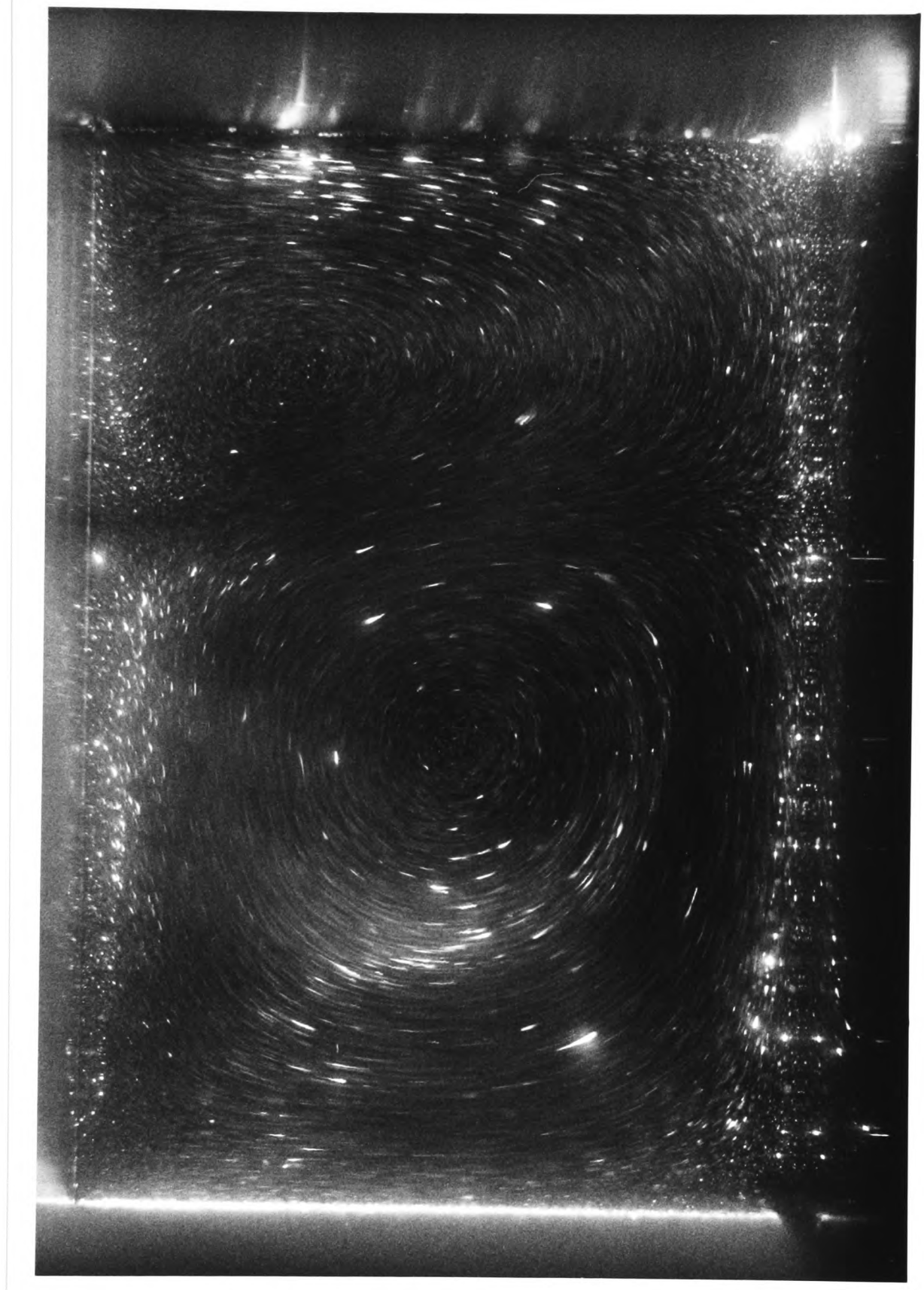

Figure 3.5 : (b) Asymmetric two-cell flow in the square system at $\Gamma = 1.5$, $Re = 100.38$.

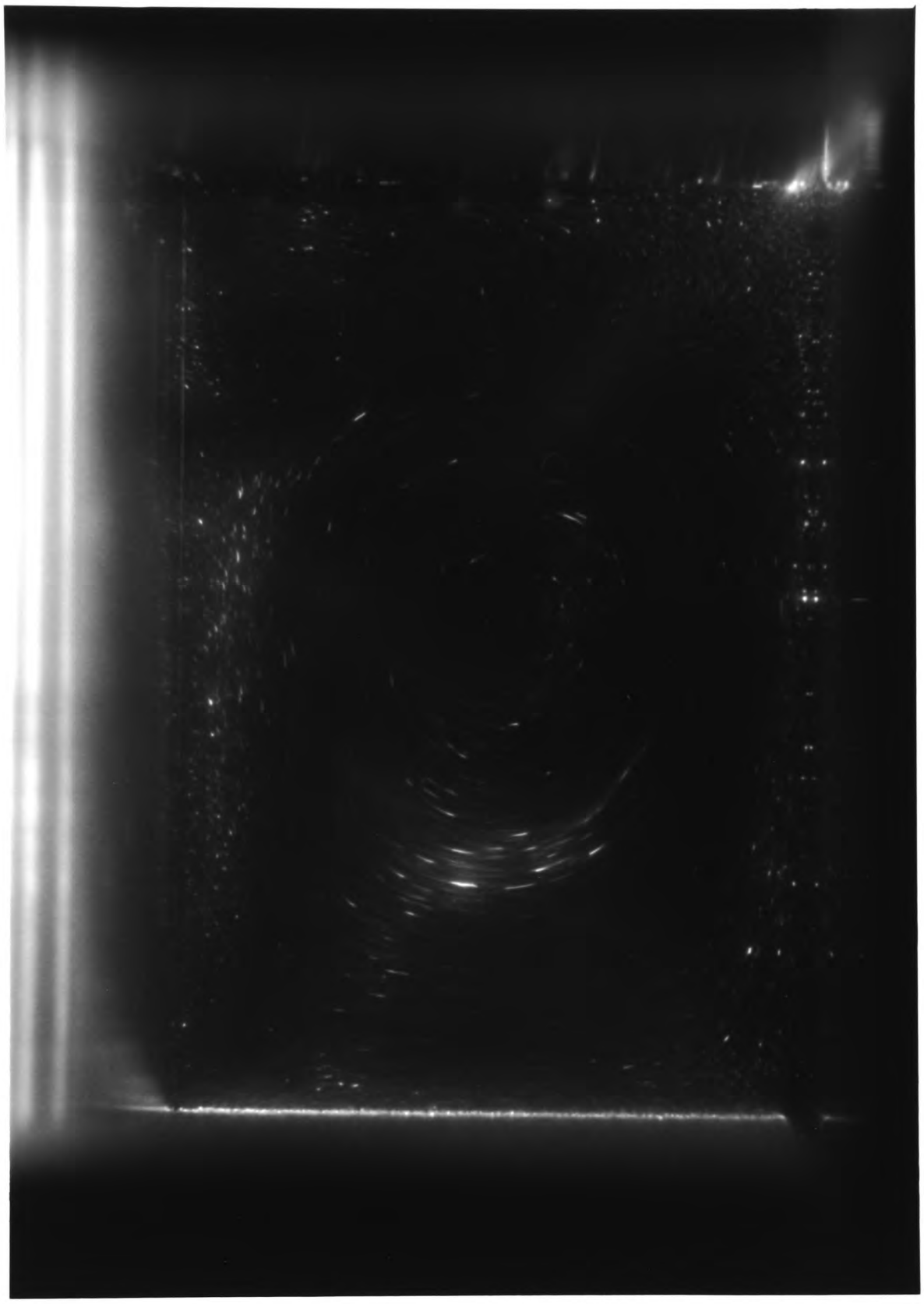

Figure 3.5 : (c) Single-cell flow in the square system at $\Gamma = 1.5$, $Re = 121.12$.

that it coincided with the midplane of the flow domain.

A practical problem here is that the symmetry-breaking bifurcation is disconnected by unavoidable imperfections in the system. There is therefore no critical point at which the symmetry is broken, but rather a continuous transition from symmetric to asymmetric flow. However, since the extent of the disconnection is very small, it is possible to make use of the lower stability limit of the disconnected branch to obtain accurate experimental measurements.

In the experiments, the Reynolds number was increased suddenly so as to realise the single-cell flow corresponding to the disconnected branch of the pitchfork bifurcation. Once this had been achieved, the Reynolds number was gradually reduced until the lower limit of stability of the disconnected solution was encountered. Although the collapse is a very subtle event, it can nevertheless be detected by an irreversible change in the direction of the vertical flow component at a representative point on the horizontal cross-hair. The procedure was repeated several times in order to obtain successively more accurate measurements of the critical Reynolds number, which was ultimately limited to an accuracy of approximately 0.1% by the stability of the oscillator controlling the speed of the rotating cylinder. The measurement of the critical Reynolds numbers associated with the lower stability limits of the secondary two-cell flow and the secondary single-cell flow was performed using a similar refinement technique, but without the requirement to locate the symmetry plane since the transitions were of a much more definite nature.

A factor which had to be taken into account when carrying out the experimental measurements was the rate at which transient flow decayed when changes were made in the Reynolds number. It was observed that this time varied significantly depending on whether or not the system was close to one or more bifurcation points. For the majority of measurements, the decay time was found to be much less than the viscous diffusion time τ_v. Here, τ_v is approximately 43 seconds for the minimum gap between the two cylinders. However, for measurements taken when the system was close to the coalescence of the two pitchfork bifurcations, transient times of up to 10^4 seconds were recorded. The effect is to cause the system to remain for a long time in the vicinity of the unstable symmetric solution before collapsing to the final asymmetric state. Under these conditions, it was only possible to achieve repeatable results by allowing times in excess of 10^4 seconds between the small changes of Reynolds number required to locate bifurcation points accurately.

The above observations are consistent with results which were obtained by Pfister *et al.* (1988) for the decay of transients in the standard Taylor-Couette system. Time constants were measured experimentally by Pfister *et al.* for several values of the Reynolds number in the interval separating the two pitchfork bifurcations for the sequence equivalent to that shown in figure 3.4b. It was found that the time constant has a parabolic variation across the interval, with a minimum value approximately equidistant from the two bifurcation points.

The experimentally determined loci of the three different types of bifurcation are shown in figure 3.6 as a plot in the two-dimensional parameter space defined

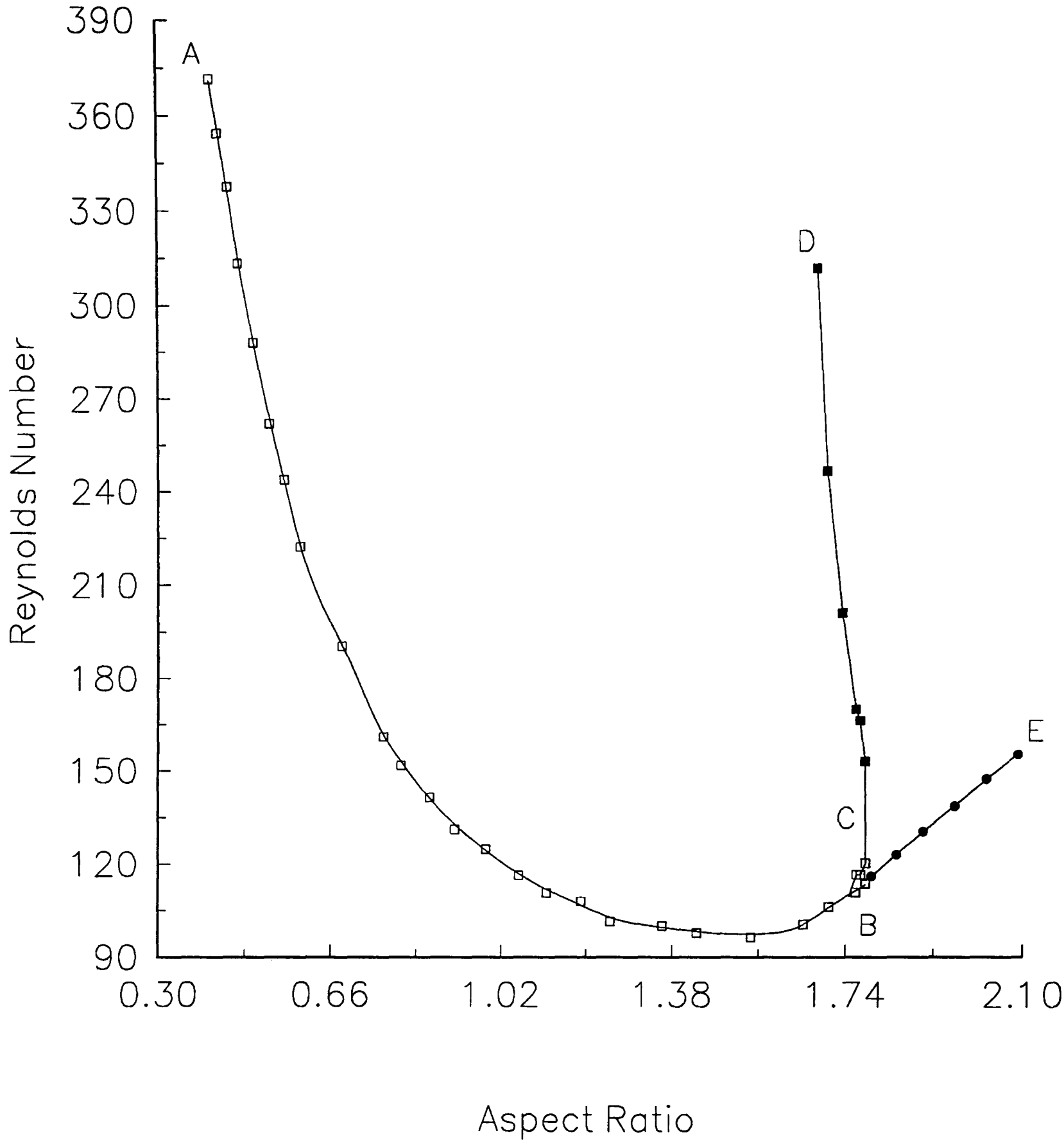

Figure 3.6 : Experimentally determined bifurcation set in the square system. AB (□) is locus of primary pitchfork bifurcations to single-cell flow. CD (■) is locus of secondary pitchforks which restabilize the two-cell flow. BE (•) is locus of saddle-node bifurcations which mark the lower stability limit of the disconnected single-cell flow. Lines are drawn purely to guide the eye.

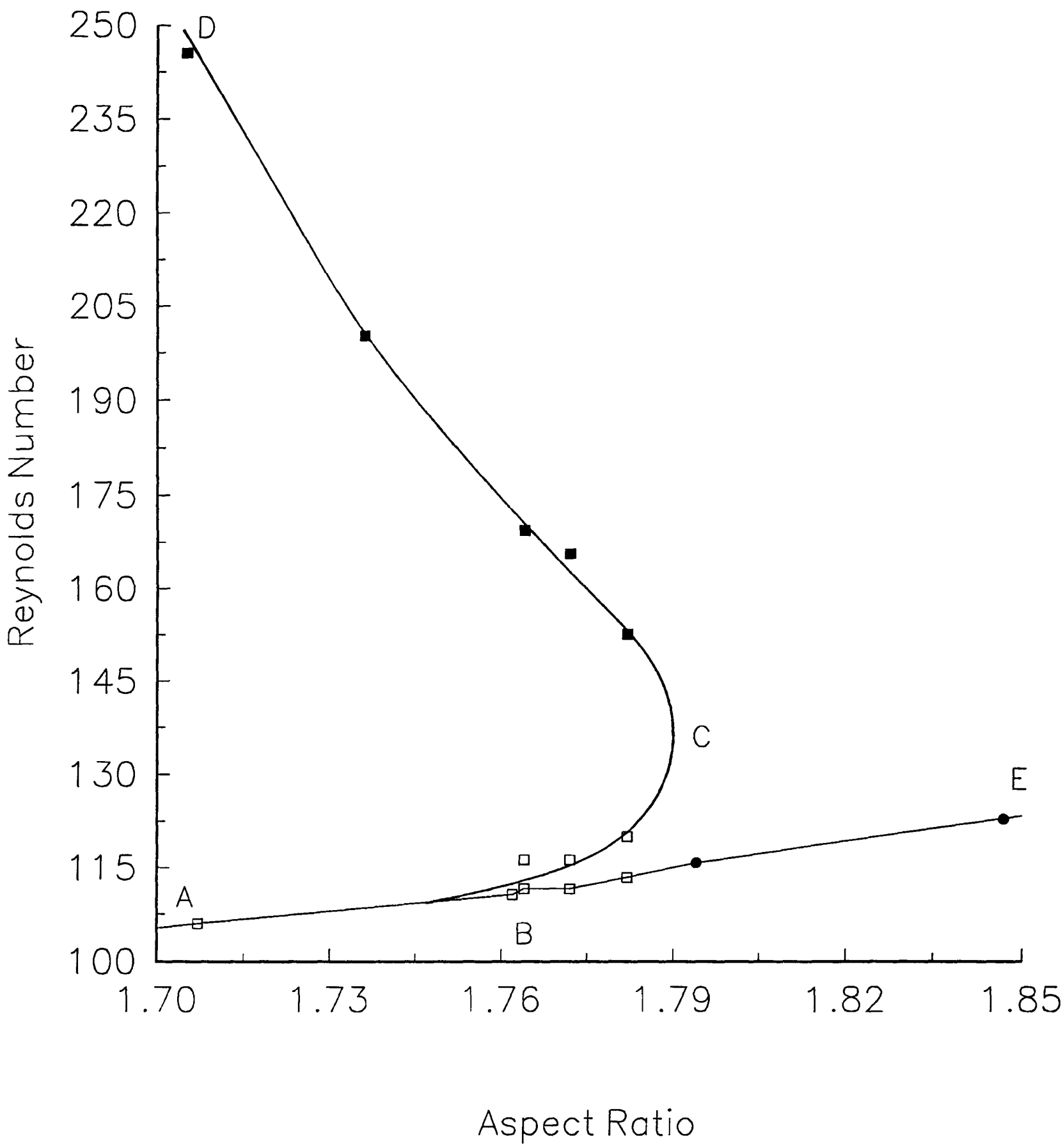

Figure 3.7 : Expanded view of figure 3.6 around point C showing hysteresis in primary symmetry-breaking bifurcation.

by aspect ratio and Reynolds number. The results show that the bifurcation sequence found in the standard system by Benjamin & Mullin (1981) also exists for this variant with a square outer boundary. The locus AB marks the path of the primary symmetry-breaking bifurcation resulting in single-cell flow. The locus CD is a similar path for the subcritical pitchfork bifurcation that restabilizes the symmetric two-cell flow. As the aspect ratio Γ is increased, these two lines of critical points converge. The primary pitchfork bifurcation goes through a quartic point and develops hysteresis, just as predicted by Benjamin & Mullin. This results in the splitting of the symmetry-breaking locus at point B in figure 3.6. The two subcritical points connect at point C, resulting in the full stabilization of the symmetric solution branch. The disconnected single-cell flow has a lower limit of stability represented by a saddle-node bifurcation whose locus is the line BE. An expanded view of the parameter space around point C is presented in figure 3.7, where the development of hysteresis and the subsequent disconnection of the single-cell can be seen more clearly.

3.5 Comparison with the standard system

We have seen in section 3.4 that there is strong qualitative similarity between the steady-state bifurcation sequences found at small aspect ratios in Taylor-Couette systems with circular and square outer cylinders. However, it is also possible to compare some quantitative aspects of results obtained from the two systems.

In order to do this, we must give consideration to the parameter equivalent to the radius ratio in the standard system. The definition adopted in this study of a clearance ratio equal to the diameter of the inner cylinder divided by the length of side of the outer cylinder follows Snyder (1968). He investigated the flow in an apparatus with a clearance ratio which varied from 0.652 at the narrowest part of the gap to 0.461 in the corner. Specifically, Snyder measured the Reynolds number at which Taylor vortices were seen to appear in the flow.

The results of Cliffe *et al.* (1992) show that the Reynolds number for the onset of cells in the standard Taylor-Couette system is independent of aspect ratio in practice for $\Gamma \gtrsim 4$, and depends only on the radius ratio of the system. Thus it is possible to compare the value of Reynolds number obtained from the square Taylor-Couette system with similar measurements for the onset of cells in standard systems with various radius ratios. The value measured by Snyder corresponds to a radius ratio of 0.67 if the outer boundary had been circular, and within the limits of error this value equates to the clearance ratio based on the minimum gap between the inner circular cylinder and the outer square cylinder.

Further justification for this choice can be found by considering the nature of the two-dimensional flow field as shown in figures 3.1 and 3.2. The radial extent of the main flow is essentially determined by the minimum gap between the inner and outer cylinders. A correspondence can therefore be considered with the standard Taylor-Couette geometry that has an outer cylinder diameter equal to the length of side of the present square cylinder.

The symmetry-breaking bifurcation set for a standard system with radius ratio $\eta = 0.5$ has been determined experimentally and numerically by Pfister *et al.* (1988). It is therefore possible to make a direct quantitative comparison of the results of measurements of bifurcation points, as long as the defining length scale is taken as the gap (the minimum gap in the case of the square configuration) between inner and outer cylinders. An overlay of the results of the present study with those of Pfister *et al.* is shown in figure 3.8. It can been seen that the two lines of bifurcations become quantitatively very similar as the aspect ratio is decreased below $\Gamma = 1$.

An explanation of this convergence phenomenon can be found by considering the nature of the three-dimensional flow that is driven by the inner cylinder at very small aspect ratios. The frictional effect of the stationary ends on the flow is now very strong, with the result that the only significant motion is confined to fluid close to the rotating cylinder. The form of the two-cell flow at very small aspect ratios for both the standard and the modified system is shown schematically in figure 3.9a. The two Taylor cells are confined to a region whose radial extent is approximately equal to the vertical spacing between the end plates. This symmetric flow undergoes

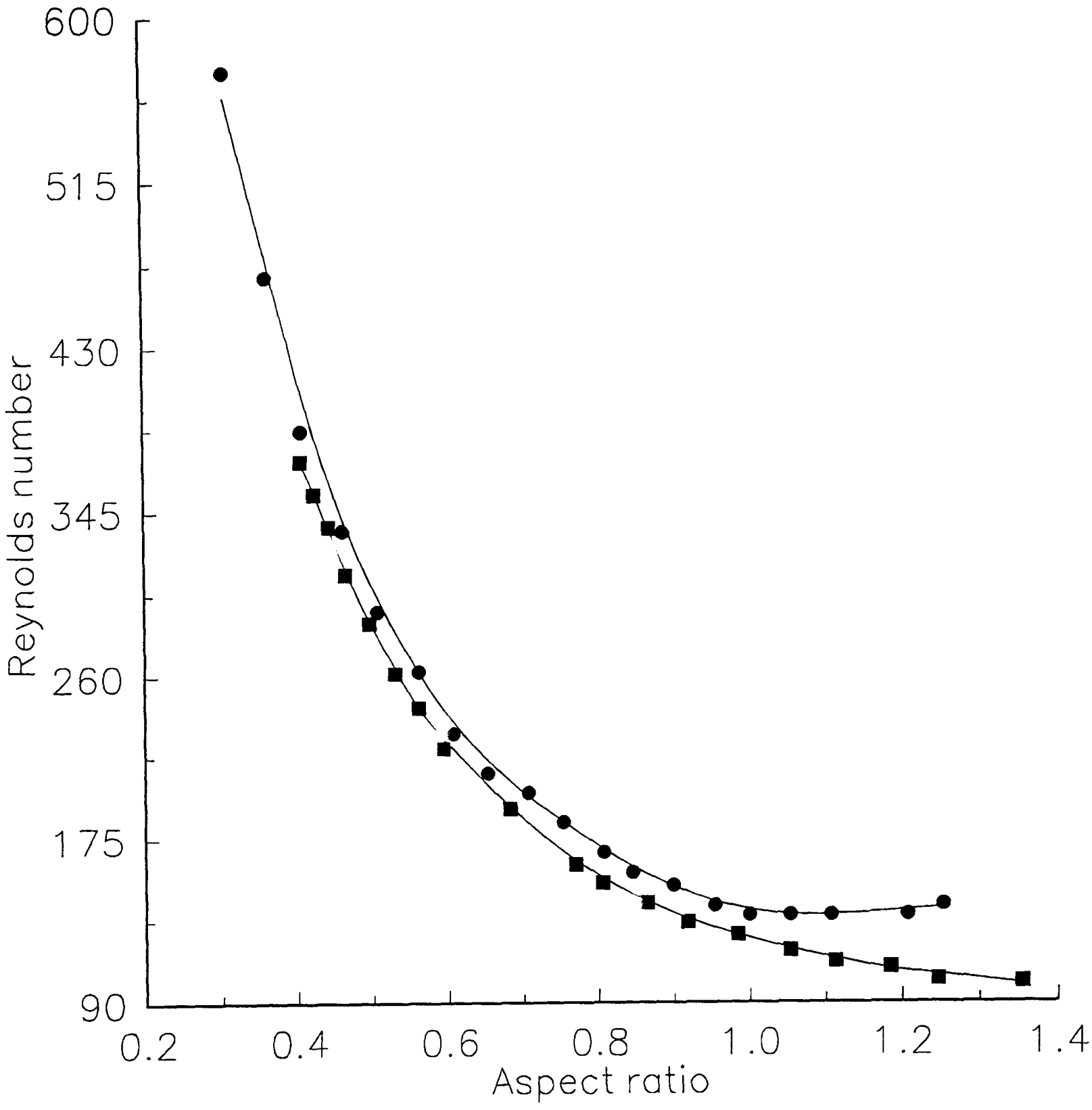

Figure 3.8 : Overlay of loci of symmetry-breaking bifurcations for the standard (●) and square (■) systems.

(a)

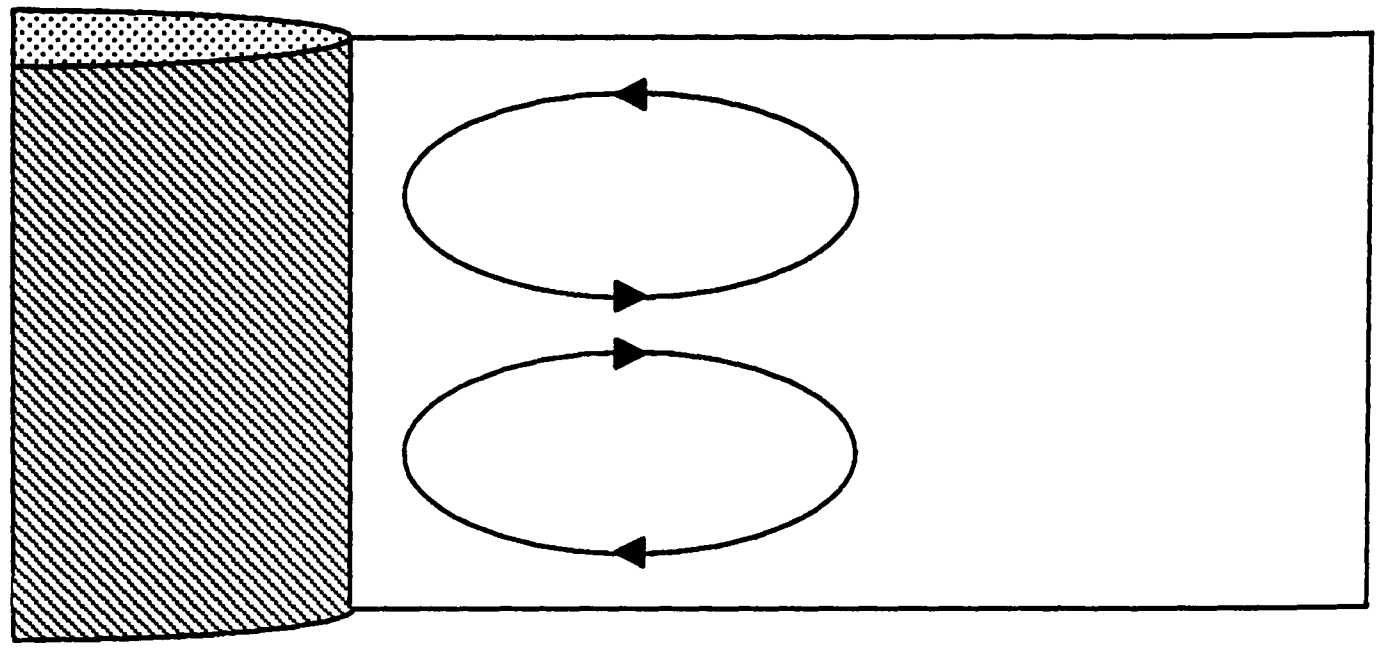

(b)

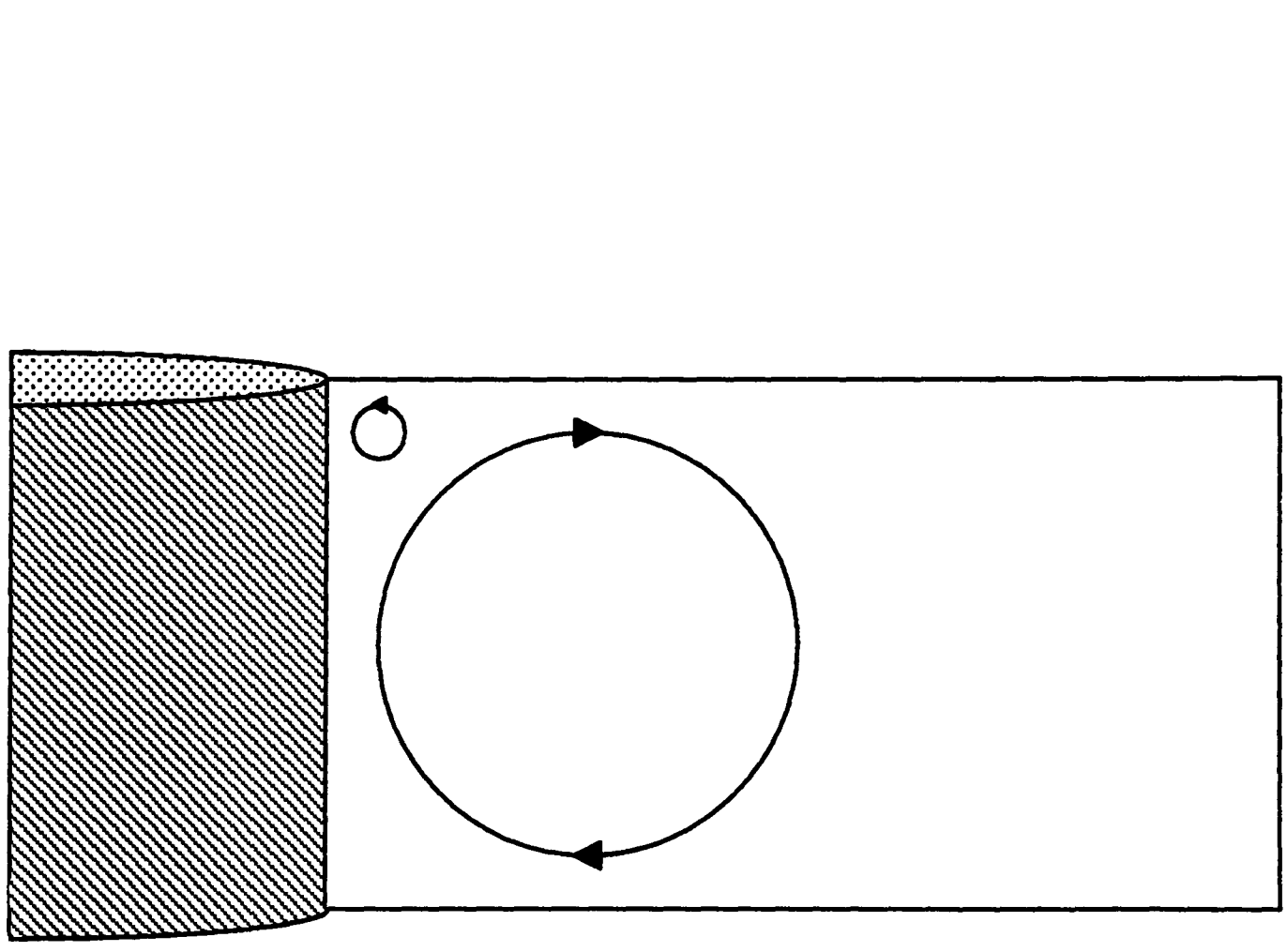

Figure 3.9 : Flows in both the standard and square systems at very small aspect ratio. (a) symmetric two-cell flow. (b) single-cell flow.

a symmetry-breaking bifurcation to a single-cell flow as shown in figure 3.9b. The single Taylor cell occupies the same region as was previously determined by the two-cell flow. A consequence of this restriction of cellular flow to the proximity of the inner cylinder is that the exact details of the shape of the outer boundary become less significant as the aspect ratio is decreased below the value of one. Thus it is possible to understand how two systems, one with a circular outer boundary and the other with a square outer boundary, can be practically indistinguishable through experimental measurement of the critical Reynolds number for symmetry-breaking.

However, the results of Pfister *et al.* (1988) also indicate that the argument given above cannot necessarily be extended to cover all other types of flow in the two systems at very small aspect ratios. A major contribution of Pfister *et al.* was the discovery in the standard system of a new symmetric two-cell flow which is stable for aspect ratios $\Gamma \lesssim 0.55$. This new flow, although similar in form to that which exists prior to the symmetry-breaking bifurcation, is a disconnected solution and has a lower limit of stability that is greater than the Reynolds number at which the primary two-cell flow loses stability. Pfister *et al.* were able to measure and calculate the lower stability limit of this new flow over a range of aspect ratio, and obtained very good agreement between experiment and computation.

Several attempts were made as part of the present study with a square outer boundary to locate a similar flow experimentally. A series of sudden starts and sudden increases of Reynolds number were performed at various aspect ratios less than one. However, no disconnected symmetric flows were located using these techniques.

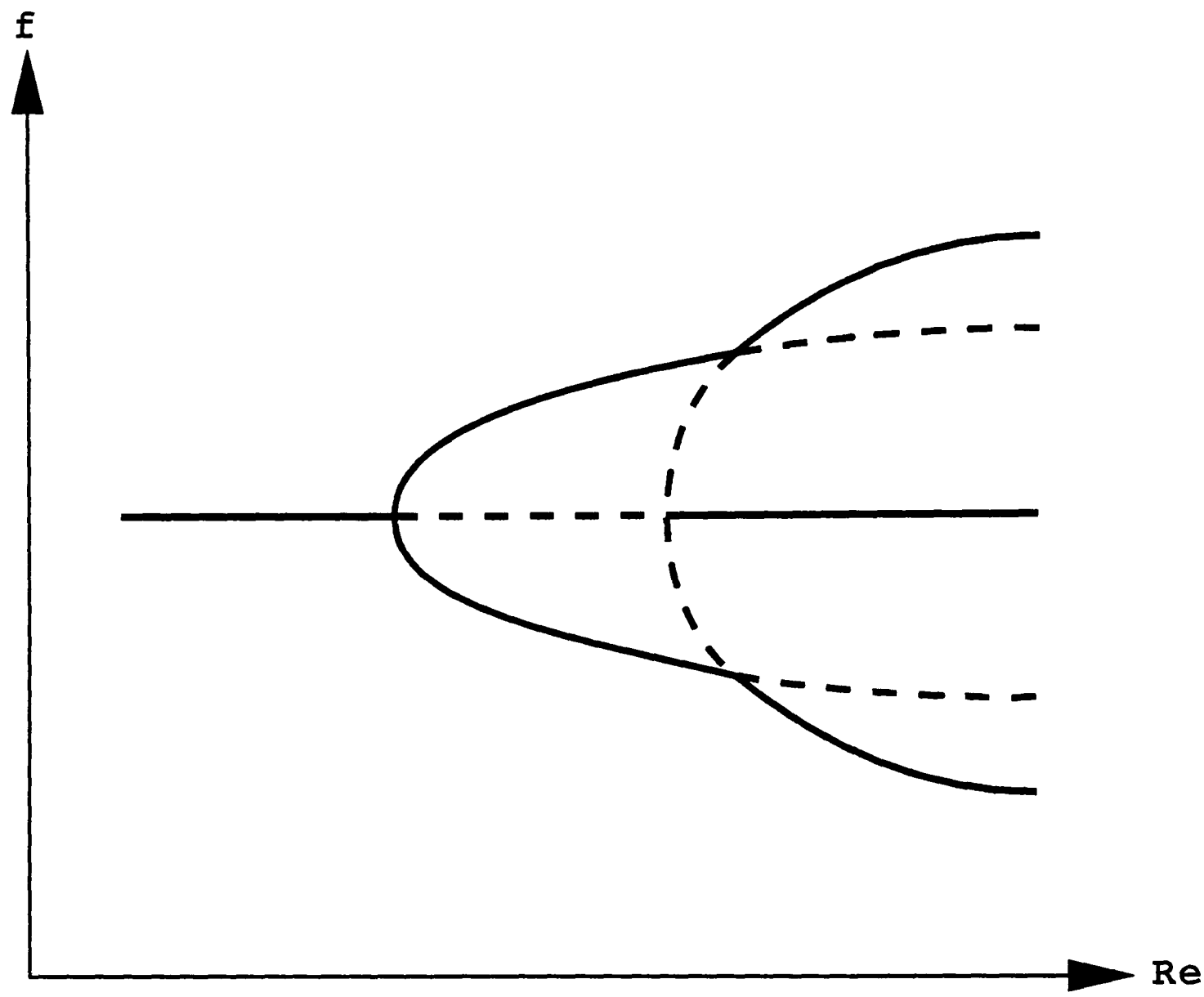

Figure 3.10 : Bifurcation sequence found by Pfister et al. (1991) at very small aspect ratios involving transcritical bifurcations.

A recent study by Pfister *et al.* (1991) in the standard system showed that at certain aspect ratios the unstable asymmetric solution branches which are created when the symmetric flow restabilizes go on to interact with the stable asymmetric solutions, giving rise to transcritical bifurcations. An example of the corresponding bifurcation diagram is shown in figure 3.10. The transcritical bifurcations are observed experimentally in plots of the vertical velocity component at a point midway between the horizontal ends with gradual increase of the Reynolds number. Although no such bifurcations were observed in the present study, there is no guarantee that they do exist over a small range of aspect ratio.

However, the results of Pfister *et al.* (1988) also show that the restabilized flow becomes time-dependent via a Hopf bifurcation at Reynolds numbers only marginally greater than the value associated with the lower stability limit of the steady flow. These two bifurcations coalesce to form a codimension-2 bifurcation at an aspect ratio $\Gamma \approx 0.55$, beyond which the new two-cell flow is unstable and therefore unobservable in experiment. It will be seen in Chapters 4 and 5 that the major effect of altering the geometry of the outer boundary is on the nature of time-dependent flows in the system. It is therefore supposed that the apparent absence of a stable secondary two-cell flow at very small aspect ratios is a result of a displacement of the line of Hopf bifurcations in parameter space. Given that the two-cell flow is unstable for aspect ratios greater than the value associated with the codimension-2 point, a shift of this point to extremely small values of aspect ratio would render the two-cell flow unobservable in practice. It appears that a resolution to the question of existence of the secondary two-cell flow in

the system with $\mathbb{Z}_4 \times \mathbb{Z}_2$ symmetry will only be achieved by the application of numerical bifurcation techniques to the problem at such a time when this becomes computationally viable.

3.6 Summary

The results presented in this chapter show that for the case of steady single-cell flow phenomena at least, the standard and the square Taylor-Couette problems have very similar solution structures. It was shown that the bifurcation sequence proposed by Benjamin & Mullin (1981) for the standard system also holds for the square system. It was argued that a direct quantitative comparison between the two systems is possible if the clearance ratio in the square system is based on the minimum separation between the cylinders. Thus it was found that the loci of primary symmetry-breaking bifurcations at aspect ratios less than one show strong quantitative similarity. This fact was attributed to the confined nature of the cellular flows in the two systems when the end-plates are closer together than the inner and outer cylinders.

Thus a framework of bifurcations of equilibrium solutions exists for the case of steady flows in a domain with discrete azimuthal symmetry. This framework is now built upon by extending the scope of the study to consider time-dependent flows. It is the role of low-dimensional dynamics in particular that is in question in Chapters 4 and 5, and whether it is possible to establish similar consistent solution sets as was the case for the steady flows.

CHAPTER FOUR

Time-dependent single-cell flows in the square Taylor-Couette system

In this chapter, we consider the nature of the basic time-dependent flows which develop from the steady single-cell flow that was discussed in Chapter 3. Experimental results are presented which show that the onset of time-dependence in the flows under investigation occurs via Hopf bifurcations to two qualitatively different singly-periodic modes. The selection of these modes is determined by the aspect ratio of the system, and results are presented which show a consistent bifurcation structure linking the two regimes. Finally, comparisons are made with certain qualitative and quantitative aspects of the time-dependent single-cell flows in the standard Taylor-Couette system.

4.1 Time-dependent flow for $\Gamma < 1$

We begin this section by recalling the description given in section 3.5 of the nature of the steady single-cell flow for aspect ratios less than one. When viewed in vertical cross-section, the cell is seen to be approximately circular with its centre close to the rotating inner cylinder. There is no discernible motion of the fluid in the outer region of the bounded domain. Although in principle such motion must exist, it must be very weak. Another point which is worth recalling is that the symmetry-breaking bifurcation which gives rise to the single-cell flow acts only on the $\mathbb{Z}_2$ symmetry group. The single Taylor cell still has the same $\mathbb{Z}_4$ symmetry property as the outer boundary. As such, the four corner circulations which were identified in Chapter 3 as being part of the underlying flow must still be present, although again they are too weak to be detected.

We will now consider the behaviour of single-cell flow at an aspect ratio $\Gamma = 0.5$ with increase of the Reynolds number. For the sake of consistency within the results, we choose to study the flow which corresponds to the connected solution branch of the symmetry-breaking bifurcation. However, identical features are found in the other single-cell flow which corresponds to the disconnected solution branch.

The symmetry-breaking bifurcation to single-cell flows is encountered at $Re \approx 300$ for the aspect ratio $\Gamma = 0.5$. Initially, the only effect of further increase of Re is to intensify the secondary circulation which we use to define the Taylor cell. However, there is a fundamental qualitative alteration in the nature of the flow at

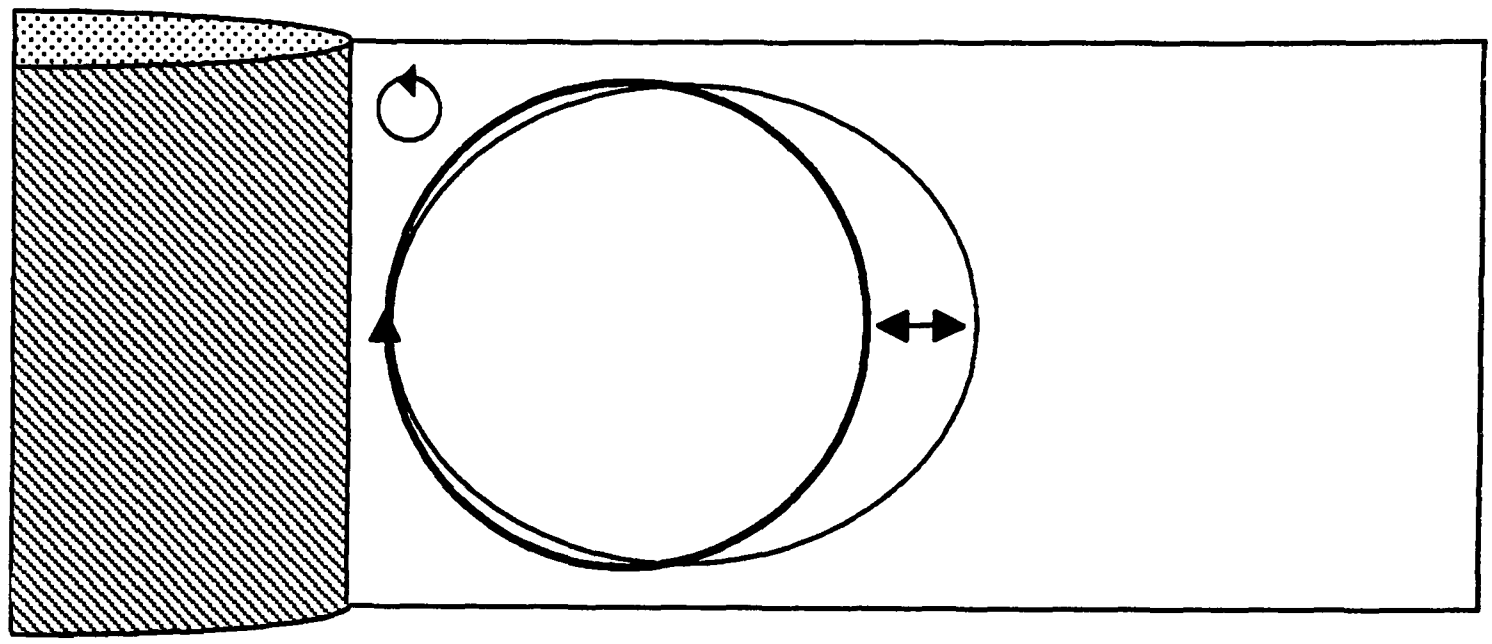

Figure 4.1 : Basic oscillation sequence observed in the single-cell flow at $\Gamma = 0.5$.

$Re \approx 600$. The flow field changes from one which is steady to one in which there is an oscillatory motion. The sequence of the oscillation is shown schematically in figure 4.1 as a vertical cross-section through the flow in the region where the gap between inner and outer cylinders is smallest. The central circulation region of the previously steady single cell now has a profile which oscillates in time between a circular and an oblate shape. The oscillation is predominantly in the radial direction, with the maximum amplitude occurring approximately half way between the horizontal ends.

The sequence of events described above for $\Gamma = 0.5$ is typical of the onset of time-dependence in single-cell flows for the range of $\Gamma < 1$ in general. Close observation of the oscillating flow using flow-visualization shows that it is periodic in time. The frequency ω of the oscillation, when normalized by the frequency ω_c of the rotating cylinder, gives a value of $\omega/\omega_c = 0.3$ for the dimensionless frequency of this particular time-dependent flow for all aspect ratios at which it is observed. This value is also independent of the Reynolds number, at least within a range of 10% of the critical value for the onset of the oscillation.

In addition to observing the nature of the oscillation in the profile of the single cell, the structure of the time-dependent flow around the annulus can also be determined using flow-visualization techniques. This was achieved by measuring the differences in phase between planes of cross-section at different azimuthal positions. Phase differences were determined by eye, based on the average time between the maximum radial displacement of the flow as observed at two different positions si-

multaneously. The results for $\Gamma < 1$ indicate a variation in phase around the flow domain which would normally correspond to an azimuthal wave-number $k = 2$. However, it must be realised that the use of a wave-number in a flow such as this is not strictly justified because of the discrete symmetric nature of the flow domain in the azimuthal direction. Thus we will proceed with this flow labelled with wave-number $k = 2$ subject to the qualification that it refers to the temporal rather than the spatial azimuthal structure.

4.2 Time-dependent flow for $\Gamma > 1$

The nature of the time-dependent single Taylor cell for aspect ratios $\Gamma > 1$ is qualitatively different from that which was discussed in the previous section for $\Gamma < 1$. We begin by considering the flow at the fixed value of $\Gamma = 1.5$ as an example.

The steady single-cell flow at $\Gamma = 1.5$ has already been shown in the photograph of figure 3.5c, but is shown schematically here in figure 4.2 for reference. The main cell fills the full vertical and horizontal extent of the section. This is in contrast to the profile for $\Gamma < 1$, which is approximately circular as does not extend as far as the outer boundary. The fact that the steady-state structures are different between the two aspect ratio regimes is an indication that the time-dependent flows might also be distinct.

The transition from steady to oscillatory flow occurs at a Reynolds number of approximately 400 for $\Gamma = 1.5$. The nature of the time-dependence is shown schematically and sequentially in figure 4.3. A cycle begins with the appearance of a small vortex at the inner cylinder approximately half way between the horizontal end-plates (figure 4.3a). The circulation of this new vortex is in the opposite sense to the single Taylor cell. Once formed, the vortex moves with the main flow and causes a local deformation of the cell outline. The strength of the vortex reaches a maximum as it is swept radially outwards along the end-plate (figure 4.3b). Finally, the vortex dissipates at the stationary outer boundary of the flow domain (figure 4.3c). This cycle is seen to repeat with a regular period. For $\Gamma = 1.5$, the

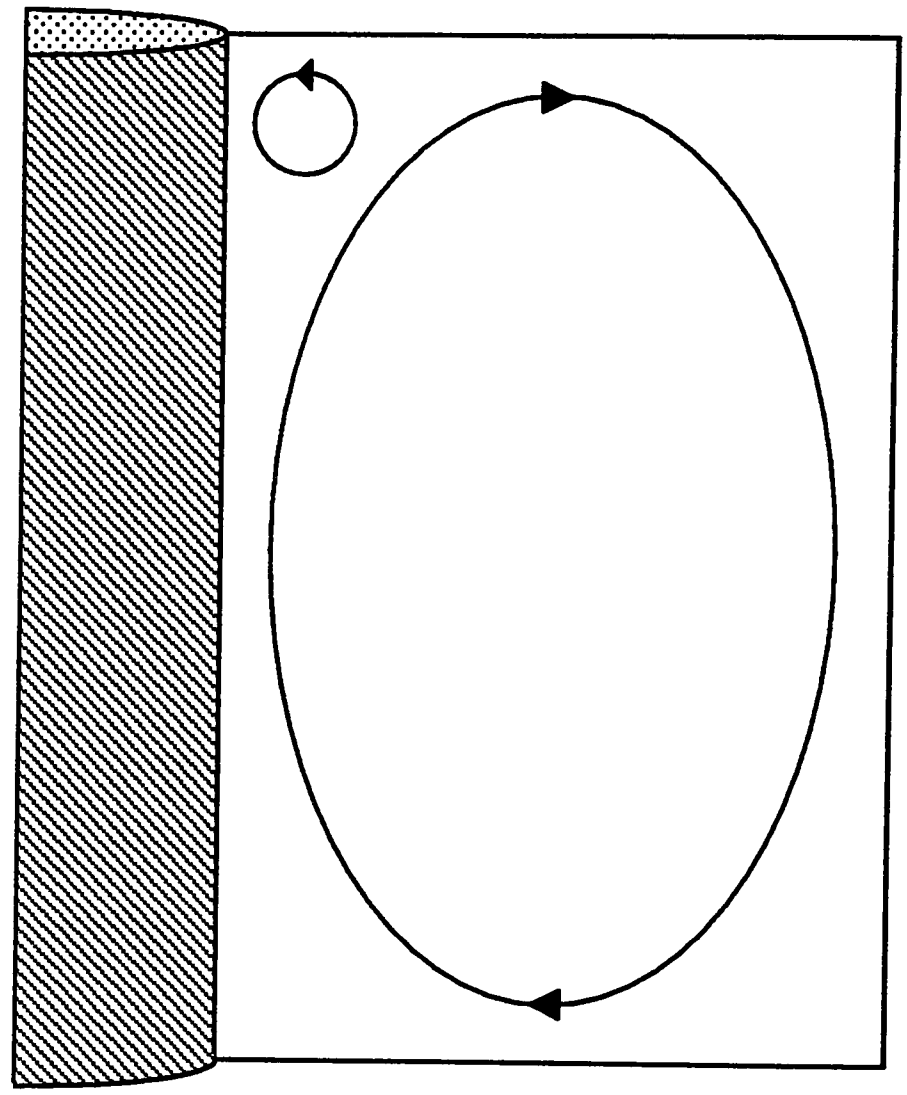

Figure 4.2 : Steady single-cell flow in the square system for $\Gamma = 1.5$.

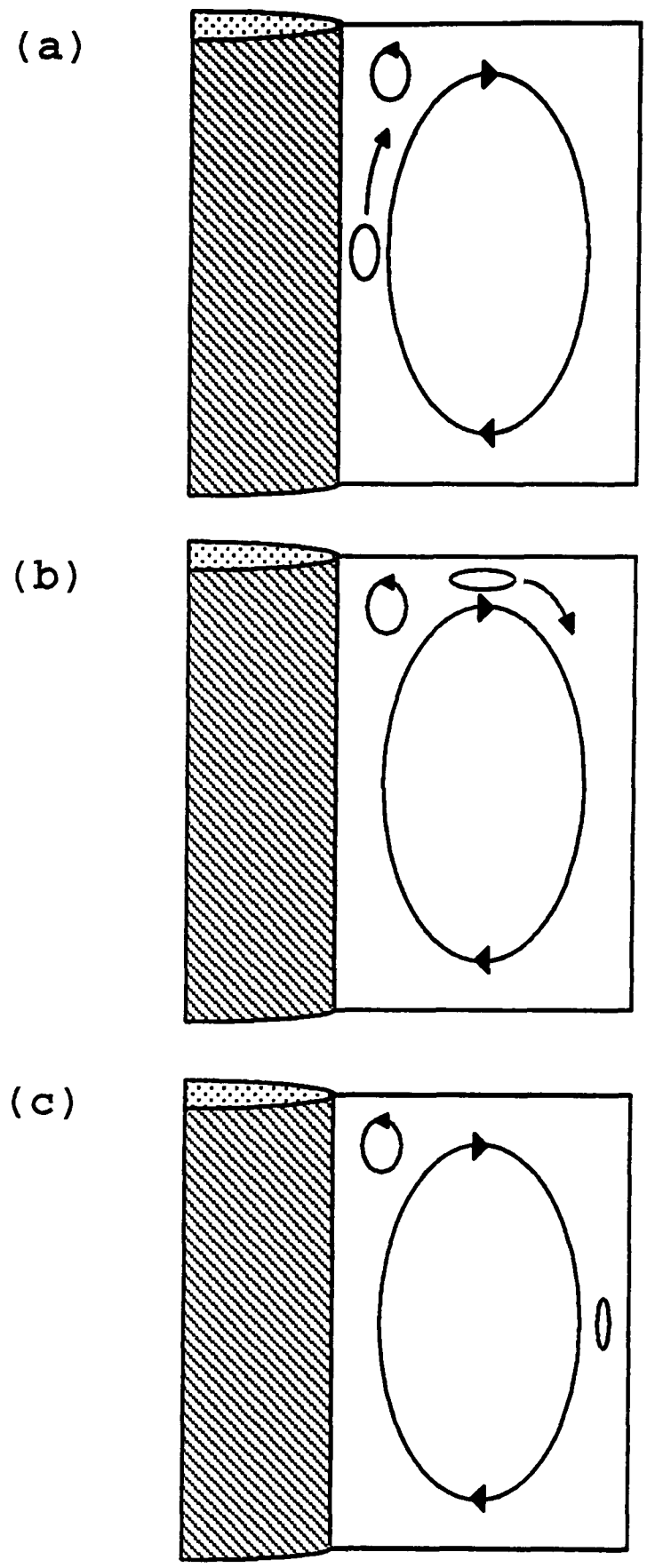

Figure 4.3 : Time-dependent single-cell flow for $\Gamma = 1.5$. (a) A small vortex forms between the main cell and the inner cylinder. (b) The vortex moves around the outside of the main cell. (c) The sequence ends when the vortex reaches the outer cylinder, where it dissipates.

dimensionless frequency of the oscillation is given by $\omega/\omega_c = 0.2$. Unlike the characteristic dimensionless frequency for $\Gamma < 1$, this value does not remain constant over the range of aspect ratios for which the above flow occurs. Indeed, it will be seen in Chapter 5 that the dynamic nature of flows for $\Gamma > 1$ is highly dependent on both the aspect ratio and the Reynolds number of the system.

The azimuthal structure of this time-dependent flow for aspect ratios greater than one was investigated using the techniques described in section 4.1. The variation of the phase of the oscillation around the flow domain now indicates a temporal wave-number is now $k = 3$, as opposed to the value $k = 2$ for the mode when Γ is less than one.

4.3 Identification of Hopf bifurcations

The Hopf bifurcation (Appendix A) represents the simplest mechanisim for the loss of stability of a steady solution to a singly-periodic solution with variation of a control parameter μ. There are two characteristic properties which hold local to the Hopf bifurcation at $\mu = \mu_c$. Firstly, the amplitude of the oscillation grows as $(\mu - \mu_c)^{1/2}$ for $\mu > \mu_c$. Secondly, the frequency of the oscillation is independent of μ. We shall use these two properties to determine if the onset of time-dependence in single-cell flow is as a result of a Hopf bifurcation.

In order to obtain accurate quantitative information from the time-dependent flows, a laser Doppler velocimeter was used as described in Chapter 2. For both $\Gamma = 0.5$ and $\Gamma = 1.5$, the Reynolds number was gradually increased from zero until an oscillation in the output voltage of the LDV was detected. Two series of measurements were then made of the amplitude and the dimensionless frequency of the oscillation for Reynolds numbers Re greater than the critical value Re_c. Measurements were made from the screen of a cathode ray oscilloscope, allowing the amplitude and frequency of the oscillation to be determined with accuracies of 6% and 0.5% respectively. The results are shown in figure 4.4 for $\Gamma = 0.5$ and figure 4.5 for $\Gamma = 1.5$.

The solid lines in figures 4.4a and 4.5a are least-squares fits of the form

$$A = k(Re - Re_c)^{1/2}, \tag{4.1}$$

where A is the amplitude of the oscillation and k is the fitting parameter. In both

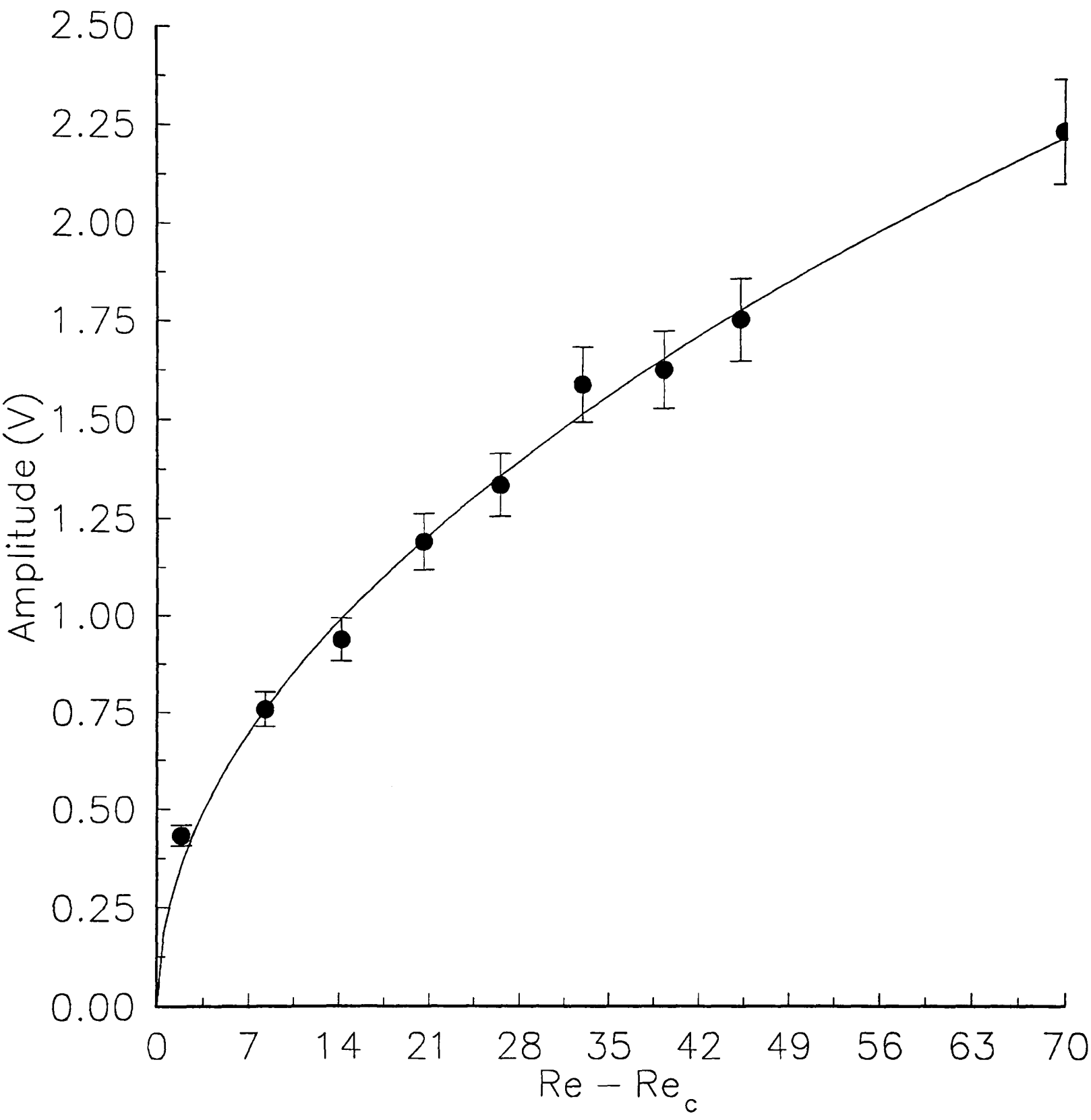

Figure 4.4 : Hopf bifurcation for $\Gamma = 0.5$. (a) Amplitude variation. Critical Reynolds number $Re = 587.24$.

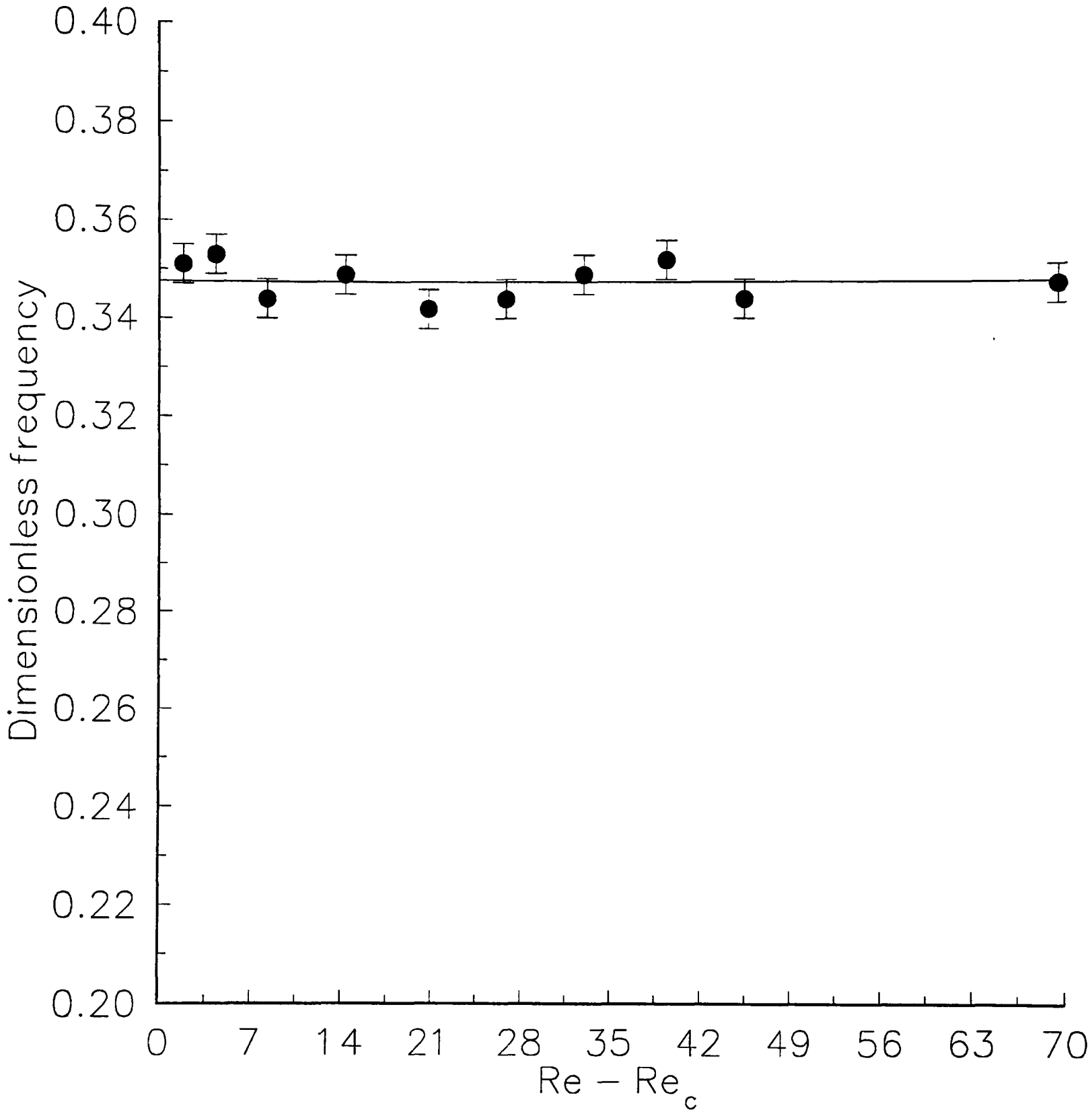

Figure 4.4 : Hopf bifurcation for $\Gamma = 0.5$. (b) Frequency variation. Critical Reynolds number $Re = 587.24$.

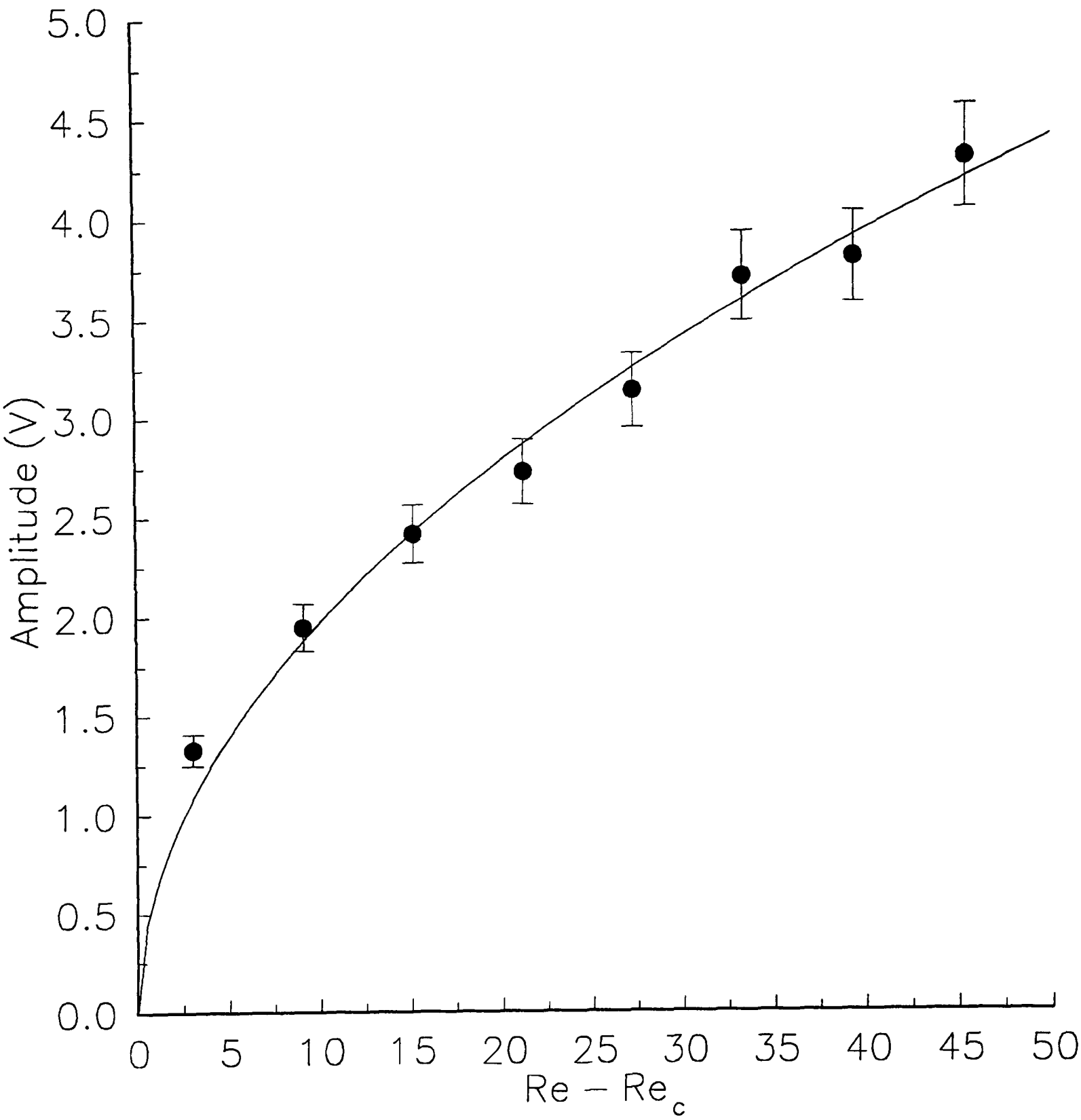

Figure 4.5 : Hopf bifurcation for $\Gamma = 1.5$. (a) Amplitude variation. Critical Reynolds number $Re = 452.76$.

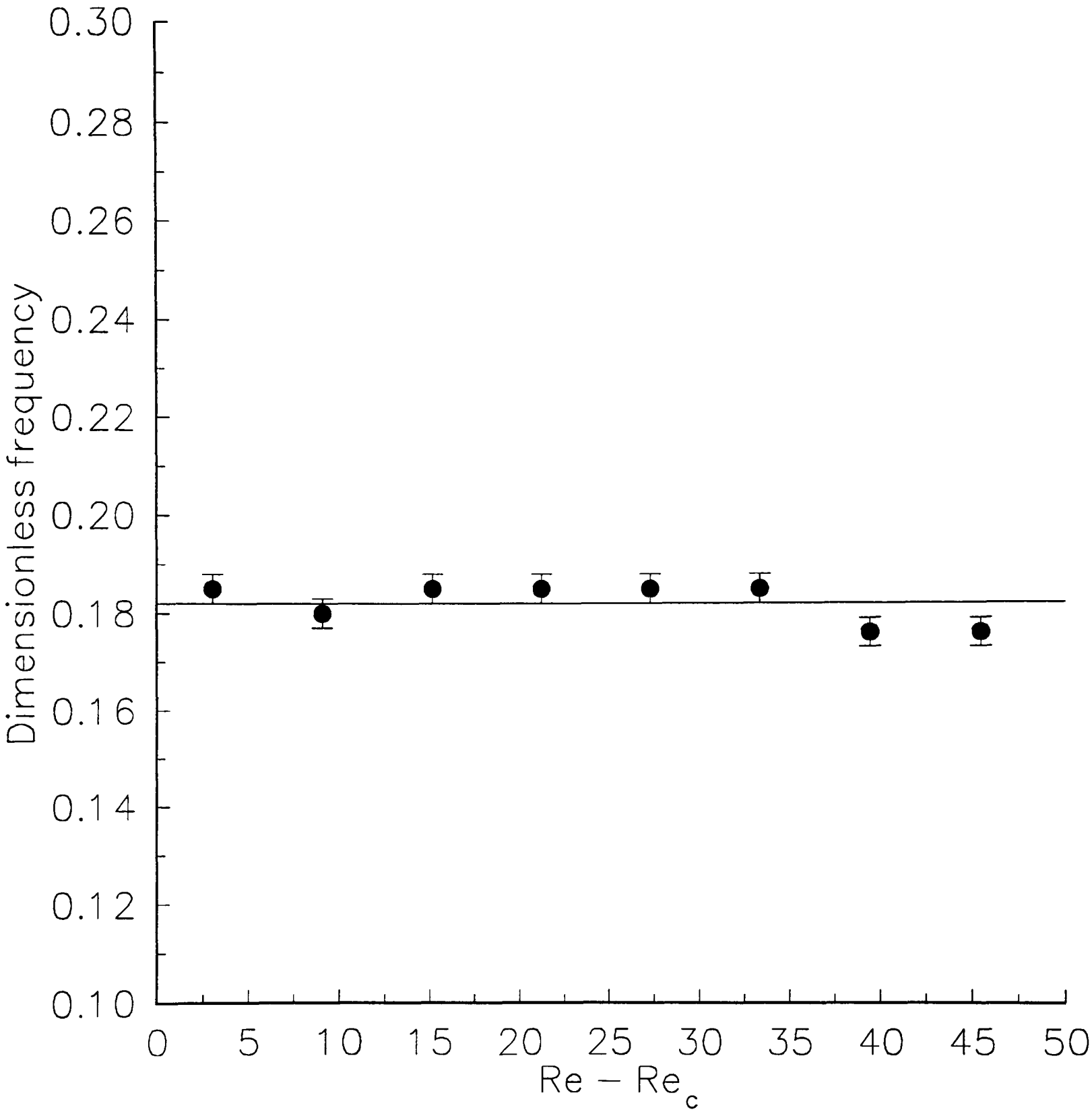

Figure 4.5 : Hopf bifurcation for $\Gamma = 1.5$. (b) Frequency variation. Critical Reynolds number $Re = 452.76$.

cases, the experimental results show good agreement with equation 4.3. The results for the dimensionless frequencies of the two oscillations are shown in figures 4.4b and 4.5b. The horizontal lines are obtained from linear regression performed on each set of data. They show that both dimensionless frequencies remain constant to within experimental error for Reynolds numbers in a range of 10% of the critical value. Thus it is the case that the onset of time-dependence in the single-cell flow in the square Taylor-Couette system is the result of Hopf bifurcations to two qualitatively different singly-periodic modes.

4.4 Bifurcation structure at small aspect ratios

It has been established in the previous sections that there exist two qualitatively different time-dependent forms of single-cell flow in the square Taylor-Couette system. Both these modes occur as the result of Hopf bifurcations on the asymmetric branches of the symmetry-breaking bifurcation which first gives rise to single-cell flow. The bifurcation diagram for this process is shown in figure 4.6. The selection of the mode which appears when the Hopf bifurcation is encountered is seemingly determined by the aspect ratio of the system, there being one mode for $\Gamma < 1$ and another for $\Gamma > 1$.

We now wish to address the problem of how the change between the modes takes place as the aspect ratio is varied between the two regimes. Experiments were carried out using a laser Doppler velocimeter to map out the loci of various bifurcations over a region of parameter space centred on the aspect ratio $\Gamma = 1$. The results presented below show a self-consistent solution structure in which the existence of the two modes may be understood.

Measurements were made first of the critical Reynolds numbers for the onset of each mode over a range of aspect ratio. The results are shown in figure 4.7, where the lines ABC and DE are the loci of Hopf bifurcations leading to the $k = 2$ and $k = 3$ modes respectively. The dashed line is the path of steady symmetry-breaking bifurcations which were discussed in Chapter 3, and is shown again here for reference. The aspect ratio associated with point A was the smallest value at

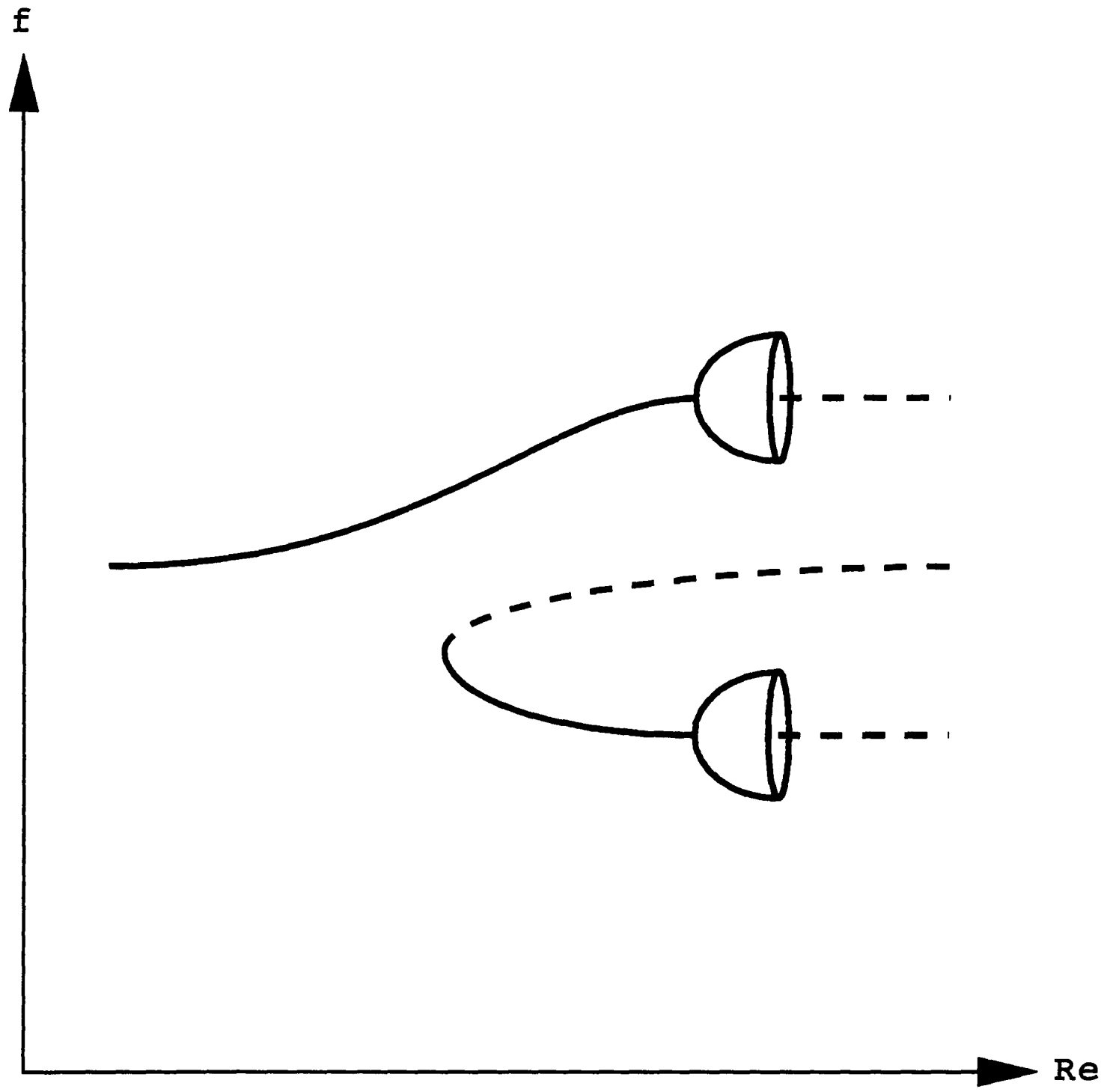

Figure 4.6 : Bifurcation diagram for single-cell flow incorporating Hopf bifurcations of the asymmetric solution branches.

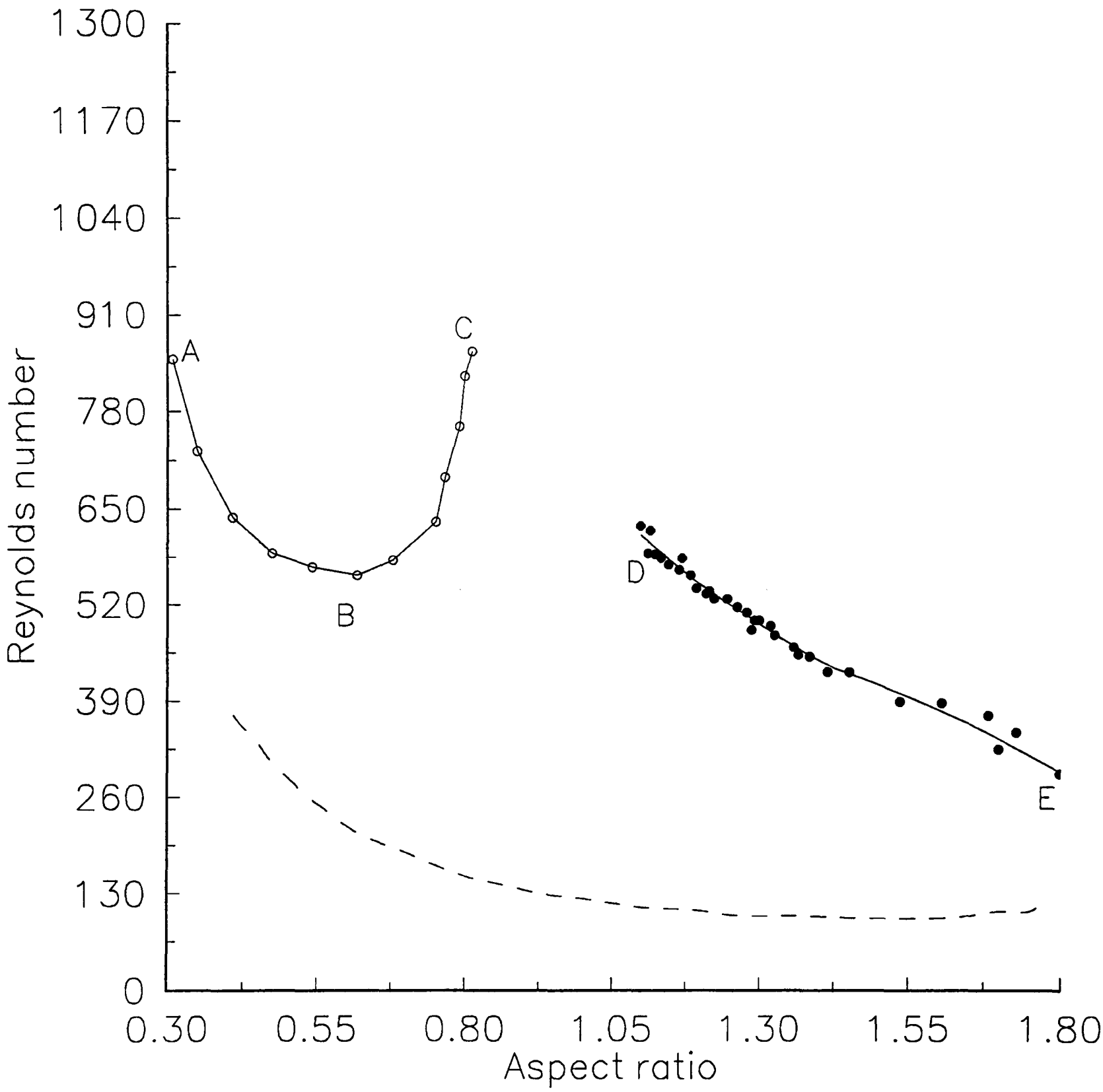

Figure 4.7 : Loci of Hopf bifurcations to time-dependent single-cell modes. ABC (o) is to $k = 2$ mode. DE (•) is to $k = 3$ mode. Dashed line is locus of symmetry-breaking bifurcations to steady single-cell flow.

which the LDV could be operated, while that for point E was the chosen limit beyond which the locus was not followed. However, points C and D mark aspect ratios at which the two lines of Hopf bifurcations were found to terminate. For this to happen in a way which is consistent with dynamical systems theory, there must be other lines of bifurcations through these points. Therefore, attention in the experiments was focussed on the regions of parameter space surrounding points C and D.

It was found that the parameter range between points C and D involves a hysteretic transition between two types of steady single-cell flow. The steady single cell which first develops above the point of symmetry-breaking for $\Gamma < 1$ was shown in Chapter 3 to have a circular cross-section and be limited in the radial direction to a region close to the rotating inner cylinder. The new single-cell flow which appears at higher values of the Reynolds number differs from this because it extends to fill the full radial extent of the flow domain. A photograph of the new cellular flow in the narrowest section of the annulus is shown in figure 4.8. This should be compared with the sketch of the circular single cell shown in figure 3.9b.

A bifurcation sequence which describes the exchange between the two flows is shown in figure 4.9. This has the form of two saddle-node bifurcations which are connected by an unstable solution branch. The circular cell persists with increase of Reynolds number until the saddle-node bifurcation at Re_1 is encountered. The flow then changes catastrophically to the extended form of the single cell. The reverse transition occurs upon decreasing the Reynolds number to the point Re_2, where

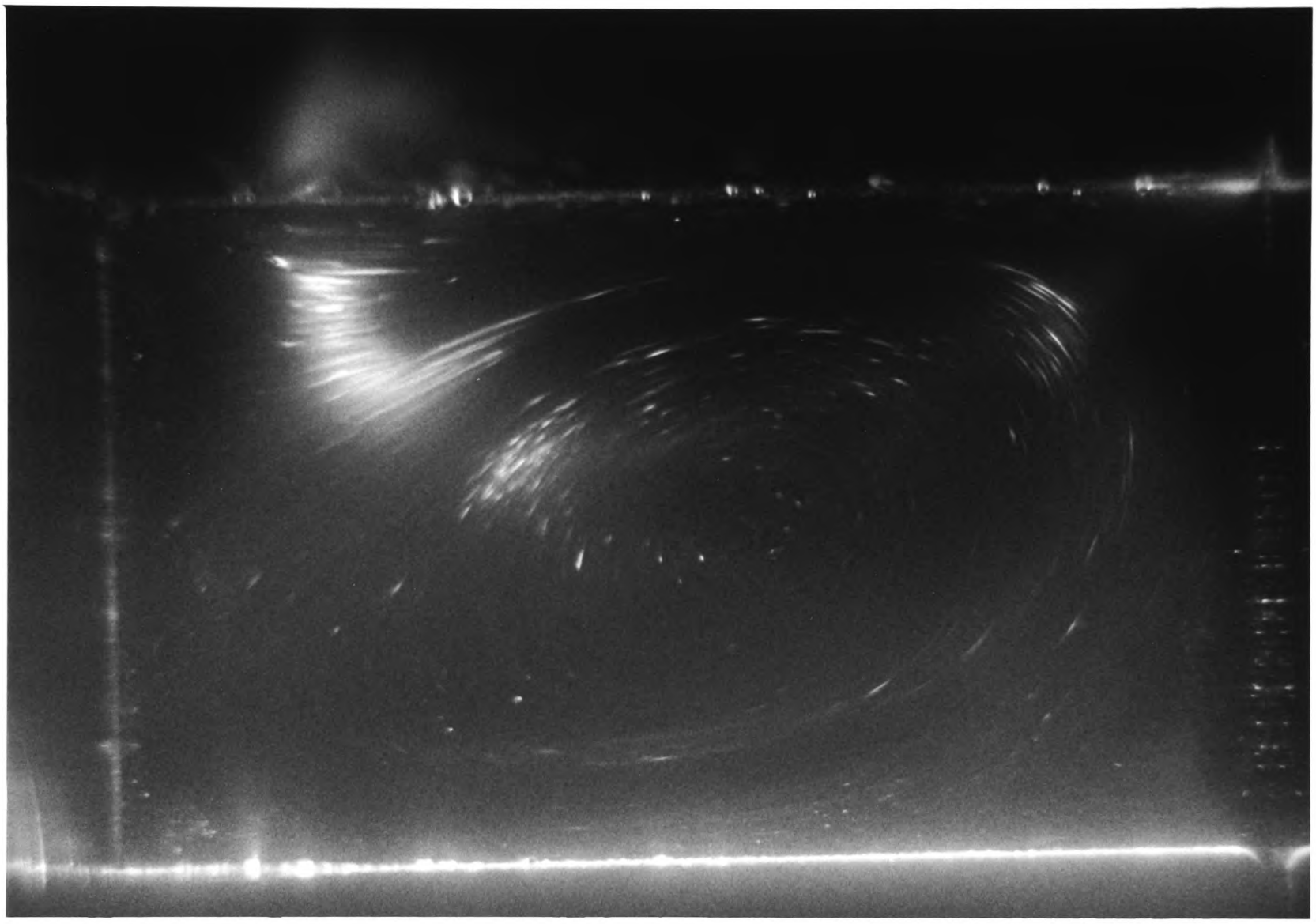

Figure 4.8 : Photograph of new steady single-cell flow at $\Gamma = 0.55$, $Re = 1003$.

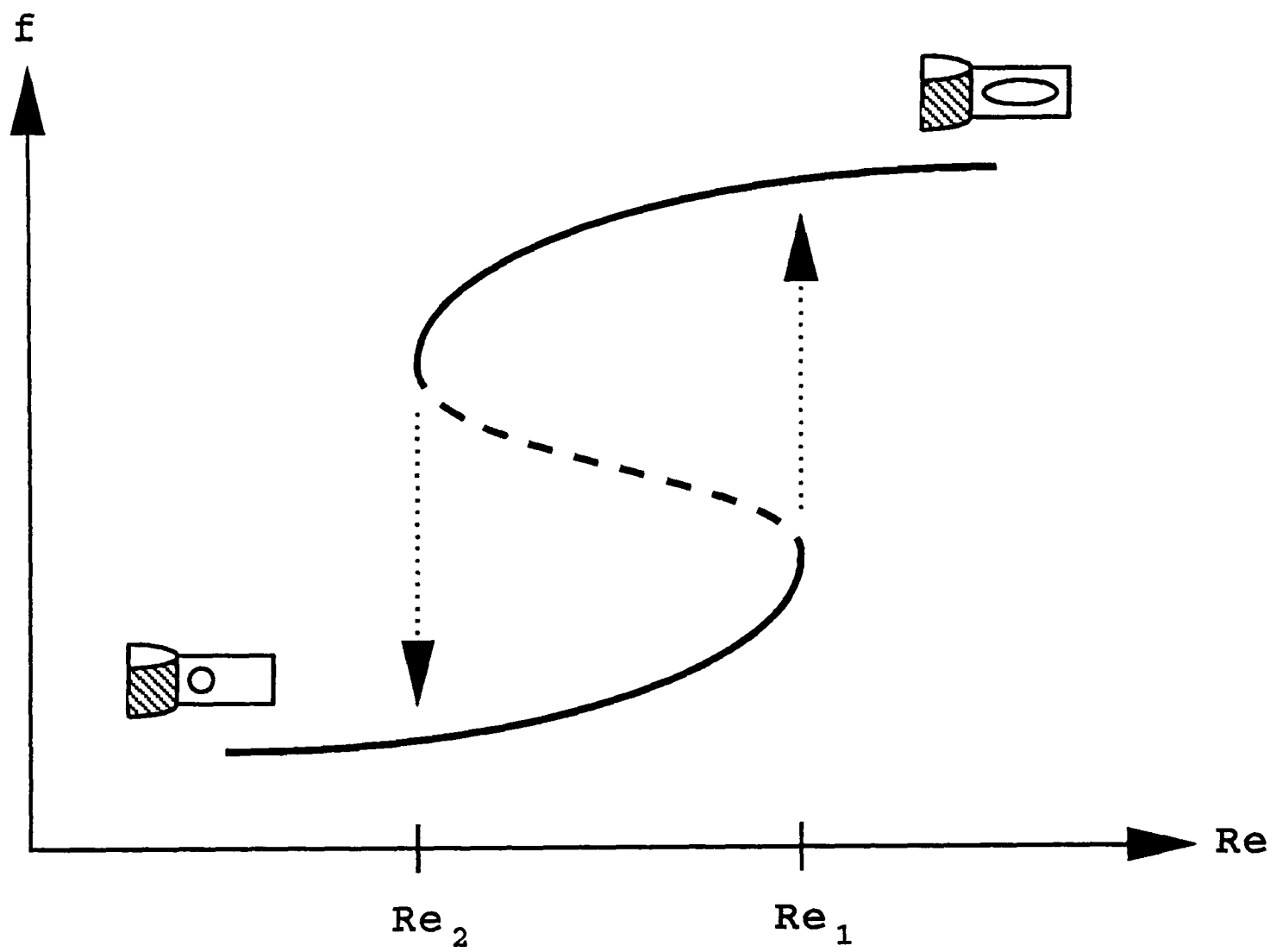

Figure 4.9 : Bifurcation diagram for the transitions between circular and extended forms of single-cell flow.

Re_2 is less than Re_1. Qualitatively identical bifurcations sequences were found to exist on both of the asymmetric branches of the pitchfork bifurcation from two-cell to single-cell flow. Measurements were always made on the connected branch of this bifurcation.

Results of LDV measurements of the hysteretic transition over a range of aspect ratio are shown in figure 4.10. The locus FGH of critical points forms a standard hysteresis cusp in parameter space. For aspect ratios between points C and G in figure 4.10, the circular single-cell flow exists until the line CG is crossed from below. The flow then evolves to the extended form of the single cell, and remains so until the line FG is crossed from above. The upper and lower limits of the hysteresis region coincide at the point G, which corresponds to an aspect ratio of approximately 0.95. This convergence can be understood in terms of the progressive lack of distinction between the two types of single-cell flow as the aspect ratio is increased towards one.

The effect of the hysteretic transition between two different types of single-cell flow is that the locus ABC of Hopf bifurcations does not continue past the point C where it meets the locus CG of saddle-node bifurcations. Thus there is a codimension-2 bifurcation formed near the point C, where a Hopf bifurcation and a saddle-node bifurcation are encountered simultaneously. However, it proved impossible to locate the codimension-2 bifurcation point exactly in the experiments because of the sensitivity of the system to changes in the control parameters in the region where the two lines of bifurcations are close together.

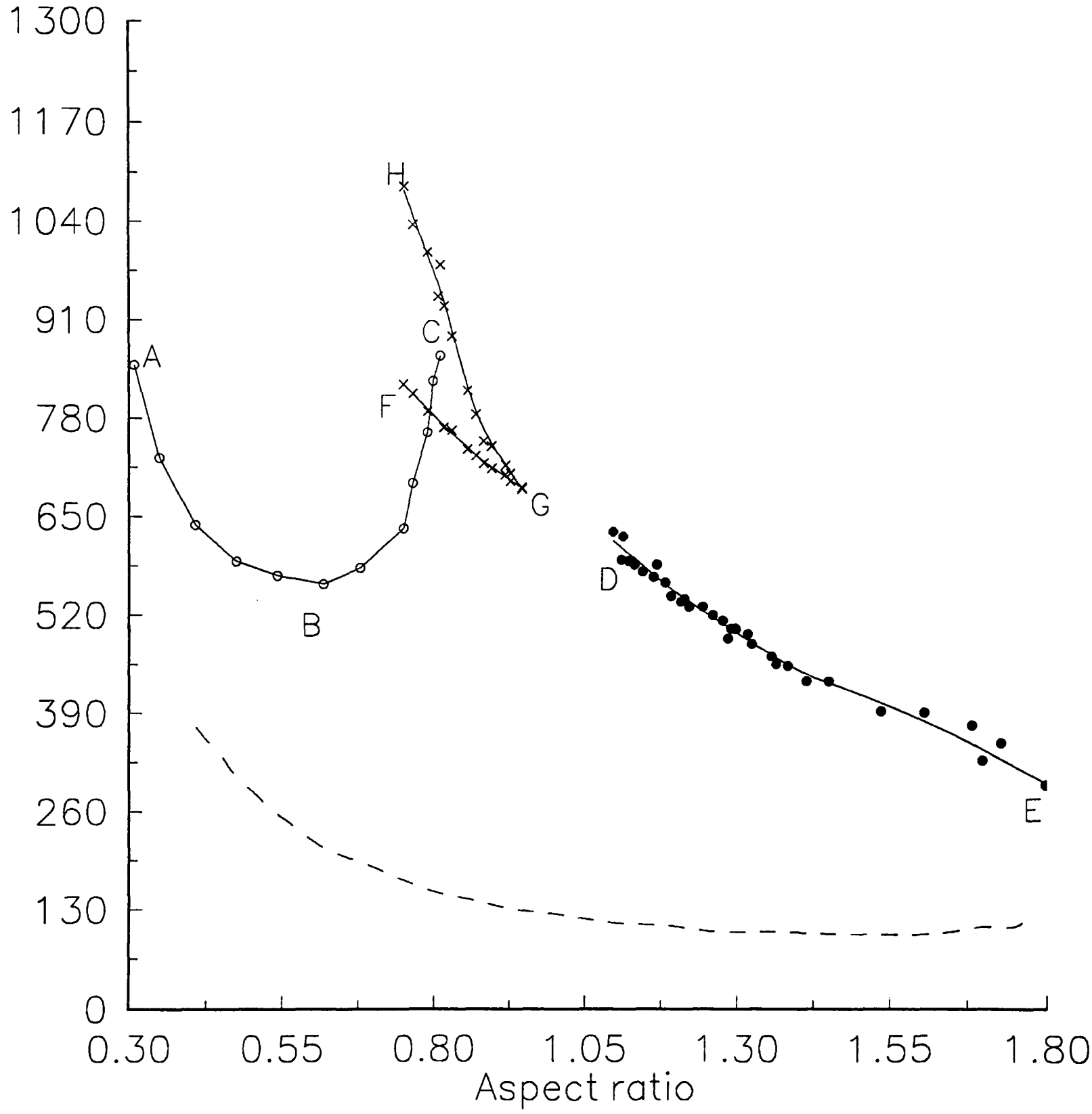

Figure 4.10 : Parameter space diagram incorporating the lines FG and HG ($\times$) of saddle-node bifurcations which mark the hysteretic transitions between the circular and extended forms of the single-cell flow.

For aspect ratios below that associated with the point C, the result of increasing the Reynolds number beyond the Hopf bifurcation at BC is that a cyclic fold bifurcation is encountered (see Appendix A). The oscillatory form of the circular single cell persists with unchanged dimensionless frequency until a critical Reynolds number is reached, at which point there is a catastrophic collapse to the extended single-cell flow. The experimentally determined locus CH of these cyclic folds is shown in figure 4.10. Once achieved, the extended single-cell flow does not revert to the circular form until the line FG of saddle-node bifurcations is crossed from above.

A feature of the hysteretic transition from both the steady and the time-dependent circular cell to the extended cell is that the latter flow was typically encountered in a time-dependent form. The bifurcation diagram was explored at a fixed value of the aspect ratio. This revealed the existence of two Hopf bifurcations on the solution branch corresponding to the extended single cell. A schematic bifurcation diagram is shown in figure 4.11. The time-dependent solution exists as an isola on the solution branch, with inward-facing Hopf bifurcations at each end of the isola. Thus the steady extended cell can be restabilized from its time-dependent form by either increasing or decreasing the Reynolds number.

Measurements of the critical Reynolds numbers of the two Hopf bifurcations were made over a range of aspect ratio using an LDV. The results are shown in figure 4.12 as the locus JKL, and thus the point K is an isola formation point in parameter space. The extended single-cell flow is time-dependent for all parameter

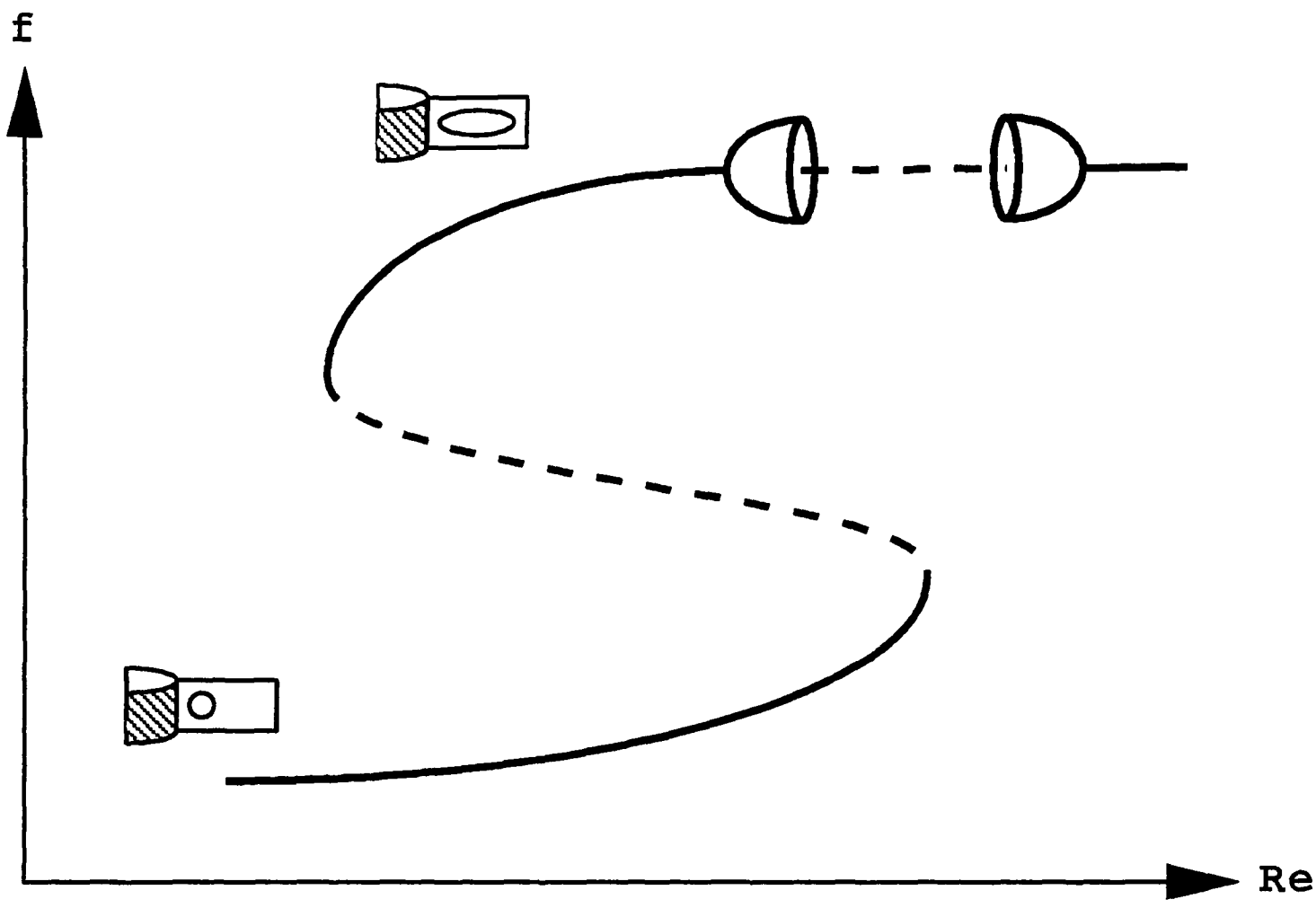

Figure 4.11 : Bifurcation diagram showing the time-dependent isola in the solution branch for the extended single-cell flow.

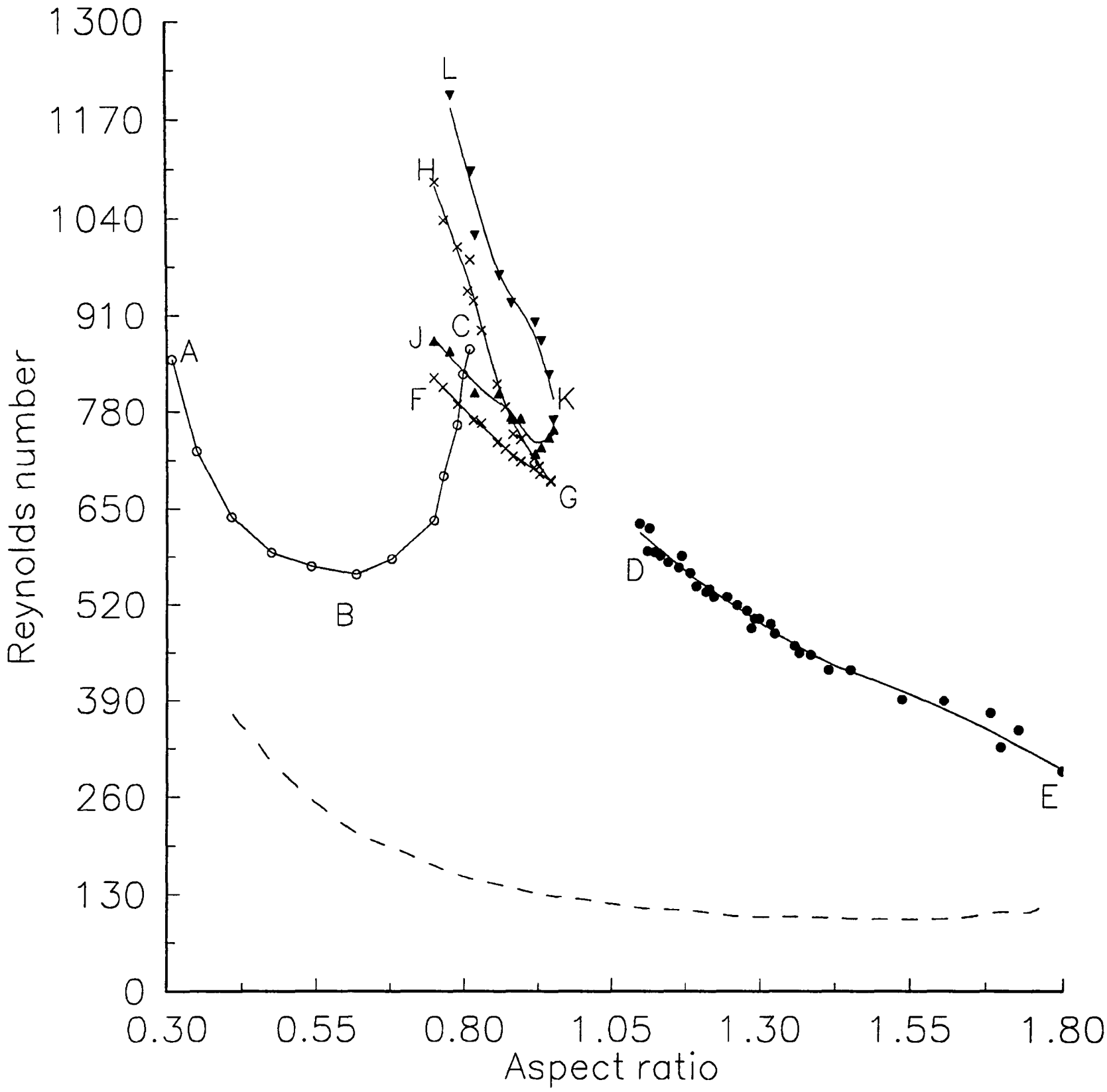

Figure 4.12 : Parameter space diagram incorporating the line JKL of Hopf bifurcations which mark the limits of the time-dependent isola in the extended single-cell solution.

values within the region defined by the line JKL. The proximity of the locus JK of Hopf bifurcations to the locus FG of saddle-node bifurcations which mark respectively the upper and lower limits of stability of the steady extended cell shows that there is only a narrow range of parameter values at which the steady flow can be observed experimentally at the lower end of the time-dependent isola.

The dimensionless frequency of the oscillation in the extended single-cell flow was found to have the value $\omega/\omega_c = 0.04$ over the range of aspect ratio which was considered. This is in contrast with the value of $\omega/\omega_c = 0.3$ which is associated with the time-dependent circular cell. Observation of the spatial structure of the oscillating extended cell using flow visualization revealed a cycle which was reminiscent of the time-dependent flow found in general for aspect ratios greater than one. There was the periodic formation of a small vortex between the inner cylinder and the main cell. This vortex then moved around the outside of the extended cell, but in the opposite direction to that of the time-dependent sequence shown in figure 4.3 for $\Gamma > 1$. A cycle of the oscillation in the extended single cell is shown schematically in figure 4.13.

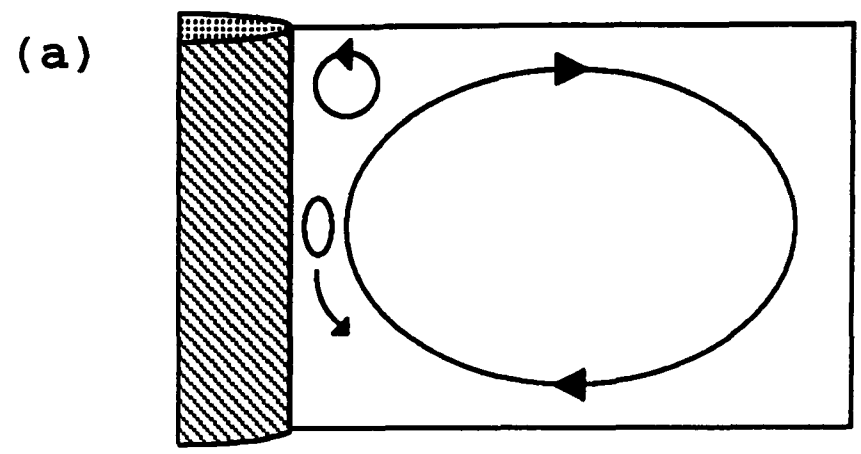

Figure 4.13 : Schematic diagram showing sequence of oscillation in the extended single cell. (a) A small vortex forms between the main cell and the inner cylinder. (b) The vortex moves round the outside of the cell in the opposite direction to the prevailing flow. (c) The vortex dissipates upon reaching the stationary outer cylinder.

4.5 Homoclinic phenomena

The results in section 4.4 provide a consistent framework of solutions to account for the original observation of a termination in parameter space of the locus ABC of Hopf bifurcations. However, it is also necessary to consider the region of parameter space around the point D which marks the observed end of the other primary locus of Hopf bifurcations.

For aspect ratios just less that the value associated with point D in figure 4.12, observations were made of homoclinic phenomena in the problem. A homoclinic orbit in phase-space is one which asymptotically approaches the same fixed point as time $t \rightarrow \pm\infty$. In the context of a dynamical system, this is when the period of an oscillatory solution becomes infinite with variation of one or more control parameters. In an experimental situation, obviously no oscillation can be observed as having infinite period. Rather, the system is said to be approaching a state of homoclinicity when the period of an oscillation is far in excess of the typical time-scale of the problem. A careful investigation of flow phenomena was made using an LDV for aspect ratios just less than the point where the locus DE of Hopf bifurcations ends. The results are shown in figure 4.14 in the context of the previously determined bifurcation structure.

The line MD in figure 4.14 marks a locus of sudden transitions from steady to time-dependent flow with increase of Reynolds number. The oscillation appeared with non-zero amplitude as the line MD is crossed from below. Once established, the

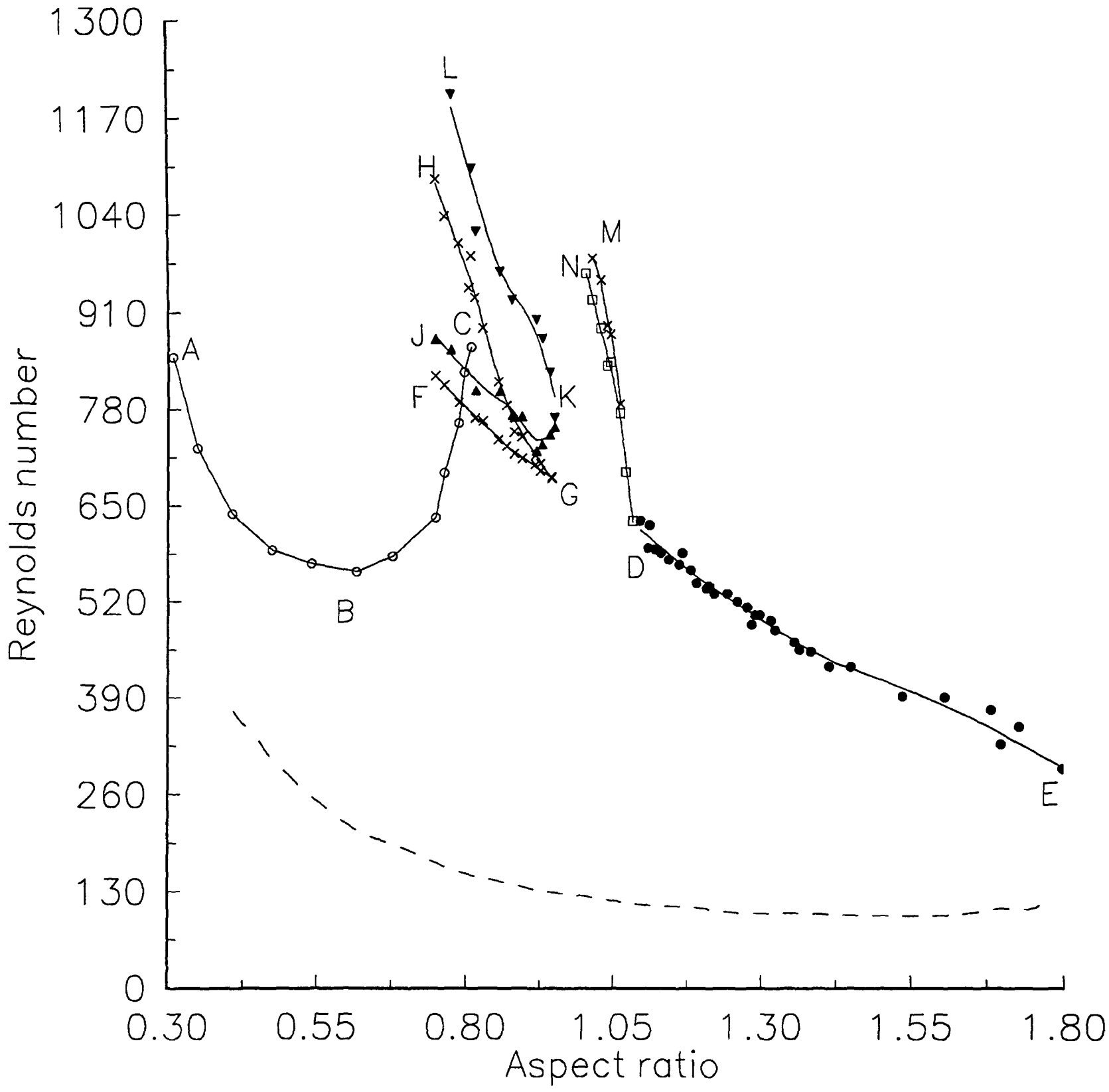

Figure 4.14 : Parameter space diagram incorporating the locus MD ($\times$) of saddle-node bifurcations and the locus ND ($\square$) of homoclinic bifurcations.

oscillation was found to persist with decrease of Reynolds number to a value which was slightly lower than the value associated with the critical point for the onset of the oscillation. The approach towards the lower limit of stability was accompanied by a continuous drop in the value of the dimensionless frequency, indicating that the oscillation was becoming homoclinic. The locus of homoclinic bifurcations back to the steady flow is shown in figure 4.14 as the line ND. It should be noted that these two lines of bifurcations exist in very close proximity in parameter space. Careful experimental procedure was therefore required in order to make measurements of the respective critical points. Nevertheless, it proved to be impossible to resolve the very small amount of hysteresis which almost certainly exists close to the point D in figure 4.14.

The loci MD and ND both rise steeply in the given representation of parameter space. The critical points were therefore much more easily investigated by fixing the Reynolds number and varying the aspect ratio. The variation of dimensionless frequency as the locus ND of homoclinic bifurcations was approached in this way is shown in figure 4.15 for the Reynolds number $Re = 900$. Here we can clearly see the continuous decrease in dimensionless frequency over a narrow range of control parameter which is characteristic of an impending homoclinic bifurcation. It should be noted that all the behaviour in this region was observed to be non-chaotic.

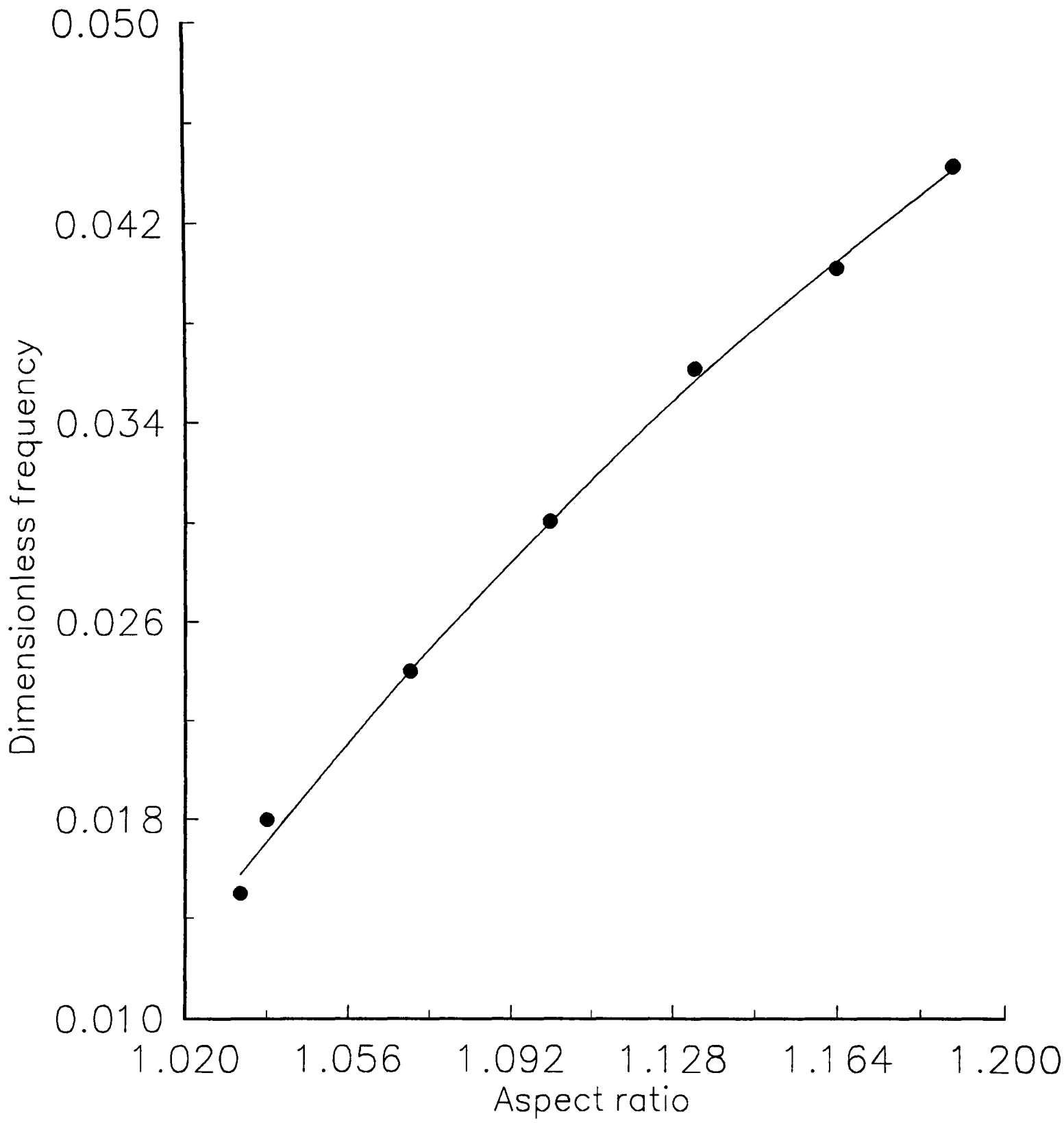

Figure 4.15 : Variation of dimensionless frequency with aspect ratio in single-cell flow at $Re = 900$.

4.6 Comparison with the standard system

We end this chapter by considering how the time-dependent single-cell flows in the system with a square outer boundary compare with those which are found in the standard system with a circular outer boundary. An experimental study of the dynamics of single Taylor vortex flow in the Taylor-Couette system has been carried out by Lensch (1988). The radius ratio η was equal to 0.5, and the flow was driven by rotation of the inner cylinder alone. The height of the annulus was set by the position of two stationary horizontal end-plates. Aspect ratios which were studied ranged from $\Gamma = 0.4$ to $\Gamma = 1.3$.

The qualitative nature of time-dependent single-cell flows in the standard system was found to be the same as has been discussed above for the square configuration. For aspect ratios less than one, the cell profile oscillates between circular and oblate in a predominantly radial direction. The oscillation for Γ greater than one consists of the periodic formation of small vortices at the inner cylinder which then move round the outside of the main cell and are destroyed at the outer boundary.

A quantitative comparison can be achieved by considering the respective dimensionless frequencies of each mode in the two systems. For aspect ratios less than one, Lensch reports a value of $\omega/\omega_c = 0.3$ in the standard system. This is the same as the value for the corresponding mode in the square system. However, the agreement does not persist for $\Gamma > 1$. A value of $\omega/\omega_c = 0.06$ is quoted by Lensch, whereas the modified system gives $\omega/\omega_c = 0.2$. A possible explanation for

the different values of dimensionless frequency for one range of aspect ratio and the agreement for another comes from the distinct nature of the two time-dependent modes. The oscillating single cell for $\Gamma < 1$ in both the standard and modified systems is effectively localized to a region of the flow domain close to the inner cylinder. It is therefore possible that this type of flow is insensitive to the exact details of the outer wall geometry. However, the oscillation for $\Gamma > 1$ has a strong effect on the whole flow field. Hence it is not surprising that a change in shape of the outer boundary might produce a change in a quantitative aspect of the flow.

A second quantitative comparison is possible in terms of the wave-numbers of the flows. We saw in sections 4.1 and 4.2 that subject to certain qualifications about the use of a wave-number in an annulus without continuous rotational symmetry, the modes for $\Gamma < 1$ and $\Gamma > 1$ can be labelled with wave-numbers $k = 2$ and $k = 3$ respectively. However, Lensch reports a value of $k = 3$ for $\Gamma < 1$ and $k = 2$ for $\Gamma > 1$ in the standard system, which is the reverse of the case for the modified system. The reasons for the reversal are not understood at present, and this result clearly shows the limitation of arguments based simply on the qualitative nature of the single-cell flows.

Finally, it is worth considering here a possible mechanism for the formation of these small vortices at the inner cylinder. The observations of this phenomenon are reminiscent of a hypothesis developed for the case of the standard Taylor-Couette system by Barcilon *et al.* (1979) and extended by Barcilon & Brindley (1984). This is that conditions exist at high values of the Reynolds number for the formation of

Görtler vortices (see Drazin & Reid (1981), for example) close to the cylinder walls . The hypothesis has been tested experimentally by Wei *et al.* (1991), who presented results showing the creation of small vortices close to the inner cylinder at Reynolds numbers of approximately 3×10^3. These vortices then moved away from the inner cylinder and ultimately contributed to the overall disordered structure of the Taylor vortex flow. Although the formation of vortices in the single-cell flows in both the standard and the square systems occurs at Reynolds numbers much less than those considered by either Barcilon *et al.* (1979, 1984) or Wei *et al.* (1991), the basic similarity of the respective processes does suggest that there may be an underlying connection between the present observations and the Görtler vortex phenomenon.

4.7 Summary

The results presented in this chapter show that a framework of low-dimensional dynamics exists for the basic time-dependent single-cell flows which are found in the square Taylor-Couette system. This was uncovered as a progression from similar considerations of the solution set for the steady flows. The time-dependent mode for aspect ratios less than one consists of an oscillation between circular and oblate forms of the single cell, while that for aspect ratios greater than one involves a periodic motion of small vortices around the main Taylor cell. In establishing a connection between these two modes, a new type of steady single cell was discovered for $\Gamma < 1$. Homoclinic behaviour was also observed in the solution set of the problem.

Up to this point, the observed dynamical phenomena have all been relatively simple occurrences of low-dimensional behaviour. The existence of a codimension-2 bifurcation at an aspect ratio less than one does not appear to be the source of more complicated dynamics in the immediate vicinity of this point. The general conclusion is that the system is restricted at very small aspect ratios to such an extent that only basic behaviour exists for the values of Reynolds number which were investigated. However, in Chapter 5 we will consider behaviour at aspect ratios greater than one which is more complex than anything observed so far. In doing so, a much clearer picture will emerge of the role which low-dimensional dynamics have to play in this system with discrete azimuthal symmetry.

CHAPTER FIVE

Low-dimensional dynamical flow phenomena in the square Taylor-Couette system

The results and discussions which have been presented in Chapters 3 and 4 are aimed at establishing a consistent understanding of basic flow phenomena in the square Taylor-Couette system at small aspect ratios. It was shown first that the steady flows can be described in terms of a bifurcation sequence involving symmetry-breaking bifurcations which lead to single-cell flow. This framework was then built upon by considering the onset of time-dependence in the single Taylor cell. It was found that two qualitatively different time-dependent modes exist, and that each of these is the result of a Hopf bifurcation from steady flow. Work was undertaken to establish the connection between the two modes. The results showed the existence of an intricate but robust solution set which can be understood in terms of simple bifurcation mechanisms applying to equilibrium and singly-periodic solutions.

It is now possible to extend the study to dynamical regimes where more complicated flow behaviour occurs. This was done experimentally by focussing on the effects of increasing the Reynolds number for a particular time-dependent mode. The results of these investigations are presented in this chapter.

5.1 Basic dynamical phenomena

The present state of understanding of the solution structure of the problem is summarized in the parameter space diagram shown in figure 4.14. The connection between the two different time-dependent modes was established by following the various loci of bifurcations which are found to exist between points C and D that mark the respective limits of the two sets of Hopf bifurcations.

The results as shown in figure 4.14 suggest that the effect of varying the aspect ratio for $\Gamma > 1$ is simply a monotonic change in the critical Reynolds number associated with the Hopf bifurcation. However, a plot of the dimensionless frequency of the oscillation at its onset versus the aspect ratio, as shown in figure 5.1, indicates that the behaviour is more complicated than this. For aspect ratios greater than $\Gamma = 1.235$, the dimensionless frequencies are of the order of $\omega/\omega_c = 0.2$. This is the value quoted in Chapter 4 for the typical time-dependent mode where there are small vortices moving around the perimeter of the main cell in the same direction as the secondary flow in the cell. However, there appears to be a discontinuous change in the value of the dimensionless frequency at $\Gamma = 1.235$. For aspect ratios below this value, the frequency drops suddenly to values of the order of $\omega/\omega_c = 0.01$. The presence of such a change in the dimensionless frequency requires explanation, and it will be shown below that the answer is to be found in the detailed bifurcation structure which manifests itself at values of the aspect ratio around $\Gamma = 1.235$.

We begin by considering the qualitative nature of the time-dependent flow

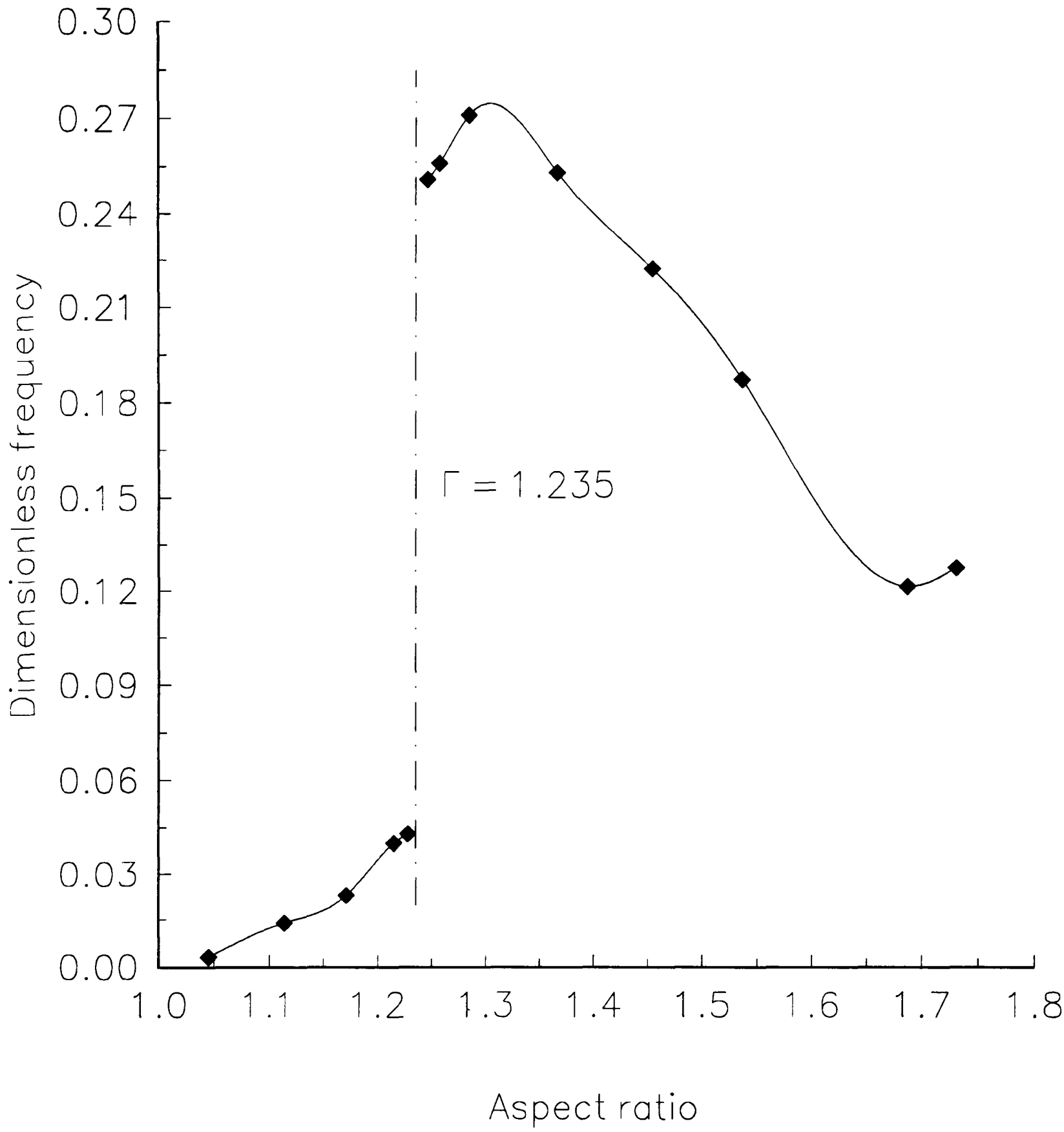

Figure 5.1 : Plot of dimensionless frequency versus aspect ratio along the locus of Hopf bifurcations for $\Gamma > 1$.

for aspect ratios greater than one using flow visualization techniques. The critical aspect ratio at which the discontinuous change in the dimensionless frequency occurs was identified as $\Gamma = 1.235$. Aspect ratios of $\Gamma = 1.22$ and $\Gamma = 1.25$ were therefore used to observe the time-dependent flow on either side of the critical value. For $\Gamma = 1.25$, the Hopf bifurcation leads to the time-dependent flow which was described in Chapter 4 as being typical for the majority of aspect ratios greater than one. This is the mode in which small vortices are formed between the main cell and the rotating inner cylinder and move around in the same direction as the prevailing flow. Such behaviour has already been shown sequentially for $\Gamma = 1.5$ in figure 4.4. However, a qualitatively different type of time-dependent flow was encountered at the Hopf bifurcation for $\Gamma = 1.22$. This flow still involves the periodic formation of a small vortex beside the inner cylinder, but now its motion around the perimeter of the main cell is in the opposite direction to the secondary flow in the cell. This is the same sequence that was found for the time-dependent form of the extended single-cell flow for $\Gamma < 1$, and was illustrated in figure 4.15. Thus it is reasonable to conclude that the Hopf bifurcation which is encountered for aspect ratios just below $\Gamma = 1.235$ is the same Hopf bifurcation which is found at the values of Γ associated with the extended single cell.

In order to determine the mechanism whereby the nature of the time-dependent flow changes suddenly along the line of Hopf bifurcations, it was necessary to consider the dynamical behaviour of the system at parameter values away from the immediate vicinity of the onset of time-dependence. To begin with, the aspect ratio was set to a value below $\Gamma = 1.235$ so that gradual increase of the Reynolds number

resulted in the onset of the lower-frequency mode. Once this mode was established, the Reynolds number was held fixed and the aspect ratio was gradually increased beyond the value of 1.235. The system was then in the regime in which the Hopf bifurcation from steady flow results in the higher-frequency mode. However, the result of varying the control parameters in the manner described above was that the system persisted in being in the lower-frequency mode for $\Gamma > 1.235$. Thus there is a multiplicity of time-dependent single-cell flows, with both the lower-frequency and the higher-frequency modes being observed at the same set of control parameters. The same multiplicity was found for $\Gamma < 1.235$. If the higher-frequency mode is first established at $\Gamma > 1.235$, then the aspect ratio can be decreased without any change in the qualitative nature of the time-dependent flow.

We will use the nomenclature of Benjamin (1978a) to describe the relative characteristics of the two time-dependent modes. The mode which results from the quasistatic variation of only one control parameter through one or other of the Hopf bifurcations will be termed the *primary mode*. The mode which is necessarily realised by the variation of both parameters or by a sudden change in one of the parameters will be referred to as the *secondary mode*. Thus for $\Gamma \gtrsim 1.235$, the primary mode is the higher-frequency oscillatory flow and the secondary mode is the lower-frequency oscillatory flow. For $\Gamma \lesssim 1.235$, the roles of the two modes are reversed.

A characteristic feature of a secondary mode is that it is terminated by a saddle-node bifurcations and thus has a lower limit of stability (Benjamin 1978a).

This is indeed found to be the case for both the higher-frequency and the lower-frequency secondary modes in the present study. The secondary mode collapses catastrophically at a critical set of control parameters, and the system reverts to the dynamics of the appropriate primary mode. The lower stability limits of the two secondary modes were measured experimentally over a range of aspect ratio using an LDV system. The results are shown in the context of the full parameter space in figure 5.2, and in an expanded view in figure 5.3. The locus PQ represents the lower stability limit of the lower-frequency flow, while the locus PR is that of the higher-frequency flow. In the expanded view given in figure 5.3, it can be seen that the two loci KP and PL of Hopf bifurcations intersect at approximately the aspect ratio $\Gamma = 1.235$, thus giving the apparent single line of Hopf bifurcations which was suggested by the preliminary results presented at the end of Chapter 4.

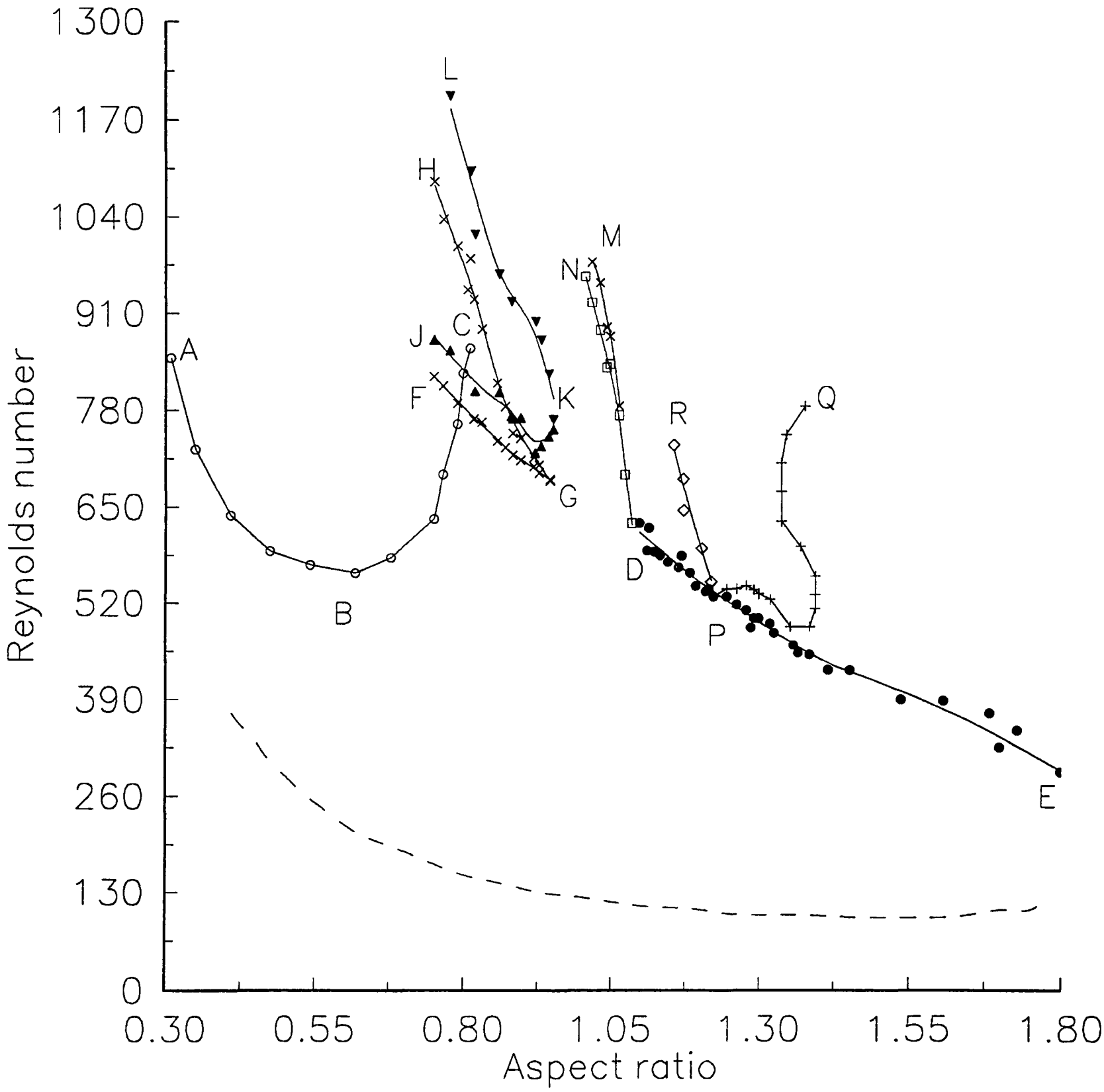

Figure 5.2 : Parameter space diagram incorporating the lower stability limits of the lower-frequency (PQ +) and higher-frequency (PR ◊) modes.

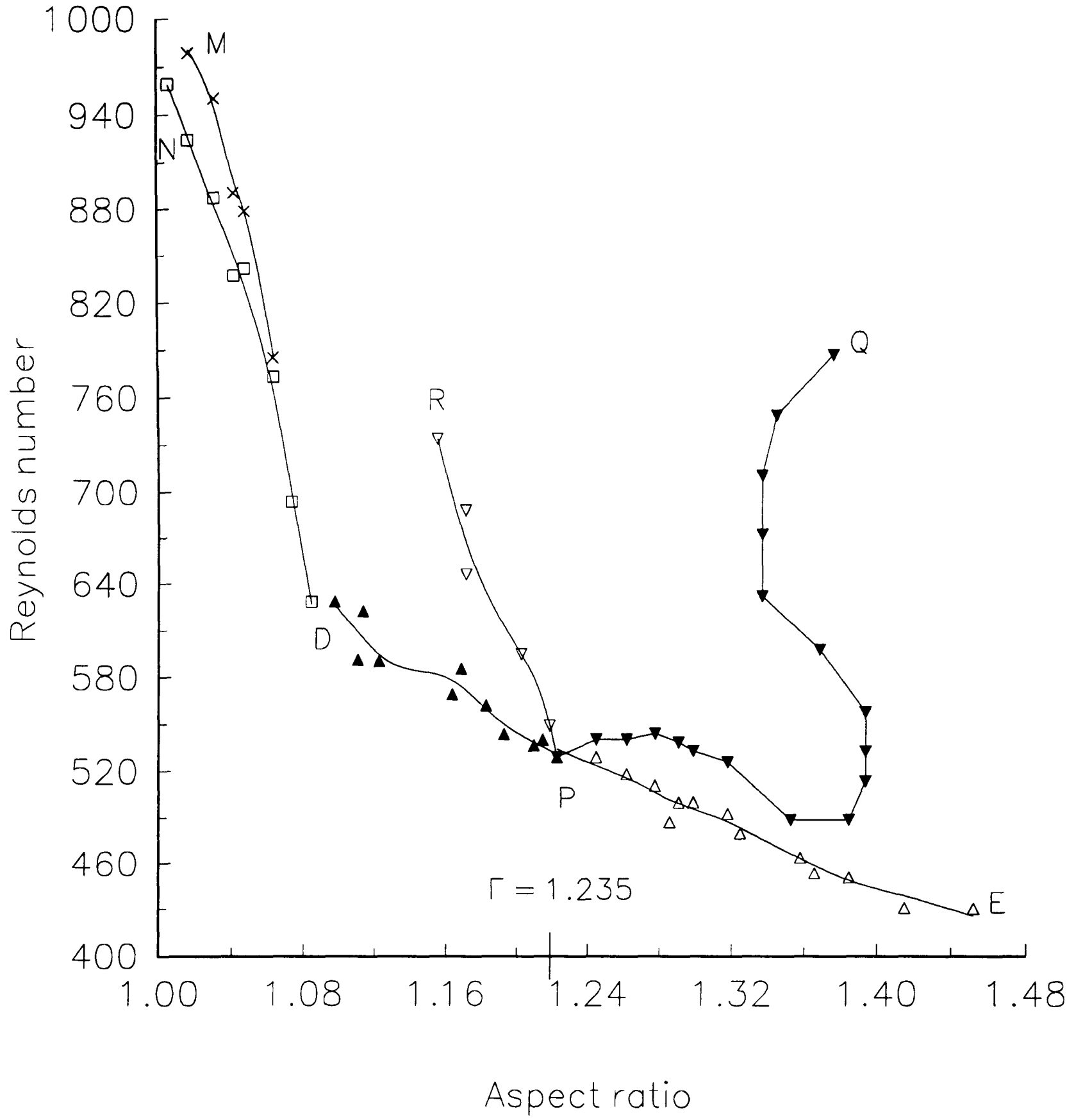

Figure 5.3 : Expanded view of figure 5.2 about the point P. Symbols have been changed to indicate the two different types of behaviour. PE (△) Hopf bifurcations leading to higher-frequency mode. PR (▽) stability limit of higher-frequency mode. PD (▲) Hopf bifurcations leading to lower-frequency mode. PQ (▼) stability limit of lower-frequency mode.

5.2 Higher-order dynamical phenomena

Up to this point, we have considered only the simplest dynamical behaviour of flows between a rotating circular cylinder and a stationary square cylinder. This was necessary in order to establish the role of finite-dimensional effects in the onset and interaction of the various time-dependent modes which have been encountered so far. We now proceed to investigate more complicated dynamical behaviour in one mode in particular, with a view to identifying features of the dynamics which are of interest in relation to the change from continuous to discrete azimuthal symmetry in the flow domain.

The mode which was chosen for the study is the one which begins at the locus PE of Hopf bifurcations in figures 5.2 and 5.3. This has been referred to previously as the higher-frequency mode, and is the one which may be considered typical for the single cell at aspect ratios greater than one. We consider first the results of increasing the Reynolds number at a single value of the aspect ratio, namely $\Gamma = 1.28$. The singly-periodic mode which arises from the Hopf bifurcation at $Re = 500$ was found to persist until $Re = 665$. At this point, a *secondary* Hopf bifurcation was encountered. This is a bifurcation from a singly-periodic mode to a doubly-periodic mode, which is an oscillation comprising two distinct frequency components. Time-series obtained experimentally using an LDV system consist of the original oscillation with a regular modulation of the amplitude envelope. An example of the above sequence is shown in figure 5.4 for $\Gamma = 1.28$, where the measuring position using the dimensionless system proposed in Appendix B was

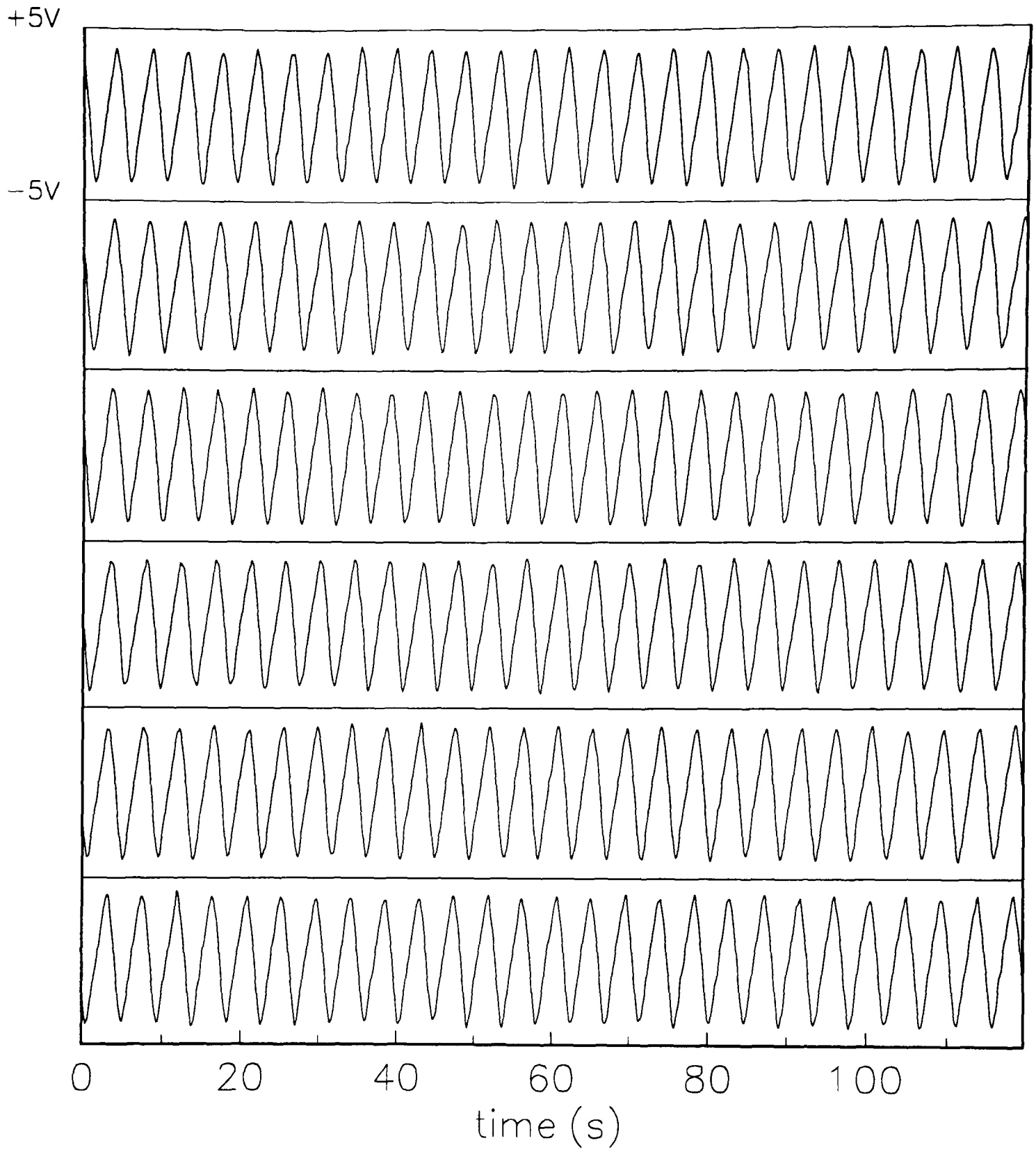

Figure 5.4 : Effect of a secondary Hopf bifurcation at $\Gamma = 1.28$. (a) Singly-periodic oscillation at $Re = 660.69$. Measuring position $h = 0.53$.

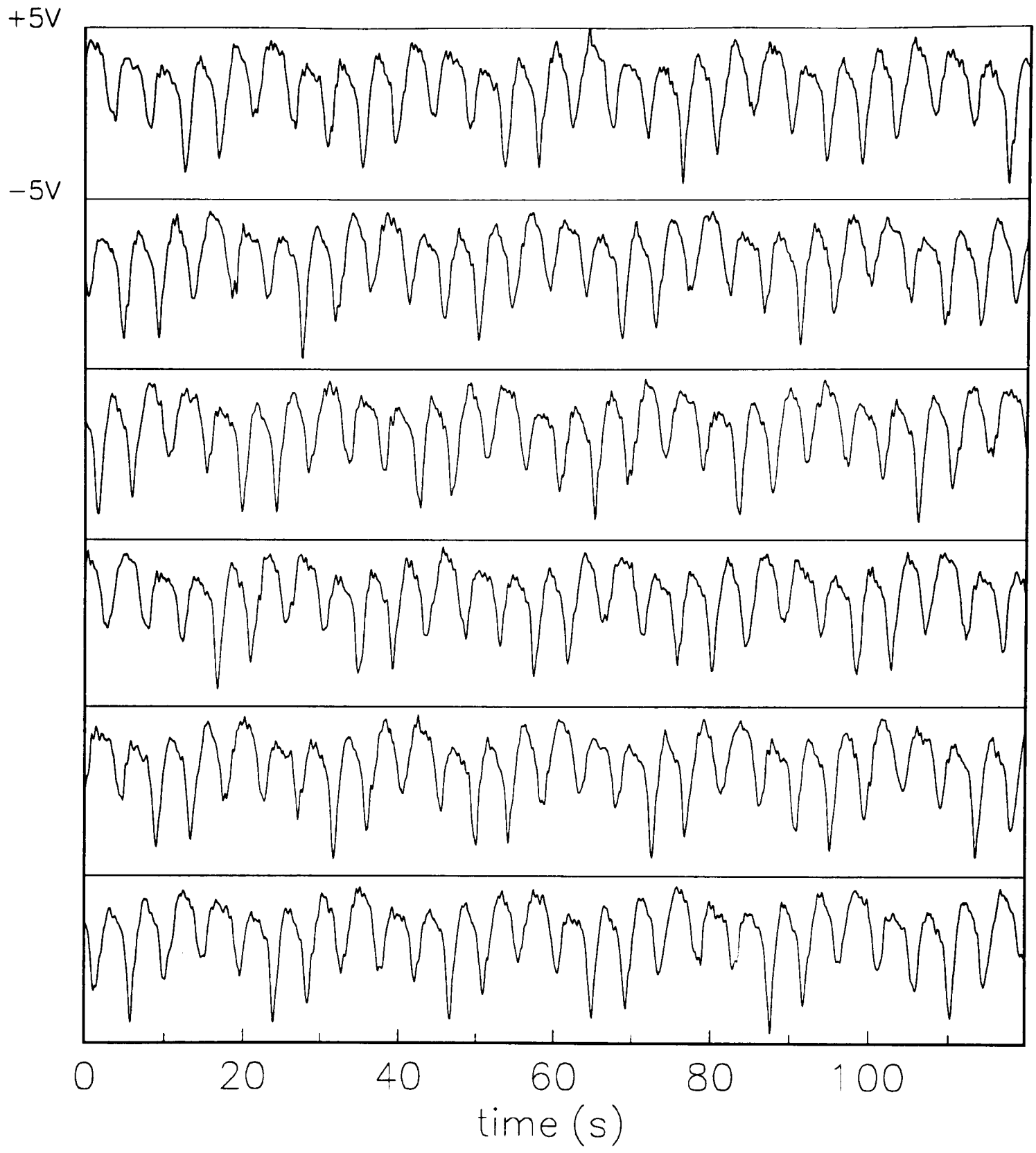

Figure 5.4 : Effect of a secondary Hopf bifurcation at $\Gamma = 1.28$. (b) Doubly-periodic oscillation at $Re = 677.24$. Measuring position $h = 0.53$.

$h = 0.53$. In figure 5.4a, the Reynolds number was at a value which was just below that associated with the secondary Hopf bifurcation. Here the time-series shows a regular oscillation with a constant amplitude. The Reynolds number was then increased to a value which was just above the secondary Hopf bifurcation and the resulting time-series is shown in figure 5.4b. The basic oscillation remains, but now the amplitude envelope is no longer constant. Instead there is a modulation at a frequency which is lower than the frequency of the basic oscillation.

An alternative representation of the effect of the secondary Hopf bifurcation is in terms of the phase-space reconstruction of the dynamics. This is performed computationally using the method of delays combined with singular value decomposition (SVD) as developed originally by Broomhead & King (1986). The two dynamic modes which were presented in the form of time-series in figure 5.4 are shown in figure 5.5 as phase-space reconstructions instead. The singly-periodic mode appears as a limit cycle in figure 5.5a, with the time taken for one orbit around the loop being equal to the period of the oscillation. The onset of a second frequency results in a torus in phase space, as shown in figure 5.5b. The basic oscillation corresponds to orbiting in the azimuthal sense, with the modulation producing the windings around the core. The utility of this form of representation of dynamics will become clearer shortly for the case of a particular oscillatory behaviour. However, it is important to state that the form of trajectories in phase space can be effected by the choice of measuring position within the time-dependent flow. A fuller discussion of this issue is given in Appendix B. It is stated here that all dynamic modes which were encountered in the course of this study were subjected to a vertical tra-

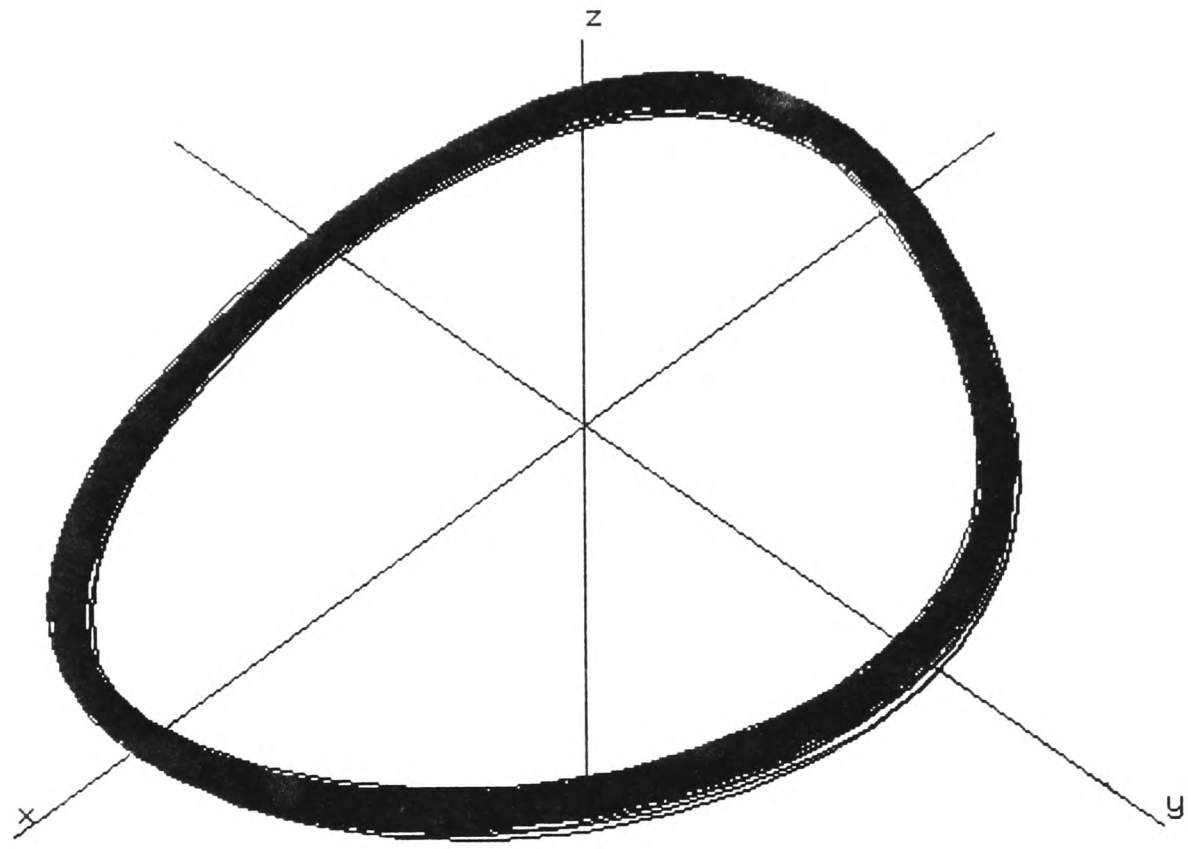

Figure 5.5 : (a) Reconstructed phase portrait from the time-series shown in figure 5.4a.

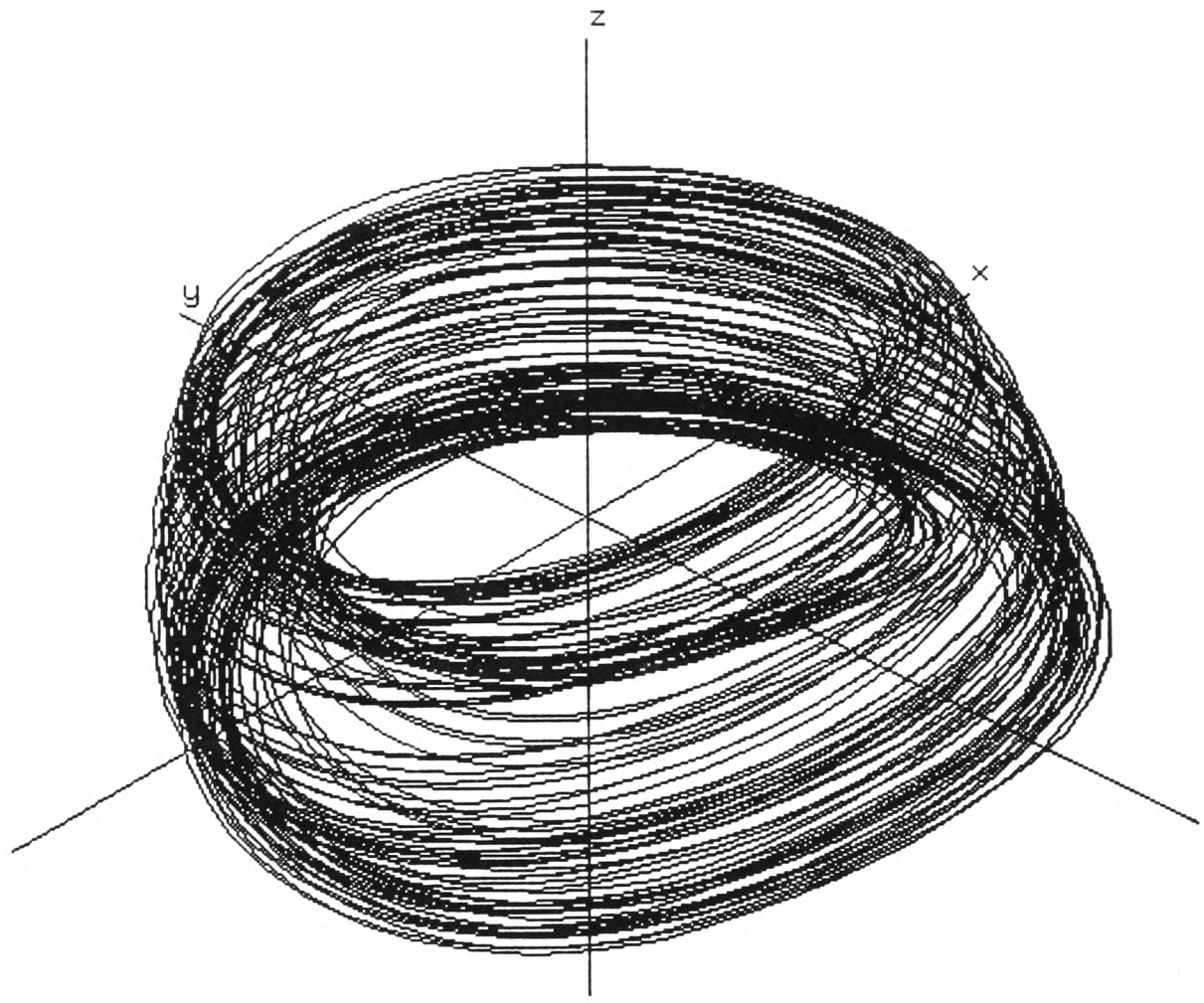

Figure 5.5 : (b) Reconstructed phase portrait from the time-series shown in figure 5.4b.

verse of the LDV measuring position through the flow. This was in order to ensure that measurements and recordings were made at a representative point within the domain.

The variation of the critical point for the secondary Hopf bifurcation was investigated experimentally over a range of aspect ratio. The results are shown in figure 5.6 as the locus ST, where the point T was the chosen limit on the range of measurement. The significant feature of these results is that they indicate an intersection of the line of secondary Hopf bifurcations with the locus RP of cyclic folds which marks the lower stability limit of the singly-periodic mode. Thus there is a codimension-2 bifurcation in parameter space, close to the point S in figure 5.6, where a cyclic fold and a secondary Hopf bifurcation occur simultaneously. The exact position of this bifurcation could not be determined experimentally because of the extreme sensitivity of the system to changes in the control parameters as the locus RP of cyclic folds is approached. The point S represents the closest position which was attainable with the present system, whose main limitation was the degree to which the aspect ratio could be varied without causing an excessive perturbation to the flow. Nevertheless, the experimental results strongly suggest that the locus ST intersects the locus RP. This is further attested to by the fact that the section of the locus RP above the point S marks the lower stability limit of the *doubly*-periodic mode, that is the modulated oscillation was found to persist with decrease of aspect ratio until this upper section of the line RP was crossed. The mode then collapsed catastrophically to the singly-periodic lower-frequency mode which originates at the Hopf bifurcation indicated by the locus DP in figure 5.6.

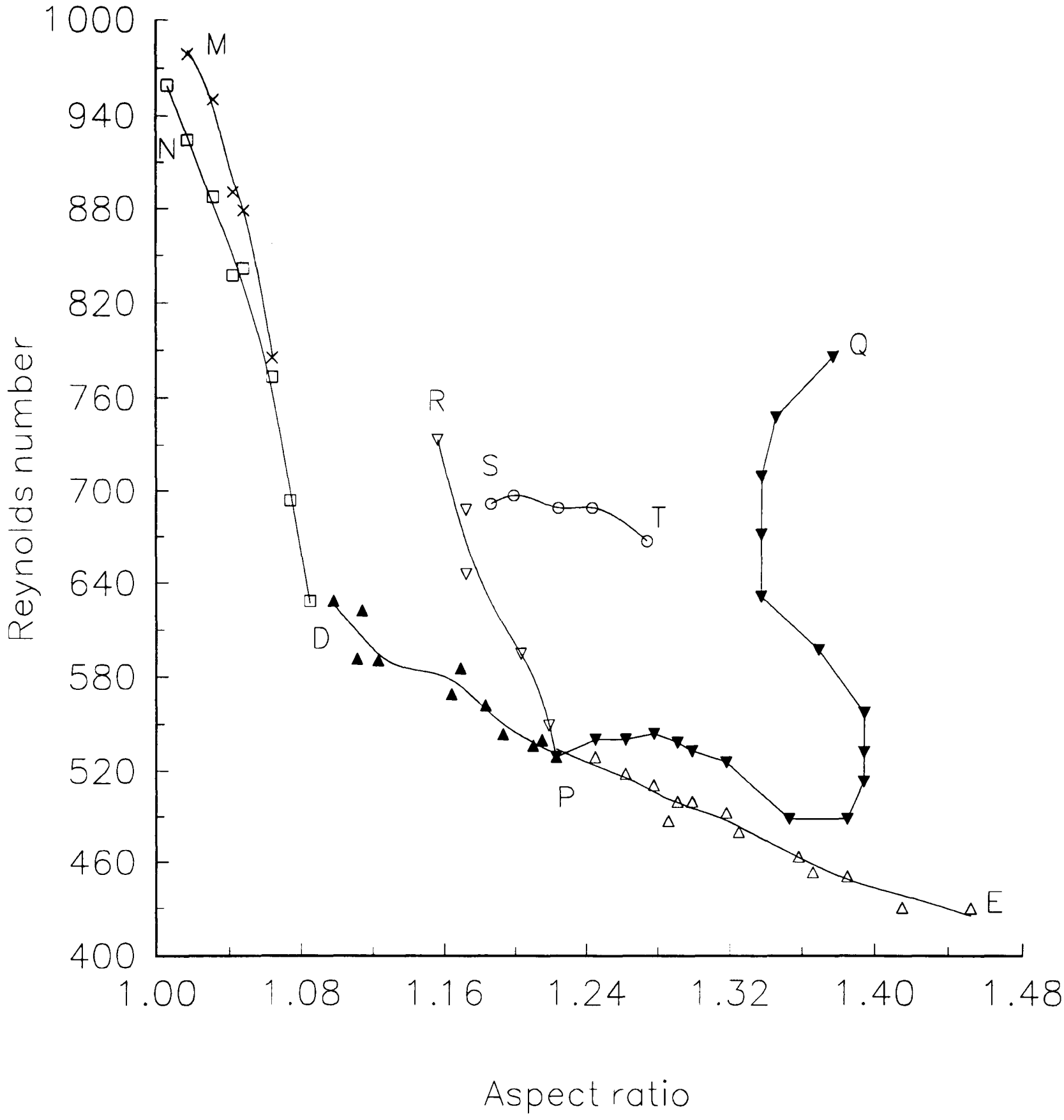

Figure 5.6 : Parameter space diagram incorporating locus ST (o) of secondary Hopf bifurcations from the singly-periodic mode established at PE.

The effect of increasing the Reynolds number from the regular doubly-periodic regime was investigated for a fixed value of aspect ratio $\Gamma = 1.25$. The behaviour of the flow remained qualitatively unchanged in the modulated oscillatory state until $Re = 766$. At this point, the previously regular modulated behaviour developed an irregular character. After a transient time corresponding to approximately 2400 revolutions of the inner cylinder, the flow was then observed to change to a new dynamic state. A time-series which captures the change in the flow is shown in figure 5.7. It was taken at a fixed set of parameter values ($\Gamma = 1.25$ and $Re = 766.07$), and the recording began immediately the Reynolds number was increased from $Re = 761$ to $Re = 766$. The long transient phase consists of the basic short-period oscillation together with a highly irregular modulation of the amplitude envelope. This eventually gives way to an apparently regular long-period oscillation with a dimensionless frequency of $\omega/\omega_c = 0.05$.

It would appear that the system has simply reverted to the basic long-period oscillation which we have already discussed in previous sections. However, we will see that the dynamics of this new state are quite different from anything which has been observed so far in this study. The next section of this chapter is given over to a description of the new mode, and to a discussion of the implications of its discovery for the role of symmetries in the Taylor-Couette problem in general.

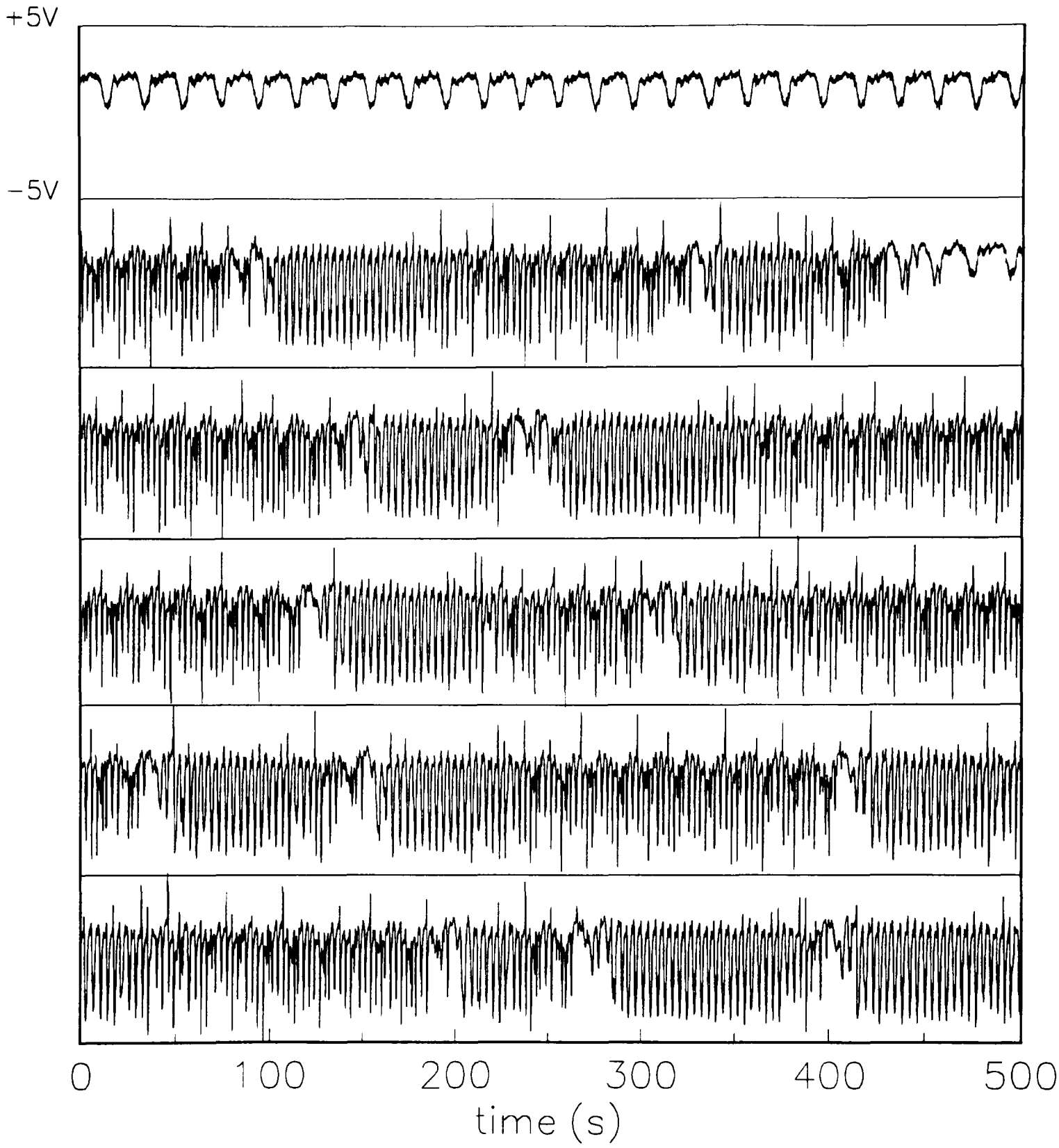

Figure 5.7 : Time-series recorded at $\Gamma = 1.25$, $Re = 766.07$. There is a long transient phase of irregular modulated behaviour before the system settles to a persistent regular oscillation. Measuring position $h = 0.50$.

5.3 Experimental dynamics and the Šilnikov mechanism

The time-series which is shown in figure 5.7 was recorded at a position in the flow approximately half-way between the two horizontal end-plates. In this representation, it appears that the new mode, which is established after the breakdown of the modulated flow, is a simple long-period oscillation of the type which has already been encountered. However, the results which are presented in Appendix B make it clear that the choice of measuring position can have an effect on the extent to which certain aspects of the fluid motion are captured by the measuring process. With this in mind, the measuring position was varied in order to determine whether the representation shown in figure 5.7 was typical of the actual dynamical mode.

It was found that when the measuring position was moved closer to the end corresponding to outward radial flow in the single Taylor cell, a significant change took place in the information content of the signal obtained from the laser Doppler velocimeter. The time-series which is shown in figure 5.8 was recorded at the same parameter values which were used to obtain the persistent state shown in figure 5.7, namely $\Gamma = 1.25$ and $Re = 766.07$. The only difference is that the location of the measuring point has been changed. It is now clear that there are in fact *two* elements in this particular flow. There is the lower-frequency oscillation which was detected initially at the first measuring position. In addition, there is a higher-frequency component which appears in finite sections throughout the time-series. This element was not detected at the earlier measuring position, where its amplitude was below the noise level in the LDV signal.

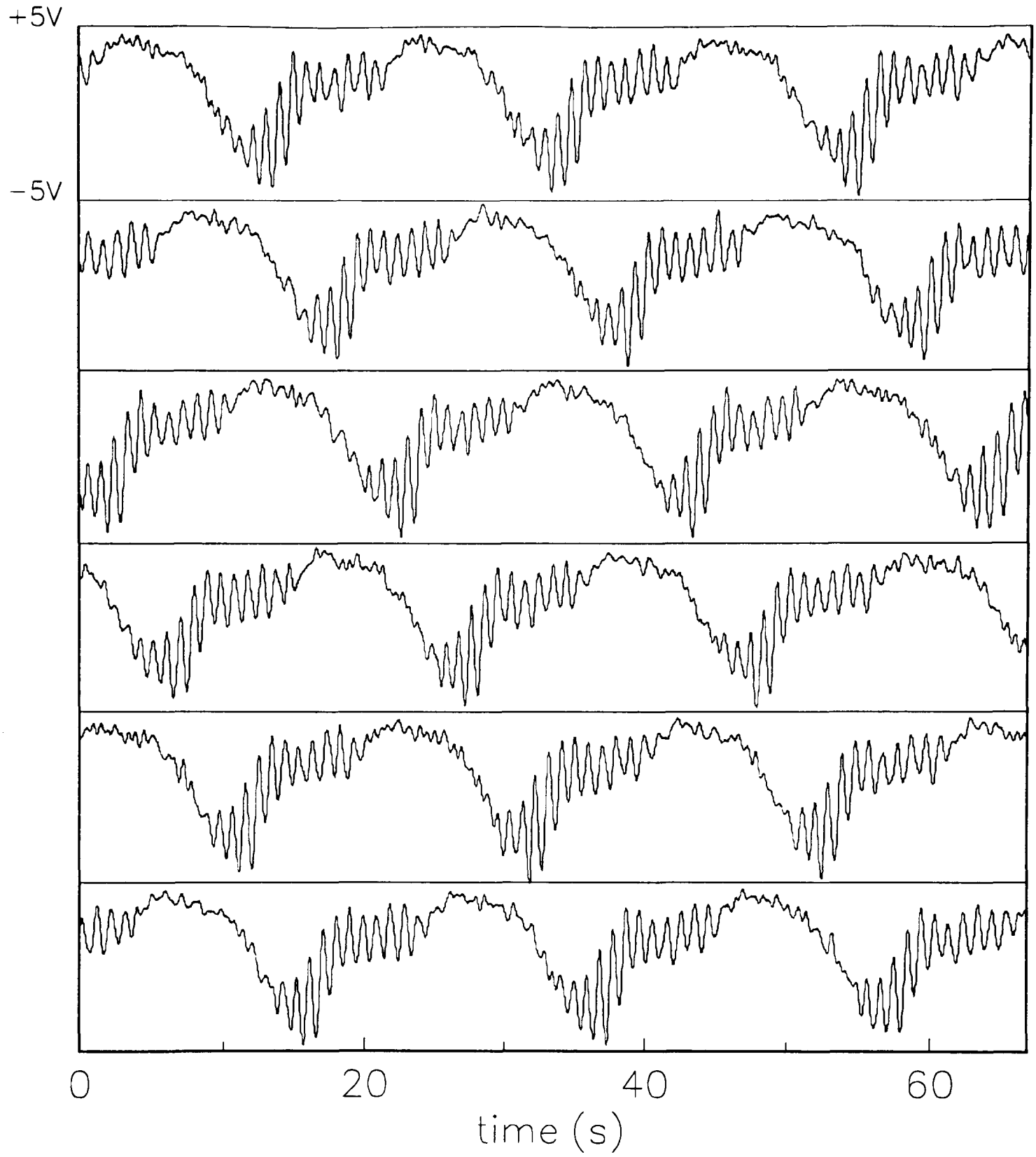

Figure 5.8 : Time-series recorded at $\Gamma = 1.25$, $Re = 766.07$ in the square system. Behaviour is that of persistent state shown in figure 5.7. New measuring position $h = 0.79$.

We have seen in the case of the collapse of the modulated flow that the system under investigation can exhibit relatively long transient phases before settling into a stable mode of behaviour. Thus it was important to consider the possibility that the time-series shown in figure 5.8 could be a mixed-mode transient, involving the system alternating between lower-frequency and higher-frequency behaviour before converging to one or the other as a final state. In order to settle this question, the system was left running for a time which corresponded to approximately 10^5 rotations of the inner cylinder. The dynamical state of the system was found to be unaltered at the end of this time, and so it was concluded that the motion being observed was a genuinely stable and persistent feature. Indeed, the mode in question was established several times from $Re = 0$, and its form was found to be the same each time.

Modern signal processing techniques were applied to the time-series shown in figure 5.8. In particular, the phase portrait of the dynamics was reconstructed. This allowed any significant temporal structures which may be of importance in controlling the dynamics as a whole to be observed geometrically. The phase portrait which was reconstructed from the time-series of figure 5.8 is shown in figure 5.9. It shows that the motion takes place on a somewhat distorted torus which has a narrow central core. The core begins at the far end of the torus, where the high concentration of points indicates that the flow spends a relatively long time in this region. Such behaviour suggests the presence of a weakly unstable fixed point, with the unstable direction being along the core of the torus. At the other end of the core, the motion appears to become unstable to perturbations in a plane perpen-

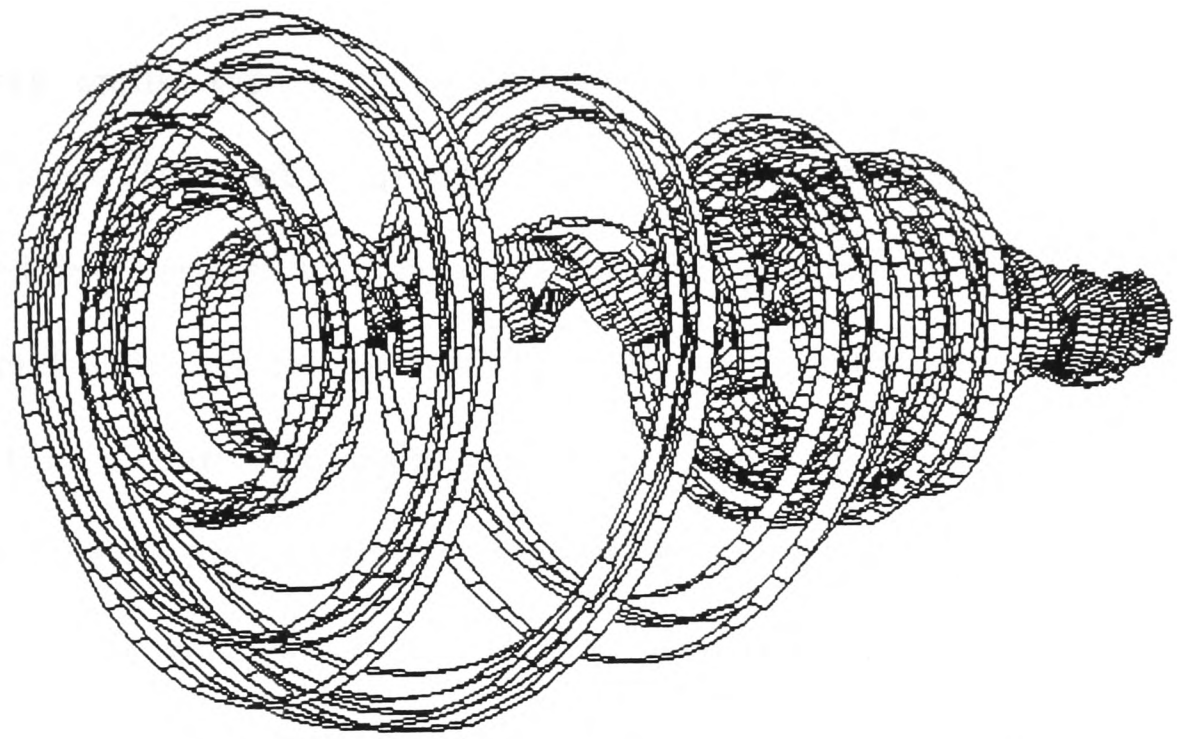

Figure 5.9 : Phase-space reconstruction using the time-series shown in figure 5.8.

dicular to the core. Individual trajectories can be seen to spiral outwards initially, and then wind back towards the far end of the attractor. A feature of this return mechanism is the high concentration of orbits just before the trajectories return to the weakly unstable fixed point. There is the suggestion of a weakly unstable limit cycle around the core which causes the system to spend a disproportionate length of time in its vicinity.

A very similar type of dynamical behaviour was observed experimentally by Mullin & Price (1989) while investigating a different Taylor-Couette problem. They considered flow between two concentric circular cylinders where the inner cylinder and the end-plates rotate together. The symmetries which are associated with the flow are thus a continuous azimuthal $SO(2)$ symmetry group around the annulus and a discrete $\mathbb{Z}_2$ mirror symmetry about the midplane of the annular gap. The particular mode which was studied was a time-dependent four-cell flow which had undergone a symmetry-breaking bifurcation with respect to the $\mathbb{Z}_2$ symmetry group. A time-series which was obtained from the flow by Mullin & Price using LDV is shown in figure 5.10, along with the reconstructed phase portrait in figure 5.11. The dynamics, in the form of the time-series in figure 5.10, involve two components of very different frequencies. There is a higher-frequency component which appears in short bursts, separated by a long quiescent phase. This is to be compared with the time-series data which has been obtained in the present study and is shown in figure 5.8. Here too we see similar bursts with quiescent phases in between. The comparison can be continued with the respective reconstructed phase portraits. The data of Mullin & Price is shown geometrically in figure 5.11, and is the result of the

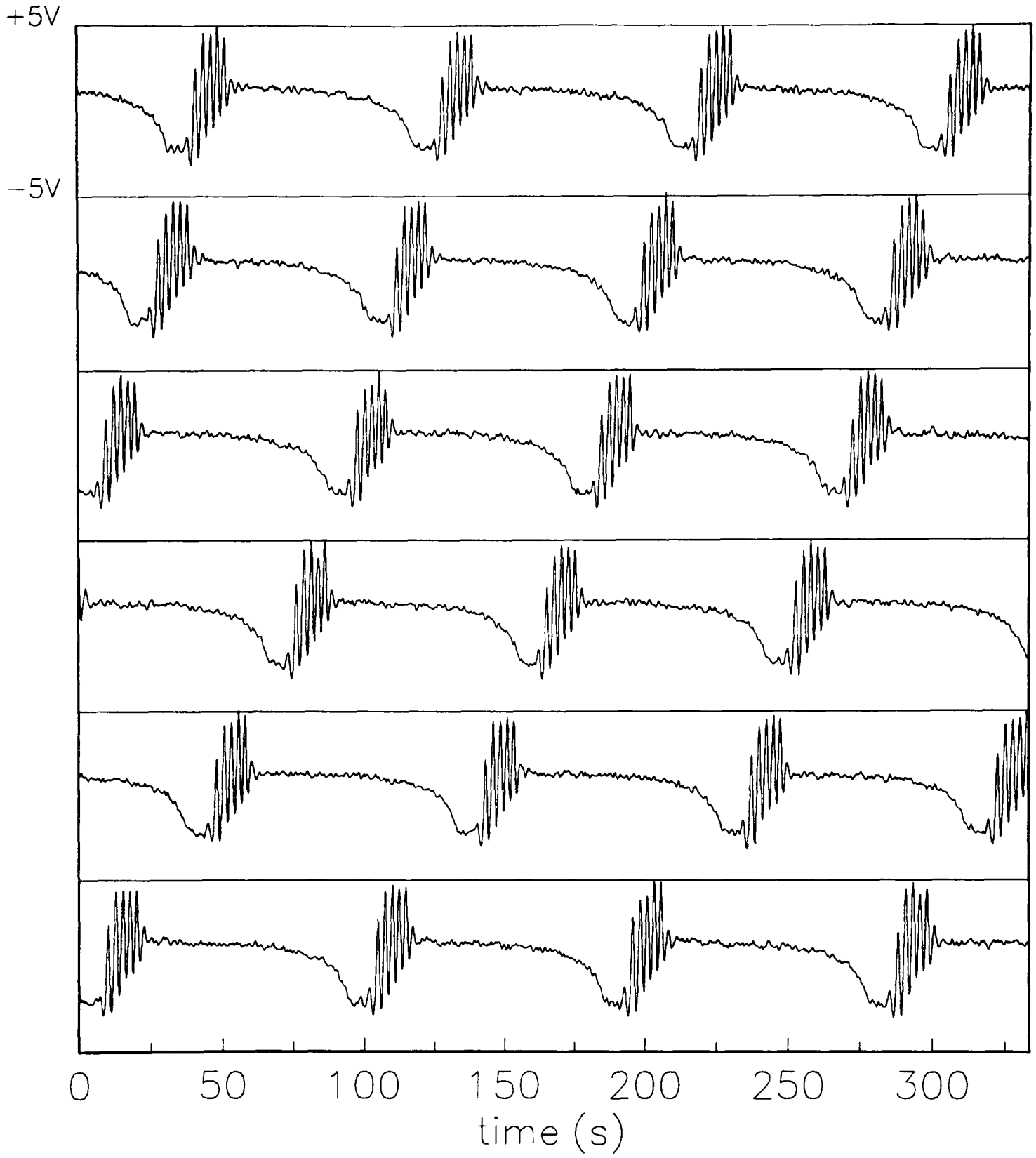

Figure 5.10 : Time-series recorded by Mullin & Price (1989) from an asymmetric four-cell flow in a Taylor-Couette system with SO(2) azimuthal symmetry.

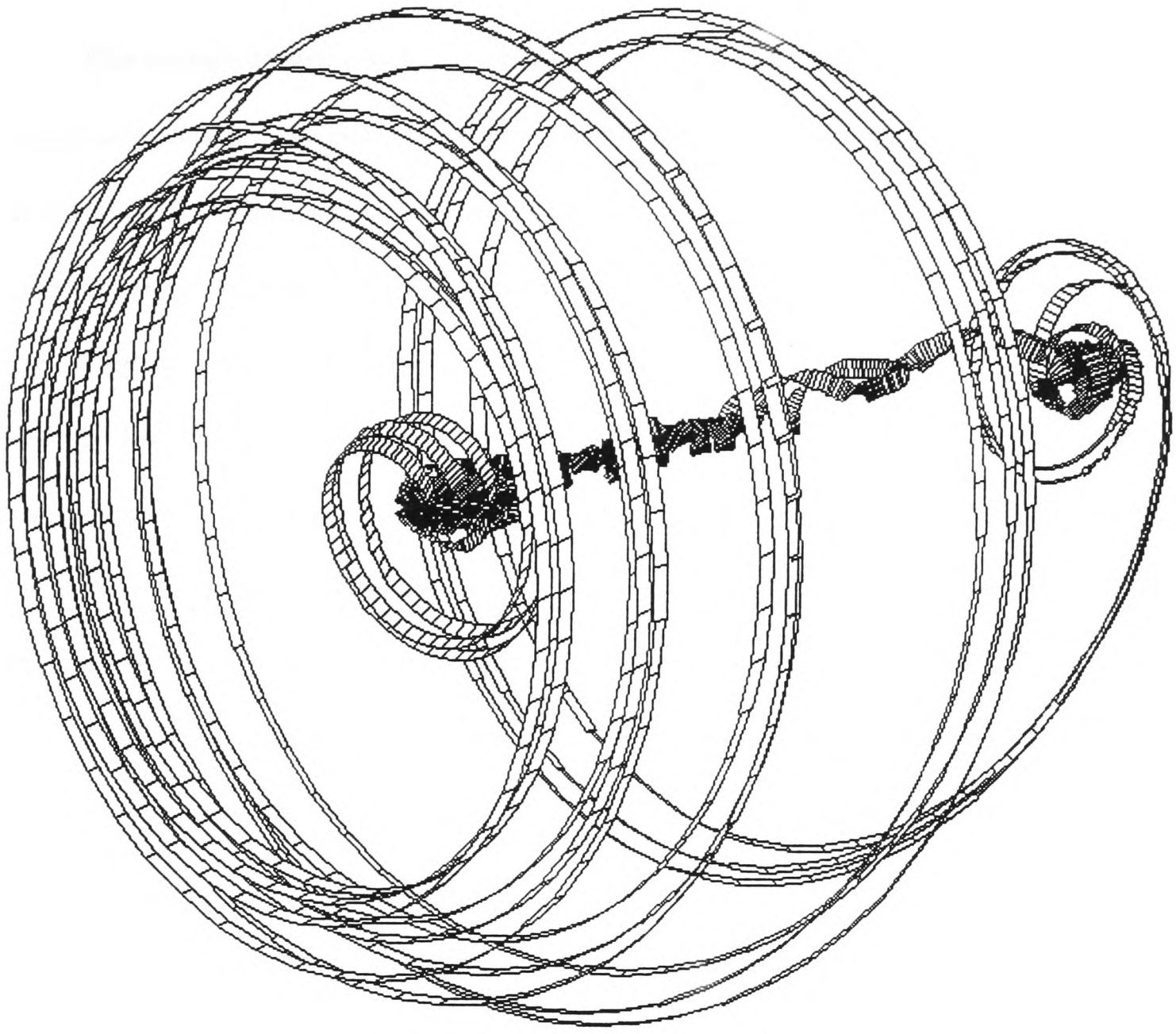

Figure 5.11 : Phase-space reconstruction using the time-series shown in figure 5.10. From *Mullin & Price (1989).*

same reconstruction procedure which was used to form the phase portrait shown previously in figure 5.9. We see in figure 5.11 the same type of structure, with a tight central core of trajectories and a spiralling motion around the outside.

The experimental results of Mullin & Price (1989) are significant because of the qualitative similarity between the reconstructed phase portrait and those obtained from a finite-dimensional mechanism for the onset of chaos known as the *Šilnikov phenomenon* (Šilnikov 1965). A comprehensive account of this mechanism is given by Wiggins (1990). It involves an orbit in phase space which is homoclinic to a saddle point where one of the manifolds is a spiral on a sheet and the other is a line perpendicular to the sheet. Such behaviour can indeed be seen to be consistent with the structures at either end of the core in figure 5.11, where the spiralling motion is inward at one end and outward at the other end. The relatively long period ($\sim$ 90s) associated with the oscillatory flow is an indication that the system is near a state of homoclinicity. Mullin & Price also showed that a small change in one of the control parameters (they varied the aspect ratio by 0.14%) results in a transition from the regular dynamics as shown in figure 5.10 to an irregular regime. In this state, the higher-frequency bursts arrive at intervals which are no longer equally spaced but vary in an unpredictable manner. Chaotic motion exists in the Šilnikov mechanism in the vicinity of the spiral homoclinic point, and can be shown to result from the variation of some external control parameter. Thus the results of Mullin & Price are strong indicators towards a possible connection between the Navier-Stokes equations, which are partial differential equations and hence infinite dimensional, and systems which are governed by ordinary differential equations and

result in finite-dimensional dynamics.

5.4 Comments

The results of the present study involving Taylor-Couette flow in a square configuration are also very suggestive of dynamics of the type which were considered by Šilnikov (1965) and have been observed experimentally in the Taylor-Couette system by Mullin & Price (1989). However, it was found in the present case that this mode of behaviour exists in only a very small region of parameter space and is therefore very difficult to investigate systematically. In particular, there was no clear observation of the transition between regular and irregular behaviour as reported by Mullin & Price. It is possible that the present system was not sufficiently close to a state of homoclinicity to allow such a transition to occur, and that the degree of control which was exerted over the governing parameters needed to be even greater to allow the resolution of events that exist very close to the limits of stability of this particular flow.

We end by stressing the similarities between the present results and those obtained by Mullin & Price. The key elements are those of linear and spiral trajectories in phase space, and long-period behaviour suggesting homoclinicity. In both cases the system had previously undergone a symmetry-breaking bifurcation to an asymmetric state, there being one cell in the present study and four cells in the study of Mullin & Price. The fact is that dynamics of this form have been found in both a four-cell flow under an $SO(2)$ symmetry group and in a single-cell flow under a

$\mathbf{Z}_4$ symmetry group. Thus it is proposed here that the Šilnikov mechanism for the onset of chaos is one which is related to the Navier-Stokes equations in a sense that is not necessarily restricted to a high degree of inherent symmetry.

CHAPTER SIX

Flows in a stadium Taylor-Couette system

The flows which have been considered up to this point have existed in a domain with $\mathbb{Z}_4 \times \mathbb{Z}_2$ symmetry. It has been shown that ideas from low-dimensional dynamical systems are valid in describing transitions which occur in both steady and time-dependent flows, and that such an approach provides a suitable context for comparisons with similar flows in the standard Taylor-Couette system. Novel fluid behaviour has been discovered, and in particular there is evidence that the Šilnikov mechanism, as observed by Mullin & Price (1989) in the standard system, persists under the change to the $\mathbb{Z}_4 \times \mathbb{Z}_2$ group.

The next stage of the present study was to take a further step in reducing the overall symmetry of the flow domain. To this end, the shape of the outer boundary was changed to that of a *stadium*, while retaining the rotating circular cylinder on the inside. This geometry has been illustrated previously in figure 2.3 of Chapter 2. The symmetry of the flow domain is now that of a $\mathbb{Z}_2 \times \mathbb{Z}_2$ group. The $\mathbb{Z}_2$ mid-plane symmetry of the majority of previous studies of Taylor-Couette flow is retained, but the azimuthal symmetry is reduced further from the continuous $SO(2)$ group of the standard system and the discrete $\mathbb{Z}_4$ group of the square system.

In sections 6.1 and 6.2, the steady two-dimensional flow is investigated using numerical and experimental approaches respectively. Preliminary results from a prototype apparatus are then presented in section 6.3 of time-dependent behaviour in the three-dimensional flow over a range of aspect ratios. Low-dimensional dynamics are observed at relatively small aspect ratios, but there is evidence of a direct transition to irregular flow at higher aspect ratios. This transition is compared in section 6.4 with similar behaviour which has been reported in other fluid systems. A second stadium apparatus was used to obtain more accurate results of the observed phenomena, and these are presented in section 6.5. Finally, the implications of the observations for Taylor-Couette flow in general are considered in section 6.6.

6.1 Numerical study of two-dimensional flow pattern

Studies of two-dimensional flows in systems which are geometrically similar to the present one have been carried out by Schumack *et al.* (1991) and Hellou & Coutanceau (1992). Schumack *et al.* used the spectral element method to solve for flow between a rotating circular cylinder and a cylinder which was formed from two circular arcs and is similar to an ellipse. The two-dimensional flow takes the form of approximately circular streamlines around the inner cylinder, and recirculation regions in both corner ends of the outer container. The problem which was tackled by Hellou & Coutanceau was that of two-dimensional flow which is driven by the rotation of a circular cylinder at the centre of a rectangular box. The solution was obtained both analytically using a truncated-series approach to the biharmonic equation, and experimentally using flow visualization techniques. Both methods give a flow field which comprises a main circular flow around the inner cylinder and driven recirculations in the outer regions of the domain.

On the basis of the results of the above studies, it should be expected that the two-dimensional flow between a rotating circular cylinder and a stationary stadium-shaped cylinder will have a similar qualitative form to that described above. In order to establish the exact nature of the flow, a numerical and an experimental approach were used together, and the results compared. The details of the numerical method are given in this section, along with the results in the form of a stream-function plot. The experimental approach is outlined in section 6.3, and photographs are shown of the two-dimensional motion.

The numerical technique is similar to the one adopted by Price (1991) for the calculation of two-dimensional flows in a triply-connected Taylor-Couette system. We will consider here the essential elements of the procedure. The governing equations for the motion of a viscous fluid are the Navier-Stokes equations. We are interested in steady flows where the inertia terms are negligible in comparison to the viscous terms, or equivalently when $Re \ll 1$. Under this approximation, the Navier-Stokes equations reduce to the equations for *creeping flow* as discussed by Acheson (1990), for example. These are

$$-\nabla p + \mu \nabla^2 \mathbf{u} = 0 \tag{6.1a}$$

and

$$\nabla \cdot \mathbf{u} = 0. \tag{6.1b}$$

The incompressibility condition (equation 6.1b) is automatically satisfied by the introduction of a scalar stream-function ψ. If $\mathbf{u} = (u, v, 0)$, then ψ is defined by $u = \partial\psi/\partial y$ and $v = -\partial\psi/\partial x$. It follows from this definition that

$$\nabla \wedge \mathbf{u} = (0, 0, -\nabla^2 \psi). \tag{6.2}$$

Taking the curl of both sides of equation 6.2 gives the *biharmonic equation* $\nabla^4 \psi = 0$.

Thus the problem is essentially one of solving the biharmonic equation with the appropriate boundary conditions. This was done here using the *finite-difference method* as discussed by Press *et al.* (1988). Differential operators were discretized on a grid of points which represented the flow domain, and calculations were performed iteratively on a *Masscomp 5600* computer. Ideally, the coordinate system

describing the grid should be chosen to match the flow domain. However, there is no convenient system for the present geometry. An alternative approach is that taken by Lewis (1979) for calculating the two-dimensional flow between a rotating circular cylinder and a square outer cylinder. A cartesian grid was used with a variable spacing to force grid points to lie on the boundaries of the flow domain. However, the approach adopted here followed that of Price (1991), who used a uniform cartesian mesh with a sufficiently small spacing to allow close approximation between the grid and the noncartesian boundaries. The excellent agreement obtained by Price between calculated and experimentally visualized flow fields is justification for this geometrical approximation.

The only appropriate form of boundary condition for the present problem is the no-slip condition applied to the inner and outer cylinders. Thus the fluid velocity is zero everywhere on the outer stadium, and directed tangentially with constant magnitude on the circular cylinder. The problem can be formulated to use these conditions by employing the *velocity-vorticity* formulation, as discussed by Churchill (1988). The vorticity of the velocity field is defined as $\nabla \wedge \mathbf{u}$, and it has already been shown in equation 6.2 that this vector quantity has only one nonzero component in this case, namely $-\nabla^2\psi$. Thus we may introduce a scalar ω for the vorticity such that

$$\nabla^2\psi = -\omega \tag{6.3a}$$

and

$$\nabla^2\omega = 0. \tag{6.3b}$$

Finally, we make use of the standard vector identity $\nabla^2\mathbf{u} = \nabla(\nabla \cdot \mathbf{u}) - \nabla \wedge (\nabla \wedge \mathbf{u})$

and the incompressibility condition $\nabla \cdot \mathbf{u} = 0$ to give

$$\nabla^2 \mathbf{u} = -\nabla \wedge (\omega \mathbf{k}) \tag{6.4a}$$

and

$$\nabla^2 \omega = 0. \tag{6.4b}$$

The computer algorithm for solving equations 6.4a and 6.4b is initiated by labelling all the points in the uniform cartesian grid on the basis of whether they are inside or outside the flow domain. Subsequent operations are then carried out on internal points only. A plot of the 200×100 grid point distribution which was used for the present calculations is shown in figure 6.1. New values of the velocity components u and v were calculated using the discretized form of equation 6.4a. These values were then used to update the boundary values of the vorticity before calculating the new vorticity field using equation 6.4b. The vorticity was then time-stepped before repeating the entire procedure. The calculation was halted when the solution had converged to an accuracy of 0.1%. The velocity field was then integrated to give the value of the stream-function at every point within the flow domain. These values were used to plot contours of constant stream-function, namely the streamlines of the flow.

The result of applying the above procedure to the present problem is the streamline plot shown in figure 6.2. Here it can be seen that there are indeed three separate regions which are analogous to those of previous studies in similar systems. There is a main circulating flow close to the inner cylinder, and two recirculations

on either side. The values of the stream-function show that the recirculations are weaker than the circular flow, although they still occupy a significant area within the flow domain.

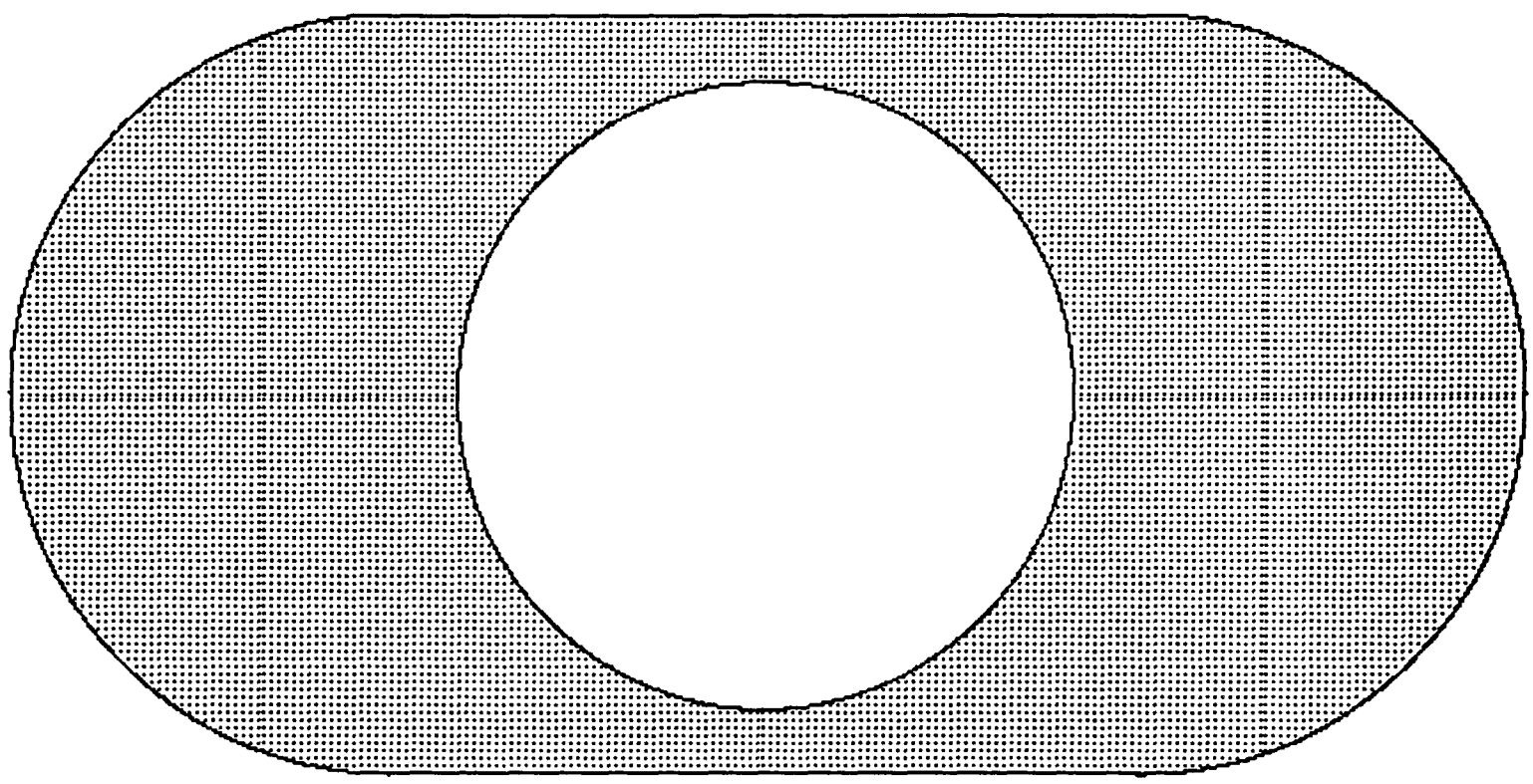

Figure 6.1 : Discretization grid of 200 $\times$ 100 points used for numerical calculations in the stadium domain with clearance ratio 0.824. Any apparent nonuniformity in the grid spacing is due to a finite resolution of printing.

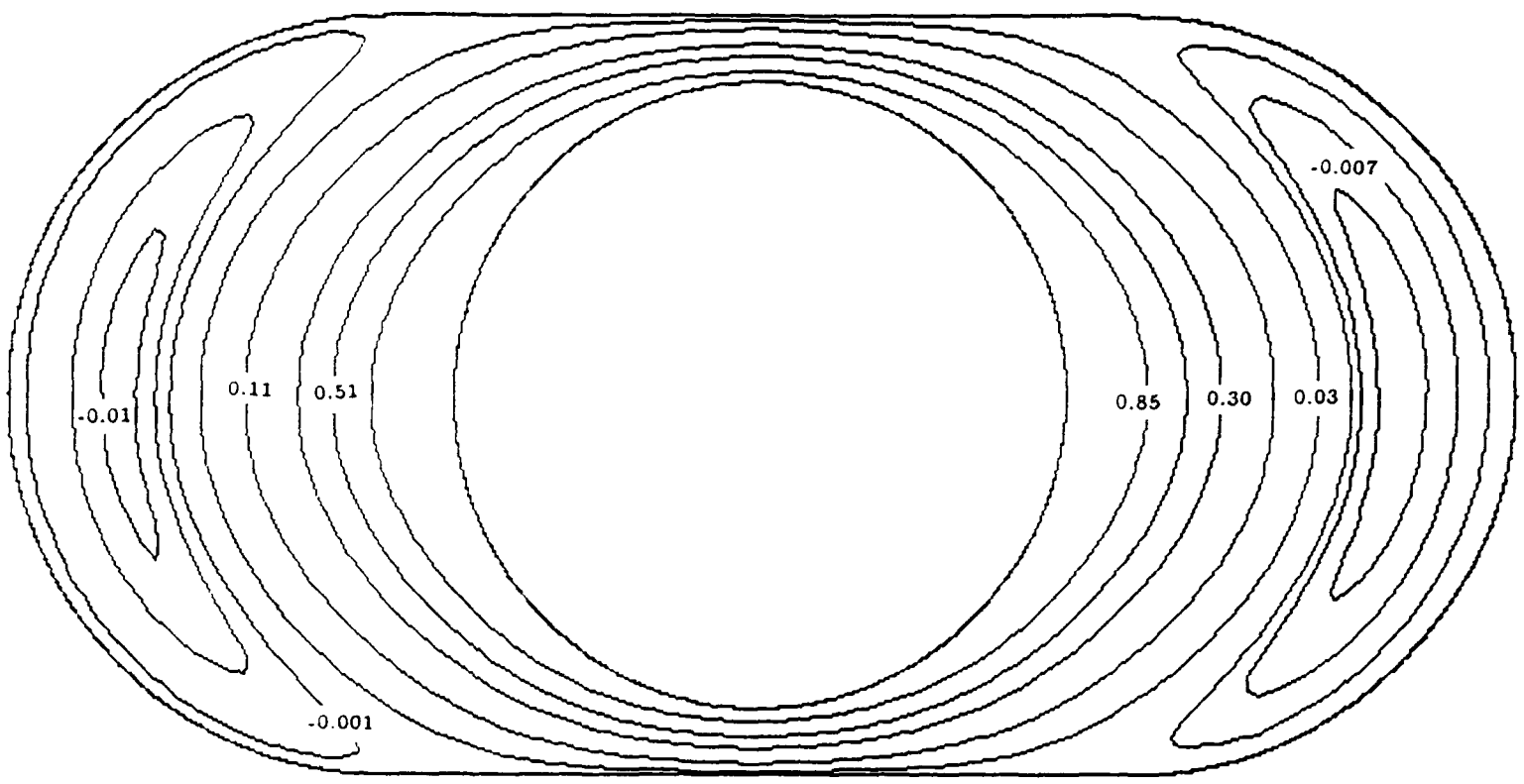

Figure 6.2 : Streamlines for two-dimensional flow in the stadium Taylor-Couette system.

6.2 Experimental study of two-dimensional flow pattern

Experimental visualization of the two-dimensional flow was carried out in order to obtain a comparison with the numerical results of section 6.1. The prototype stadium apparatus (described in Chapter 2) was filled with pure glycerol to a depth of approximately 2 cm. A small quantity of $\sim$ 0.2 mm Styrene beads was then spread uniformly on the surface of the glycerol layer. The flow which was driven by rotation of the inner cylinder was viewed from underneath the rig with a diffuse light source in the background. This had the effect of showing the Styrene beads as tiny dark specks against an otherwise uniform light field. An Olympus OM-4 Ti camera was used with Fujichrome 64T colour slide film to record the paths of the beads as they moved with the flow. Exposure times were set to approximately 10 s in order to capture the relatively weak recirculations outside the main rotating flow.

An example of the results of the visualization experiments is shown in figure 6.3. The photograph was taken with the system operating at a Reynolds number (based on the minimum gap between inner and outer cylinders) of $Re \approx 1$ and with clearance ratio $\eta = 0.824$. Only half the domain is shown to enhance the resolution of the flow pattern. The distinct regions of the flow can clearly be seen. Firstly, there is the circulating flow close to the inner cylinder. Then there is the crescent-shaped recirculation which is driven by the main flow. Exposure times were set to be sufficiently long that the relatively slow motion in the outer region would be recorded. Consequently the much faster motion near the inner cylinder does not appear as distinguishable particle paths. The slight overall skewness of the flow field is caused

by inertial effects, which are unavoidable at nonzero values of the Reynolds number. The skewness may be lessened by further reducing the Reynolds number, but the value of $Re \approx 1$ was the lowest value at which recordings could be made satisfactorily using the present system. Despite this problem, it is nevertheless clear that the experimental and numerical representations of the two-dimensional flow field are in good agreement.

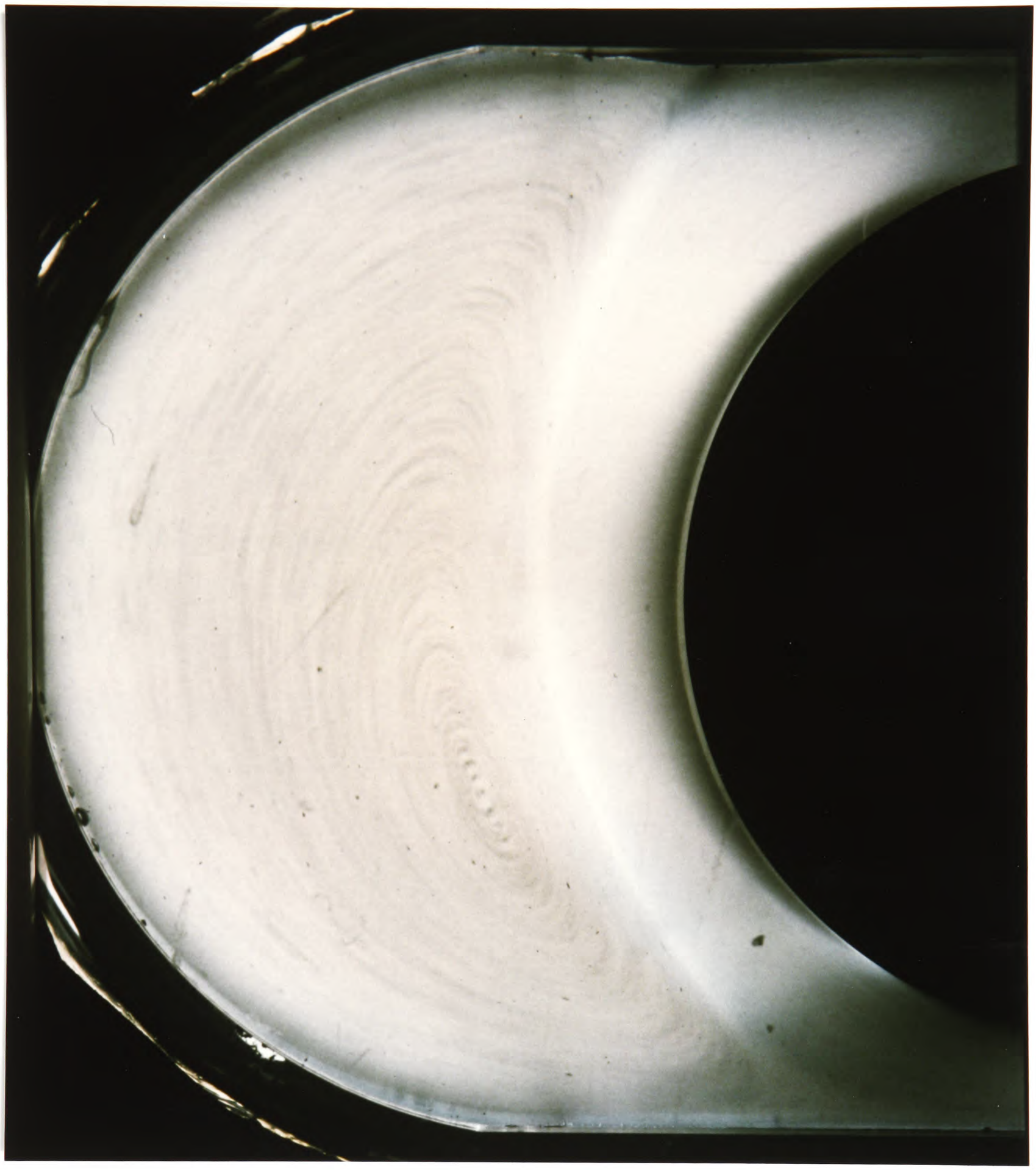

Figure 6.3 : Photograph of two-dimensional flow in one half of the stadium Taylor-Couette system at $Re \approx 1$.

6.3 First results for time-dependent flows

The main objective of studying flows in the stadium Taylor-Couette system is to determine whether the gross departure from the $SO(2)$ symmetry of the standard system has a significant effect on the nature of time-dependent flows. It is the role of finite-dimensional dynamics in particular that we wish to investigate, and whether or not such dynamics persist with this further reduction of the azimuthal symmetry of the flow domain.

Experiments were carried out to investigate the general form of the dynamics in a stadium Taylor-Couette system of finite extent. It was observed initially that steady cellular flow exists close to the inner cylinder above a certain range of Reynolds number. This is consistent with the results for the two-dimensional configuration, from which it can be seen that Rayleigh's criterion holds for the region of approximately circular flow. The Taylor vortices in the main flow in turn drive certain three-dimensional structures in the outer recirculation regions. Since the work of Benjamin (1978a,b) on the standard Taylor-Couette system, it has become clear that the number of vortices in the primary mode, which develops with quasistatic increase of the Reynolds number, is directly determined by the aspect ratio of the system. This also appears to be the case for the stadium Taylor-Couette system. Radial velocity profiles which were taken at aspect ratios $\Gamma = 4$ and $\Gamma = 8$ in a system with clearance ratio $\eta = 0.8$ show the presence of flow near the inner cylinder with four and eight vortices respectively. However, the exact details of the cellular structure of the flow and the dependence on aspect ratio are beyond the

scope of this study. A great deal of careful and intricate work of the type carried out by Mullin (1982) in the standard Taylor-Couette system is required to understand this mechanism fully. At the present stage of the investigation, it is sufficient to recognize that the flows have a cellular nature, and that there is undoubtedly a wealth of structure still to be determined for the variation of the number of cells with aspect ratio.

To begin with, a prototype apparatus was used in conjunction with a laser Doppler velocimeter to observe the time-dependent behaviour over a range of aspect ratio from $\Gamma = 3$ to $\Gamma = 11$ at a clearance ratio $\eta = 0.824$. This allowed various dynamical features to be identified, which were then studied more rigourously in a second flow rig that was made to a much higher specification than the prototype. The results of these experiments are presented below in the form of time-series, phase portraits and parameter-space diagrams.

The prototype flow rig was shown in figure 2.4 of Chapter 2. It was filled with silicone oil which had previously been seeded with latex spheres (also described in Chapter 2). Experiments were performed with a background air-conditioning system to regulate the temperature of the working fluid, which was measured using a mercury thermometer in the fluid above the movable top plate. The temperature was found to vary between 21.0°C and 23.0°C over the course of the experiments, leading to a variation in viscosity between 16.9 $mm^2s^{-1}$and 16.5 mm^2s^{-1}. Measurements of the inner cylinder rotation speed were always accompanied by measurements of the fluid temperature in order to allow the Reynolds number to be

determined reasonably accurately (approximately 2%) for the purpose of this initial study. The aspect ratio of the system was determined by using a ruler to measure externally the height of the top plate above the base of the flow rig. Again, this proved sufficiently accurate for the present purpose.

An important consideration was the position within the flow at which measurements should be made. Results which were obtained at a measuring point located in the centre of either the main rotating flow or one of the recirculations were found to be unrepresentative of the dynamics as a whole. If the measuring position was instead at the interface between the two regions, then the signal was found to capture the respective time-dependent motions without undue bias towards one or the other. Thus the measuring position was placed approximately at the interface in the widest part of the gap between inner and outer cylinders, and midway between the horizontal boundaries which define the height of the flow domain.

The results which were obtained using the above set-up are shown in figure 6.4 in the form of a parameter-space diagram whose axes are aspect ratio and Reynolds number. The initial transition from steady to time-dependent flow is marked by the locus AB. A Hopf bifurcation to a singly-periodic flow was found at each of the measured positions along this line. The dimensionless frequency of the oscillation at onset was found to be $\omega/\omega_c \approx 0.1$ across the whole range of aspect ratio which was investigated. The locus is marked with a dashed line to indicate that the measured bifurcation points are not all from the same cellular flow, but rather that this is the general trend of the Hopf bifurcation for increasing aspect ratio and therefore

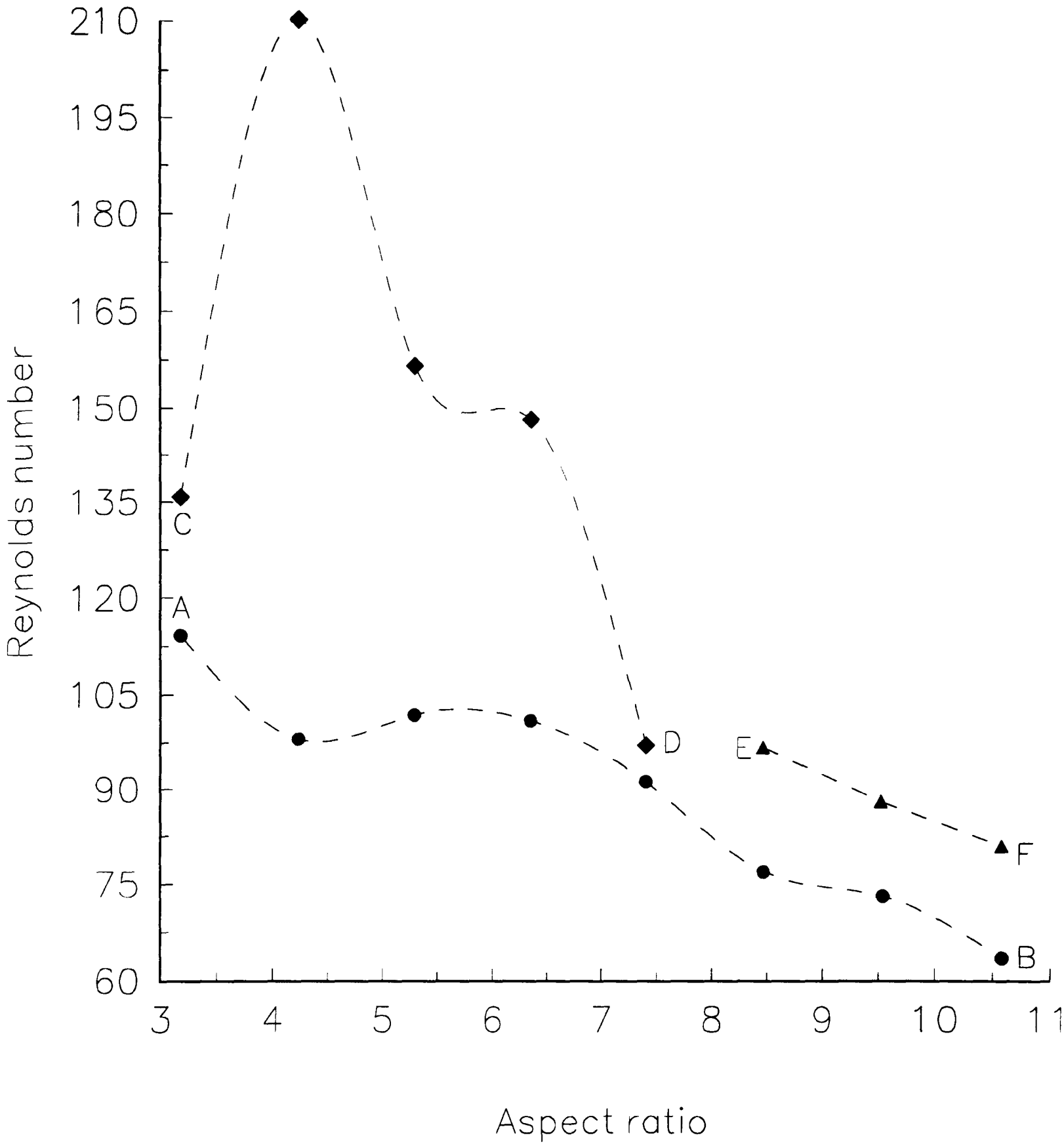

Figure 6.4 : Parameter space diagram showing bifurcation structure in the prototype stadium system with $\eta = 0.824$. AB (●) is locus of Hopf bifurcations. CD (♦) is locus of period-doubling bifurcations. EF (▲) is locus of transitions to irregular behaviour.

increasing numbers of cells in the primary mode.

The Reynolds number was then gradually increased further in order to investigate the nonlinear development of this initial oscillation. For aspect ratios between $\Gamma = 3$ and $\Gamma = 7.5$, the next qualitative change in the motion was that of a *period-doubling* bifurcation of the original oscillation. An example of this transition was recorded at $\Gamma = 5.0$ and is shown in figure 6.5. The time-series shown in figure 6.5a was taken when the Reynolds number was just below the critical value for period-doubling. The oscillation has an amplitude envelop which is constant to within the noise level of the LDV system. The presence of harmonics in the signal is presumably due to nonlinear effects which result from placing the measuring volume at the interface between the rotating flow and the recirculating flow. The Reynolds number was then increased to just beyond the period-doubling bifurcation, and the oscillation changed to having alternating high and low peaks as shown in figure 6.5b. The time-series of figure 6.5a and 6.5b are represented geometrically in figures 6.6a and 6.6b respectively as reconstructed phase portraits. The transition in phase space is between a simple limit cycle (figure 6.6a) and a 'double' limit cycle (figure 6.6b) where trajectories now take twice the original time to return to any starting position on the attractor. The effect of harmonics in the signals can be seen in this case by the fact that both the single and double limit cycles are distorted out of the plane.

As was stated in the Introduction, period-doubling bifurcations form one of the standard routes to chaos in dissipative nonlinear systems. The simplest occurrence

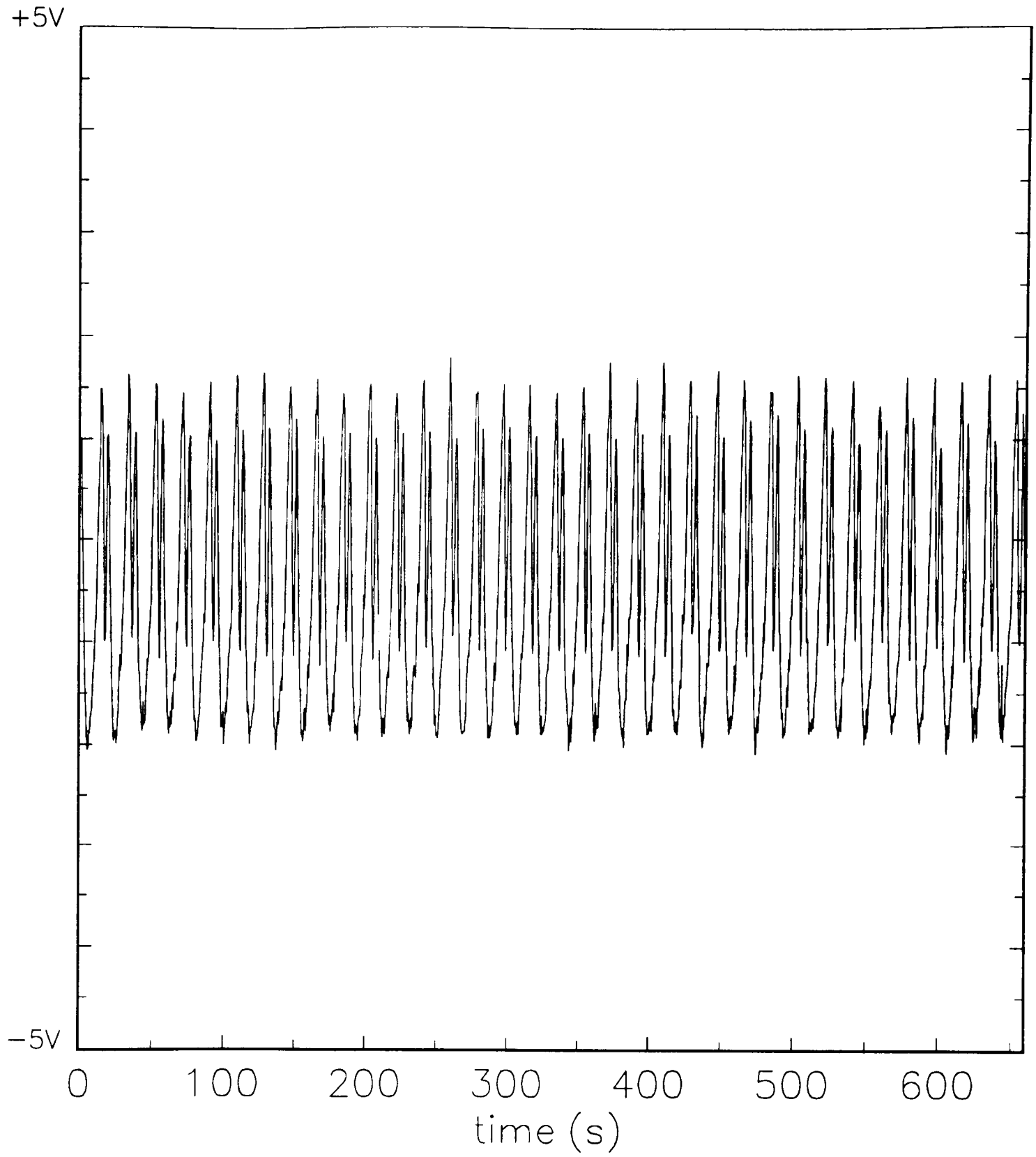

Figure 6.5 : (a) Singly-periodic behaviour in the prototype stadium system at $\Gamma = 5.0$, $Re = 168.5$.

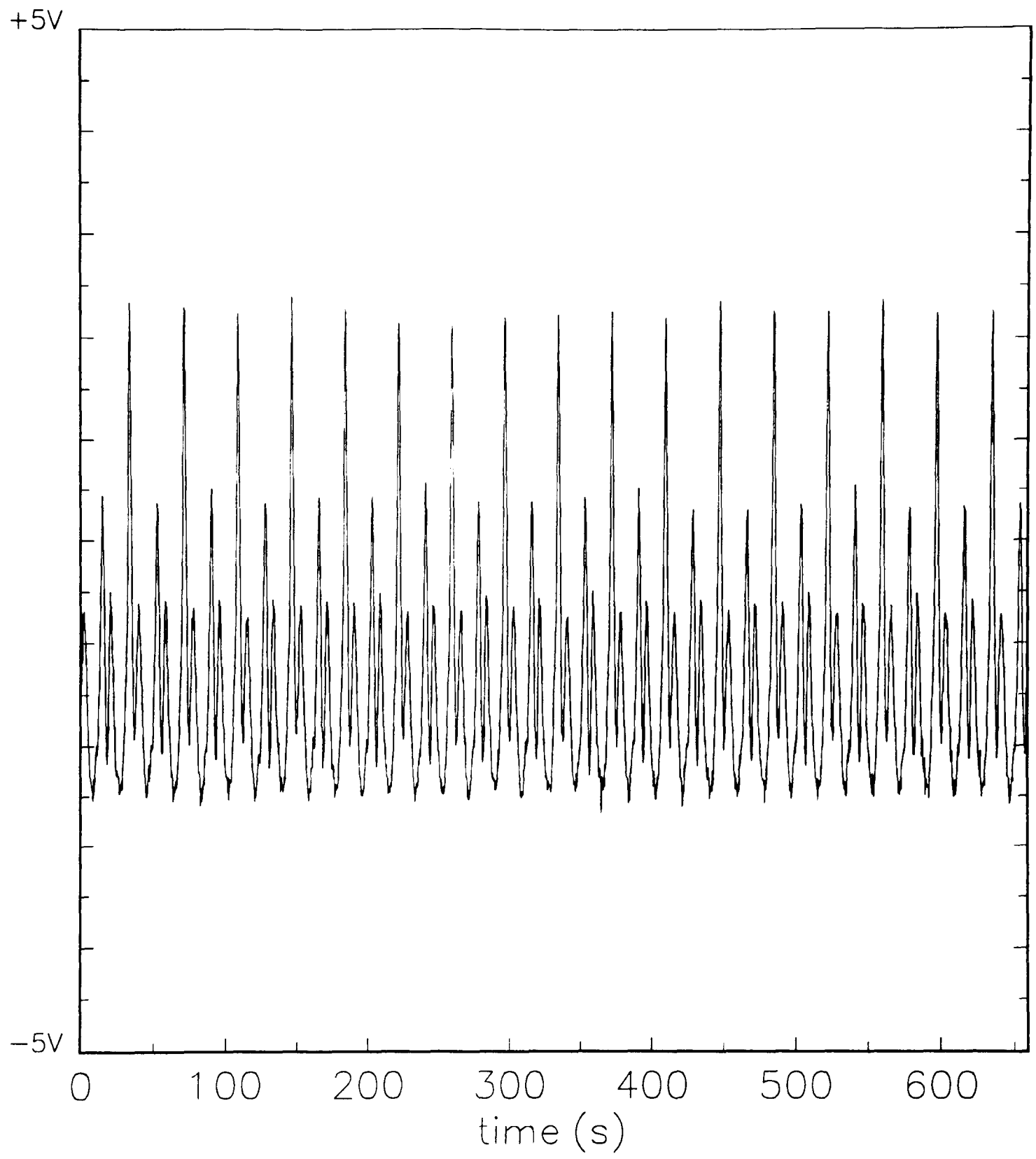

Figure 6.5 : (b) Period-two behaviour in the prototype stadium system at $\Gamma = 5.0$, $Re = 175.2$.

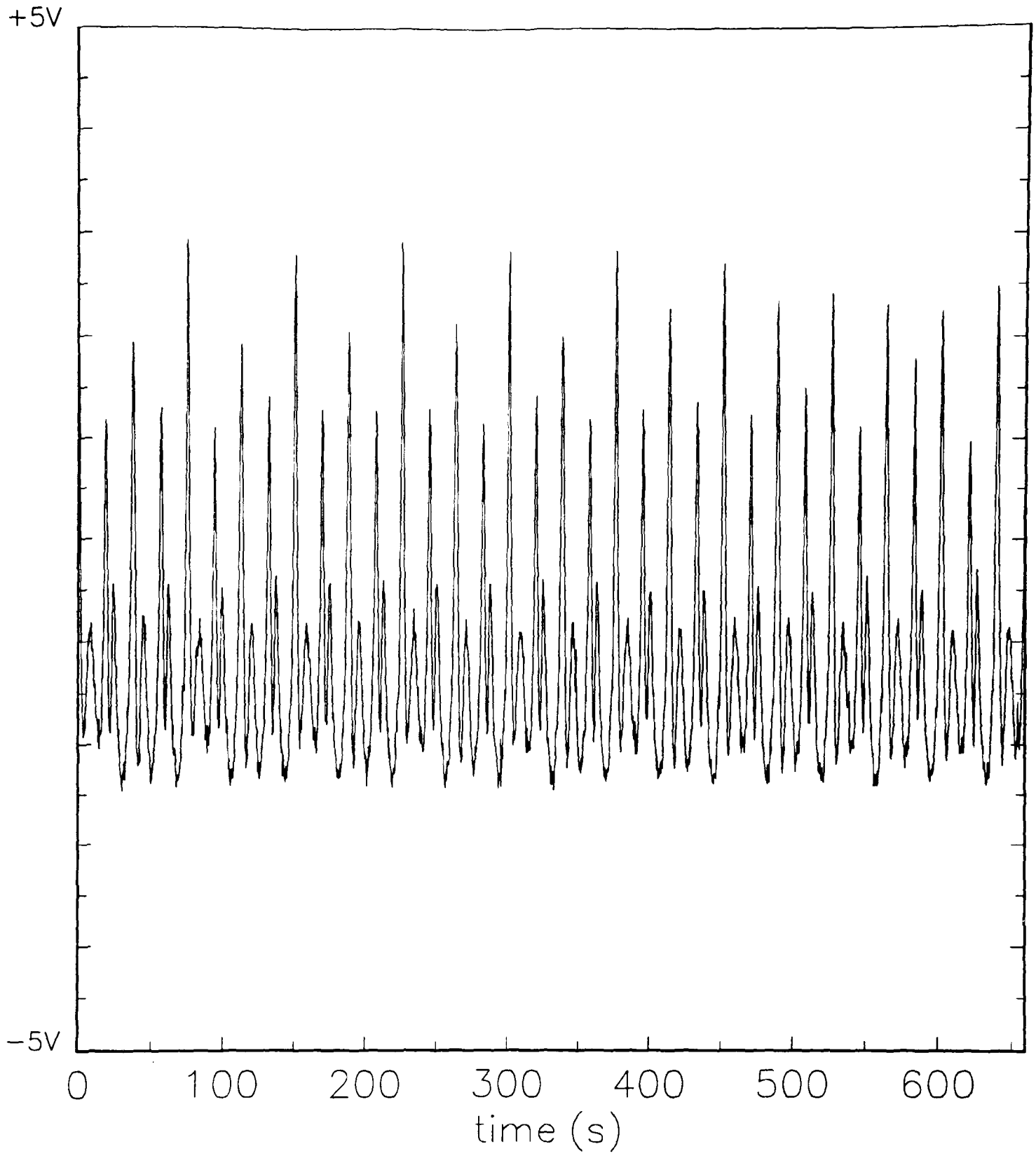

Figure 6.5 : (c) Period-four behaviour in the prototype stadium system at $\Gamma = 5.0$, $Re = 182.7$. The system can be seen to drift back into period-two behaviour towards the end of the recording.

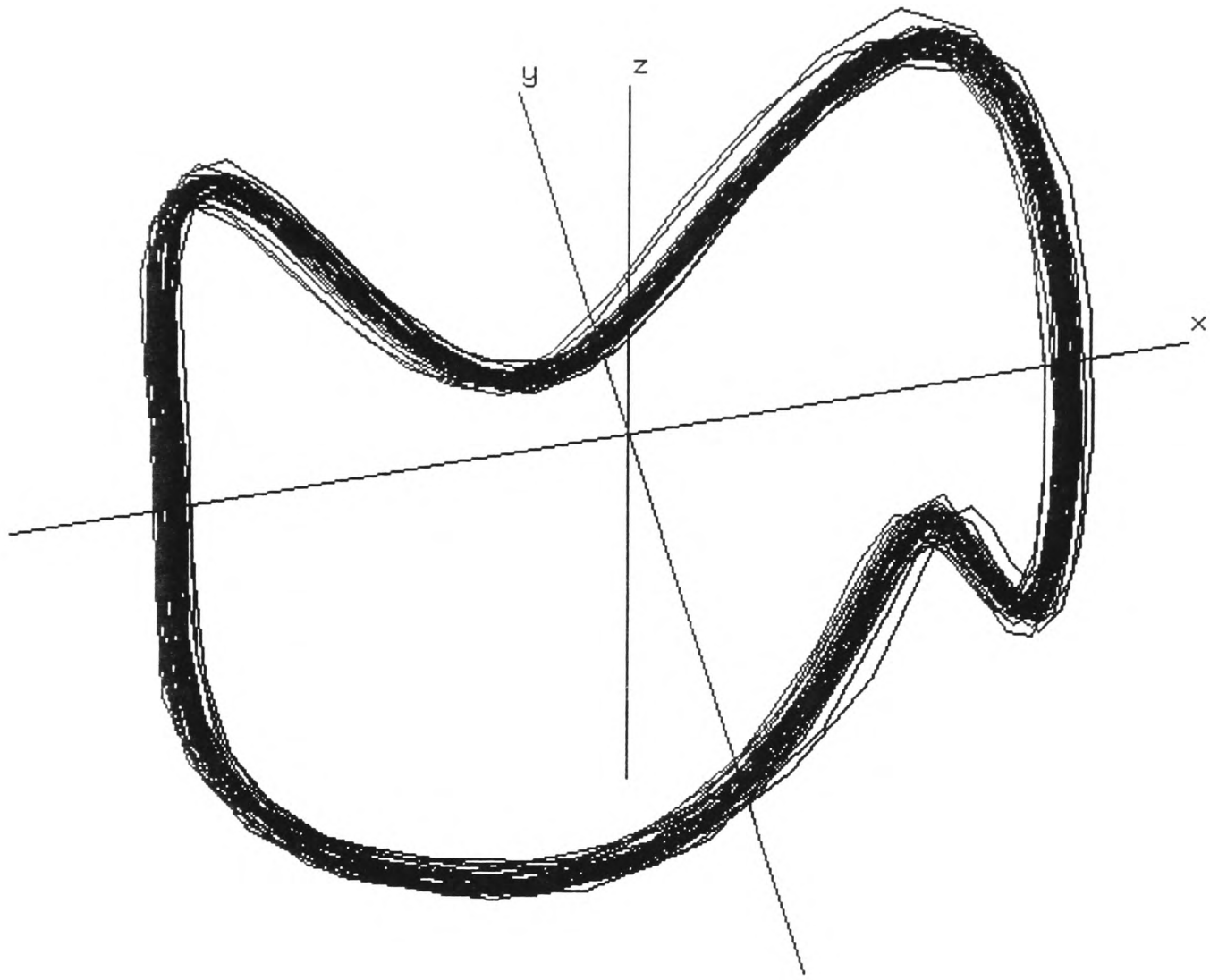

Figure 6.6 : (a) Reconstructed phase portrait from the time-series shown in figure 6.5a. This has the form of a limit cycle which is distorted by harmonic effects.

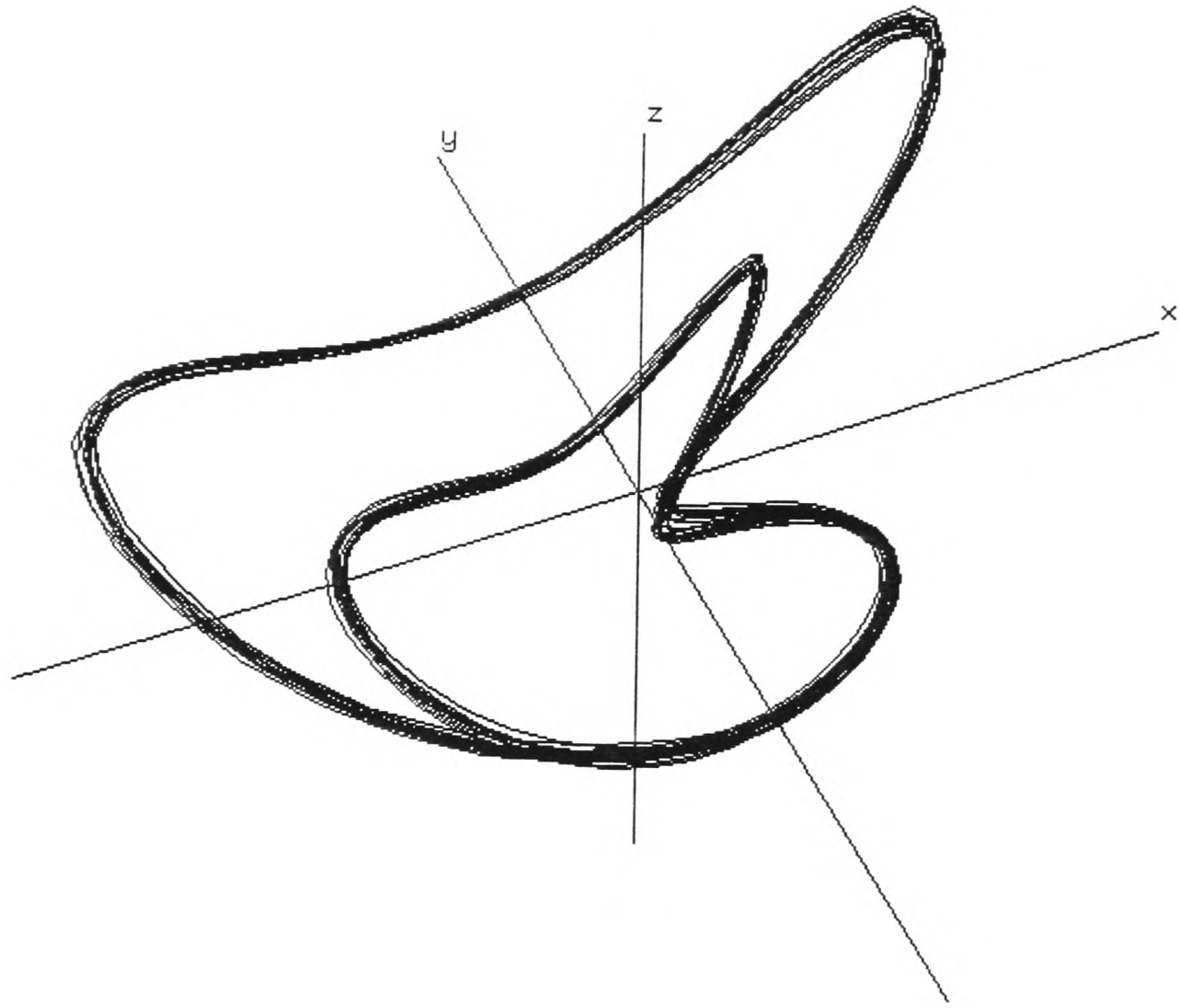

Figure 6.6 : (b) Reconstructed phase portrait from the time-series shown in figure 6.5b. The limit cycle is now split so that it takes twice the original time for trajectories to return to a given starting position. Harmonic effects are again evident.

of period-doubling is in the iteration of one-dimensional unimodal maps. It can also be found in various fluid systems, typically when the flow domain is restricted sufficiently to allow only a small number of modes to exist. Libchaber & Maurer (1980) reported period-doubling in the convection of liquid helium in a tiny cell where only two convective rolls existed. The first observation of period-doubling in Taylor-Couette flow was made by Pfister (1985) in a single-cell flow at aspect ratios much less than one.

It is possible in the present system to observe a second period-doubling bifurcation from the period-two oscillation to one where the period is four times that of the original mode. A universal feature of the period-doubling cascade is that each bifurcation occurs after successively smaller increases of the control parameter. The variation of Reynolds number in the present system as a results of changes in temperature prevents the system from remaining within the period-four 'window' indefinitely. Rather, it is found to drift slowly between the period-two and period-four behaviour. An example of the period-four oscillation is shown in figure 6.5c, where it can be seen that the system reverts to period-two behaviour towards the end of the recording.

Nevertheless, it is possible to make relatively accurate measurements of the critical Reynolds number for the first period-doubling, and this was done for several aspect ratios across the range in question. The results are shown in figure 6.4 as the locus CD. The general trend with increasing aspect ratio is for the critical Reynolds number for period-doubling to drop towards that for the Hopf bifurcation. Indeed, it

proved impossible to observe a period-doubling bifurcation for aspect ratios greater than that associated with point D in figure 6.4. This suggests that there is a critical aspect ratio at which the Hopf and the period-doubling occur simultaneously as a codimension-2 bifurcation.

The behaviour which has been encountered so far can be understood fully in the context of finite-dimensional systems. However, observations were also made of dynamics at higher aspect ratios which do not fall into one of the standard low-dimensional categories. The locus EF in figure 6.4 consists of points at which there was a sudden and reversible transition between regular oscillatory behaviour and a type of motion which was highly irregular. An example of this transition is shown in figure 6.7 for the aspect ratio $\Gamma = 10.6$. The motion at $Re = 75.6$ consists of a regular oscillation as shown in figure 6.7a. The dimensionless frequency had increased continuously from $\omega/\omega_c = 0.1$ at onset to $\omega/\omega_c = 0.2$ at the present parameter values. When the Reynolds number was increased to $Re = 81.7$, the behaviour changed to the form of the time-series shown in figure 6.7b. There are now long phases of apparently stationary behaviour punctuated irregularly by certain large low-frequency structures. The average time-scale of these excursions is approximately fifty times the period of the rotating inner cylinder. The Reynolds number was varied carefully between the two values which are quoted above, and the flow was observed to alter between the two types of behaviour without any evidence of hysteresis.

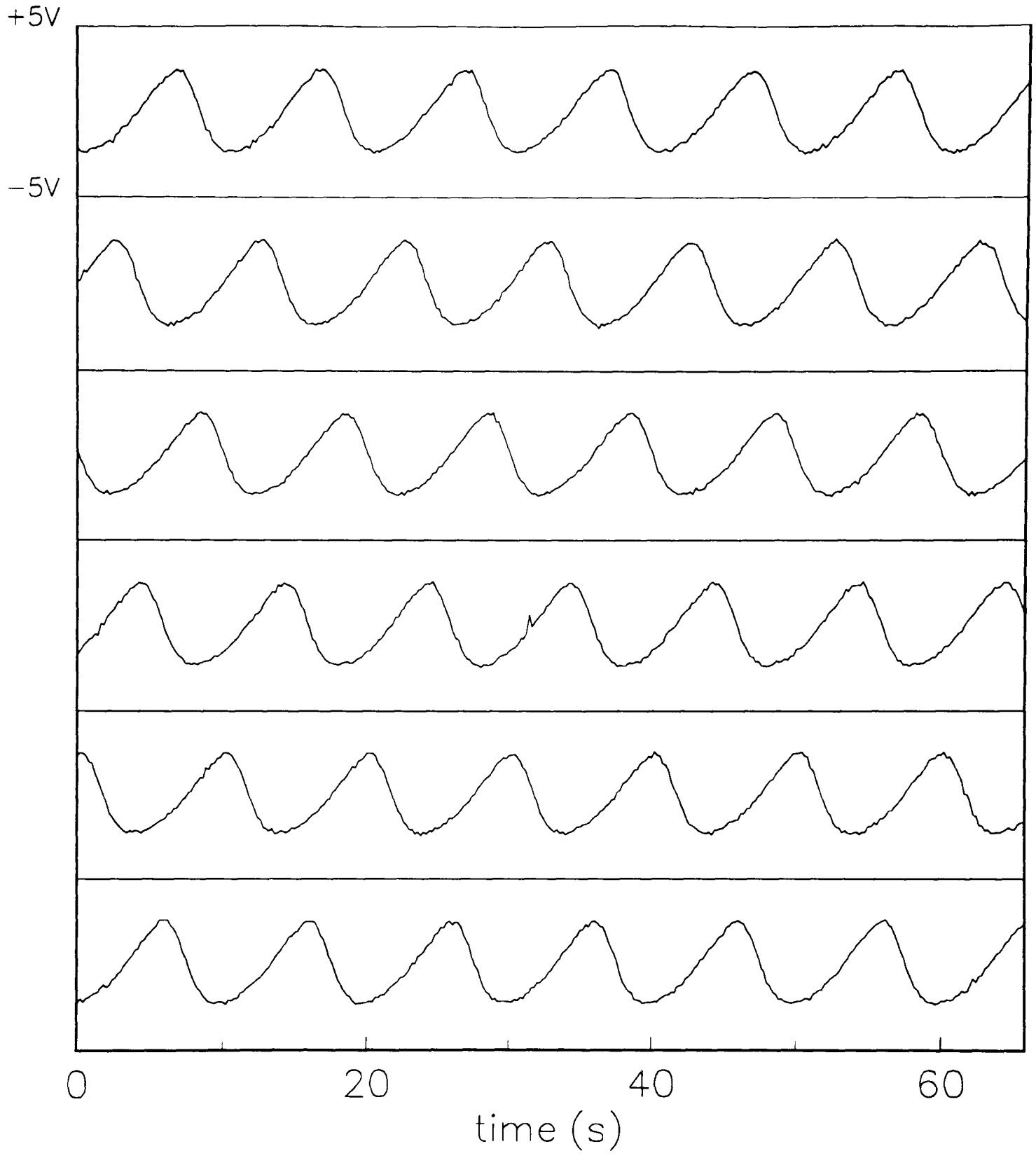

Figure 6.7 : (a) Singly-periodic behaviour in the prototype stadium system at $\Gamma = 10.6$, $Re = 75.6$.

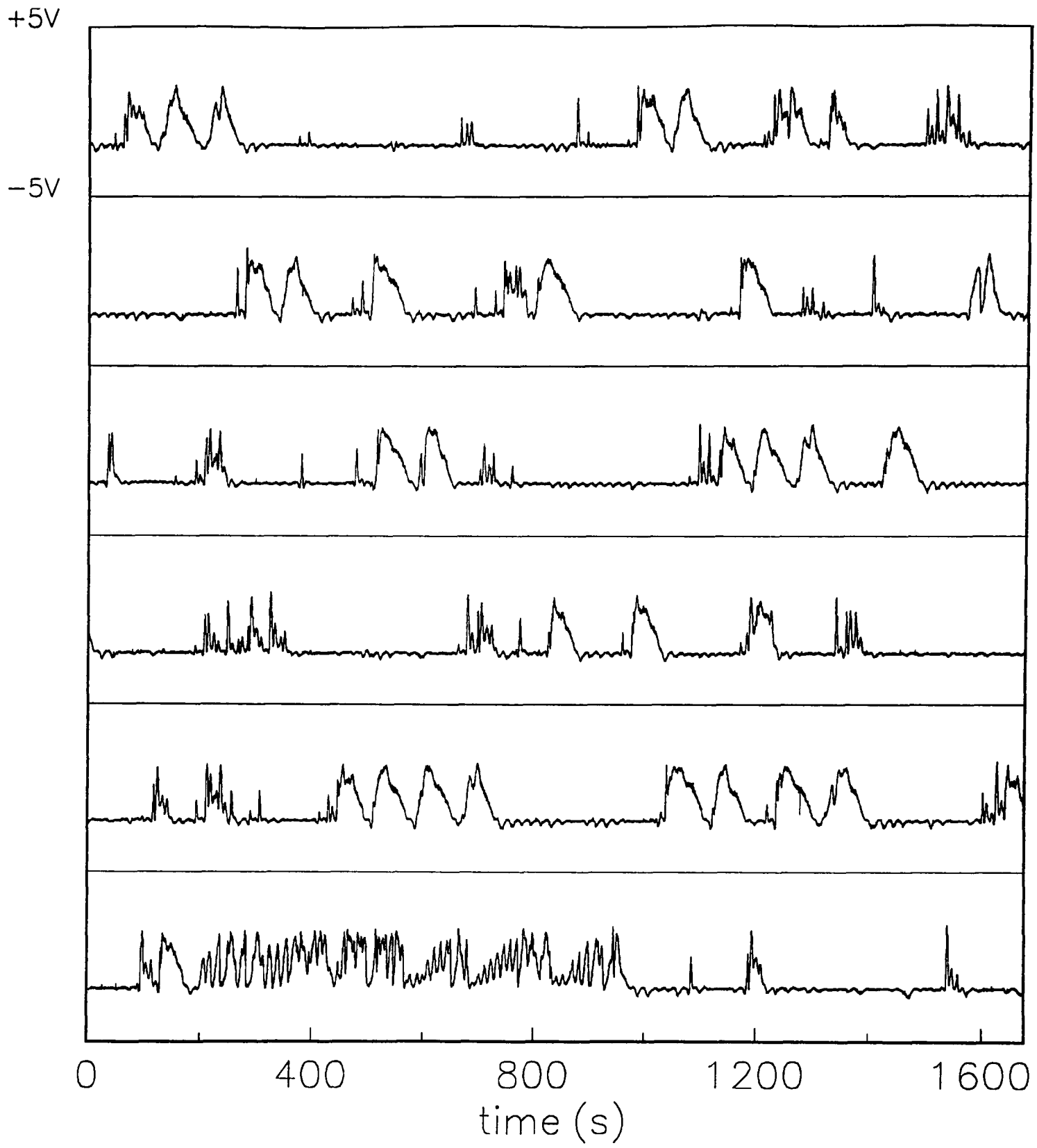

Figure 6.7 : (b) Strongly irregular behaviour in the prototype stadium system at $\Gamma = 10.6$, $Re = 81.7$. There is a sudden and reversible transition between this type of behaviour and that shown in figure 6.7a.

6.4 Comparison with other fluid systems

Irregular behaviour similar to that described in section 6.3 was observed by Sullivan & Ahlers (1988) in a fluid convection experiment. A binary fluid mixture was contained in a long rectangular box with a temperature difference between the top and bottom surfaces. The system was governed by two dimensionless parameters, namely the Rayleigh number R and a separation ratio ψ which determines whether concentration gradients help or hinder convection. Over a certain range of the parameter ψ, it was observed that the first time-dependent flow to appear with gradual increase of R consisted of slow bursts which were separated by irregular intervals that were long on the scale of the vertical thermal diffusion time. The transition was found to be reversible, with no evidence of hysteresis. At other values of ψ, however, the onset of time-dependence was observed to take place via a Hopf bifurcation to a regular singly-period mode.

An experimental study made by Mullin (1992) of flows in a triply-connected Taylor-Couette system revealed the existence of both low-dimensional behaviour and a nonstandard transition to irregular motion at one particular aspect ratio. The configuration in question consisted of two rotating cylinders placed symmetrically inside a larger stationary circular cylinder. Flow was driven by counter-rotation of the inner cylinders at equal speeds. In this way, the system was governed by a Reynolds number and an aspect ratio, and could be treated in a similar manner to other two-parameter systems. The flow was considered at an aspect ratio of $\Gamma = 3.675$ both for quasistatic increase of the Reynolds number from zero and for

sudden increases. It was observed that the onset of time-dependence in the primary mode occurred as the result of a Hopf bifurcation to a singly-periodic state, and that further increase of Re resulted in the appearance of doubly-periodic mode followed by the onset of weakly chaotic behaviour. Such a sequence has been observed in a variety of fluid systems, and is a familiar finite-dimensional route to chaos.

In addition, a secondary mode was located in which very different dynamics were found. A Hopf bifurcation to singly-periodic flow was again detected, but this time with very much smaller amplitude. On increasing the Reynolds number, occasional large-amplitude bursts were observed to occur within the otherwise regular oscillation. The average separation between these intermittent features decreased as the Reynolds number was increased. The behaviour is reminiscent of the type-1 intermittent route to chaos as proposed by Pomeau & Manneville (1980). Indeed, it was found that the average period of recurrence close to the first appearance of the bursts scaled in the same way as that predicted by Pomeau & Manneville. However, the theory also predicts that there should be a low-frequency cut-off in the distribution. This was not found in the behaviour observed by Mullin (1992), and it was concluded that this transition to chaos is not governed by one of the known finite-dimensional mechanisms.

The above observations are similar to the transition found in the prototype stadium system at relatively large aspect ratios. There is therefore reason to believe that the present results show a genuine feature of this particular problem.

6.5 Further results for dynamical phenomena

The dynamical phenomena which were described in section 6.3 show that the change to a domain with $\mathbb{Z}_2$ azimuthal symmetry does not prevent the occurrence of finite-dimensional behaviour in the flow. Although there is evidence of transitions at large aspect ratios which do not appear to be low-dimensional, these are preceded nevertheless in each case by a Hopf bifurcation from steady to singly-periodic flow. It is also the case that period-doubling can be observed up to an aspect ratio of $\Gamma = 7.5$. This contradicts the vast majority of observations of period-doubling in fluid systems, which are restricted to flows of very limited spatial extent. It is worth noting here that a claim has been made by Coughlin & Marcus (1992a) of period-doubling in a numerical simulation of Taylor vortex flow in the standard system under periodic boundary conditions. If this is the case, then it would support the present observations of period-doubling in an extended system. However, the exact details of the claim (Coughlin & Marcus 1992b) are unavailable at present.

However, it is not sufficient to rely solely on the results obtained from the prototype apparatus. Therefore a second flow rig was constructed which would allow precise control of the governing parameters, and in particular a constant temperature of the working fluid over the lengths of time which are required to observe the various phenomena. The new apparatus was shown in figure 2.5 of Chapter 2.

The clearance ratio was set initially to $\eta = 0.824$ as in the prototype system.

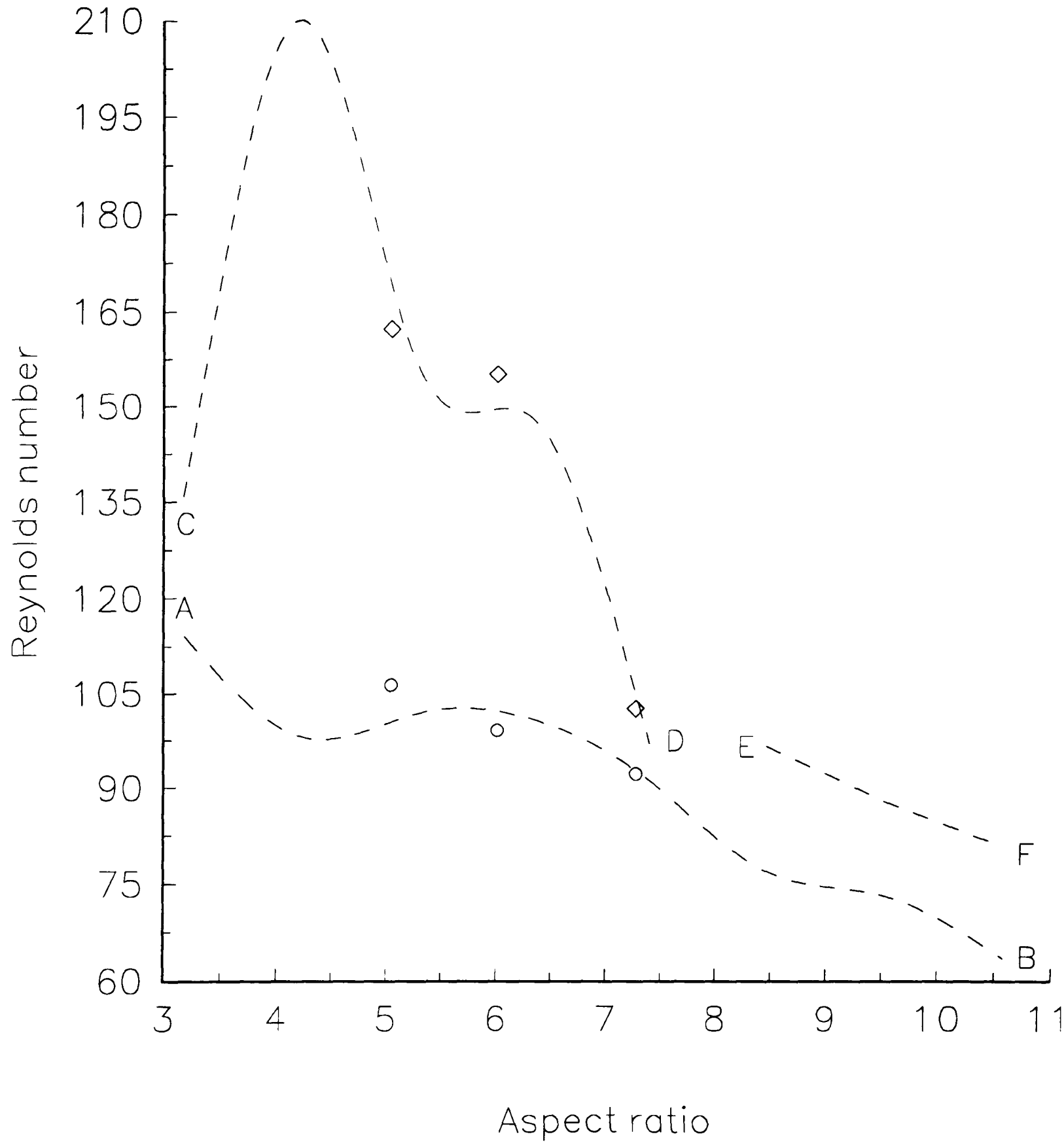

Figure 6.8 : Parameter space diagram showing overlay of results from prototype and precision stadium systems with $\eta = 0.824$. AB (o) Hopf bifurcations. CD ($\Diamond$) Period-doubling. EF Irregular behaviour. Dashed lines are from prototype system. Open symbols are from precision system.

Measurements were made once again using an LDV system with the measuring volume located approximately at the boundary between the main rotating flow and one of the recirculations. The sequence of a Hopf bifurcation followed by a period-doubling bifurcation was found qualitatively as before at moderately low values of aspect ratio. The critical Reynolds numbers for both bifurcations were measured over a range of aspect ratio in order to obtain a quantitative comparison with the prototype system. An overlay of the results from the two systems is shown in figure 6.8. The discrepancy is approximately 5%, which is highly satisfactory considering that the results were obtained from systems made to different specifications. Most importantly, the data for the new apparatus also show that the loci of Hopf and period-doubling bifurcations converge with increasing aspect ratio.

Irregular behaviour was observed once again at moderately large aspect ratios, but to a lesser degree than was the case in the prototype system. An example of the motion in question is shown in figure 6.9 for the aspect ratio $\Gamma = 10.5$. The Reynolds number was increased slowly from zero until the first appearance of a regular oscillation at the Hopf bifurcation. The Reynolds number was then increased to $Re = 90.1$, where the motion changed to the form shown in figure 6.9. As before, there is the irregular occurrence of low-frequency structures, along with intervals of approximately steady behaviour. The time-scale of an individual peak is approximately fifty times the period of the inner cylinder, which is the value that was recorded for similar features in the prototype system. However, the average extent of the quiescent phases is now markedly reduced. The form of the time-series in figure 6.9 is suggestive of the system jumping irregularly between two

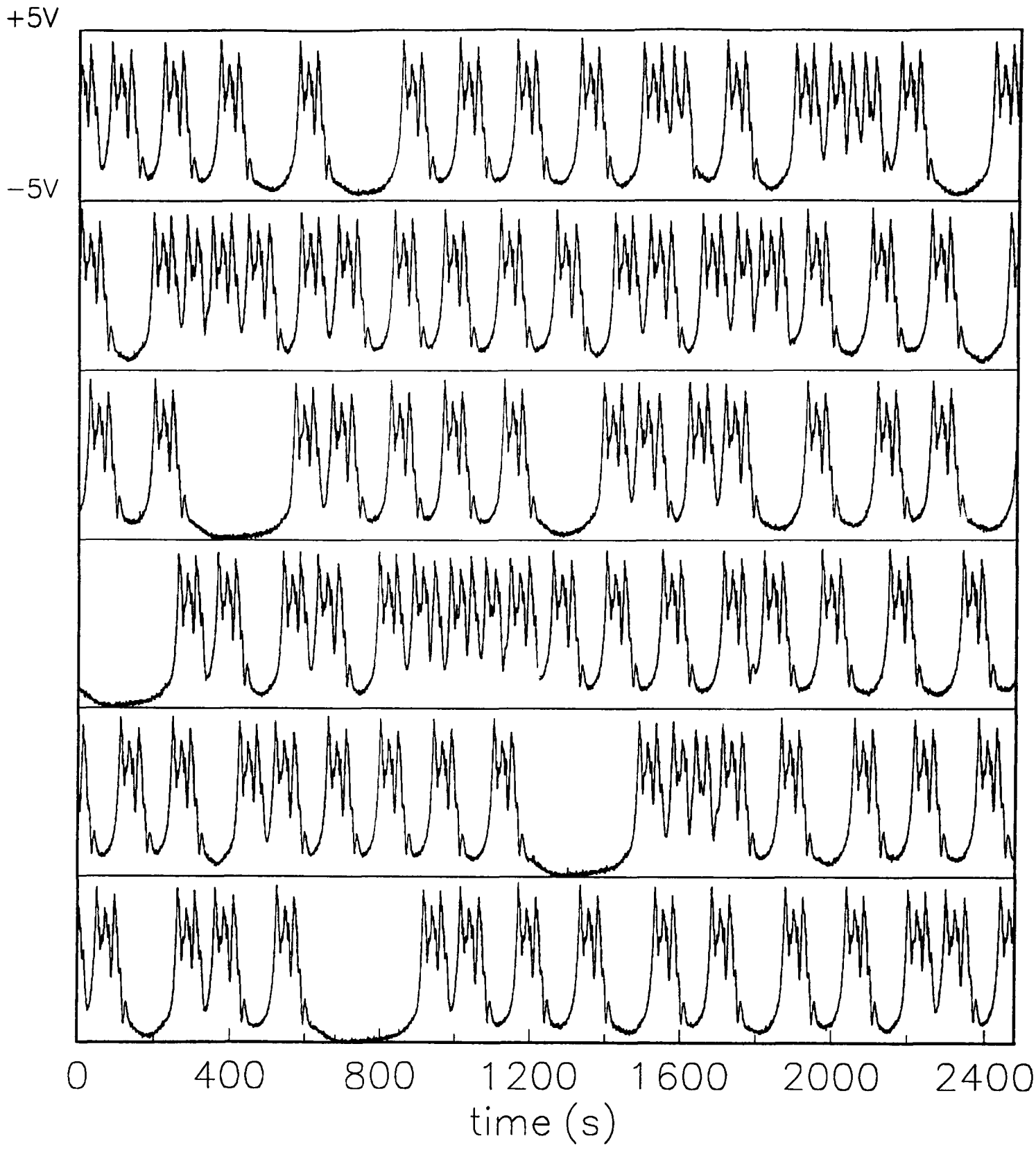

Figure 6.9 : Irregular behaviour found in the precision system with $\eta = 0.824$. Parameter values for recording were $\Gamma = 10.5$, $Re = 90.1$.

different states. If this is indeed the underlying process, then it is possible that the stronger irregularity in the prototype system was the result of thermal variations in the Reynolds number which exaggerated the basic effect.

All the observations which have been reported up to this point were obtained for a clearance ratio $\eta = 0.824$. However, measurements were also made in the precision apparatus with $\eta = 0.800$. In particular, attention was focussed on the range of aspect ratio where the previous change from finite-dimensional behaviour to nonstandard behaviour had been observed. Results for $\eta = 0.800$ are shown in figure 6.10 as a parameter-space diagram. Once again, the sequence of Hopf bifurcation followed by period-doubling bifurcation was recorded. However, it proved impossible to reproduce the transition to any form of irregular behaviour similar to that found in the previous systems at higher aspect ratios. A possible reason for this absence can be found in the variation of the paths of Hopf and period-doubling bifurcations in parameter space. As was seen in figure 6.4, the irregular behaviour occurred for aspect ratios above an apparent coalescence of the two bifurcations. The loci of bifurcations shown in figure 6.10 approach each other initially, but then diverge with further increase of aspect ratio. Thus it would appear that the small change in the value of the clearance ratio between the two systems either prevents a simultaneous occurrence of a Hopf and a period-doubling, or at least removes it to an aspect ratio which is outside the accessible experimental range. Either way, the existence of the irregular behaviour seems to be related, in a sense yet to be determined, to the interaction of the two bifurcations.

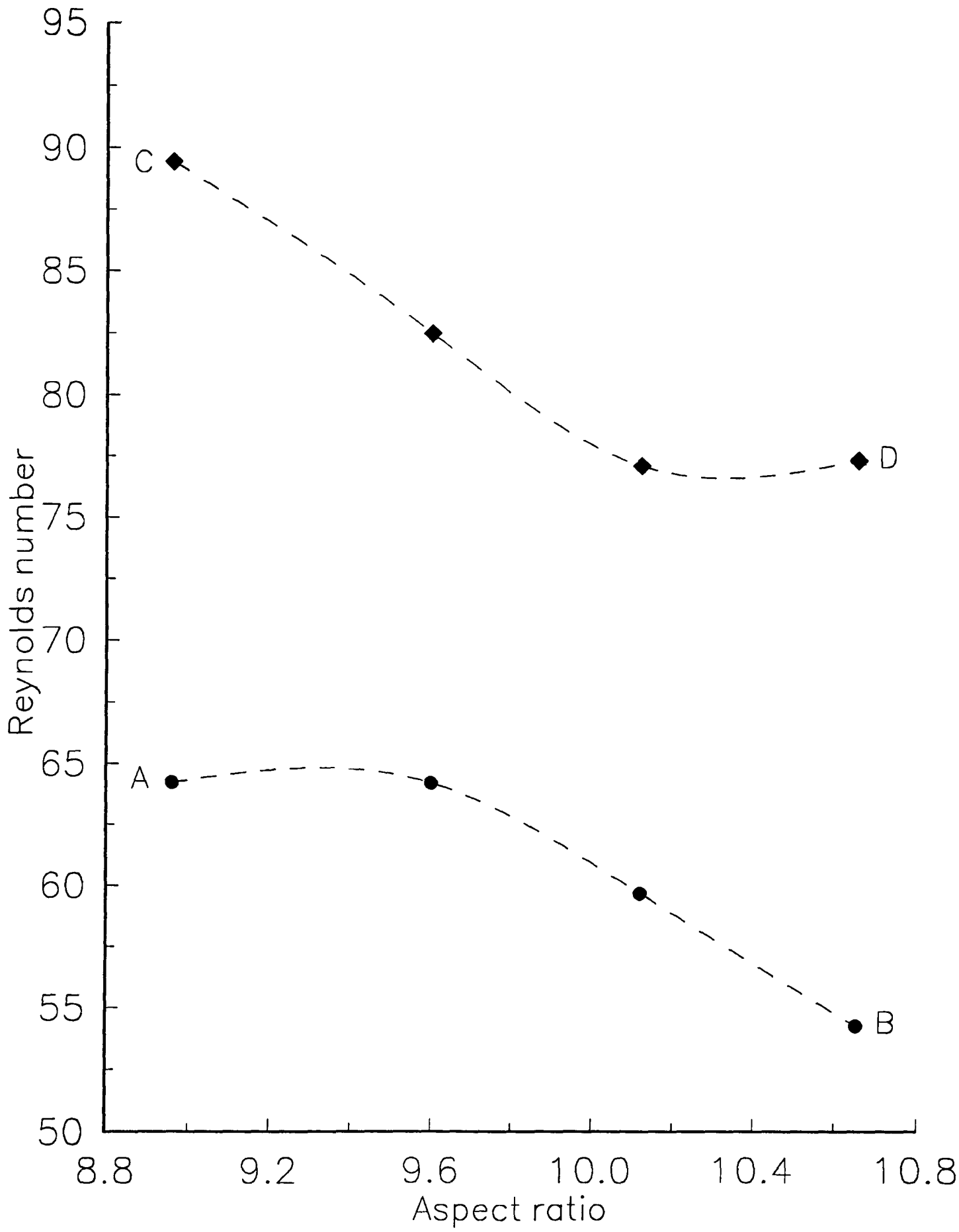

Figure 6.10 : Results from the precision stadium system with $\eta = 0.800$. AB (●) is locus of Hopf bifurcations. CD (⧫) is locus of period-doubling bifurcations.

6.6 Comments

These first results which have been obtained from the stadium Taylor-Couette system have interesting implications for the dynamics of Taylor vortex flows generally. It was shown by Mullin (1991) that a view exists linking the continuous $SO(2)$ symmetry of the standard system with the prevalence of finite-dimensional transitions in flows at moderate values of the Reynolds number. Such behaviour would then be highly nongeneric in the wider context of fluid dynamical mechanisms in arbitrary domains. However, the stadium configuration displays arguably the most basic type of finite-dimensional behaviour, namely Hopf bifurcations and period-doubling, over a wide range of aspect ratios. This is despite a substantial reduction of the azimuthal symmetry from the original $SO(2)$ group. Thus it is proposed that dynamics under a high degree of spatial symmetry are not necessarily as unrepresentative of the underlying processes in closed fluid systems as has been thought to be the case.

CHAPTER 7

Conclusions

We have been concerned in this study with the flow of a viscous fluid in two different systems which are derivatives of the standard Taylor-Couette system of concentric circular cylinders. Flow phenomena have been investigated experimentally using both flow visualization and laser Doppler velocimetry, and the results have been interpreted in the context of ideas from dynamical systems. The aim was to investigate if previously reported low-dimensional flow behaviour is restricted to the special case of continuous azimuthal symmetry, or if it is robust and can be found in systems with lesser degrees of spatial symmetry.

Most of the study is concentrated on the case of a fixed square cylinder with a rotating circular cylinder at its centre. The vertical extent of the annulus is determined by two solid stationary end-plates. Thus the domain in which flow takes place possesses the same $\mathbb{Z}_2$ midplane symmetry of the standard system, but a discrete $\mathbb{Z}_4$ azimuthal symmetry instead of the continuous $SO(2)$ group.

Attention was focussed on the particular regime of small aspect ratios for the purpose of limiting the extent to which there is multiplicity in the solution set of the problem. It was found that the steady solution set under these conditions consists

of only two- or single-cell flows. Results were presented which show that a steady bifurcation sequence first proposed by Benjamin & Mullin (1981) for single-cell flows in the standard system persists under this change to $\mathbb{Z}_4$ azimuthal symmetry. This can be attributed to the fact that the steady bifurcations in the problem are symmetry-breaking bifurcations which act only on the $\mathbb{Z}_2$ midplane symmetry. In addition it was found that the critical values of Reynolds number at which symmetry-breaking occurs in the two systems show a strong degree of quantitative similarity when the aspect ratio is reduced below $\Gamma = 1$. Since the cellular flow is restricted to a region close to the inner cylinder under these circumstances, it is argued that this renders the exact details of the outer boundary unimportant.

The onset of time-dependent behaviour in the single-cell flow in the square Taylor-Couette system was studied by building on the knowledge which had been obtained about the steady flows. It was found that two different oscillatory modes exist depending on the value of the aspect ratio relative to one. For $\Gamma < 1$, the motion takes the form of a periodic cycle between circular and oblate forms of the single cell close to the inner cylinder. For $\Gamma > 1$, there is a sequence involving the motion of small vortices around the main Taylor cell. In both cases, it was shown experimentally that the time-dependent motion arises as a result of a Hopf bifurcation on the single-cell solution branch. There is a region of parameter space around $\Gamma = 1$ which separates the regimes in which these two modes are found to exist. The details of the solution structure were explained in the context of simple bifurcations that occur in low-dimensional dynamical systems. Central to this is a steady single-cell flow at aspect ratios less than one which extends to fill

the full radial extent of the flow domain. No such flow has ever been reported for the standard Taylor-Couette system at small aspect ratios. In addition, homoclinic phenomena were observed in the single-cell flow. This is when the period of an oscillation becomes very large in comparison to the typical time-scale of the problem.

Dynamical phenomena of a more complicated nature were explored in the time-dependent mode which exists for aspect ratios greater than one. It was found that there is a multiplicity of states involving modes in which the small peripheral vortices move either with or against the prevailing flow. The two dynamical states were distinguishable by markedly different dimensionless frequencies. A locus of secondary Hopf bifurcations was encountered with increase of Reynolds number for the case of the higher-frequency mode, which results in a modulation of the amplitude envelope of the oscillation. The transition is viewed in reconstructed phase-space as being between a simple limit cycle and a torus. The locus of secondary Hopfs was observed to meet the locus of cyclic folds which mark the lower limit of stability of the higher-frequency mode. This results in a critical set of parameter values at which there is a catastrophic collapse of the doubly-periodic mode.

The effect of further increase of Reynolds number is that the doubly-periodic mode develops a long irregular transitory phase before undergoing an irreversible transition to a new dynamical state. This consists of isolated sections of oscillatory behaviour separated by relatively quiescent phases. When viewed in reconstructed phase-space, this motion takes places on an attractor with a central core connected at each end by spiralling trajectories. This structure shows strong similarity with

results obtained by Mullin & Price (1989) for flow in a Taylor-Couette system with continuous $SO(2)$ symmetry. Their results were the first observations in a fluid system of behaviour relating to the Šilnikov mechanism for chaotic motion which had previously been restricted to systems governed by ordinary differential equations. Thus the present results suggest that this mechanism is robust, and exists in systems with lesser degrees of symmetry.

A second configuration was used in the investigation of the relationship between symmetry and low-dimensional flow phenomena. This was again based on the Taylor-Couette system, but this time the outer cylinder had the cross-sectional shape of a stadium. Thus the symmetry group is reduced further to $\mathbb{Z}_2 \times \mathbb{Z}_2$ symmetry. The two-dimensional flow which exists in such a system was calculated numerically using a finite-difference scheme applied to the equations for creeping flow. This was compared with experimentally visualized two-dimensional flow at a Reynolds number $Re \approx 1$. Both approaches show a flow field which consists of a main circulating flow driven by the rotation of the inner cylinder, and two outlying crescent-shaped recirculation regions.

Time-dependent phenomena were investigated in a prototype stadium system over a relatively wide range of aspect ratio. A sequence of a Hopf bifurcation followed by a period-doubling bifurcation is observed for aspect ratios up to a value of $\Gamma = 7.5$, beyond which there is a sudden and reversible transition between a singly-periodic mode and strongly irregular behaviour. Similar transitions have been found to occur in other closed flows, namely binary convection in a rectangular

contained and triply-connected flow in a Taylor-Couette system with two rotating inner cylinders. Irregular behaviour is also observed in a precision apparatus, and its existence appears to be connected with a probable intersection of the locus of Hopf bifurcations with the locus of period-doubling bifurcations at a slightly lower aspect ratio. This is supported by measurements at a different value of the geometrical clearance ratio which show there to be no intersection of the two lines of bifurcations, and also no irregular behaviour of the form encountered previously.

Considered as a whole, the results presented in this thesis form a strong body of evidence in support of the role of finite-dimensional dynamics in describing the origins of simple and more complicated behaviour in fluid flows. It had previously been supposed that the success of applying such ideas to phenomena in the standard Taylor-Couette system was due to the high degree of spatial symmetry embodied in the problem, particularly the continuous $SO(2)$ azimuthal symmetry. However, we see now that low-dimensional dynamics also lie at the heart of much of the behaviour found in systems with $\mathbb{Z}_4$ and $\mathbb{Z}_2$ azimuthal symmetry groups. In particular, observation were made of oscillatory motion in the square system which suggests the possibility of temporal chaos arising from the finite-dimensional Šilnikov mechanism. In the stadium system, a transition which does not fit into one of the standard low-dimensional categories still seems to be related to the existence of a simultaneous occurrence of two standard bifurcations nearby in parameter space.

Thus, the utility of a finite-dimensional approach in overcoming the substantial obstacles presented by the infinite-dimensional Navier-Stokes equations promises to

be of use in systems of a more general nature than the special Taylor-Couette problem. In particular, there is the case that the use of numerical bifurcation calculations for fluid flows could be extended from the current regime of two-dimensional problems to implementations which tackle fully three-dimensional flows of the type considered here. Given that simple bifurcations mechanisms persist under the breaking of continuous symmetries which have previously been used to simplify the computations, it is still the case that standard numerical bifurcation techniques such as path following and centre-manifold reductions can employed, albeit at greatly increased computational expense.

Finally, there is growing interest in the possible role that finite-dimensional dynamics might have to play in describing the origins of highly complicated behaviour in open flow systems. Much of this work is summarized in the comprehensive review given by Holmes (1990) for the case of turbulent boundary layer flow. Essentially, the approach is based on the fact that certain large-scale vortices, known as *coherent structures*, exist in turbulent flows. The suggestion is that these structures can be thought of as being coupled together by nonlinear interactions, resulting in a finite-dimensional dynamical system. Experimental observations have been reported by Gaster (1990) of certain phenomena in a turbulent boundary layer which appear to have low-dimensional characteristics. However, the fact that the flow has a strong spatial dependence as well as a temporal one makes it difficult to gather data of a sufficient consistency to allow extensive investigation of the underlying dynamical structure. The result presented in this thesis show that, far from being a closed subject, the role of finite-dimensional dynamics in closed fluid flows is something about

which there is still much to be discovered. The fact that complicated behaviour is found in closed systems with reduced geometrical symmetries provides an opportunity to study low-dimensional phenomena in detail, without being hindered by strong spatio-temporal effects which serve to mask the underlying processes.

APPENDIX A

Notes on dynamical systems and bifurcations

We are concerned throughout the present study with qualitative changes which occur in various fluid flows under the variation of certain governing parameters. The particular context in which these changes are considered is that of nonlinear dynamical systems, and in particular the bifurcation of equilibrium solutions. This subject has been covered in great detail by Guckenheimer & Holmes (1986) and Wiggins (1990), and we review here only the essential elements.

An example of a dynamical system is a set of n first-order autonomous ordinary differential equations, which can be written as

$$\dot{x} = f_\mu(x), \quad x = x(t) \in \mathbb{R}^n. \tag{A.1}$$

The vector field f in equation A.1 has a functional dependence on a set of parameters μ, where $\mu \in \mathbb{R}^k$ if there are k parameters. The solution space $\mathbb{R}^n$ is known as the *phase space* of the system. Given an initial starting condition $x(0)$ at time $t = 0$, the solution $x(t)$ to equation A.1 traces out a particular *trajectory* in phase space.

An important class of solutions of equation A.1 are those which satisfy the condition that $\dot{x} = 0$. An initial solution of this form remains unchanged with time, and is referred to as an *equilibrium solution.* In terms of the phase-space representation, such solutions are known as *fixed points* of the particular phase

space $\mathbb{R}^n$. The stability of equilibrium solutions is of particular importance here, since it is the case that the only observable solutions of this class in physical systems are those which are stable to infinitesimal perturbations.

If we consider a fixed point x^*, then by definition $\dot{x}^* = f_\mu(x^*) = 0$. The stability of the fixed point may then be investigated by applying an arbitrary perturbation ξ. This results in the perturbed equation

$$\dot{\xi} = f_\mu(x^* + \xi). \tag{A.2}$$

If ξ is now specified as an infinitesimal perturbation, then equation A.2 can be linearized about x^* to give

$$\dot{\xi} = \frac{Df_\mu(x^*)}{Dx}\xi, \tag{A.3}$$

where $Df_\mu(x^*)/Dx$ is the Jacobian of f_μ evaluated at the fixed point. Equation A.3 leads to the conditions for the linear stability of x^*, namely that all the eigenvalues of the Jacobian matrix evaluated at x^* must have non-positive real part. Since the eigenvalues themselves are functions of μ, it is the case that varying the control parameters may cause one or more eigenvalues to cross the imaginary axis of the complex plane. Such an occurrence is known as a *bifurcation* of the equilibrium solution.

The simplest type of bifurcations are those which result from the variation of only one parameter. The *codimension* of a bifurcation is defined here as the smallest dimension of parameter space in which the bifurcation can occur generically (we use here the definition of Guckenheimer & Holmes (1986) rather than that of

Golubitsky & Schaeffer (1985)). Thus the most basic bifurcations are codimension-1 type, whereas those which require the variation of two parameters are classed as codimension-2 type. In a two-parameter problem such as the ones which are studied here, codimension-1 bifurcations appear as lines in parameter space which separate regions of qualitatively different behaviour in the system. The intersection of two such lines marks the point at which there is a codimension-2 bifurcation. The advantage of this formalism is that it allows bifurcation phenomena to be studied in general terms. Thus knowledge of the solution structure associated with one particular type of bifurcation may be used to interpret similar behaviour in a wide class of systems.

There are only two codimension-1 bifurcations possible in a general system with no symmetries. These are the *saddle-node* and *Hopf* bifurcations. The two bifurcations are illustrated in figures A.1a and A.1b respectively by means of a *bifurcation diagram.* This is a plot of the evolution of a linear functional of solutions with variation of the bifurcation parameter through the critical value at which the bifurcation occurs. The convention in these diagrams is to show stable solutions as solid lines and unstable solutions as dashed lines. It must be emphasised that these graphical representations are only of the lowest-order behaviour local to the bifurcation point. Nevertheless, they are a highly effective way of communicating the essence of the bifurcation mechanism.

The saddle-node bifurcation is shown in figure A.1a. This is the result of a single real eigenvalue passing through the origin. A stable and an unstable solution

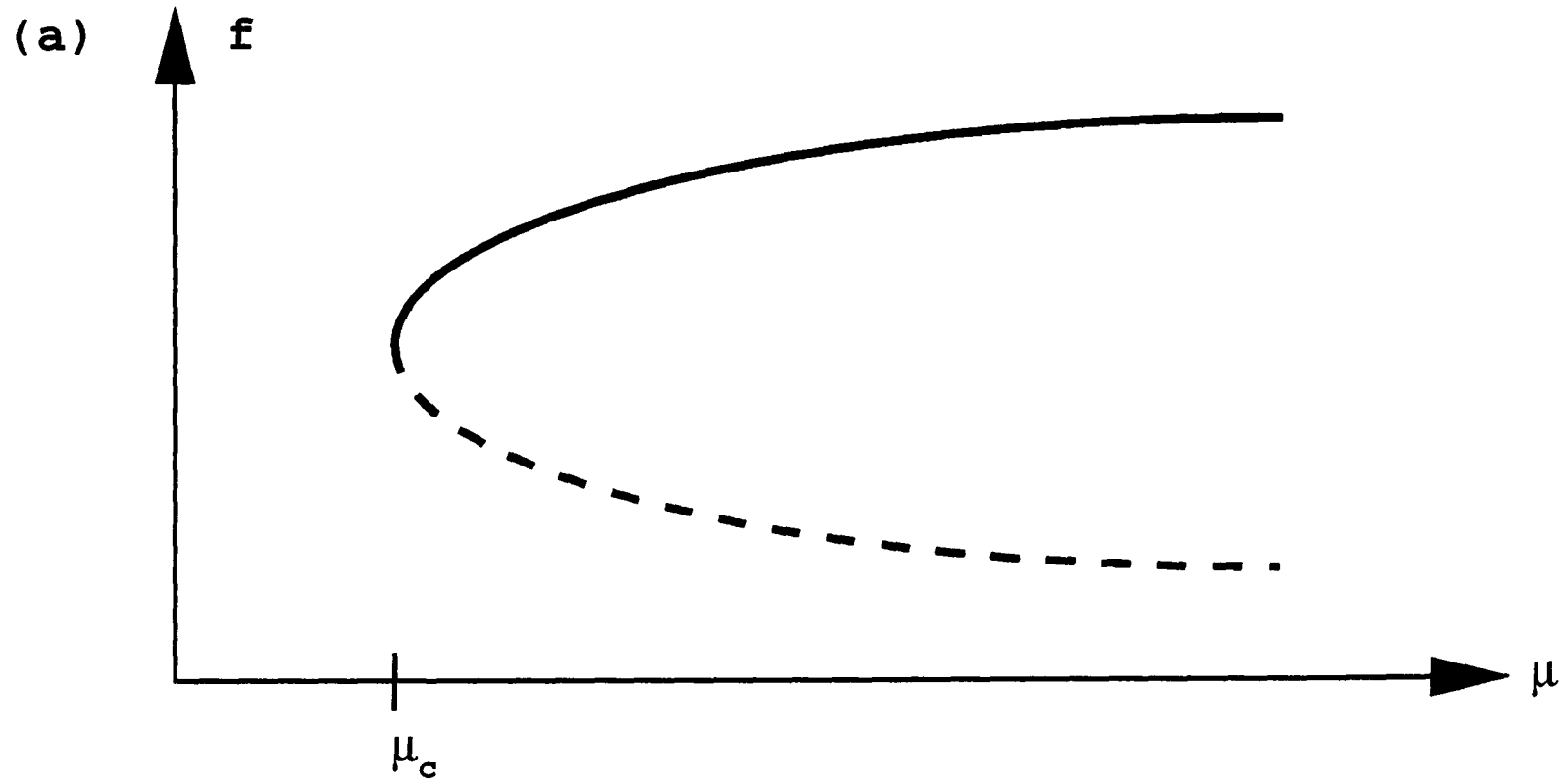

Figure A.1 : Basic codimension-1 bifurcations. (a) saddle-node bifurcation. (b) Hopf bifurcation. Solid lines represent stable solutions. Dashed lines represent unstable solutions.

branch exist for values of the parameter μ greater than the critical value μ_c. The two solutions coalesce at $\mu = \mu_c$, beyond which there are no local solutions. In a physical system, the result of passing through a saddle-node bifurcation is typically that the system 'falls off' onto a new solution branch which corresponds to a different type of behaviour. The saddle-node bifurcation is *structurally stable* in the sense that it is not destroyed by small perturbations of the system in whose solution structure it occurs.

The other basic codimension-1 bifurcation is the Hopf bifurcation, as shown in figure A.1b. Here, a complex conjugate pair of eigenvalues crosses the imaginary axis transversely with variation of the parameter. For $\mu < \mu_c$, the fixed point is stable, with decaying oscillatory transients. At the bifurcation point, the fixed point becomes unstable and trajectories now spiral out to a stable *limit cycle* surrounding the unstable fixed point. The system has undergone a change from a steady time-invariant solution to a periodic time-dependent solution. The Hopf bifurcation represents the simplest way in which a physical dynamical system can develop an oscillation with variation of a control parameter. As with the saddle-node, the Hopf bifurcation is also structurally stable in the presence of imperfections.

Other codimension-1 bifurcations are possible when a solution is constrained in a particular way. Of particular importance here is the case when an equilibrium solution is invariant under a reflectional symmetry. There is then the possibility of a *pitchfork* or *symmetry-breaking* bifurcation as shown in figure A.2. The bifurcation which is shown in figure A.2a is for conditions of perfect symmetry. The symmetric

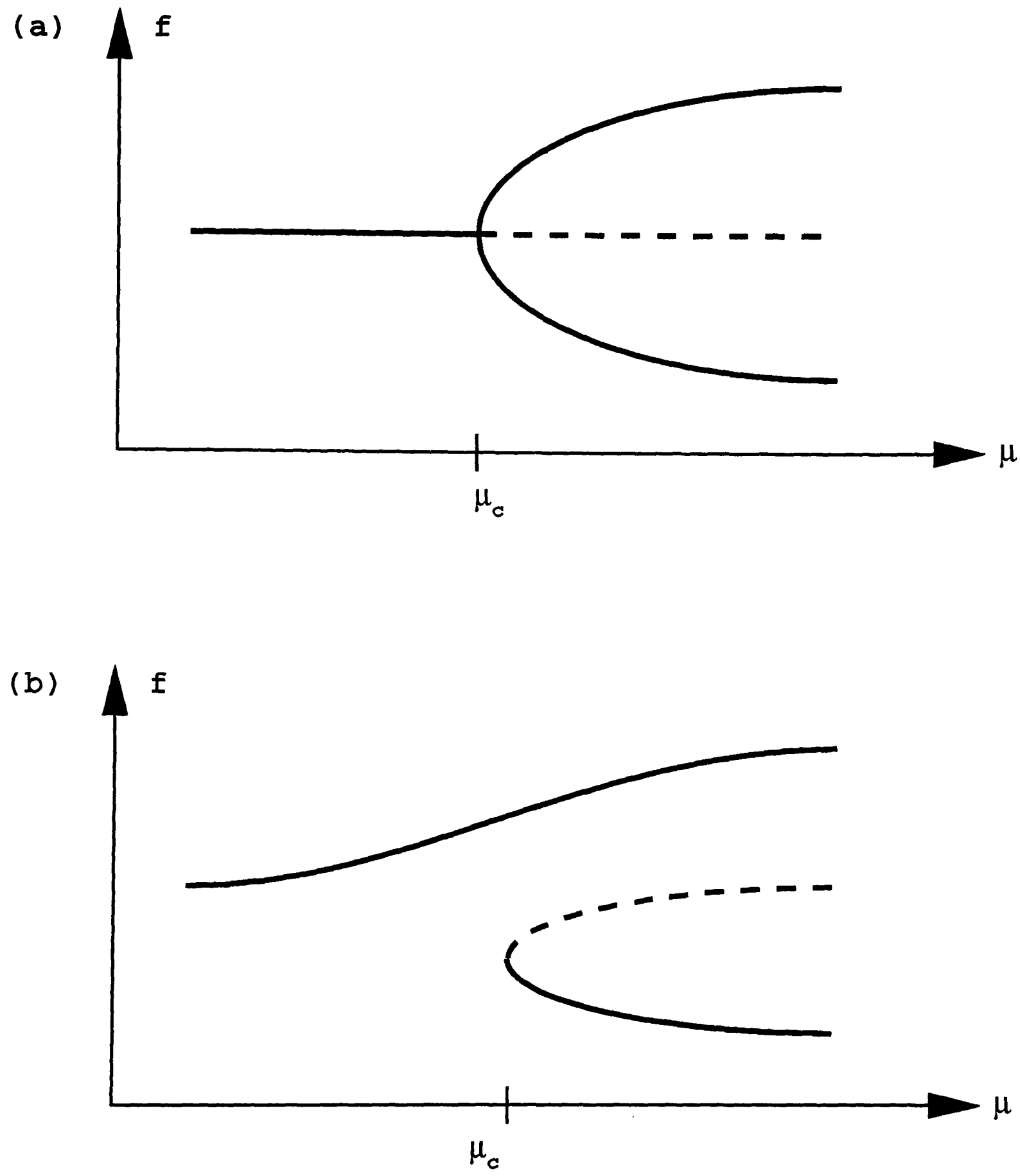

Figure A.2 : Pitchfork bifurcation. (a) symmetric bifurcation. (b) imperfections cause one asymmetric branch to disconnect.

solution becomes unstable at a critical value of the bifurcation parameter μ, at which there is the appearance of two stable asymmetric solution branches. However, unlike the cases of the saddle-node and Hopf bifurcations, the symmetric pitchfork bifurcation is not structurally stable in the presence of imperfections. A physical system can never be perfectly symmetric, and the effect of imperfections is to bias the system towards one particular sense of asymmetry. The effect on the bifurcation diagram can be seen in figure A.2b, where there is the disconnection of one of the asymmetric solution branches. Thus the system now always evolves along the same branch with quasistatic increase of the bifurcation parameter. However, the other asymmetric solution remains stable, and can be accessed by suitable initial conditions which allow the system to settle on this branch. Subsequent decrease of the bifurcation parameter results in a saddle-node bifurcation being encountered, whereupon the system falls back to the connected solution.

The pitchfork bifurcation is an example of the phenomena of *multiplicity of solutions* in a nonlinear system. In a linear system, there is a unique solution for any set of control parameters. However, in a nonlinear system there is the possibility of more than one solution existing for the same operating conditions. In the bifurcation diagrams of figure A.2, there is only one local solution for $\mu < \mu_c$. This changes to three local solutions for $\mu > \mu_c$, where two are stable and one is unstable. The selection of one particular stable solution is determined by the choice of initial conditions which are given to the system. This defines a *basin of attraction* for each solution, in which all trajectories are drawn towards the same final state.

We consider the Taylor-Couette system in this study as a particular example of a dynamical system, in which the various bifurcations which have been discussed above are encountered. The focus up to this point has been on systems whose phase spaces have a finite number of dimensions. However, the governing equations of fluid flow, the *Navier-Stokes equations*, are for a continuum and are therefore infinite dimensional. Nevertheless, we see that there are circumstances under which the behaviour of flow in the Taylor-Couette system is very similar to that of systems with a finite number of degrees of freedom.

APPENDIX B

Local measurements in oscillatory flows

It is shown in Chapter 4 that the different time-dependent forms of the single Taylor cell in the square domain posses interesting spatial characteristics. For example, there is the oscillatory mode that is found at aspect ratios greater than one which involves the motion of small vortices around the outside of the main cell. Such behaviour is an inherently global feature of the flow field, since the fluid is a continuum and this implies that all points within the flow must experience the oscillation. The qualitative nature of the flow is therefore best studied using flow visualization, since this is a technique which allows the global nature of a flow to be observed directly. On the other hand, the use of laser Doppler velocimetry (LDV) to obtain a quantitative measure of the flow provides by nature a local measurement since the signal is produced by the scattered light from a small measuring volume. This raises the question of the extent to which a local measurement can represent the global aspects of the flow.

For the case of a Taylor-Couette system, the problem can be viewed at its simplest level by considering a singly-periodic Taylor vortex flow. The velocity at all points within the flow will be oscillating at the same frequency, but by no means at the same amplitude. The action of the no-slip boundary condition causes the oscillation to be very small at points close to the stationary surfaces, whereas it

may well be much larger at other points within the body of the flow. This fact has important consequences relating to the application of signal processing techniques to time-series which are obtained using LDV. If the measuring position is close to one of the end-plates, then a signal with a relatively small amplitude will be recorded. The power spectrum of this signal can be expected to contain just a single component, and the reconstructed phase portrait will take the form of a planar limit cycle. However, the signal-to-noise ratio in this regime is likely to be quite low. If instead the measuring position is moved away from the stationary ends, then a signal of much larger amplitude will normally be recorded. Although still singly-periodic, the signal is almost always found to have a higher harmonic content than before due to the adverse effects of velocity gradients. This, along with the fact that there can be apparent nonlinear interaction between the various harmonics, results in a power spectrum of greatly increased complexity. The same is true for the topology of the reconstructed phase portrait. It will still be a limit cycle, but one which is distorted out of the plane by the action of the higher harmonic components.

The problem becomes more significant when the flow contains not one but *two* independent modes, since there is now also the question of the relative contributions of the two modes. Many of the results in Chapter 5 relate to flows of this type, and so it is worth considering an example of the effect of measuring position on the representation of a doubly-periodic mode. A number of recordings were made at different positions in a doubly-periodic single-cell flow in the square Taylor-Couette system. The details of the measuring process are given in section B.1. The results are presented in section B.2 in the form of time-series plots, and various

comments are made regarding the different points at which the flow was sampled. In section B.3, the time-series are used to reconstruct phase portraits, and the structure of these are shown using Poincaré sections. Finally, certain conclusions arising from the results are made in section B.4.

B.1 Experimental details

All the time-series were recorded in the square Taylor-Couette system at a constant set of parameter values, namely the aspect ratio $\Gamma = 1.25$ and Reynolds number $Re = 723.94$. These values are shown in the context of the neighbouring bifurcation structure in figure B.1. The aspect ratio was set first, and then the Reynolds number was increased slowly from zero to the final value. The first bifurcation encountered was the symmetry-breaking bifurcation to steady single-cell flow as described in Chapter 3. The flow then becomes time-dependent as the locus PE of Hopf bifurcations is crossed. This bifurcation is to a singly-periodic flow where small vortices are formed at the inner cylinder and move round in the same direction as the secondary flow in the main cell (see Chapter 4). This motion persists until the system crosses the locus ST of secondary Hopf bifurcations. The singly-periodic flow now becomes doubly-periodic, with the appearance of a lower-frequency modulation of the original oscillation. Flow visualization studies suggest that this second frequency is the result of a slow oscillation in the main Taylor cell, whereas the higher frequency is due to the motion of the small peripheral vortices. The dimensionless frequencies of the basic oscillation and the modulation are $\omega/\omega_c = 0.34$ and $\omega/\omega_c = 0.06$ respectively.

The LDV was aligned so that the measuring volume was at a radial position midway between the inner and outer cylinders and at an azimuthal position where the gap between the two cylinders is a minimum. These two positions were held fixed, while the vertical position was varied by raising or lowering the flow rig on

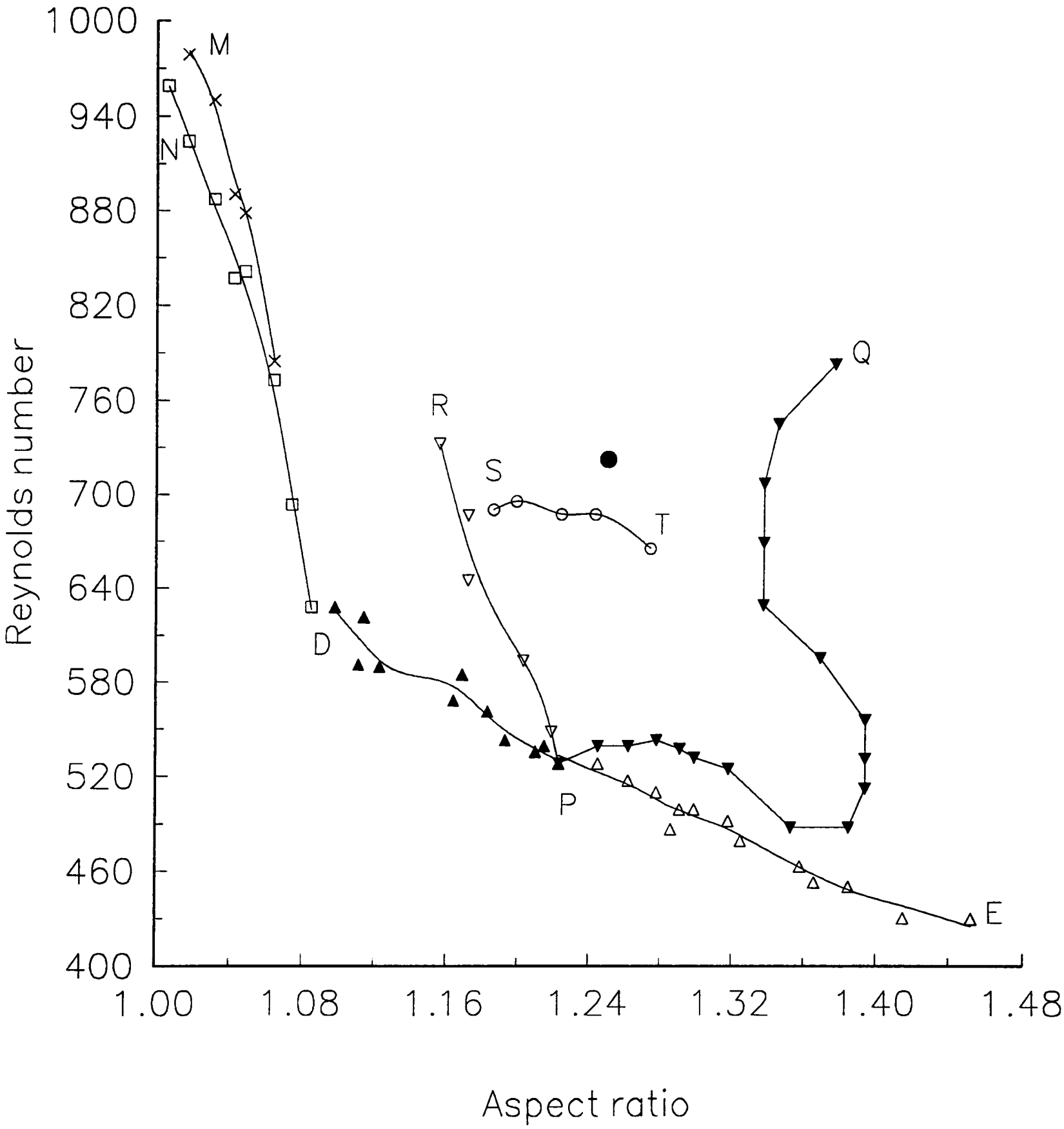

Figure B.1 : Parameter space diagram showing bifurcation structure in the vicinity of the point at which measurements were made. The full details of this figure can be found in Chapter 5.

a computer-controlled lift (see Chapter 2). The vertical position of the measuring volume will be labelled by the dimensionless linear coordinate $h \in [0, 1]$, where $h = 0$ indicates the end-plate corresponding to inward radial flow of the single cell and $h = 1$ that for outward radial flow.

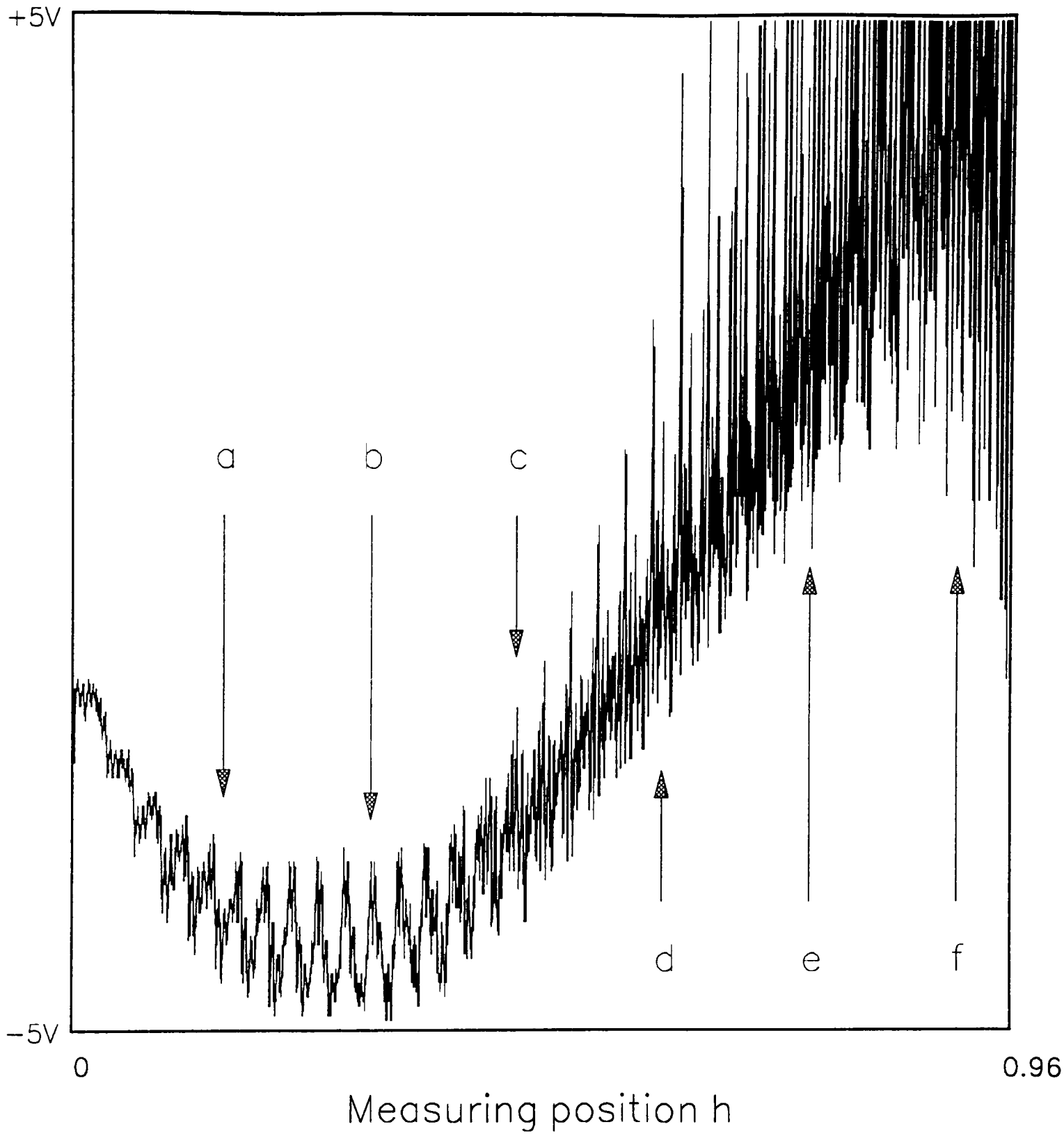

Figure B.2 : Radial velocity profile through flow at $\Gamma = 1.25$, $Re = 723.94$. a : h = 0.15. b : h = 0.30. c : h = 0.45. d : h = 0.60. e : h = 0.76. f : h = 0.91.

B.2 Time-series from different measuring positions

The radial velocity profile of the flow at $\Gamma = 1.25$ and $Re = 723.94$ is displayed in figure B.2 as a sweep of the measuring volume from $h = 0$ to $h = 1$ in a time corresponding to approximately 600 rotations of the inner cylinder. The vertical scale is not absolute, since the output of the LDV was amplified and shifted so as to capture as much of the profile as possible within the range of the analogue-to-digital converter. Even so, there is a certain amount of unavoidable cut-off of the large amplitude oscillations towards $h = 1$. The trace does not extend all the way to $h = 1$ as a result of the requirement that there be a slight angle of inclination of the photomultiplier relative to the plane of the LDV beams. There is thus a small region towards one end-plate where the measuring volume is hidden from the photomultiplier.

Six different values of h were chosen at which the signal was recorded. These values are $h = 0.15, 0.30, 0.45, 0.60, 0.76$ and 0.91, and the positions on the profile are marked in figure B.2 as a, b, c, d, e and f respectively. In each case, the signal was amplified and shifted in order to obtain the best resolution on the A-to-D converter. However, it should be remembered that the amplitude envelop varies considerably with vertical position, as can be seen from the radial velocity profile. The time-series which were obtained at positions a—f in figure B.2 are shown in the same order in figures B.3a—f. The feature which is most interesting in relation to the measuring position h is the relative contribution of the high- and low-frequency components in each of the time-series, and how this relates to the qualitative nature

of the flow at that position.

In figures B.3a and B.3b, the low-frequency component appears to be dominant over the high-frequency component, even though it is known that the former is a modulation of the latter. This can be understood from the way that the small peripheral vortices which contribute the high-frequency mode are created beside the inner cylinder and then move off towards the $h = 1$ end of the flow domain. These vortices are then destroyed as they pass in between the Taylor cell and the stationary outer cylinder. Thus, measurements close to the $h = 0$ end do not experience a significant contribution from these small vortices. However, the low-frequency oscillation, being associated with the main cell, is still easily detected at this end since the cell extents to fill the full vertical extent of the annulus. As the measuring position is advanced, so the relative contribution of the high-frequency mode increases. Evidence of this increase can be seen by inspection of figures B.3c—e. The final time-series presented in figure B.3f was taken at the position $h = 0.91$. It can be seen that the high-frequency mode is now dominant over the low-frequency mode, and that the latter is clearly a modulation of the former.

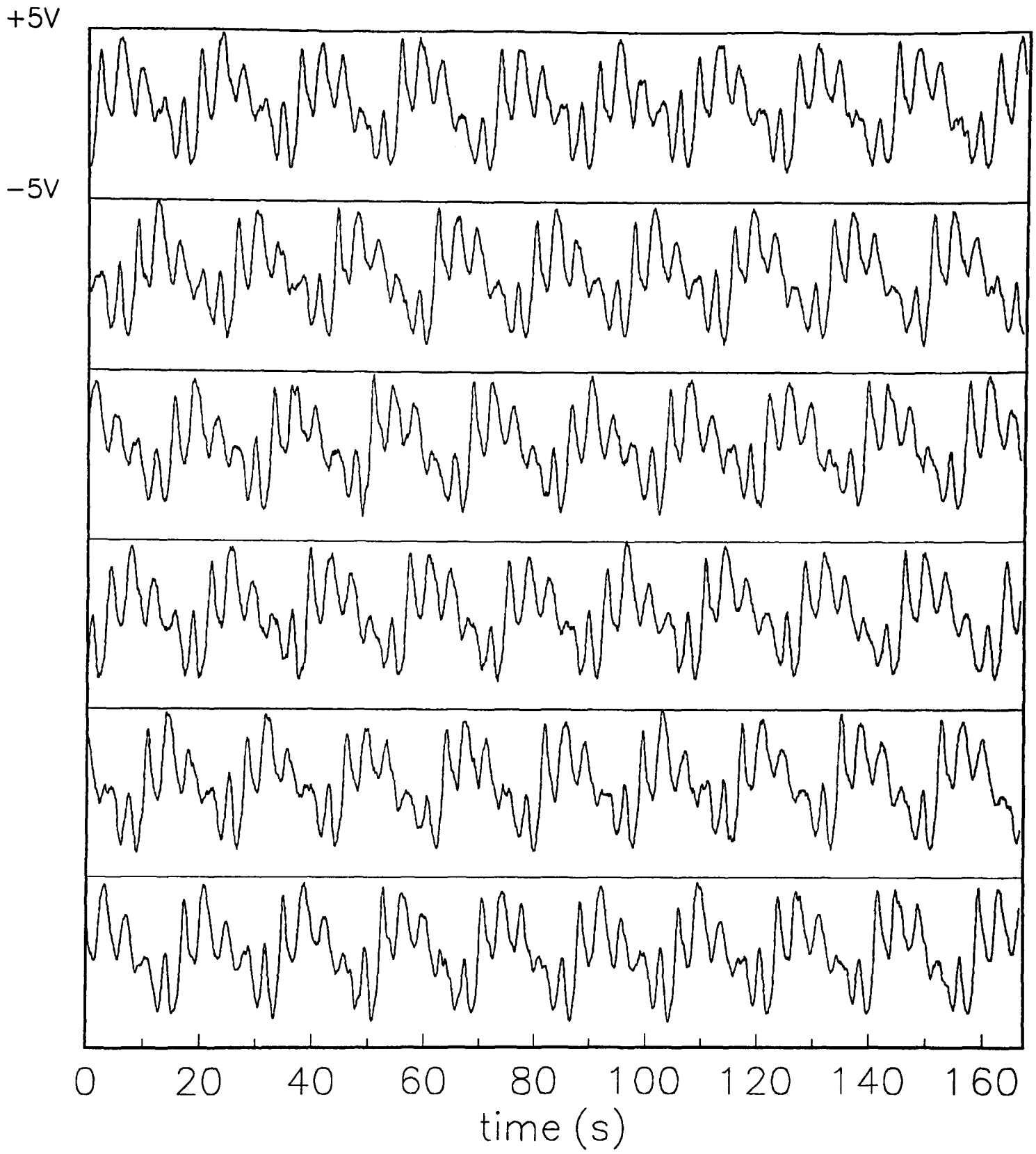

Figure B.3a : Time-series measured at h = 0.15

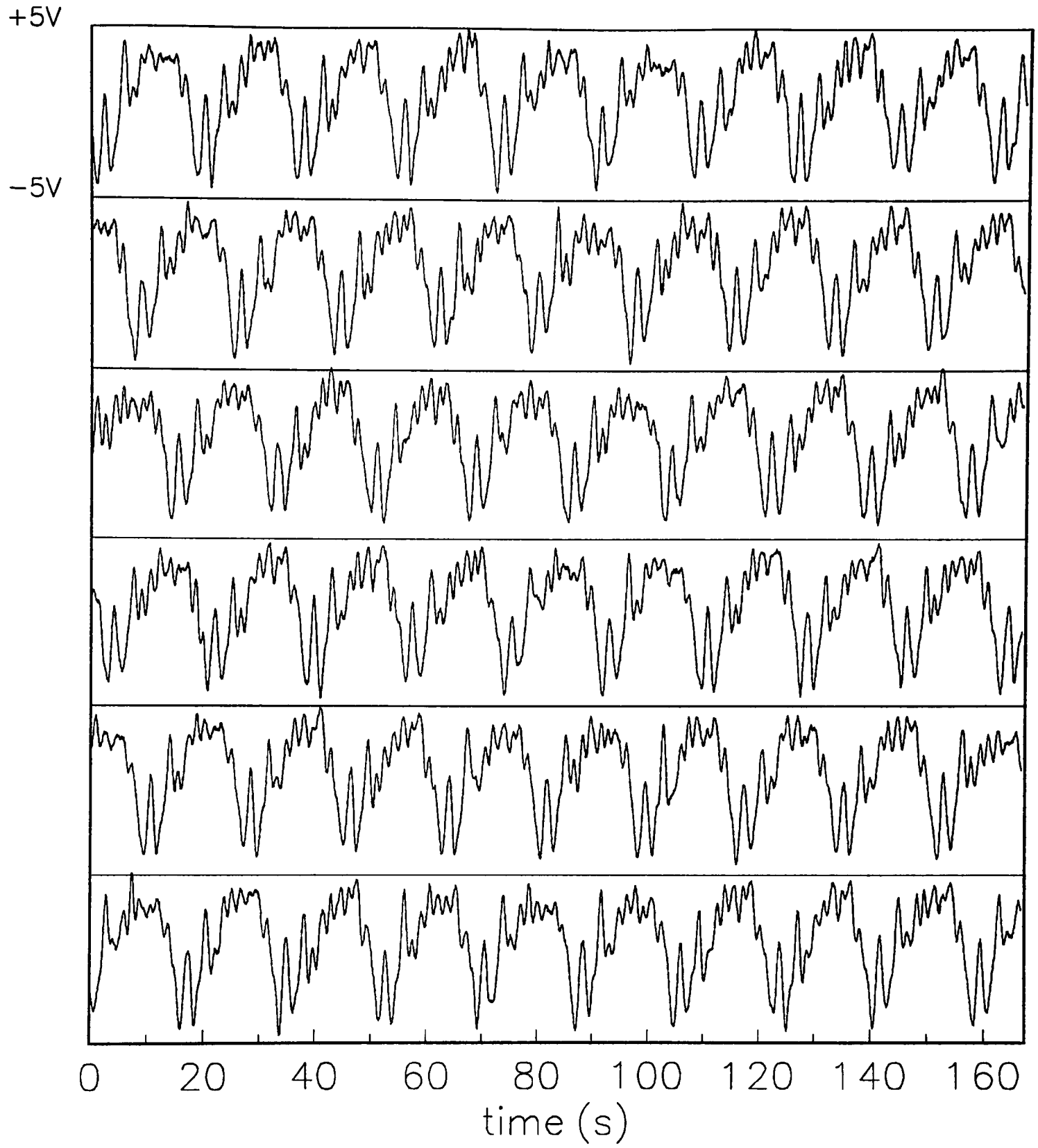

Figure B.3b : Time-series measured at h = 0.30

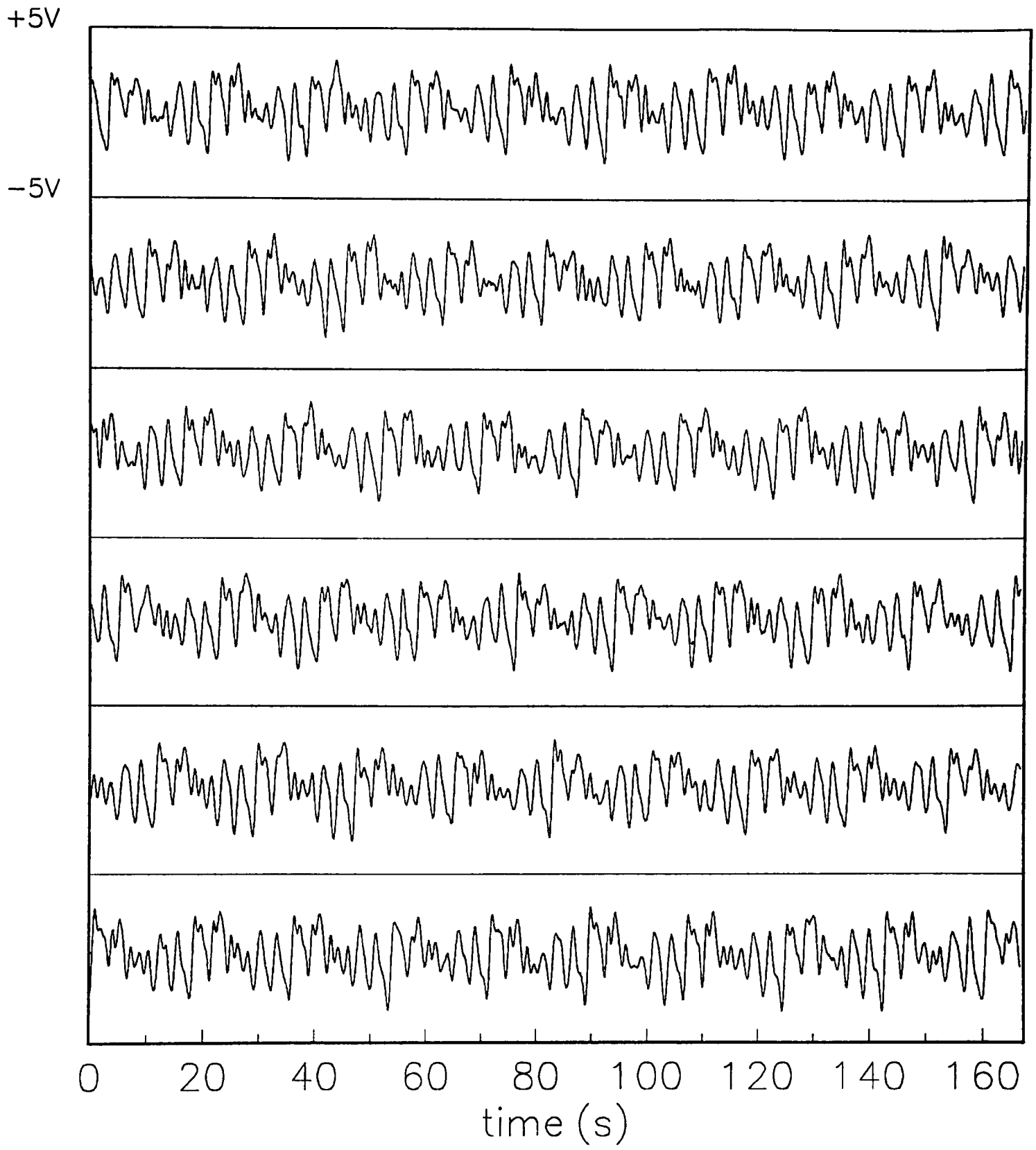

Figure B.3c : Time-series measured at h = 0.45

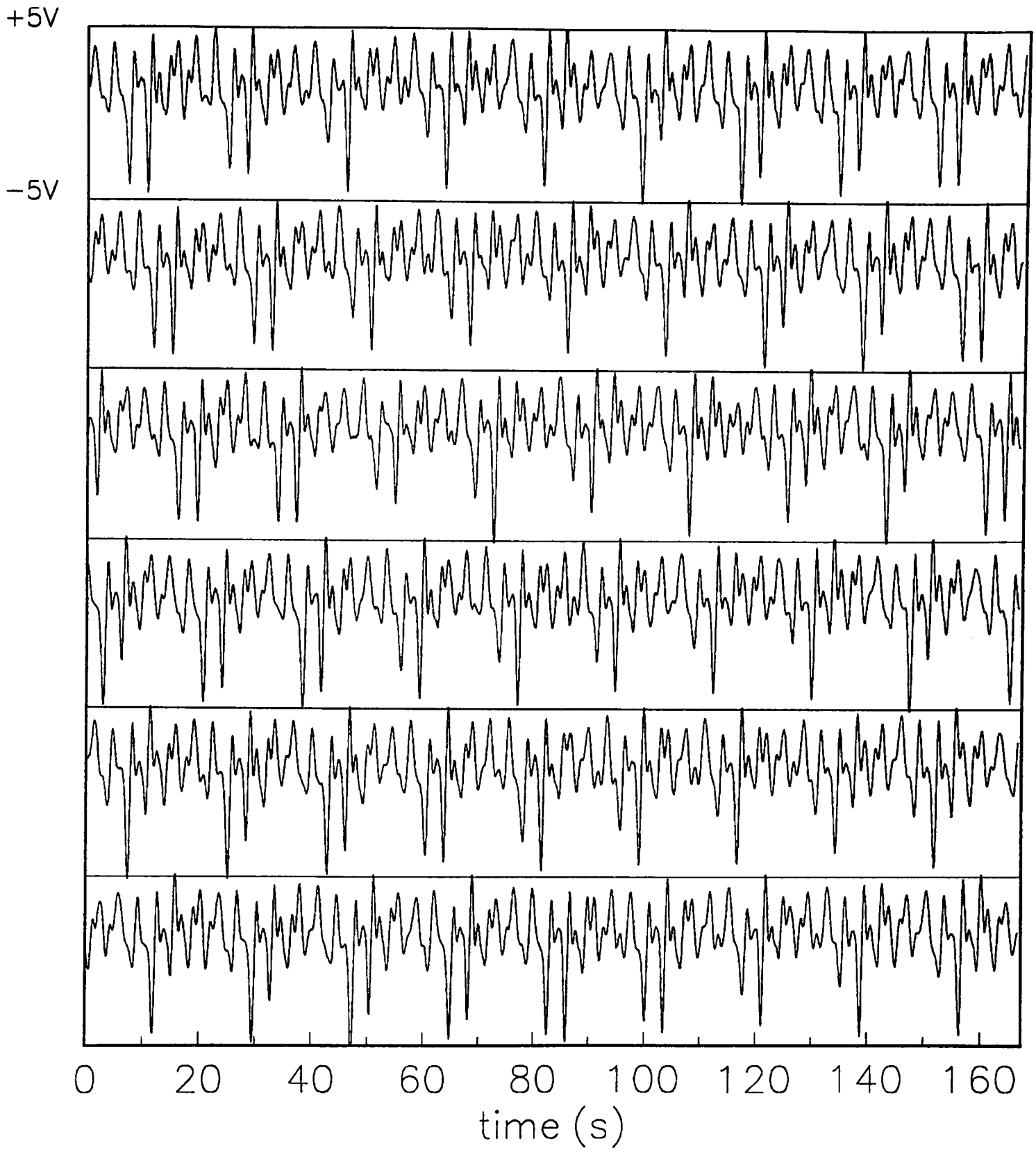

Figure B.3d : Time-series measured at h = 0.60

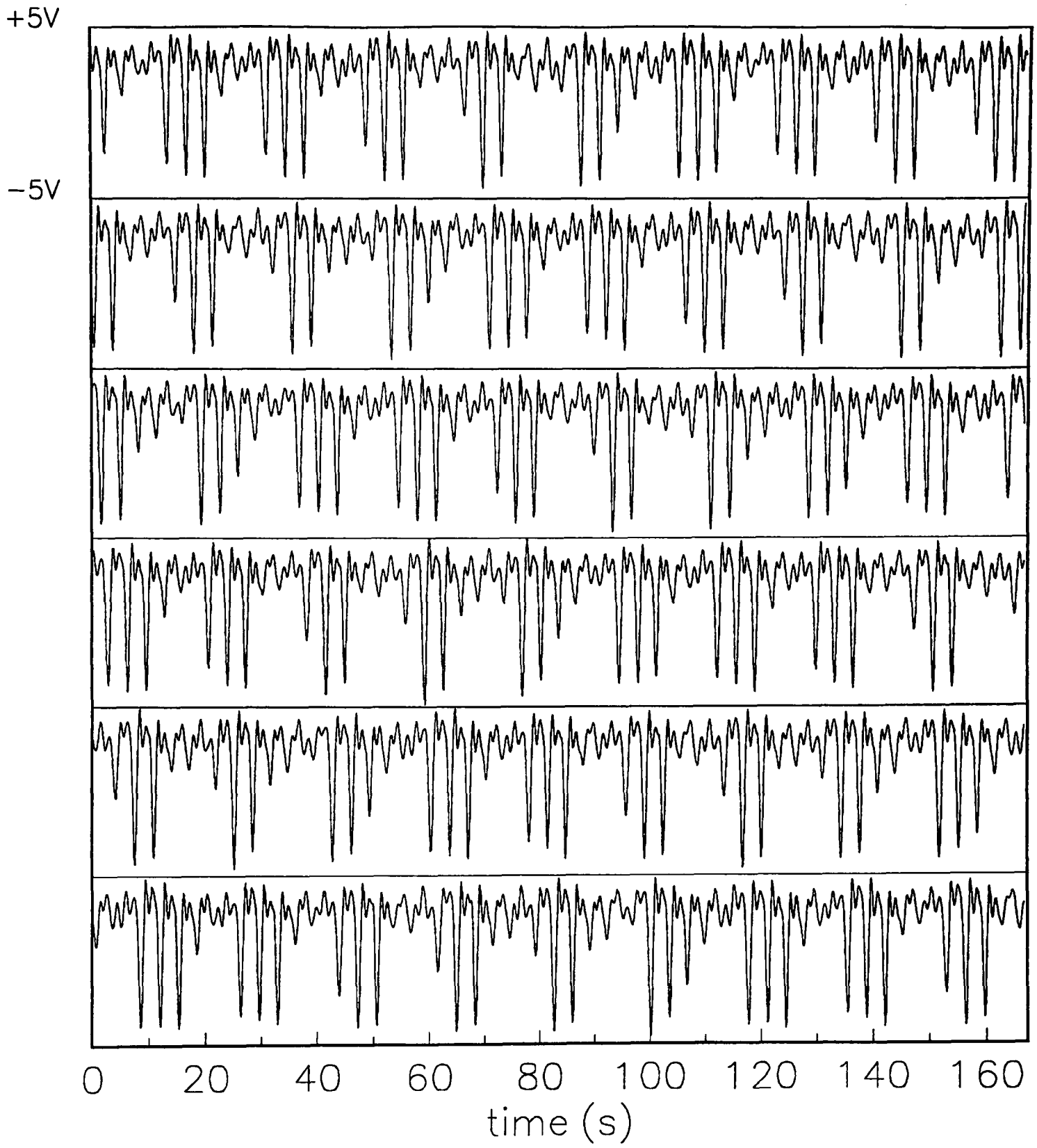

Figure B.3e : Time-series measured at h = 0.76

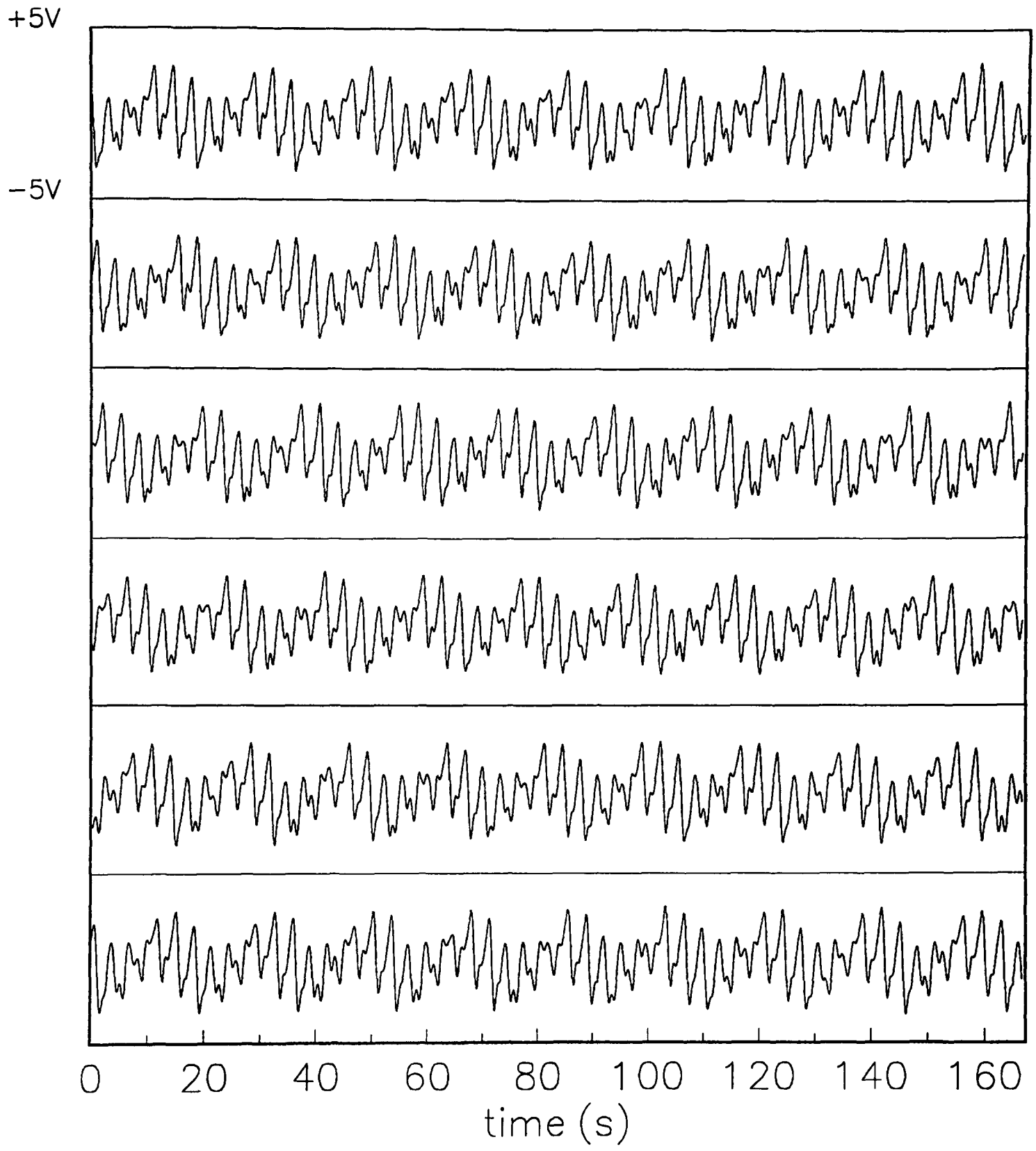

Figure B.3f : Time-series measured at h = 0.91

B.3 Structure of reconstructed phase portraits

Each of the time-series shown in figures B.3a—f was used to reconstruct an associated set of trajectories in phase space. This process was carried out using the techniques set out by Broomhead & King (1986) for the geometrical interpretation of experimental time-series. The techniques are now relatively standard, and a comprehensive review is given by Broomhead & Jones (1989). The aim of this study is to consider to what extent the choice of measuring position affects the general geometric form of the reconstructed phase portrait.

An ideal singly-periodic oscillation will be represented in phase space as a planar limit cycle. Correspondingly, and ideal doubly-periodic oscillation will appear as a torus when the data are viewed geometrically. The two independent frequency components in the flow are $\omega/\omega_c = 0.34$ and 0.06, and since these are not rationally related to each other, it is to be expected that the set of trajectories in phase space will form a well-defined torus. However, the two components will provide different relative contributions to the total signal as the measuring position varies. The extent to which this affects the form of the reconstructed phase portrait can be seen in figures B.4a—f, which run in order from $h = 0.15$ (figure B.4a) to $h = 0.91$ (figure B.4f). Here, the structure of trajectories in phase space is illustrated by taking Poincaré sections (see Bergé *et al.* (1986), for example) through the full attractor.

The sections shown in figure B.4 show the toroidal structure of the attractor becoming progressively clearer as the measuring position h is moved from the in-flow

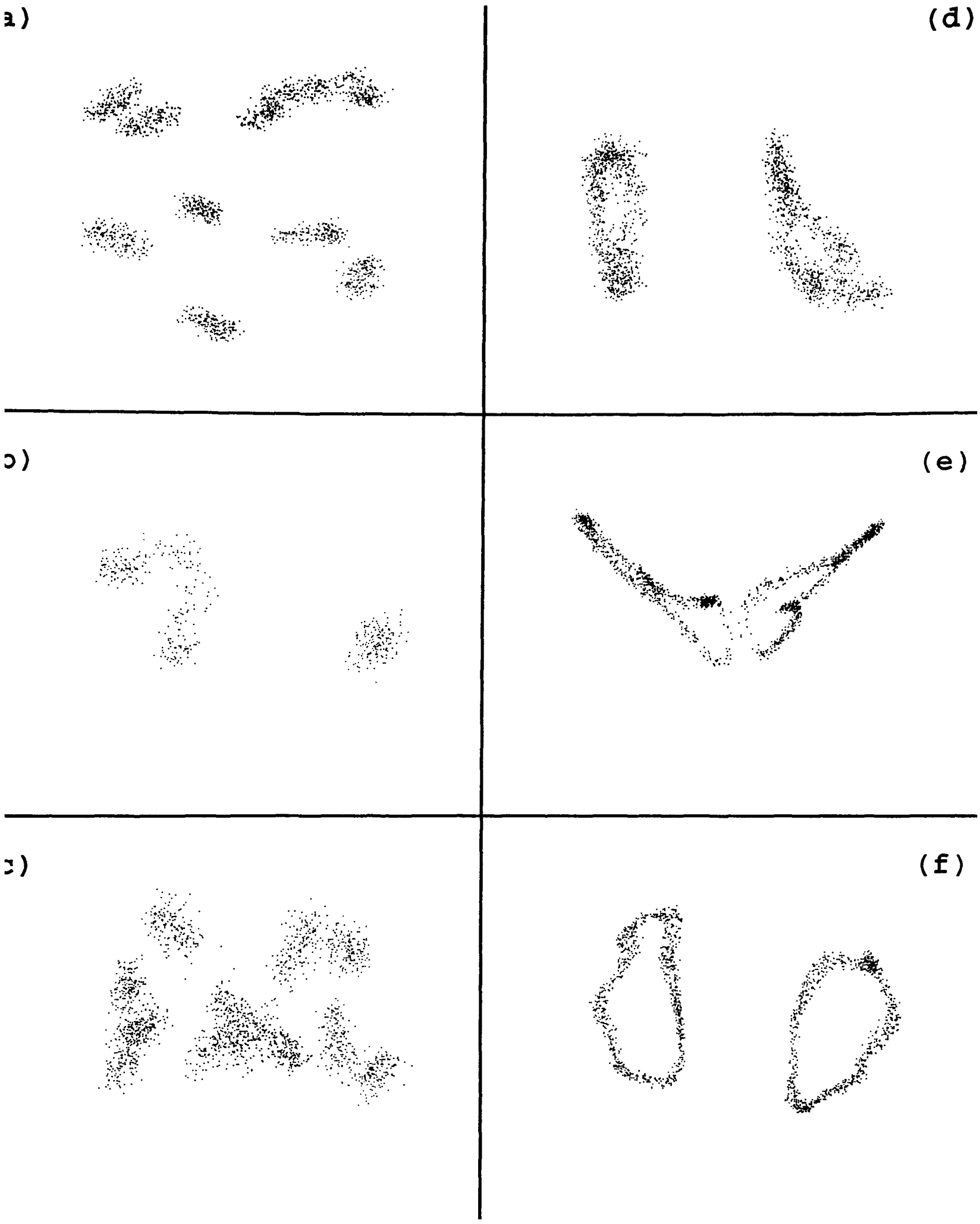

Figure B.4 : Poincaré sections through attractors reconstructed using time-series shown in figure B.3. (a) h = 0.15. (b) h = 0.30. (c) h = 0.45. (d) h = 0.60. (e) h = 0.76. (f) h = 0.91.

boundary ($h = 0$) to the out-flow boundary ($h = 1$). This is the same conclusion which is drawn from inspection of the time-series in figure B.3. The data recorded at positions (a) and (b) in figure B.2 do not give any indication that there are two incommensurate frequencies in the flow. The first suggestion of a toroidal structure comes in figure B.4c, where the points on the Poincaré section are arranged approximately into two groups. Two closed loops can be seen in figures B.4d—f, with the clearest form being that shown in figure B.4f.

B.4 Conclusions

It is very difficult to quantify the criteria for an 'ideal' measuring position in the circumstances which are considered in this appendix. However, there are various qualitative features which may be used with experience to identify certain positions as being more representative than others. Certainly, a knowledge of the behaviour of the system at parameter values other than those at which measurements are being made can lead to distinctions between representative and unrepresentative signals. In addition, reference to the spatial structure of the flow can indicate points at which measurements might be made that would capture more accurately the significant features of the time-dependent motion. In conclusion, care must be taken when positioning the measuring volume within the flow to ensure that local measurements are representative of the whole flow field. However, given this recognition, it is the case that investigations of the type reported in previous chapters can be carried out successfully to give consistent results.

REFERENCES

Acheson D.J. 1990. Elementary Fluid Dynamics. *Clarendon Press, Oxford.*

Barcilon A. & Brindley J. 1984. Organized structures in turbulent Taylor-Couette flow. *J. Fluid Mech.* **143**, 429.

Barcilon A., Brindley J., Lessen M. & Mobbs F.R. 1979. Marginal instability in Taylor-Couette flows at a very high Taylor number. *J. Fluid Mech.* **94**, 453.

Benjamin T.B. 1978a. Bifurcation phenomena in steady flows of a viscous liquid. 1. Theory. *Proc. R. Soc. Lond.* A **359**, 1–26.

Benjamin T.B. 1978b. Bifurcation phenomena in steady flows of a viscous liquid. 2. Experiments. *Proc. R. Soc. Lond.* A **359**, 27–43.

Benjamin T.B. & Mullin T. 1981. Anomalous modes in the Taylor experiment. *Proc. R. Soc. Lond.* A **377**, 221–249.

Benjamin T.B. & Mullin T. 1982. Notes on the multiplicity of flows in the Taylor experiment. *J. Fluid Mech.* **121**, 219–230.

Bergé P., Pomeau Y. & Vidal C. 1986. Order Within Chaos. *Wiley/Hermans, New York/Paris.*

Broomhead D.S. & Jones R. 1989. Time-series analysis. *Proc. R. Soc. Lond.* A **423**, 103–121.

Broomhead D.S. & King G.P. 1986. Extracting qualitative dynamics from experimental data. *Physica* D **20**, 217–236.

Chandrasekhar S. 1961. Hydrodynamic and Hydromagnetic Stability. *Clarendon Press, Oxford.*

Churchill S.W. 1988. Viscous Flows: the Practical Use of Theory. *Butterworth, New York.*

Cliffe K.A. 1983. Numerical calculations of two-cell and single-cell Taylor flows. *J. Fluid Mech.* **135**, 219–233.

Cliffe K.A., Kobine J.J. & Mullin T. 1992. The role of anomalous modes in Taylor-Couette flow. Submitted to *Proc. R. Soc. Lond.* A.

Coles D. 1965. Transition in circular Couette flow. *J. Fluid Mech.* **21**, 385–425.

Coughlin K.T. & Marcus P.S. 1992a. Modulated waves in Taylor-Couette flow. Part 2. Numerical simulation. *J. Fluid Mech.* **234**, 19–46.

Coughlin K.T. & Marcus P.S. 1992b. Period-doubling in a three-dimensional flow. Unpublished.

Cvitanović P. 1989. Universality in Chaos. 2nd edition. *Adam Hilger, Bristol.*

Davey A., DiPrima R.C. & Stuart J.T. 1968. On the instability of Taylor vortices. *J. Fluid Mech.* **31**, 17–52.

DiPrima R.C. & Swinney H.L. 1981. Instabilities and transition in the flow between concentric rotating cylinders. In *Hydrodynamic Instabilities and the Transition to Turbulence.* H.L. Swinney & J.P. Gollub (eds.). *Springer, Berlin.*

Drain L.E. 1980. The Laser Doppler Technique. *John Wiley & Sons Ltd., New York.*

Drazin P.G. & Reid W.H. 1981. Hydrodynamic stability. *C.U.P., Cambridge.*

Fearn R.M., Mullin T. & Cliffe K.A. 1990. Nonlinear flow phenomena in a symmetric sudden expansion. *J. Fluid Mech.* **211**, 595–608.

Gaster M. 1990. The nonlinear phase of wave growth leading to chaos and breakdown to turbulence in a boundary layer as an example of an open system. *Proc. R. Soc. Lond.* A **430**, 3–24.

Gollub J.P. & Swinney H.L. 1975. Onset of turbulence in a rotating fluid. *Phys. Rev. Lett.* **35**, 927–930.

Golubitsky M. & Schaeffer D. 1985. Singularities and Groups in Bifurcation Theory. Volume 1. *Applied Mathematical Sciences* **51**. *Springer-Verlag, New York Inc.*

Guckenheimer J. 1981. On a codimension-2 bifurcation. *Lecture Notes in Mathematics* **898**. *Springer-Verlag, Berlin.*

Guckenheimer J. & Holmes P. 1986. Nonlinear Oscillations, Dynamical Systems and Bifurcations of Vector Fields. 2nd edition. *Applied Mathematical Sciences* **42**. *Springer-Verlag, New York Inc.*

Hellou M. & Coutanceau M. 1992. Cellular Stokes flow induced by rotation of a cylinder in a closed channel. *J. Fluid Mech.* **236**, 557–577.

Holmes P. 1990. Can dynamical systems approach turbulence? In *Lecture Notes in Physics* **357** – *Whither Turbulence? Turbulence at the Crossroads* (ed. J.L. Lumley). *Springer-Verlag, Berlin Inc.*

Langford W.F. 1983. In *Nonlinear Dynamics and Turbulence* (ed. G.I. Barenblatt, G. Ioos and D.D. Joseph). *Pitman, New York.*

Lensch B. 1988. Über die Dynamik der Einwirbelströmung im Taylor-zylinder. Diplomarbeit. University of Kiel, Germany.

Lewis E. 1979. Steady flow between a rotating circular cylinder and a fixed square cylinder. *J. Fluid Mech.* **95**, 497–513.

Libchaber A. & Maurer J. 1980. Une experience de Rayleigh-Bénard de géométrie réduite; muliplication, accrochage et démultiplication de fréquencies. *J. de Phys.* **41**, Colloq. C3–51.

Moffat H.K. 1964. Viscous and resistive eddies near a sharp corner. *J. Fluid Mech.* **18**, 1–18.

Mullin T. 1982. Mutations of steady cellular flows in the Taylor experiment. *J. Fluid Mech.* **121**, 207–218.

Mullin T. 1991. Finite-dimensional dynamics in Taylor-Couette flow. *IMA J. Applied Maths.* **46**, 109–119.

Mullin T. 1992. Disordered fluid motion in a small closed system. Submitted to *Physica D.*

Mullin T. & Cliffe K.A. 1986. Symmetry breaking and the onset of time-dependence in fluid mechanical systems. In *Nonlinear Phenomena and Chaos* (ed. S. Sarkar). *Adam Hilger, Bristol.*

Mullin T., Cliffe K.A. & Pfister G. 1987. Unusual time-dependent phenomena in Taylor-Couette flow at moderately small Reynolds numbers. *Phys. Rev. Lett.* **58**, 2212–2215.

Mullin T. & Lorenzen A. 1985. Bifurcation phenomena in flows between a rotating circular cylinder and a stationary square outer cylinder. *J. Fluid Mech.* **157**, 289–303.

Mullin T., Lorenzen A. & Pfister G. 1983. Transition to turbulence in a non-standard rotating flow. *Phys. Lett.* **96A**, 236–238.

Mullin T. & Price T.J. 1989. An experimental observation of chaos arising from the interaction of steady and time-dependent flows. *Nature* **340**, 294–296.

Mullin T., Tavener S.J. & Cliffe K.A. 1989. An experimental and numerical study of a codimension-2 bifurcation in a rotating annulus. *Europhys. Lett.* **8**, 251–256.

Pfister G. 1985. Deterministic chaos in rotational Taylor-Couette flow. *Lecture Notes in Physics* **235**, 199–210.

Pfister G., Schmidt H., Cliffe K.A. & Mullin T. 1988. Bifurcation phenomena in Taylor-Couette flow in a very short annulus. *J. Fluid Mech.* **191**, 1–18.

Pfister G., Schulz A. & Lensch B. 1991. Bifurcations and the route to chaos of a one-vortex state in Taylor-Couette flow. Unpublished.

Pomeau Y. & Manneville P. 1980. Intermittent transition to turbulence in dissipative dynamical systems. *Comm. Math. Phys.* **74**, 189–197.

Press W.H., Flannery B.P., Teukolsky S.A. & Vetterling W.T. 1988. Numerical Recipes in C: the Art of Scientific Computing. *C.U.P., Cambridge.*

Price T.J. 1991. Experiments on nonlinear flows in triply-connected systems. D. Phil. Thesis. University of Oxford, United Kingdom.

Savaş Ö. 1985. On flow visualization using reflective flakes. *J. Fluid Mech.* **152**, 235–248.

Schaeffer D.G. 1980. Analysis of a model in the Taylor problem. *Math. Proc. Camb. Phil. Soc.* **87**, 307–337.

Schumack M.R., Schultz W.W. & Boyd J.P. 1991. Taylor vortices between elliptical cylinders. Phys. Fluids A, 4, 2578–2581.

Šilnikov L.P. 1965. A case of the existence of a denumerable set of periodic motions. *Sov. Math. Dokl.* **6**, 163–166.

Smith G.P. & Townsend A.A. 1982. Turbulent Couette flow between concentric circular cylinders at large Taylor numbers. *J. Fluid Mech.* **123**, 187–217.

Snyder H.A. 1968. Experiments on rotating flows between noncircular cylinders. *Phys. Fluids* **11**, 1606–1611.

Sullivan T.S. & Ahlers G. 1988. Nonperiodic time dependence at the onset of convection in a binary liquid mixture. *Phys. Rev.* A **38**, 3143–3146.

Taylor G.I. 1923. Stability of a viscous liquid contained between two rotating cylinders. *Phil. Trans. R. Soc. Lond.* A **223**, 289–343.

Terada T. & Hattori K. 1926. Some experiments on the motions of fluids. 4. Formation of vortices by rotating disc, sphere or cylinder. *Rep. Tokyo Univ. Aeronaut. Research Inst.* **2**, 287–326.

Tritton D.J. 1988. Physical Fluid Dynamics. 2nd edition. *Clarendon Press, Oxford.*

Wei T., Kline E.M. & Lee S.H.K. 1991. Görtler vortex formation at the inner cylinder in Taylor-Couette flow. Unpublished.

Wiggins S. 1990. Introduction to Applied Nonlinear Dynamical Systems and Chaos. *Texts in Applied Mathematics* **2**. *Springer-Verlag, New York Inc.*

Winters K.H. 1987. A bifurcation study of laminar flow in a curved tube of rectangular cross-section. *J. Fluid Mech.* **180**, 343–369.